N69-27775
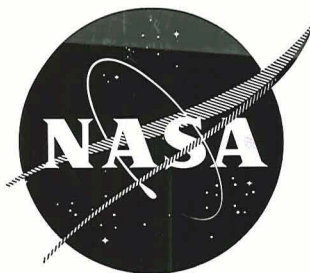
DEVELOPMENT OF DUCTILE CLADDINGS FOR DISPERSION-STRENGTHENED NICKEL-BASE ALLOYS

by

V. L. Hill, S. K. Misra, and H. L. Wheaton

IIT RESEARCH INSTITUTE

Prepared For

NATIONAL AERONAUTICS AND SPACE ADMINISTRATION

FINAL REPORT

DEVELOPMENT OF DUCTILE CLADDINGS FOR
DISPERSION-STRENGTHENED NICKEL-BASE ALLOYS

by

V. L. Hill, S. K. Misra, and H. L. Wheaton

IIT RESEARCH INSTITUTE
10 W. 35th Street
Chicago, Illinois 60616

Prepared For

NATIONAL AERONAUTICS AND SPACE ADMINISTRATION

October 30, 1968

Page ii (backside of title page) is blank

TABLE OF CONTENTS

ABSTRACT

The objective of this program was to develop ductile, oxidation-resistant cladding alloys for thoria dispersion strengthened nickel (TD Ni) and nickel-chromium (TD NiCr).

Cyclic furnace oxidation tests were conducted on modified alloys in the Fe-Cr-Al, Ni-Cr-Al, and Ni-Cr-Ta systems at 2300°F for periods of up to 800 hr. Supplemental evaluation included torch oxidation, sulfidation-corrosion, and bend tests. Interdiffusion studies were also conducted on selected Fe-Cr-Al and Ni-Cr-Al alloys in contact with TD Nickel and TD NiCr.

The most oxidation-resistant alloys were Fe-25Cr-4Al modified with Y and Th and Ni-20Cr-5Al modified with Th. A Fe-25Cr-4Al-0.08Y-0.5Ta alloy is of particular interest. This alloy survived a 800 hr cyclic furnace exposure and retained ductility as a 10 mil sheet; the others did not. Diffusion studies revealed that extensive interdiffusion occurred in 100 hr at 2300°F and nearly complete homogenization in 300 hr with both TD Ni and TD NiCr substrates. Oxidation mechanisms and interdiffusion based on microprobe examination are discussed.

LIST OF TABLES

LIST OF TABLES (Continued)

LIST OF TABLES (Continued)

LIST OF FIGURES

LIST OF FIGURES (Continued)

LIST OF FIGURES (Continued)

LIST OF FIGURES (Continued)

I. SUMMARY

The objective of this program was to develop ductile, oxidation-resistant cladding alloys for TD Nickel and TD NiCr for use at temperatures to 2300°F.

The experimental program consisted of two tasks. In Task I, 56 alloys in the Fe-25Cr-4Al, Ni-20Cr-5Al, and Ni-Cr-Ta systems were fabricated and furnace oxidation tested at 2300°F for 100 hr. Alloy modification to the three alloy systems included 0.25 a/o additions of Y, Be, Mg, Ce, La, Th, Ti, Zr, Hf, Ta, Si and Ge. The oxidation resistance was determined by gravimetric analysis during cyclic furnace testing and subsequent metallographic measurement of metal recession. It was found that the best oxidation resistance was obtained in Fe-25Cr-4Al alloys modified with Y, Ti, Th, and Hf and in Ni-20Cr-5Al modified with Th and Hf. No promising alloys were obtained in the Ni-Cr-Ta system.

The most oxidation-resistant Fe-Cr-Al and Ni-Cr-Al compositions were then further modified and evaluated at 2300°F in a second series of cyclic furnace oxidation tests. Selected modified alloys were also subjected to supplemental evaluation including torch oxidation, sulfidation-corrosion, and bend tests. The results demonstrated that none of the alloys were subject to sulfidation corrosion. Furthermore, the furnace oxidation rate was equivalent to the oxidation rate in an air-natural gas torch flame at 2300°F. All of the Ni-Cr-Al alloys, but only the Fe-Cr-Al alloys containing Hf and Ta, were ductile after oxidation exposure at 2300°F for 100 hr.

Effort in Task II consisted of further modification of Fe-Cr-Al and Ni-Cr-Al alloys based on Task I oxidation behavior. Eighteen alloys, including six compositions from Task I were fabricated into 10-mil thick oxidation samples and exposed at 2300°F for 800 hr, or failure. The alloys selected for evaluation included Fe-25Cr-4Al modified with Ti, Hf, Th, and Y, and Ni-20Cr-5Al with Th additions. Selected alloys of each base material were also evaluated with Ta and Hf secondary additions. Again, the oxidation rates were measured by gravimetric analysis and metallographic examination. The most oxidation-resistant compositions were three Fe-Cr-Al-Y alloys, which were the only ones that survived 800 hr exposure. One of the three Fe-Cr-Al-Y alloys containing 0.50 Ta and 0.25Y was ductile after the 800 hr exposure. Oxidation life in the range of 500-700 hr was also obtained for Fe-Cr-Al-Th and Ni-Cr-Al-Th alloys. The poorest oxidation resistance found in Task II was exhibited by Fe-Cr-Al-Hf and Fe-Cr-Al-Ti alloys, although all compositions survived exposure for more than 100 hr.

Microprobe examination of oxidation samples demonstrated that the oxidation resistance of Fe-Cr-Al alloys depended upon

the Al_2O_3-rich surface oxide layer. The microprobe data and oxidation behavior suggested that the improvement in oxidation resistance due to minor additions consisted of modification of this surface oxide. This was concluded although no detectable concentration of minor additions could be found in the scale after exposure. Alloys in the Ni-Cr-Al system had a similar tendency to develop an Al_2O_3-rich oxide, but the rate of scale growth was much slower. In contrast to alloys in the Fe-Cr-Al system which failed abruptly, modified Ni-Cr-Al alloys exhibited a gradual metal recession during exposure.

Interdiffusion studies were conducted in argon for 100 and 300 hr at 2300°F using Fe-Cr-Al and Ni-Cr-Al cladding on TD Ni and TD NiCr. Metallographic examination of inter-diffused samples indicated extensive porosity at the cladding/substrate interface with Fe-Cr-Al cladding, especially on TD Ni substrates. Porosity was also evident with Ni-Cr-Al cladding, but no continuous band of porosity existed at the cladding/sub-strate interface. Microprobe scans revealed that extensive inter-diffusion had occurred in 100 hr and nearly complete homogeniza-tion had occurred after 300 hr. Bend tests of interdiffused samples did not cause separation of the cladding, in spite of the observed interfacial porosity. Furthermore, it was concluded that the life of a composite system could not be predicted on the basis of interdiffusion data alone. Further evaluations of clad composites in air environments are necessary to define the influence of interdiffusion on the mechanical properties and oxidation resistance of the composites.

Six of the most oxidation-resistant Task II alloys were fabricated into 5-mil sheet material for further evaluation at NASA as a concluding phase of the program. These alloys in-cluded five Fe-Cr-Al alloys and one Ni-Cr-Al alloy. The fabrica-tion procedure used for preparing both the 5-mil and 10-mil material was a combination of hot and cold rolling.

II. INTRODUCTION

One interesting and potentially useful group of high-temperature materials is based on dispersion strengthening a metallic matrix with fine, well-dispersed particles of a refractory oxide. TD Nickel (TD Ni), which is representative of this system, has a number of properties which make it attractive for gas turbine applications, such as nozzle guide vanes, combustion cans, and after-burner liners. Guide vane materials, for example, must possess a high degree of oxidation and corrosion resistance and be capable of withstanding severe thermal gradients without cracking or bowing. Fortunately, the applied stress resulting from the gas bending load is only of the order of 4000 psi. The superalloys currently used for vane applications generally fail as a result of oxidation or thermal fatigue, although thermal fatigue cracking is often initiated or augmented by intergranular oxidation. In order to extend the vane life at current operating conditions, it is necessary to make significant improvements in these areas. The potential of increasing turbine inlet temperatures, without resorting to design techniques such as air cooling, also requires improvements in high-temperature load-bearing capability beyond that provided by current superalloys.

TD Ni possesses a number of properties desirable for turbine vane materials: useful strength in the 2000°-2400°F range, higher melting temperature than current superalloys, good conductivity, and good thermal stability. Unfortunately, its resistance to oxidation is nearly that of pure nickel and is therefore inadequate for many potential turbine applications. Attempts to improve the oxidation resistance of TD Ni have included the use of aluminum and aluminum-rich diffusion coatings and alloying. To date, the best aluminide coatings cannot be used over about 2200°F if a reasonable life is required. Improvement of oxidation resistance through alloying has resulted in the development of TD NiCr which contains 20% Cr, but this alloy is also not adequate for long-time service in a dynamic environment over about 2100°F.

The objective of this program was to develop a ductile, oxidation-resistant cladding alloy which would protect TD Ni and TD NiCr from oxidation and sulfidation corrosion for extended periods of time in the 2000°-2400°F range. The initial goal was to provide a 5 mil cladding capable of surviving a 800 hr exposure in air at 2300°F. In addition to oxidation and sulfidation resistance, the alloy had to possess the following properties:

1. Sufficient ductility to permit fabrication of thin foil.

2. Adequate ductility after long-time cyclic exposure in order to maintain resistance to failure by mechanical impact.

3

3. Resistance to extensive interdiffusion in contact with the TD Ni or TD NiCr substrates.

4. Expansion coefficient similar to that of the substrate in order to avoid damaging thermal stresses.

Obviously, the development of a single cladding alloy with all the above requirements is difficult. Accordingly, the initial approach was to develop cladding alloys with the requisite oxidation resistance and ductility, keeping in mind the requirement of diffusional stability. Diffusion barriers could subsequently be employed to maintain diffusional stability, if required. However, selection and evaluation of appropriate diffusion barriers was considered beyond the scope of the current program.

The experimental program was divided into two tasks. The first task consisted of alloy system development and screening oxidation testing at 2300°F. Based on the results of the initial oxidation tests, modifications of the most resistant alloys were selected for additional cyclic furnace oxidation evaluation. Subsequently, selected modified Task I alloys were oxidation tested in a torch flame and exposed to a sulfidation environment.

The second task involved the development and evaluation of improved alloys based on information obtained in the first task. One major difference in the test samples existed for oxidation tests conducted in Task II from those in the previous task. Oxidation samples during the second task were fabricated from 10 mil sheet material, rather than 0.060 in. thick material used previously, to simulate alloy depletion effects in a 5 mil cladding layer. Effort during this phase included 800 hr cyclic furnace oxidation testing and investigation of interdiffusion of selected cladding alloys on TD Ni and TD NiCr substrates. Finally, 5 mil sheet material of selected alloys was prepared for further evaluation by NASA.

The research effort in this program was chronological and will generally be discussed in the same order as the work was conducted. However, some deviation in this order will be exercised in this report to avoid excessive repetition of the discussion of experimental data. For example, the results of metallographic examination in Task I will be assimilated into a single section. Furthermore, the alloys selected for the various tests did not always represent those which had the best oxidation resistance. Ductility was also considered. Some alloy compositions were selected to bracket initially selected compositions, however, with the intention of obtaining the maximum possible information during the experimental program.

In this report, all compositions are given in weight percent unless specifically identified as atomic percent.

III. BACKGROUND

A review of the literature indicated two general types of materials which could meet the objective of the program: (1) alloys based on iron, nickel, or cobalt alloyed with chromium and other elements; or (2) precious metals such as platinum, iridium or rhodium, or an alloy thereof. The precious-metal approach was technically attractive since these metals could have fair compatibility with TD Ni, good ductility, and excellent resistance to oxidation. Unfortunately, materials cost made this approach impractical.

The oxidation-resistant alloy (Ni, Fe, or Co) approach was, therefore, chosen. A literature review to establish the effect of composition on oxidation resistance, fabricability, stability, and thermal expansion characteristics, however, revealed a dearth of information on the oxidation behavior of thin sheet material of these alloys. For that matter, few quantitative data existed on the oxidation behavior of any form of such alloys above 2200°F. Moreover, with the possible exception of heater element materials, most available materials were developed to obtain high-temperature strength, often obtained at the expense of oxidation resistance.

Based on the analysis of existing oxidation data, three systems were selected for investigation of the series Fe-Cr-Al, Ni-Cr-Al, and Ni-Cr-Ta. No problems in thermal expansion were expected for any of these systems because of a basic similarity with TD Ni and TD NiCr. This conclusion was verified for the Fe-Cr-Al system[1,2] and the Ni-Cr-Al[2] system by existing data. The chemical similarity of the Ni-Cr-Ta system to many nickel-base superalloys also indicated no difficulty with thermal expansion in this system.

It was also expected that all of these systems could be worked provided that the alloying additions of chromium, aluminum, and/or tantalum were maintained within the solid solubility limits. These limits were known for Ni-Cr-Al and Fe-Cr-Al systems and are above the range at which good oxidation resistance can be obtained in these systems. It was expected that tantalum additions would decrease the workability of Ni-Cr alloys, but the tantalum concentration limits were not known.

Considerable oxidation data existed on bulk Fe-Cr-Al and Ni-Cr-Al alloy systems at 2100-2300°F. Oxidation resistance had been obtained in these alloys which approached that required by the program objectives. Consequently, these alloys could meet the program objective of several hundred hours life at 2300°F if further improvement could be obtained. Accordingly, attempts to improve the oxidation resistance in these systems were based on additions of a variety of metals as quaternary additions to a single base composition. The selected base compositions Fe-25Cr-4Al and Ni-20Cr-5Al were both expected to be in the workable range.

The oxidation resistance of the alloys in the Ni-Cr-Ta system at 2300°F was not known, although there were some indications that tantalum improves the oxidation resistance of Ni-Cr-Al alloys at lower temperatures. It was hoped that good oxidation resistance could be developed in this system, since these alloys might provide greater elevated temperature stability in contact with TD Ni or TD NiCr. Since no quantitative elevated temperature oxidation data existed for this system, more extensive compositional variation was studied. Alloys consisting of variations in both chromium and tantalum were studied, as well as alloys with quaternary additions to the base composition Ni-25Cr-10Ta. As a result, a greater number of Ni-Cr-Ta alloys were selected for oxidation testing in the initial phase than Fe-Cr-Al or Ni-Cr-Al alloys.

Quaternary additions to the three base compositions were maintained at 0.25 a/o for the initial alloy selection. This was intended to assess the influence of the various alloying elements at a fixed nominal atomic concentration. The relatively low level of addition was selected because of the limited solubility of many of the alloying elements and the unknown influence of the additions on the workability of the alloys, particularly the rare earth metals. Furthermore, data existed on high-temperature oxidation resistance of similar alloys which suggested that considerable improvement in oxidation resistance could be obtained by very small additions.[3]

IV. EXPERIMENTAL PROCEDURE AND RESULTS

A flow sheet of the experimental program is shown in Figure 1. During the program, three major groups of cyclic furnace oxidation tests were conducted. After the initial alloy election, compositions evaluated in modified Task I and Task II alloys were based on the results of previous tests. The arbitrary criterion used in the screening of alloy compositions was the total weight gain of less than 11 mg/cm^2 in 100 hr at 2300°F.

All of the cyclic furnace oxidation tests were conducted in a similar manner. The samples were contained in Al_2O_3 crucibles in order to record both total weight gain and sample weight change. The cyclic conditions were 2 hr cycles to 20 hr, followed by 20 hr cycles to either 100 hr or 800 hr. Evaluation of selected alloys in the torch flame was conducted in a similar manner except that 8 hr cycles were used after 20 hr. In addition to weight change data, the rate of oxidation was also measured by metallographic measurement of the oxide thickness and metal recession rate.

Metallography of samples of all alloys in both the as-fabricated and the oxidized conditions was evaluated routinely for each of the three oxidation tests. In addition, samples subjected to the sulfidation test, torch oxidation tests, and interdiffusion were also examined metallographically. Bend tests and microhardness measurements were also made on selected alloys throughout the

program to indicate the ductility of the various alloys. During Task II, all alloy compositions were evaluated in the as-fabricated and the oxidized condition by 4t bend testing.

Chemical analysis of selected compositions was employed to verify the nominal composition of the alloys. A total of 23 of the 67 Task I and modified Task I alloys and all 18 alloys during Task II were analyzed by wet chemical analysis. Chemical analysis was required for alloys which exhibited weight losses greater than 1 percent during arc-melting. In no case did this occur; consequently, selection of alloys for chemical analysis in Task I was arbitrary.

Electron microprobe examination was employed extensively during Task II to augment other evaluation techniques. Selected alloys were examined in the as-fabricated condition and at various exposure times during the 800 hr oxidation test. All diffusion couples were examined both in the as-fabricated condition and after exposure for 100 and 300 hr at 2300°F.

A. Task I - Screening Studies and Alloy Modification

1. Alloy Selection and Sample Fabrication

As previously discussed, all of the alloys selected, with one exception, were in the three basic alloy systems Fe-Cr-Al, Ni-Cr-Al, and Ni-Cr-Ta. The nominal compositions of the 56 Task I alloys in weight percent are given in Table 1. The code letters for the various types of alloys shown in Table 1 will be employed throughout this report. Alloys designated as M1, M2, and M3 are identified separately since they represent special cases, as will be discussed subsequently.

In the Fe-Cr-Al system, the base composition selected was Fe-25Cr-4Al. Each addition of 0.25 a/o Y, Be, Mg, Ce, La, Th, Ti, Zr, Hf, Ta, Si, and Ge was made to this base composition. Similarly, these same additions, with the exception of tantalum, were made to the Ni-20Cr-5Al base composition in the Ni-Cr-Al system. The alloy Ni-16Cr-5Al was also included in order to assess the effect of lower chromium concentration.

Alloys in the Ni-Cr-Ta system represented variations in both chromium and tantalum, in addition to 0.25 a/o quaternary additions of the above elements to the base composition Ni-25Cr 10Ta. The chromium concentration was varied from 20 to 40 w/o attendant with tantalum variation from 5 to 15 w/o. It was expected that some difficulty in working would be encountered at the higher concentration of chromium and tantalum. Since no data existed for the Ni-Cr-Ta system, it was decided to define the concentration limits for workable alloys.

Three additional alloys were included for evaluation during Task I. One of these alloys was Ni-20Fe-20Cr-1Mn-0.15La (M1), which was selected to investigate reports that additions of manganese and lanthanum significantly improve the oxidation resistance of Hastelloy through the formation of a $MnCr_2O_4$ scale. The other two alloys were Ni-20Cr-5Ta-5Al (M2) and Fe-35Cr-7.5Al (M3) which were intended to approach the maximum of alloying addition for fabricable alloys in these systems.

The raw materials used for alloy fabrication were carefully selected since the alloys would be consolidated by arc melting. Thus, no major refinement of the raw material could be expected. Therefore, the melting stock of the major alloying elements was selected upon consideration of a large number of sources. It was considered appropriate to consider only commercial metals, rather than high cost, high purity melting stock. Iron, chromium, nickel, aluminum, and tantalum were selected with minimal interstitial and tramp element content.

The typical compositions of the Fe, Ni, Cr, Al, and Ta melting stock are summarized in Table 2. Oxygen is the major detrimental impurity, being about 130 ppm in iron, 400 ppm in chromium, and 150 ppm in tantalum. It was considered likely that most of the oxygen would be scavenged during arc melting since all of the alloys contained at least one strong metallic deoxidizer. In arc melting, the slag which floats to the surface of the ingot during repeated melting can result in reduced concentration of oxide formers such as Y, Th, and Hf. It is quite likely that fractions of some alloying additions were lost by this means. The importance of sulfur and tramp element levels is noted because of their possible detrimental effect on hot workability.

The source and purity levels of the minor alloying elements are shown in Table 3. No attempt was made to determine the types and concentrations of impurities for these materials. Addition of these elements to the various alloys was generally less than 1.0 w/o so that impurities introduced should be insignificant if reasonable purity is assumed.

Fifty-gram heats of the 56 Task I alloys were prepared by nonconsumable electrode melting in a water-cooled copper crucible under a protective atmosphere of argon. All melts were originally made by the Oregon Metallurgical Company, except the two Be-containing alloys which were melted at IITRI. During arc-melting, a minimum of eight remelts were made on each ingot in order to obtain a homogenized structure.

The ingots were weighed after arc melting to determine the melt losses. Weight losses during arc-melting are summarized in Table 4. Only one alloy (NT24) showed a weight loss greater than 1%, and a new heat of this alloy was melted at IITRI. The weight loss of the second heat was 0.14%. Melt loss data did not illustrate any definable trend relating either to the base composition or to the specific alloying elements in the nickel-base systems. Iron-base alloys, however, tended to have higher weight losses than the nickel-base alloys.

Prior to hot rolling, the ingots were conditioned using a small hand grinder in order to remove surface defects such as shrinkage, cold shuts, oxides, etc. Interestingly, the nickel-base alloys were much more prone to shrinkage and dirt than the iron-base materials. During the conditioning process, five alloys were found to contain small amounts of unalloyed or partially alloyed material on the surface. These included F7 (Th), F9 (Zr), F10 (Hf), NA9 (Hf), and NT27 (Hf). The small degree of segregation observed was mainly associated with the hafnium-containing alloys. These alloys were remelted several times at IITRI, and with the exception of F9, homogeneous ingots were obtained. However, chemical analysis of this alloy showed that the actual composition was very near the nominal composition.

After surface conditioning, the ingots were given a homogenization treatment of 2100°F for 24 hr in air followed by air cooling. The alloys were then hot rolled using a preheat temperature of 2150°F with reheating between each pass. In general, the ingots were given about 5 to 10 passes at 5% reduction per pass for initial breakdown, followed by 5 to 10 passes of 7.5% and finally passes of 10% until the sheet was approximately 0.080 to 0.090 in. thick. The number of reductions varied depending on the initial thickness and workability of the material, since the reductions cited are nominal rather than actual. The rolling process was interrupted after reduction of about 30% and again at 50 to 60% for inspection and further surface conditioning. At these points, any surface defects not evident in the as-cast ingot were carefully removed by grinding.

Examples of the various types of sheet material produced are shown in Figure 2. F5 is representative of total failure of the ingot during hot rolling. M1 exhibited large edge cracks, but some usable material was available. The conditions of moderate, light, and no edge cracking are represented by NT10, NT2, and F1, respectively. Another rather common occurrence with the Ni-Cr-Al alloys was one or two large tears resulting from ingot defects, and NA2 is representative of this condition. The workability of the Fe-Cr-Al alloys studied was generally very good. These materials appeared to have low hot strength, a wide working range, and apparently a relative insensitivity to ingot defects. As will be noted, however, alloys with rare earth additions were more prone to fabrication difficulties than those without these additions.

All of the Fe-Cr-Al alloys produced sheet free of edge cracks with the exception of F5 (Ce) and F6 (La) although occasional minor surface imprefections resulting from ingot defects were noted. The rare earth containing alloys were completely unworkable by the techniques employed. An intermetallic compound, located primarily at the grain boundaries was visible metallographically and is believed to have caused the failure. The exact failure mechanism (i. e., liquation, intergranular attack, or grain boundary weakness), however, was not determined. Specimens of F5 and F6 were prepared by grinding buttons which were arc-melted at IITRI.

Most of the Ni-Cr-Al alloys produced good quality sheet material with only light edge cracking. Exceptions were again those alloys containing the rare earths Ce and La (NA5 and NA6); the situation appears to be analogous to that in the Fe-Cr-Al system. Although considerable cracking occurred, however, it was possible to roll NA6 and obtain specimens from the wrought material. An attempt was made to grind oxidation samples from an arc-melted button of NA5, but the material crumbled before reaching finished dimensions. In general, the workability of the Ni-Cr-Al alloys was not as good as their Fe-Cr-Al counterparts. The reasons for this appear to be higher hot strength, a narrower working range, and a greater sensitivity to ingot defects. Nickel-base alloys appeared to be prone to cracking when the temperature loss during transfer from the preheat furnace was excessive. During the initial breakdown portion of the hot working process, small, undetected shrinkage cavities probably resulted in some of the large cracks which developed. Thus, with sound, properly conditioned ingots, light initial reductions and good temperature control, good quality sheet material of Ni-Cr-Al alloys can be produced.

The fabricability of the Ni-Cr-Ta alloys was in general better than the Ni-Cr-Al types, but not as good as the Fe-Cr-Al materials. The Ni-Cr-Ta alloys, like Ni-Cr-Al alloys, had high hot strength, but did not appear to be as prone to cracking due to temperature loss during transfer from the preheat furnace. A reason for this behavior may be that the precipitation of Ni_3Ta is sluggish, whereas the precipitation of Ni_3Al is rapid. Gamma prime is also a more potent hardener than Ni_3Ta. Satisfactory sheet was produced from all the ternary Ni-Cr-Ta alloys although at the higher Cr and Ta levels, the alloys were very stiff. Compositions containing up to about 30% Cr resulted in sheet with light edge cracking, whereas higher Cr materials produced sheet with moderate edge cracking.

The 0.25 a/o additions of Y, Mg, Th, Ti, Hf, Si, and Ge had no apparent effect on the workability of the basic Ni-25Cr-10Ta alloys. As with the Fe-Cr-Al and Ni-Cr-Al alloys, heavy edge cracking occurred in the alloys containing Ce and La, although the yield was sufficient to obtain oxidation test specimens. The poor performance of the zirconium-bearing materials is more likely due to ingot quality rather than alloy composition.

10

The only remaining alloy which could not be worked was M2 (Ni-20Cr-5Al-5Ta). It is believed that this material is simply too saturated with hardeners (Al, Ta) to be worked by the methods employed in this investigation. Since this alloy was not included in the initial program, samples of the M2 alloy were not prepared for oxidation testing.

Following hot rolling of each alloy, samples approximately 1.0 x 1.0 in. were cut from the 0.080 to 0.090 in. thick hot rolled sheet. After straightening, the specimens were surface ground to 0.060 ± 0.0005 in. and polished through 600 grit paper to ensure constant surface conditions. The close thickness tolerance was intended to permit accurate metallographic thickness measurements on oxidized samples. Finally, the edges and corners were rounded, and the samples were washed in acetone prior to testing.

2. Oxidation Screening Tests

Cyclic oxidation tests were accomplished in static airs in a Globar heated furnace at 2300° ± 10°F. Duplicate specimens of each alloy were placed in Norton Alundum crucibles, which were baked in air at 2300°F for 24 hr prior to use. The crucibles containing the samples were then mounted in alumina refractory bricks, and Alundum covers were suspended above the crucibles. This was intended to prohibit debris from falling into the crucibles. Cyclic furnace oxidation testing consisted of 2 hr cycles for the first 20 hr followed by 20 hr cycles to 100 hr. After removal from the furnace, the crucibles were quickly capped to prevent any losses due to spalling. The weights of the crucibles containing the samples plus spalled scale (if any) and the weights of the samples after light brushing were then determined. From these weights, both total specific weight gain including spalled scale and specific sample weight change were calculated. When a 20 hr exposure was completed, one-third of one sample of each alloy was removed for metallographic examination. Similarly, a metallographic sample was removed from the sectioned sample after 60 hr, and the remaining part used for metallography after 100 hr of testing. An attempt was made to obtain reduced weight and dimensions after each sectioning operation for weight change calculations. However, the specific weight gains that were calculated did not show good agreement with the results of the duplicate samples that were not sectioned. This appeared to be mainly the result of additional spalling induced by the clamping and cutting operation.

Oxidation screening tests in Task I were conducted in six groups, with 18 specimens in each group. Finally, the two remaining alloys were evaluated in a seventh run. This was intended to avoid mixing of test samples, as well as to permit initiation of oxidation testing prior to fabricating all of the 110 test samples. In general, the six groups of test samples consisted of a variety of test samples of the three alloy systems. Duplicate samples of TD NiCr were exposed in the second run as control specimens for the oxidation test.

a. **Fe-Cr-Al Alloys**

The oxidation data for Task I Fe-Cr-Al alloys are sum-
marized in Table 5. The total specific weight change (including
spalled scale) and the specimen specific weight changes for
selected alloys are plotted in Figures 3 and 4, respectively.
Although weight changes were measured and calculated at each
2 hr interval during the initial 20 hr, data in Table 5 are given
only at 20 hr intervals. Furthermore, data at 20 hr represents
the average of two samples, whereas the remaining weight changes
were calculated from a single sample. This is because one of the
samples of each alloy was sectioned periodically for metallographic
examination, as previously discussed.

The oxidation resistance of the basic Fe-25Cr-4Al (F1)
is not adequate for 2300°F service. During the first few cycles,
a very thin, white oxide, resembling onion skin, formed which com-
pletely peeled from the surface and left the base metal exposed.
After about 4 cycles, a thin dark gray oxide formed which partially
spalled on cooling. The spalling process was characterized by
ejection of small areas of oxide, as opposed to the gentle flaking
noted earlier, resulting in a spotted appearance. During this
portion of oxidation, the increments of weight gain between the
2-hr cycles increased as the number of cycles increased. After
about 60 hr of oxidation, a thick black oxide which did not spall
as readily as its predecessor began to form. The effect of the
third oxide layer is reflected in the specimen weight change curve
(Figure 3) as a change in slope after about 60 hr.

The addition of 0.25 a/o Mg (F4) or Ge (F13) had no
significant effect on the oxidation resistance of Fe-25Cr-4Al.
These alloys appeared identical on the basis of macroscopic appear-
ance, total weight gain, and sample weight change. Similarly, no
real improvement was achieved by the addition of Si (F12) although
the weight loss was somewhat less due to less spalling. This
apparently resulted from the formation of the thick black oxide
observed on the base alloy after about an equal exposure time.

The rare earth additions of Ce (F5) and La (F6) provided
improved scale adherence, but the overall level of oxidation resis-
tance remained poor. The 100 hr total specific weight gains of
these alloys were very close to the value of 24 mg/cm^2 exhibited
by the base composition; however, the sample weight change was
positive, indicating improved adherence of the oxide scale.

The addition of 0.25 a/o Y resulted in a marked improve-
ment in oxidation resistance as evidenced by a total weight gain
of 3.50 mg/cm^2 and a specimen weight change of +2.35 mg/cm^2 after
100 hr. During the first few cycles of oxidation, this alloy
formed a very thin, adherent, light-gray oxide, rather than the
flaky, white oxide observed on the basic Fe-25Cr-4Al alloy. The
protective oxide appeared to remain essentially unchanged for the
duration of the test although there were a few tiny, bright specks

on the sample after 100 hr. The bright areas were presumably the metal substrate revealed in some areas as a result of localized spalling. Since this occurred only over a small portion of the surface and the protective oxide was very thin, the weight changes were quite small.

The addition of 0.25 a/o Th (F7) produced an effect quite similar to that of the Y addition. A total weight gain of 4.67 mg/cm^2 and a positive sample weight change of 2.26 mg/cm^2 were recorded. The oxide was thin, gray, and adherent, and only a few small bright spots (presumably spalling) were noted after the 100 hr test.

The Group IV-A metals (Ti, Zr, and Hf) all had a marked effect on the oxidation resistance of the basic Fe-25Cr-4Al alloy. The titanium-containing alloy (F8) formed a thin adherent gray oxide and had a total weight gain of 2.82 mg/cm^2 with a sample weight change of +0.52 mg/cm^2. A few small bright spots indicative of spalling were noted on the sample during the later stages of the test.

Zirconium, at the level investigated, did not result in an alloy with desired degree of improved oxidation resistance. The alloy formed a thick, adherent, black oxide with a rough surface. A positive sample weight gain of 15.5 mg/cm^2 as compared to a total weight gain of 18.6 mg/cm^2 is indicative of good scale adherence.

The 0.25 a/o Hf addition to Fe-25Cr-4Al produced a most interesting appearance. This alloy developed a very adherent oxide as evidenced by a sample weight change of +6.18 as compared to a total weight gain of +7.56 mg/cm^2 after 100 hr of oxidation testing. While the previous additions which improved the oxidation resistance of the base alloy resulted in the formation of a gray oxide, the hafnium addition resulted in a dark gold oxide.

The last 0.25 a/o addition which produced improvement in the oxidation resistance of Fe-25Cr-4Al was tantalum (F11). The total weight gain of this alloy was 7.52 mg/cm^2 after 100 hr of oxidation testing, but the sample weight change was -4.32 mg/cm^2 indicating a lack of oxide adherence. The alloy formed a thin protective gray oxide, but a good portion of the oxide spalled during cooling giving the sample a speckled appearance.

The Be-containing alloy and the high-chromium (35%), high-Al (7.5%) version (M3) of the base alloy were quite similar. F3 had a total weight gain of 12.1 and M3, 15.4 mg/cm^2--as compared to 24.0 mg/cm^2 for the base composition. However, the protective oxide was not very adherent and appreciable spalling occurred, resulting in sample weight losses of 6.9 and 10.7 mg/cm^2.

Comparison of both the total and sample weight changes in Figures 3 and 4 provides some insight into the oxidation behavior of the various alloys. It is difficult, perhaps dangerous, to generalize for all of the alloys studied since the data can be influenced by several competing factors (spalling, vaporization, internal oxidation, etc.). Obviously, the total weight gain must be always positive and equal to or greater than the sample weight change. The sample weight change can be positive or negative and is generally a measure of the spalling tendency of the alloy. A positive sample weight change is indicative of an adherent oxide layer. On the other hand, a large negative weight gain indicates little or no scale adherence and, normally, high total weight gain because metallic surface is continually presented to the environment. Alloys which exhibit high positive total and sample weight gains can be suspected to undergo internal oxidation.

Weight change data are plotted only for selected alloys in Figures 3 and 4 because of a similarity of the data for many of the alloys. Thus, the curves for the base alloy (F1) are also representative of alloys F4 (Mg), F13 (Ge), and, with minor differences, M3 (Fe-35Cr-7.5Al). Similarly, F3 (Be) also represents F11 (Ta), the F2 (Y) curves are very similar to F7 (Th), and F10 (Hf) is also generally representative of F9 (Zr).

Alloys F2, F3, F8, F9, and F10 all indicate approximately parabolic oxidation rates and adherent oxide layers, although F8 does show minor spalling after about 60 hr. The higher weight gains for F9 and F10 indicate either more rapid growth of the oxide layer or internal oxidation, or both. Thus, the oxides developed on alloys containing Hf and Zr may have a higher oxygen mobility than alloys containing Y, Ti, and Th, or more cracks in the scale.

The sample weight change for F5 (Ce) is a classic example of oxidation behavior for many materials which form solid oxides. Initially, a protective oxide is formed which increases in thickness until the oxide can no longer accommodate the stress developed by oxide growth. At this point, spalling begins and the sample weight change becomes negative with further exposure. This curve generally applies to most of the alloys tested, but the time scale varies widely for the various compositions because the rate of oxide growth is significantly different.

Alloy F6 (La) is the only composition which exhibits a linear oxidation rate over the 100 hr exposure period. The oxide was adherent, as evidenced by a positive sample weight change. Thus, it appears that F6 may have been subject to rapid internal oxidation, possibly by a short circuit diffusion process. The grain boundary precipitate found in this material may have provided a means for rapid, internal diffusion of oxygen. If this was the case, a similar situation may have also been operative in alloy F5 (Ce).

One other factor is evident in Figure 3. The sharp break in the total weight gain curve at 20 hr for alloys F1 and F5 indicates a sensitivity of these and similar alloys to the rate of cycling. These alloys show a more rapid oxidation during the first 20 hr, which consisted of 2 hr cycles, than during the 20 hr cycles subsequently employed. Alloys which had the best oxidation resistance do not show a similar effect.

b. Ni-Cr-Al Alloys

The oxidation data for the Task I Ni-Cr-Al alloys and the TD NiCr control sample are summarized in Table 6. The total weight and sample weight changes for selected alloys are plotted in Figures 5 and 6. In general, these alloys were not as oxidation resistant as the Fe-Cr-Al compositions.

Two ternary Ni-Cr-Al alloys were investigated: Ni-16Cr-5Al and, the base composition for alloying additions, Ni-20Cr-5Al. During the initial 2 hr of oxidation, both alloys formed a very thin white oxide which gently flaked off the specimens leaving the bare metal exposed. This oxide presumably was alumina-rich. Additional oxidation layers were also present which partially spalled during the cooling cycle resulting in a spotty appearance. The secondary oxide spalled as small pieces, rather than large flakes. The lack of oxide adherence is reflected in the weight change data which show a sample weight loss after 100 hr of -24.5 and -21.1 mg/cm^2 for NA1 and NA2, respectively. The total weight gains after 100 hr were 17.0 and 14.8 mg/cm^2 for NA1 and NA2, respectively, indicating that the higher Cr alloy had slightly better oxidation resistance.

The additions of Mg (NA4) and Si (NA10) had no apparent effect on the oxidation behavior of the Ni-20Cr-5Al base alloy. After 100 hr, NA4 showed a total weight gain of 15.0 mg/cm^2 and a sample weight change of -21.0 mg/cm^2 as compared to values of 14.8 and -21.1 mg/cm^2 for the base alloy. The corresponding values for NA10 were 15.8 and -24.3 mg/cm^2.

Addition of Ti (NA8), Ge (NA11), and Be (NA12) appeared to have a slightly detrimental effect on 2300°F cyclic oxidation resistance. The macroscopic behavior of these alloys was identical to the base; after the first few cycles a greenish-black oxide formed which spalled on cooling. On the basis of total weight gain, the oxidation resistance of these compositions was slightly less than that of NA2.

Additions of 0.25 a/o Y (NA3) and La (NA6) produced significant changes in the oxidation behavior of Ni-20Cr-5Al. During the first oxidation cycle, these alloys formed adherent greenish-gray oxides. As the exposure time increased, the specimens remained green, but fine bright spots developed. The oxides were reasonably adherent as shown by sample weight change values of +7.40 mg/cm^2

for the Y-containing alloy and -0.36 mg/cm^2 for the La modification. However, the total weight gain of 19.1 and 23.3 mg/cm^2 was greater than that of the base alloy after 100 hr. It is quite possible, however, that Y and/or La might be more effective at levels other than 0.25 a/o.

The most effective addition (at the 0.25 a/o level) for improving the oxidation resistance of Ni-20Cr-5Al was thorium. This alloy (NA7) had a total weight gain of 6.08 mg/cm^2 and a sample weight change of -4.69 mg/cm^2 after 100 hr, as compared to corresponding values of 14.8 and -21.1 mg/cm^2 for the base composition. An adherent, light gray-green oxide was formed in the initial stages of the oxidation test. As the exposure time increased, bright spots were developed on the green oxide, although it was not clear if this represented exposed base metal or another oxide.

Hafnium was also effective in increasing the oxidation resistance of Ni-20Cr-5Al, although not to the same extent as thorium. The weight change value was about half that of the Ni-20Cr-5Al base composition. However, this alloy also exhibited spalling, as indicated by a sample weight loss of 15.5 mg/cm^2.

The oxidation data obtained for the TD NiCr samples are also included in Table 6. This material formed a thin, adherent, greenish-black oxide which showed only a minor amount of spalling especially in the later stages of exposure. The total weight gain of 2.90 mg/cm^2 after 100 hr was the lowest of any nickel-base material tested.

Weight change data in Figures 5 and 6 are plotted only for selected alloys because of a similarity in the curves for many of the alloys. Thus, the plots of NA1, NA2, and NA12 (Be), generally represent a group also consisting of NA4 (Mg), NA8 (Ti), NA10 (Si), and NA11 (Ge). In contrast to Fe-Cr-Al alloys, only NA3 (Y) and NA6 (La) had positive sample weight changes during any portion of the 100 hr exposure. However, these alloys also exhibited the highest total weight gains, and NA6 illustrates increasing spalling after about 60 hr. Thus, the results show that in no case was a stable, adherent oxide layer formed on any of the Ni-Cr-Al alloys.

The sample weight change curves in Figure 6 also indicate some sensitivity on the part of some alloys to cycling rate, as shown by the change in slope after 20 hr. Furthermore, with the exception of NA3 and NA6, the surface weight loss for all alloys is approximately twice the total weight gain.

TD NiCr exhibited the lowest total weight gain of any of the Ni-Cr alloys. Thus, aluminum had no apparent influence on the Ni-Cr alloys in the 2300°F furnace test. It is interesting that the two most oxidation-resistant Ni-Cr alloys contained thorium

16

as either the metal (NA7) or as the oxide (TD NiCr). The oxidation performance of the TD NiCr alloy was very good in the static test. However, this material had much poorer oxidation resistance in the dynamic environment of the torch test, as will be shown in Section III-A-4.

c. **Ni-Cr-Ta Alloys**

A summary of the weight change data at 20 hr intervals for the 28 Ni-Cr-Ta alloys during cyclic furnace oxidation at 2300°F is given in Table 7. The total and sample weight changes are plotted for selected alloys in Figures 7 through 9.

None of the Ni-Cr-Ta alloys approached the preselected criterion of 11 mg/cm^2 total weight gain in 100 hr. Visually, all of the alloys developed a fairly thick, brownish green oxide which spalled extensively compared to Ni-Cr-Al alloys. The increments of weight gain and change increased with increasing exposure time in the initial 20 hr period. This probably was the result of a combination of spalling of the oxide and depletion of chromium from the underlying metallic layer. The overall result was that this group of alloys showed high total weight gains, large negative sample weight loss, and (as will be shown in Section III-6-b) extensive metal loss and internal attack. All Al_2O_3 crucibles used for Ni-Cr-Ta alloys showed a greenish-brown deposit on the interior walls indicating the formation of volatile oxidation products.

The oxidation data in Table 7 also showed that alloys NT14 (Ni-35Cr-15Ta) and NT18 (Ni-40Cr-15Ta) melted during exposure at 2300°F. The minimum melting points in the Ni-Ta and Cr-Ta binary systems have been reported to be about 2460°[4] and 3060°F[5] respectively. Thus, the results indicate that a ternary eutectic exists in the Ni-Cr-Ta system with the approximate composition Ni-40Cr-20Ta.

In the Ni-Cr-Ta ternary alloys, increasing tantalum concentration in the range of 5-15 w/o decreased the oxidation resistance in alloys containing 20 to 40 w/o Cr. This is shown in Figure 7 in terms of the total weight gain. Table 7 also indicates a similar effect on the sample weight change. It is possible that Ta is only beneficial at lower temperature, or is not effective in a simple Ni-Cr matrix. However, it has been shown that Ta is beneficial in reducing oxidation of Fe-25Cr-4Al alloys at 2300°F.

Chromium, as expected, had a significant effect on the oxidation resistance. Figure 7 shows that increasing the chromium from 20 to 25 w/o significantly reduces the total weight gain, especially in alloys containing 5 and 10 w/o Ta. The weight gain curves also indicate that a situation exists at 5 and 10 w/o tantalum similar to that observed in the Ni-Cr binary system. Weight gain decreases with chromium concentration to 25 w/o followed by

little change in oxidation in behavior at 25 to 35 w/o Cr. Finally, an increase in weight gain occurs at 40 w/o Ta. In the Ni-Cr binary, the third phase is related to the formation of a Cr-rich phase when the solubility limit is exceeded. It is possible that a similar situation is operative in the Ni-Cr-Ta system.

The effects of 0.25 a/o additions on the total weight gain and sample weight change of selected Ni-25Cr-10Ta base alloys are shown in Figures 8 and 9. Data for Ni-25Cr-5Ta and Ni-25Cr-10Ta are included for comparison. Although none of the additions produced alloys with less than 11 mg/cm^2 total weight gain in 100 hr, significance differences were measured for some of the additions. Addition of 0.25 a/o Y (NT14), La (NT23), and Th (NT24) reduced both the total weight gain and the sample weight change of Ni-25Cr-10Ta to about the values measured for Ni-25Cr-5Ta. Additions of Si and Ge reduced the oxidation rate marginally and are represented by the weight change curve for the germanium addition (NT29). Alloy additions which had no significant effect included Mg, Zr, and Hf. These alloys are represented by the weight change curves of NT29 (Mg). The only addition which caused increased oxidation rate was cerium; the alloy (NT22) was completely converted to oxide in 60 hr.

It is interesting that the additions Y, Th, and La which have the most pronounced effect on Ni-20Cr-10Ta also exhibited similar effects in Ni-Cr-Al alloys. However, in the Ni-Cr-Al alloys only Th was beneficial, since Y and La caused higher total weight gains than the base alloy. The oxidation results obtained on Ni-Cr-Ta alloys demonstrated that these alloys were not promising for 2300°F service in comparison to modified Fe-Cr-Al and Ni-Cr-Al systems. Further effort on this system was therefore discontinued.

3. Oxidation Evaluation of Modified Alloys

Oxidation screening tests at 2300°F indicated that the most promising alloys for further evaluation consisted of (1) Y, Th, Ti, Hf, and Ta additions to the Fe-Cr-Al system, and (2) Th and Hf additions to the Ni-Cr-Al system. All of these alloys met the initial criterion of less than 11 mg/cm^2 total weight gain in 100 hr at 2300°F. Consequently, selection of the 11 planned modifications of Task I alloys, with one exception, were based on these alloy systems (see Table 8). Since no tantalum addition was made to the Ni-Cr-Al system in Task I, one Ta-modified alloy in this system was also selected for evaluation.

The selection of the level of addition for Task I modified alloys was also based on metallography and bend tests and of Task I alloys (as described in Section III-A-6). Bend test results revealed that the only Fe-Cr-Al alloys which were ductile after exposure were those containing Ta and Hf. Both of the best Ni-base alloys were ductile after exposure. Metallography indicated that

18

the rate of scale formation and internal oxidation was excessive in the Hf and Th modifications of both Fe-Cr-Al and Ni-Cr-Al alloys. Consequently, it was apparent that lower concentration of these elements would be beneficial.

The nominal compositions of modified Task I alloys are listed in Table 8. Alloy compositions were selected based on the above criteria and with the objective of defining the influence of varying the level of addition for the most oxidation-resistant systems. As a result, two modifications each of the best Fe-Cr-Al compositions were made with Y, Ta, and Ti. One alloy, containing less than 0.25 a/o addition of Hf and Ta, was selected in both the Fe-Cr-Al and Ni-Cr-Ta system. The remaining alloy was Ni-Cr-Al modified with 1.0 a/o Ta.

Modified Task I alloys were arc-melted and fabricated as described previously (Section III-A-1). All of the alloys were arc-melted at IITRI; the weight losses of the 100 g ingots during melting are summarized in Table 9. None of the alloys exhibited weight losses greater than 1%. No difficulties were encountered during hot rolling, and good quality sheet material was obtained for all of the alloys. Following hot rolling, the alloys were annealed, surface ground, and polished through 600 grit paper as previously described.

Weight change data for modified Task I alloys during cyclic furnace oxidation testing at 2300°F are summarized in Table 10. Weight change data for modified Task I alloys are plotted in Figures 10 through 14. Samples of TD Ni and TD NiCr were also exposed for comparison with in the cladding alloys. The specimen geometry, testing technique, and evaluation methods were identical to those described in Section II-A-2.

All of the alloys, with the exception of NA15 (1.0Ta), exhibited total weight gains less than 11 mg/cm^2. The total weight gain and sample weight change for NA15 were quite similar to the results obtained for Ni-20Cr-5Al in Task I. Thus, Ta additions are apparently innocuous in Ni-Cr-Al alloys, at least at low concentrations.

Total weight gain and sample weight change for Fe-Cr-Al alloys are plotted in Figures 10 and 11, respectively. In the Fe-base system, the highest oxidation rates occurred for additions of 0.5Ta (F19 and 1.25Ta (F18) w/o. These alloys were also the only Fe-Cr-Al systems which exhibited significant spalling as indicated by a sample weight loss. Alloys F14 (0.25Y), F15 (0.15Ti), F16 (0.5Ti), F20 (0.5Th) and F21 (0.65Y) all exhibited thin, adherent oxides. Total and sample weight gains for these alloys were between 2.5 and 3.5 mg/cm^2 and 1.3 and 2.5 mg/cm^2, respectively. The weight gains of the alloy modified with 0.5 w/o Hf (F17) were about 4.5 mg/cm^2. Thus, reduction of the Th and Hf concentration

was effective in significantly reducing the weight gain, whereas variation of Y and Ti resulted in very little change from the 0.25 a/o addition.

Total and sample weight changes for the three Ni-base alloys during cyclic furnace oxidation at 2300°F are plotted in Figures 12 and 13, respectively. Data for TD Ni and TD NiCr are included for comparison. All of these alloys, except TD Ni, had a tendency to spall, resulting in sample weight losses. However, the total weight gain of 3.46 and 2.31 mg/cm^2 for NA13 (0.5Th) and TD NiCr was comparable to the best Fe-Cr-Al alloys. The alloy with 0.6 w/o Hf (NA14) was slightly less oxidation-resistant than NA13. Addition of 1.0Ta (NA15) resulted in an oxidation rate similar to the Ni-20Cr-5Al alloy. TD Ni had a total and sample weight gain of about 31 mg/cm^2, indicating that the oxide was adherent although limited in protective capability.

4.   Torch Oxidation Test

The cyclic furnace oxidation test indicated that some of the Task I alloys were sensitive to the cycling rate. In order to evaluate the influence of cyclic conditions and higher gas flow rates, six of the Task I modified alloys were exposed for 20 cycles in an air-natural gas torch flame at 2300°F for a total exposure of 100 hr.

The alloys selected for torch oxidation included one alloy of each of the modified systems. Thus, the Fe-Cr-Al alloys evaluated included F14 (0.25Y), F15 (0.23Th), F17 (0.5Hf), F18 (1.25Ta), and F20 (0.5Th). In addition, the most oxidation-resistant nickel-base alloy, NA13 (0.5Th), was also evaluated. TD Ni and TD NiCr samples were also exposed to compare their oxidation behavior with that of the cladding alloys.

Test samples for the torch test were 1.0 x 0.5 x 0.060 in. thick and were exposed as shown in Figure 14. Two oxidation specimens were mounted in a cavity cut in an Al$_2$O$_3$ insulating refractory brick such that the flame of two air-natural gas torches impinged on one of the 1.0 x 0.5 in. surfaces of each sample. The gas flow rates provided about 20% excess air, although additional air was ingested into the cavity. Passages were cut at the rear of the sample mounting to provide an exit for the combustion gases. This was intended to minimize stagnation at the sample surface. The exposure temperature was manually controlled at 2250°F with an optical pyrometer. A 2250°F optical temperature compares to a true temperature of 2300°F assuming an emittance of 0.7, which is typical for many oxides. During the torch test, the exposure temperature was normally maintained at about ±25°F over the flame impingement surface.

The approximate heating and cooling rates during thermal cycling are shown in Figure 15. These data were obtained by mounting Pt/Pt-13% Rh thermocouples on the front and back surface of TD Ni

and monitoring the surface temperature during heating and cooling. The cooling rate shown in Figure 15 is slightly faster than that obtained during the cyclic torch test since it represents cooling augmented by the air blast after stopping the flow of natural gas. Thus, the cooling during torch testing was approximately 2 min longer than that shown in Figure 15. However, this was still much faster than the cooling rate during cyclic furnace testing.

The cycling conditions for torch tests were similar to those used for furnace tests. Samples were cycled every 2 hr for the first 20 hr, followed by 8-hr cycles to 100 hr with the sample weights measured after each cycle. Thus, the only difference from furnace tests was the substitution of 8 hr cycles for the 20 hr cycles used in furnace tests. Only sample weight change data were obtained in the torch test since the spalled oxide could not be retained for total weight gain measurements.

The weight changes of the various alloys at selected intervals during torch testing are summarized in Table 11 and plotted in Figure 16. Sample weight changes in Table 11 are calculated using both the total and the flame impingement area as the effective surface area. Although the exposure temperature of the flame impingement and back of the sample was reasonably close, as shown by Figure 15, the oxidation environment was obviously different. However, metallography did show oxidation at both surfaces for all of the alloys so that the effective exposure area was probably reasonably represented by the total sample surface.

Weight change during cyclic torch testing is plotted in Figure 16, using the data for total surface area. Major deviation from cyclic furnace oxidation exists only for TD Ni and TD NiCr. In contrast to furnace tests in which TD NiCr had one of the lowest oxidation rates, this material had the poorest oxidation resistance in cyclic torch tests. TD Ni also had a greater tendency for spalling of the oxide in comparison to furnace tests resulting in the discontinuous curve shown in Figure 16. The major difference in the data for TD and TD NiCr may have been due to greater oxide adherence on TD Ni, although the rate of metal recession may have been similar.

Weight change data for the Fe-Cr-Al alloys and NA13 were consistent with the sample weight change during furnace oxidation exposure. As in furnace tests, F14, F15, F17 and F20 had small weight gains, whereas F18 and NA13 exhibited small weight losses. Thus, the cladding alloys were not susceptible to accelerated attack in the torch test.

5. Sulfidation Test

Nickel-base superalloys with chromium concentrations below about 12 w/o are subject to sulfidation corrosion in environments containing sodium sulfate. A limited investigation was conducted to indicate the resistance of modified Task I alloys to such attack. Current data in the literature on this phenomenon generally indicate that high-chromium nickel-base alloys and iron-base alloys are not susceptible to attack by sodium sulfate environment. However, an effort was made in this program to verify these conclusions.

Effort to determine the sulfidation resistance of alloys in this program was intended only to obtain preliminary corrosion data. Accordingly, alloys were exposed in a laboratory test at 1650°F for 20 hr. The test consisted of suspending preoxidized test samples held over a bath of molten sodium sulfate. It was hoped that this would result in a refluxing action and a continued supply of condensed sodium sulfate. It was found, however, that nucleation of liquid sodium sulfate on the sample surface was difficult to control. Consequently, a modified technique consisting of pre-immersion of the samples in liquid sodium sulfate was also attempted.

Samples for sulfidation evaluation were prepared in the same manner as the oxidation samples (described in the preceding section). The compositions selected for evaluation included four iron-base alloys, F14, F15, F17, and F20 and the nickel-base alloy NA13. Samples of TD Ni and TD NiCr were also evaluated. Prior to sulfidation exposure, the samples were oxidized at 1800°F in air for 2 hr. This treatment resulted only in slight discoloration and weight gains of less than 0.06 mg/cm^2 for the iron-base alloys, NA13, and TD NiCr. TD Ni had a weight gain of about 0.5 mg/cm^2.

In the first sulfidation test, the test samples were suspended in a vertical tube furnace at 1650°F $\pm$ 10°F above a molten sodium sulfate bath held at 1700°F $\pm$ 10°F. TD Ni and TD NiCr were not exposed in the initial test. The samples were removed after 20 hr of exposure for visual examination on weighing. All of the cladding alloys exhibited only slight discoloration, and no evidence of condensed salt was visible. The weight changes for all five of the cladding alloys were less than 0.5 mg (0.06 mg/cm^2) which was within the accuracy of the balance. Thus, the fact that no apparent attack was evident on any of the alloys may have been attributable to the absence of condensed salt.

Accordingly, a second test was conducted in which the samples were immersed in the salt before suspension over the molten bath as previously. Test samples of TD Ni and TD NiCr were included in this test. Again, test samples were removed after 20 hr at 1650°F for visual examination and weight change

measurements. The salt deposit observed on the specimens after exposure was nonuniform in terms of coverage and had a yellow discoloration. The salt tended to flow down the samples and was concentrated at the bottom of the samples. None of the alloys tested showed macroscopic sulfidation attack--i.e., blisters of oxide which could readily be detached from the base. Only the nickel-base alloys looked slightly oxidized by the sulfidation environment; the iron-base alloys had only a heat tint on the surface. Since the oxides were adherent, the bulk of the salt deposit could be readily dissolved by water without influencing the weight change results. After washing in water, specimens were then given an additional desalting treatment of 1800°F for 4 hr in argon prior to weighing.

The weight gains of the various alloys after the pre-immersion test were in the range of 0.1-0.2 mg/cm^2 for the Fe-base alloys and 1.4 for TD Ni. Conversely, NA13 and TD NiCr had weight losses of 0.31 and 0.58 mg/cm^2, respectively. Thus, no significant attack of any of the alloys occurred. This was verified by metallographic examination, as will be presented in the following section.

The results of sulfidation testing did not indicate any strong susceptibility of any of the selected cladding alloys or TD Ni materials to sulfidation attack. This was not surprising since iron-base alloys and high-chromium, nickel-base alloys are not normally susceptible to attack. Thus, only TD Ni could be suspected to be subject to significant corrosion. However, difficulties with the refluxing test does indicate that the sulfidation resistance obtained may be suspect. There is some question whether adequate condensation of vapor is readily obtained in this test. It may be necessary to modify the furnace design to insure nucleation of liquid sodium sulfate on the surface. This may not be adequately circumvented by pre-immersion, since in this case the film thickness may inhibit oxygen from reaching the surface. Care must be taken to insure a balanced supply of condensed vapor and oxygen at the sample surface in order to provide an acceptable laboratory screening test.

6. Supplemental Evaluation

a. Chemical Analysis

Chemical analysis of 23 Task I and modified Task I alloys was conducted to verify the nominal analysis of selected alloys. A program requirement was that alloys which exhibited greater than 1% weight loss during arc-melting required analysis. Since this did not occur in any case, the selection of Task I alloys was arbitrary and generally included the alloys with the best oxidation resistance. All of the 11 modified Task I alloys were analyzed.

Samples for chemical analysis were sectioned from the edges and ends of hot-rolled sheet material. Chemical analysis was conducted by two organizations, Charles C. Kawin Company and W. A. Fahlbush Associates. This was necessary because the Charles C. Kawin Company did not have standard analytical processes for hafnium and thorium. Consequently, alloys containing these elements were analyzed by W. A. Fahlbush Associates. The results of wet chemical analysis of the 23 Task I and modified Task I alloys are summarized in Table 12.

Data in Table 12 represent a reasonable correlation with the nominal analysis, although some deviations are notable. The Task I results from Kawin indicated considerable deviation in aluminum from the nominal analysis. The major deviations were high values for alloys F1 and NA2. A possible explanation for this is the tendency of aluminum to be concentrated at its surface during hot rolling at 2150°F. Subsequently, samples for chemical analysis were surface ground which resulted in improved correlation with the nominal composition. Thus, the deviation in aluminum appeared to be due to a combination of the sampling technique and standard error in the analytical technique.

The analyzed compositions of the additions do indicate a definable trend. Chemical analysis of minor additions generally showed that Hf, Zr, Th, and in some cases Ta were 0.05 to 0.15 w/o lower than the nominal composition. This is probably due to gettering of oxygen from the raw materials during the arc-melting process. In contrast, the analysis of Si and Ti additions indicated that they were generally near the nominal composition.

b. Metallography

Metallographic examination of cladding alloys was conducted in this program. All of the alloys were examined in the as-fabricated (hot-rolled) condition. During oxidation tests, metallographic samples were sectioned from the various alloys after selected exposure periods for determination of metal recession and oxide thickness. All of the metallographic data generated will be presented in tabular form. Obviously, presentation of the microstructures of the 78 different alloy compositions prepared in this program would be excessive. Consequently, photomicrographs and discussion of microstructures will be limited to representative alloys.

During the 100 hr cyclic furnace tests of Task I and modified Task I alloys, metallographic samples were removed from one of the oxidation samples at 20, 60, and 100 hr of exposure at 2300°F. After these exposures, metallographic measurements were made to determine the metal recession rates and the maximum depth of oxide penetration. Metal recession measurements were intended to determine the rate at which gross oxidation progressed. This parameter was obtained by measurement of the metal remaining after

24

each exposure and averaging the reduction in metal thickness over the sample. Since the oxidation samples were ground to 60 ± 0.5 mils prior to exposure, the accuracy of the metal recession measurements was considered to be about 1 mil (0.5 mil per side).

Depth of oxide penetration measurements were intended to define additional aspects of exposure, such as internal and/or intergranular oxidation. This parameter was also determined by measurement of the thickness of metal remaining without localized internal oxidation or intergranular attack. It will be seen that considerable difference can be obtained between metal recession and depth of penetration data in cases of gross internal oxidation. However, the influence of internal oxidation on the overall oxidation resistance of the various alloys cannot be well established. The presence of extensive internal oxidation does not necessarily result in disastrous failure, as will be seen for some of the Ni-Cr-Al alloys.

(1) Task I Alloys

Metal recession and oxide penetration depth for Task I Fe-Cr-Al alloys during cyclic furnace exposure at 2300°F is summarized in Table 13. Microstructures of selected Fe-Cr-Al alloys as-hot rolled and after 100 hr at 2300°F are shown in Figures 17 through Figure 22. Table 13 indicates that there is a general correlation of metal penetration with the weight change data in Table 5. Metal recession after 100 hr of less than 1 mil were obtained for F2 (0.43Y), F7 (1.06Ta), F8 (0.25Ti), F11 (0.85Ta), and F13 (0.35Ge). These alloys with the exception of F13, had the lowest total and sample weight changes. However, the oxide thickness on alloys F7 and F11 were 4.9 and 5.6 mils, respectively, and F13 had extensive internal oxidation to a depth of 30 mils after 20 hr. The remaining alloys had metal recessions ranging from 1.5 to 0.38 mils obtained for the Fe-25Cr-4Al base alloy (F1). These compositions also exhibited extensive internal oxidation and/or porosity in most cases to a depth of 30 mils after only 20 hr at 2300°F.

The microstructure of alloy F1 as hot rolled and after 100 hr at 2300°F is shown in Figure 17. In Figure 17 and in the subsequent photomicrographs, the hot-rolled structures are etched, while the oxidized structures are unetched. The hot-rolled structure consists simply of very large grains of the ferrite solid solution. Figure 17b illustrates extensive internal oxidation and/or void formation and typifies the structures of this alloy at 20 and 60 hr. This photomicrograph is also typical of the microstructures of most of the Fe-base alloys in Table 13 which had metal penetration of 30 mils. The surface of this sample reveals the absence of surface oxide and localized pitting associated with subsurface oxide formation. The microstructures of F2 (0.43Y) and F7 (1.06Th), shown in Figures 18 and 19, respectively, show general similarities. Both of the alloys had a finely dispersed precipitate in the ferrite matrix in the as-rolled

condition. These precipitates are apparently Fe-Y and Fe-Th intermetallic compounds. Samples exposed at 2300°F for 100 hr both indicate a thin, adherent oxide at the surface. However, there is also an apparent tendency toward intergranular oxidation at the surface resulting in relatively high oxide penetration depths of about 4-5 mils.

In contrast to these alloys, alloy F8 (0.43Y), shown in Figure 20, is again a ferrite solid solution in the hot-rolled condition. The oxidized sample has a thin, adherent oxide although the interface is irregular, indicating some tendency toward spalling. Furthermore, the oxidized sample in Figure 20b shows a complete absence of either intergranular oxidation or the extensive internal oxidation present in the Fe-25Cr-4Al base alloy.

Figure 21 illustrates the influence of 0.85Hf on the hot-rolled and oxidized structures of Fe-25Cr-4Al. The hot-rolled structure also contains a dispersed precipitate, presumably an Fe-Hf compound. After 100 hr of oxidation exposure, an adherent oxide is present, but the oxide thickness is considerably greater than that observed in alloys containing Th, Y, or Ti. Furthermore, there is apparently some tendency toward precipitation of oxide particles beneath the oxide layer, although they are limited in depth.

Addition of 0.85Ta provides a slightly different behavior from that of the other alloying elements, as shown in Figure 22. Again, the hot-rolled structure in Figure 22a is a ferrite solid solution. In the oxidized condition, no intergranular or internal oxidation is visible. The interface between the thin oxide and substrate is irregular, although more pronounced than that of the Ti addition. This is apparently due to continual spalling of the oxide which is reflected in a sample weight loss for alloy F11 in Table 5. Thus, the formation of cusps of oxide is not necessarily a condition for oxide adherence. Comparison of the interface in Figure 22b with that of alloys with Y and Ti additions indicates that a well-defined interface is a manifestation of the oxidation mechanism, i.e., the formation of an adherent oxide (smooth) or one which spalls continuously (rough). This result, however, does not preclude a beneficial effect of the irregular interface on the oxide adherence of alloy F11.

The results of metal recession and depth of oxide penetration measurements on Ni-Cr-Al alloys during oxidation screening tests at 2300°F are summarized in Table 14. All of the nickel-base alloys, with the exception of TD NiCr, exhibited extensive internal oxidation to a depth of 30 mils. The rate of internal oxidation, however, was slightly slower than that of Fe-Cr-Al alloys which are susceptible to internal oxidation. Most of the alloys were not fully penetrated until 60 hr in

comparison to 20 hr for Fe-Cr-Al alloys. Metal recession for nickel-base alloys was generally less than that of iron-base alloys, ranging from 0.5 to 1.4 mils. This is in apparent opposition to the high sample weight losses and may have been due to some dimensional changes in the samples because of internal oxidation. The loss of 1 mil of metal for a material with a density of 8.0 g/cm^3 corresponds to a weight loss of about 20 mg/cm^2. Thus, the metal recession data in Table 14 are in fair agreement with sample weight loss measurements. The nickel-base alloys also show lesser tendency toward surface intergranular attack, which is included in metal loss measurements for iron-base alloys.

Figure 23 shows the microstructure of the base alloy NA2 (Ni-20Cr-5Al) as hot rolled and after 100 hr at 2300°F. The microstructure in the as-rolled condition is a single-phase nickel solid solution Figure 23b illustrates the internal oxides and/or voids that were typical of all the Ni-Cr-Al alloys. Also evident is the tendency for a surface layer virtually without porosity. Careful examination of the internal structure indicated that some of the apparent voids were partially filled with oxide. The internal structure of the nickel-base alloys also indicates that the oxide particles were more spherical and smaller than the internal defects in iron-base alloys. Thus, it appears that the apparent voids in nickel-base alloys are probably a combination of internal voids and oxide particles which are pulled out during metallographic polishing.

The microstructure of alloy NA7 (1.06Th), shown in Figure 24a does exhibit a grain boundary precipitate, presumably a Ni-Th compound, in the hot-rolled structure. In the oxidized condition in Figure 24b, this alloy shows a general similarity to the base alloy. Both alloys indicate no appreciable adherent surface oxide and internal oxidation and/or void. There is a tendency toward better definition of internal oxide particles in the alloy containing thorium, presumably as a result of oxidation of the Ni-Th compound.

Addition of 0.81Hf to the Ni-25Cr-5Al alloy also does not prohibit internal oxidation, as shown in Figure 25. The hot-rolled structure is also a single-phase solid solution. There is a tendency toward a lesser amount of internal defects, in the oxidized condition. Figure 25b does, however, indicate a tendency toward some intergranular oxidation.

The major difference between additions which improve the oxidation resistance of Fe-Cr-Al alloys in comparison to Ni-Cr-Al alloys is related to internal oxidation. Additions which effectively reduce the oxidation rate of Fe-Cr-Al as measured by weight gain also eliminate internal oxidation. In contrast, Th and Hf, which were the most effective additions in terms of weight loss, did not prohibit internal oxidation in nickel-base alloys. Thus, it is apparent that the iron-base

alloys develop a stable surface oxide which inhibits both inward oxygen diffusion and outward cation diffusion. In contrast, the nickel-base alloys do not develop adherent surface oxides. Rather the oxidation rate is controlled by the mechanism of oxidation and involves diffusion-controlled concentration changes resulting from oxide spalling and/or evaporation of oxide or metallic species.

Metal loss and oxide penetration depths for Task I Ni-Cr-Ta alloys are summarized in Table 15. The results of these measurements generally correlate with weight change data in Table 7. All of these alloys tend toward internal oxidation and/or void formation similar to Ni-Cr-Al alloys. Metal recession decreased with increasing chromium concentration, as did the weight loss. The metal recession for most of the alloys was greater than 2 mils in 100 hr. The exceptions were alloys NT23 (0.57La) and NT24 (0.91Th), which had metal recessions of 1.4 and 0.6 mils, respectively. These alloys also exhibited the lowest total weight gain of any of the modified compositions. However, both alloys exhibited internal oxidation completely across the 0.060 in. thick sample in 100 hr.

The microstructure of alloy NT5 (Ni-25Cr-10Ta) as hot rolled and after 100 hr at 2300°F is presented in Figure 26. These structures are also typical of all of the Ni-25Cr-10Ta alloys with alloying additions. Figure 26a shows that the hot-rolled structure contains a dispersed precipitate, presumably a Ni-Ta compound, in the nickel solid solution matrix. Figure 26b illustrates that internal oxidation and/or porosity was more severe than in the Ni-Cr-Al alloys, although it did not extend completely across the sample thickness. Oxide adherence was also limited on these alloys. The results of metallographic examination verified the weight change data in indicating the limited potential of protective cladding based on the Ni-Cr-Ta system in comparison to Fe-Cr-Al and Ni-Cr-Al alloys.

(2) Modified Task I Alloys

Metal recession and oxide penetration depth measurements for modified Task I alloys after cyclic furnace oxidation at 2300°F are summarized in Table 16. As for the weight loss measurements, metallographic data indicated no major deviation from the Task I alloys for the respective alloying additions. In general, modified Task I alloys had slightly reduced metal recession and depth of penetration. Thus, alloys F14 (0.25Y) and F21 (0.65Y) both had metal recession and oxide penetration of about 0.5 and 2.0 mils, respectively, corresponding to the values of 0.5 and 3.4 mils for the Task I alloy F8 (0.43Y).

The most significant metallographic effects observed for modified Task I alloys were in the result of lower additions of Hf (F17) and Th (F20) in the Fe-Cr-Al system. Reduction of

28

the hafnium concentration from 0.85 to 0.5 w/o resulted in metal recession and oxide penetration about one-half of that measured in Task I. Similarly, reduction in thorium from 1.06 to 0.5 w/o reduced the depth of penetration of alloy F20 from 4.9 to 2.0 mils. Conversely, metallographic data indicated little difference in either metal recession or depth of penetration for variation of tantalum from 0.5 (F19) to 1.25 w/o (F18).

Metallographic data for Ni-Cr-Al alloys also correlated with Task I results, as shown in Table 16. The three nickel-base alloys NA13 (0.5Th), NA14 (0.6Hf), and NA15 (1.0Ta) all exhibited intergranular oxidation and/or void formation completely across the sample after 100 hr. However, the tantalum addition indicated a slight tendency to reduce the rate of internal oxidation. The metal recession of NA15 was 1.5 mils as compared to about 0.5 for NA13 and NA14. Thus, the metal recession data showed good correlation with the sample weight loss in Table 10.

Metallographic examination of the TD Ni and TD NiCr samples also generally correlated with oxidation data. TD Ni exhibited a metal recession of 5.7 mils after 100 hr. This sample was characterized by a very thick oxide which was sufficiently adherent to permit cutting and polishing of metallographic samples without spalling. TD NiCr had a metal recession of less than 0.5 mils correlating with Task I results. The small spherical voids observed in the Task I samples were also visible in these samples. Depth of penetration measurements in Table 16 reflect the zone of spherical pores near the surface. The measurement of zone width could not be made accurately because of variable density and depth of the void structure.

Based on the 100 hr data, the most oxidation-resistant alloys were Fe-Cr-Al modified with titanium. These alloys, in addition to having among the lowest weight gain, also indicated minimal internal oxidation on surface intergranular attack. The next most resistant alloys were Fe-Cr-Al with either Y or Th additions, although these alloys had a slight tendency toward intergranular attack at the surface. Nickel-base alloys had low metal recession, but were subject to internal oxidation. The microstructures of modified Task I alloys were quite similar to Task I alloys which were presented in Figures 17 through 25.

(3) Torch Test Specimens

Metallographic examination of modified Task I alloy exposed in the air-natural gas torch flame was conducted only after 100 hr of exposure. The results of metallographic measurements on the six modified Task I alloys, TD Ni, and TD NiCr are summarized in Table 17. Also included are microhardness surveys across each of the samples after exposure. Since the original sample was 0.060 in. thick, the microhardness surveys represent the hardness profile from the center to about 2 mils of the original sample surface.

The metallographic measurements of modified Task I clad-
ding alloys indicated very little difference between the torch and
the furnace oxidation tests for most of the alloys. Only F15
(0.25Ti) exhibited greater metal recession in the torch test
than in the furnace tests. However, the furnace test also indicated
a slight tendency toward spalling of this alloy, which was verified
by the 800 hr test in Task II. The other alloy which exhibited
significant spalling was F18 (1.25Ta), but this also occurred in
the furnace test. As in the furnace test, NA13 (0.5Th) had a metal
recession of less than 0.5 mil, but was oxidized internally com-
pletely across the sample.

The most striking deviation from furnace oxidation data
was evident for TD NiCr. TD NiCr, which had a metal recession rate
of only 0.5 mil in the furnace test, indicated about 2 mils in
the torch test. In addition, internal oxidation and/or void forma-
tion was much more distinct. The size of the voids was greater
than previously observed and the zone of internal defects more
defined. TD Ni did not vary significantly from the furnace test.

The results of hardness surveys did not indicate any sig-
nificant variation in hardness for Fe-Cr-Al alloys or TD Ni, as
shown in Table 17. NA13 exhibited only a minor reduction in hard-
ness, except for the zone about 6 mils from the surface. In con-
trast, the reduction in hardness for TD NiCr began about 18 mils
from the surface and decreased continuously. This is assumed to
be due to depletion of chromium from the solid solution in both
TD NiCr and NA13. This is a probable explanation for the void for-
mation in TD NiCr, although the existence of the voids also would
tend to reduce the hardness values.

The microstructures of selected alloys after 100 hr of
cyclic torch testing are presented in Figures 27 and 28. Figure 27a
is generally representative of the Fe-Cr-Al alloys, except that most
of the alloys had a thin oxide layer on the surface. Alloy NA13
(Figure 27b) shows internal oxidation and the absence of an oxide
layer that was observed on this alloy.

Photomicrographs of TD Ni and TD NiCr after torch testing
are presented in Figure 28. The TD Ni sample shows the thick, uni-
form oxide layer that was observed on this alloy after both furnace
and torch tests, and internal precipitates which may be oxides.
Figure 28b illustrates an irregular surface and an absence of oxide,
which are both indications of spalling during the torch test. The
microstructure also shows the zone of subsurface spherical porosity
discussed previously.

(4) Sulfidation Test Specimens

Metallographic data for modified Task I alloys after the
sulfidation test are presented in Table 18. These data are for test
samples exposed at 1650°F for 20 hr after immersion in molten sodium
sulfate. The results correlate with the weight change data; metal
loss was less than 0.5 mil for all alloys.

The microstructures of selected alloys after sulfidation exposure are shown in Figure 29. Alloy F15 (Figure 29a) is representative of all the Fe-Cr-Al alloys. The surface of alloy NA13 (Figure 29b) indicates some nonuniform surface attack and a minor amount of subsurface precipitation, which may be a sulfide phase. Oxide particles may also be associated with internal oxidation of the precipitated phase in this alloy. The TD Ni samples (Figure 29c) exhibited a thin oxide layer and no subsurface attack. This structure is also similar to the TD NiCr sample, except that the oxide layer was much thinner on TD NiCr.

c. Bend Test

Bend tests were conducted on oxidized samples of Task I and modified Task I alloys to indicate the influence of exposure on bend ductility. No provision was made for bend tests in Task I in the original program plan. Bend tests were planned only on the 10-mil sheet samples in Task II. However, it was decided to conduct bend tests in Task I to augment microhardness measurements for evaluation of changes in alloy ductility during exposure. Because of insufficient hot-rolled material, bend tests were conducted on Task I alloys only after 100 hr exposure. Modified Task I alloys were subjected to bend tests in the as-fabricated and the exposed conditions.

Bend tests were conducted using the guided bend test fixture shown in Figure 30. This equipment permits variation of the mandrel diameter to accommodate samples of variable thickness. All tests employed a 4t mandrel and were continued to 180° if no failure occurred. In most cases, considerable springback occurred so that the sample bend appeared to be less than 180°.

(1) Task I Alloys

Bend samples of Task I alloys were sectioned from oxidation samples for the furnace test. Accordingly, test samples were 1 in. x 0.5 in., which was the minimum length for accommodation in the test fixture. The samples which bent 180° exhibited significant springback after release of the bend load. This is shown in the photograph of Task I bend samples, Figure 31. Although the samples were subjected to a 180° bend, springback resulted in an equilibrium position less than 180°.

The results of bend tests and microhardness surveys on Task I alloys are summarized in Table 19. These data are limited to alloys with a total weight gain of less than 11 mg/cm² during cyclic furnace oxidation. Most of the iron-base alloys, including the base composition Fe-25Cr-4Al (F1), were brittle after exposure. The only iron-base alloys which survived the bend test were F10 (0.85Hf) and F11 (0.85Ta). All three of the nickel-base alloys passed the bend test, although alloy NA7 (1.01Th) exhibited numerous small cracks on the tension side.

Microhardness data, shown in Table 19, do not explain the difference in ductility of the iron-base alloys. The base alloy failed the bend test although the microhardness is less than that of alloys F10 and F11. No significant microhardness variations occurred on any of the iron-base alloys, with the exception of F10. The hardness of 170 DPH at a distance of about 6 mils from the surface indicates some alloy depletion just beneath the relatively thick oxide layer that was present on this sample.

Microhardness data for the three Ni-Cr-Al alloys show that alloy depletion was significant only on the Ni-20Cr-5Al base composition (NA2). Furthermore, these alloys were ductile, though they had higher hardness than the iron-base alloys. The reason for surface cracking of NA7 (Th) is not well explained by the microhardness data, since it is only slightly higher than that of the Hf-modified alloy (NA9).

(2) Modified Task I Alloys

The results of bend testing and microhardness determinations of the 11 modified Task I alloys are presented in Table 20. Microhardness surveys were conducted on only 6 of the iron-base alloys and NA13. All of the Ni-Cr-Al alloys and Fe-Cr-Al alloys, except F21 (0.65Y), exhibited a degree of ductility in the hot-rolled condition. An unusual aspect of bend testing of the as-fabricated alloys was that alloys F14 and F18 failed not at the point of maximum strain, but in a region away from this point. This may have been due to microstructural inhomogeneity or laps in the hot-rolled material.

In the oxidized condition, only the nickel-base alloys and Fe-Cr-Al alloys containing Hf (F17) and Ta (F18, F19) were ductile. Thus, the bend test results of modified Task I alloys correlated with previous results. Again, microhardness data did not indicate any apparent reason for the difference in bend ductility in iron-base alloys. Furthermore, only NA13 (0.5Th) exhibited significant alloy depletion as indicated by a hardness survey across the sample.

The difference in bend ductility of iron-base alloys can probably be attributed to the ductile-to-brittle transition that is often encountered in BCC alloys. Nickel-base alloys are not susceptible to this effect because they are FCC. Hot working of the Fe-Cr-Al alloys apparently lowers the transition temperature to below room temperature. Subsequent recrystallization during oxidation exposure can increase the transition temperature depending on the alloying addition. If this is the case, Hf and Ta additions lower the transition temperature, whereas Y additions have an opposite effect. The influence of Th and Ti cannot be defined with the current data because these alloys were ductile in the hot-rolled condition and brittle after exposure, as was the Fe-25Cr-4Al base alloy.

7. Discussion

The results of oxidation tests, bend tests, and metallographic measurements in Task I were the basis for selection of alloy compositions for the 800 hr furnace oxidation testing in Task II. Oxidation data generally indicated that the Fe-Cr-Al alloys provided a wide variety of compositions with lower oxidation rates than Ni-Cr-Al alloys. Furthermore, internal oxidation did not occur in the best Fe-Cr-Al alloys, but could not be eliminated in the Ni-Cr-Al alloys. Thus, in terms of the cladding alloys alone, Fe-Cr-Al alloys appeared more promising for longer time operation at 2300°F. Obviously, they are less attractive from an interdiffusion standpoint. It was anticipated that minimal interdiffusion problems would occur with cladding alloys near in composition to TD Ni and TD NiCr (i.e., Ni-Cr alloys).

A comparison of weight change data after 100 hr at 2300°F for the best Task I and modified Task I alloys is shown in Table 21 and plotted in Figure 32. In the iron-base systems, additions of Ti and Y indicated no well-defined trend. Since the weight changes for these alloys were quite small for all levels of addition, the differences may be due to the data scatter for these systems. In contrast, lowering the concentration of Th and Hf from the 0.25 a/o level results in lower scale formation rates (lower weight gain). Tantalum was the only addition which resulted in a decrease in weight gain with increasing concentration. However the effectiveness of tantalum was not as pronounced as the other additions in reducing total weight gain.

In the nickel-base systems, reduction of Hf and Th from the initial 0.25 a/o addition level also reduced the 100 hr weight changes. Addition of Hf was considerably less effective than Th in reducing the weight gain. In contrast to the Fe-Cr-Al system, a small Ta addition (1.0 w/o) was apparently innocuous, since the weight changes were essentially that of the Ni-20Cr-5Al base alloy.

The results of Task I indicated that improved oxidation resistance could be obtained in most of the better alloys by using alloying additions below 0.25 a/o. It must be remembered that this conclusion was based on data obtained within a relatively short time period (100 hr). It was hoped that the 100 hr data could be extrapolated to longer times in Task II. This was not possible in all cases, as will be shown in Task II oxidation tests.

B. Task II - Extended Oxidation Testing
    and Interdiffusion Studies

1. Alloy Selection and Sample Fabrication

Selection of the 18 alloy compositions for evaluation
in Task II was based on all of the tests conducted in Task I.
The compositions recommended for Task II were approved by the
NASA Project Manager prior to preparation of the alloys. One
major difference between Task I and Task II oxidation tests was
planned. Oxidation samples in Task II were fabricated from 10-mil
sheet in order to simulate the oxidation behavior of a 5-mil
cladding layer. Thus, oxidation samples in Task II had a more
limited reservoir of alloying addition than did Task I specimens.

As discussed previously, Task I data indicated that most
of the alloying additions were effective at concentrations below
0.25 a/o. Furthermore, bend tests indicated that the alloying
additions, particularly Y, increased the ductile-to-brittle tran-
sition temperature in Fe-Cr-Al alloys. It was demonstrated in the
case of Y that addition of 0.65 w/o Y resulted in embrittlement
at room temperature in the hot-rolled condition. Similar effects
might possibly be expected for higher concentrations of the other
alloying elements. The use of 10-mil material introduced further
necessity for room-temperature ductility, since it was planned to
reach the final 10-mil thickness by cold rolling. All of these
factors indicated that lower concentrations of alloying additions
were appropriate. Accordingly, most of the alloys selected for
Task II had alloying additions less than 0.25 a/o.

One other factor influenced the selection of alloying
additions in Task I alloys. It was shown in Task I bend tests
that Ta additions lowered the ductile-to-brittle transition tem-
perature of Fe-Cr-Al alloys. Tantalum additions were also mildly
beneficial in improving oxidation resistance. Thus, tantalum
additions were included in combination with other additions in
the Fe-Cr-Al systems in the hope of improving room-temperature
ductility. It was hoped that improvement in room-temperature
ductility could be obtained without detriment to the oxidation
resistance.

The nominal compositions of Task II alloys are summarized
in Table 22. Alloys selected for evaluation were in five basic
systems: Fe-Cr-Al-Y, Fe-Cr-Al-Ti, Fe-Cr-Al-Hf, Fe-Cr-Al-Th, and
Ni-Cr-Al-Th. Six of the compositions were tested previously in
Task I. One alloy containing 0.5 w/o Ta was selected in each of
the four iron-base systems in the hope of increasing room-temperature
ductility. The Ta addition to Ni-Cr-Al-Th (NA17) was intended to
indicate whether any synergistic effects of the alloying elements
could be obtained. A similar alloy containing both Ti and Hf (F27)
was selected in the Fe-Cr-Al system. The remaining nickel-base
alloy, Ni-20Cr-6Al-0.75Si, was suggested by NASA based on oxidation

data from another program. This alloy could not be fabricated by hot rolling and was therefore not evaluated by oxidation tests.

Task II alloys were consolidated by arc-melting at IITRI using the raw materials and techniques described in Section III-A-1. In no case was the melt loss in excess of 1%, as shown in Table 23. Prior to hot rolling, the ingots were hand ground to remove visible surface defects such as shrinkages and cold shuts, followed by homogenization in air at 2100°F for 24 hr. The following pass sequence was maintained for the hot rolling of the Fe-Cr-Al alloys: (1) 8 to 9 passes at 5% reduction per pass, (2) 5 passes at 7.5% per pass, and (3) 10 to 12 passes at 10% per pass. The ingots were reheated for 5 min at 2150°F between each pass. During rolling of the nickel-base alloys, the reduction per pass was always about 5%. Nickel-base alloys were given a second homogenizing treatment at 2100°F for 24 hr after an initial breakdown of 25% because of greater work hardening than Fe-Cr-Al alloys.

A summary of the rolling behavior of Task II alloys is presented in Table 24. All the iron-base alloys hot-rolled exceptionally well. The few localized defects observed on the surface of some of the ingots were suspected to be due to shrinkage cavities and internal porosity. These defects were readily removed by surface grinding resulting in good quality material for cold rolling.

Nickel-base alloys were more prone to surface and edge cracking than Fe-Cr-Al, as was observed previously in Task I. However, the modified rolling schedule employed for Ni-Cr-Al alloys resulted in material of good quality, except for alloy NA18. This alloy developed severe cracks during the very early stages of rolling. In spite of more frequent surface conditioning, cracks reappeared during further hot rolling. Thus, it was apparent that cracking was due to alloy composition, rather than melting defects. In order to verify these results, a second arc-melt of alloy NA18 was prepared. As previously, hot rolling resulted in severe cracking of the second ingot. These results indicated that the high-silicon, high-aluminum concentration in alloy NA18 precluded fabrication of good quality sheet material by the methods used in this program. Consequently, this alloy was eliminated from oxidation evaluation in Task II.

The hot-rolled alloys were annealed and sliced (0.75 x 1.5 in.), transverse to the rolling direction. They were then ground about 0.01 in. per side to remove surface defects in preparation for cold rolling to 10 mil sheet. The initial thickness of all the specimens prepared for cold rolling was approximately 0.060 in.

Prior to the actual cold rolling, a pilot rolling experiment was conducted on small samples of Fe-Cr-Al alloys in order to optimize the pass sequence and annealing schedule. Reductions of

as much as 25 to 30% per pass were taken without edge cracking. Small edge cracks were generally detected after a total reduction of 60%. At this stage, the rolled sheets were annealed for 15 min at 2150°F and subsequently rolled to 0.010 in. sheet at 25 to 30% reductions without any difficulties. This procedure was followed for the actual cold rolling of alloys for fabrication of oxidation samples. However, nickel-base alloys were rolled with reductions of only about 7.5% per pass. After intermediate annealing, the very thin superficial surface oxide layer was removed by glass-bead blasting. As a result, the finished cold-rolled sheet (0.010 in.) had an excellent surface appearance.

The sequence for fabrication of 10-mil oxidation samples of the various alloys is shown in Figure 33. The three major fabrication stages of hot rolling, surface grinding, and cold rolling are illustrated. Samples for chemical analysis were removed from the cold-rolled sheet immediately adjacent to the oxidation samples, rather than from hot-rolled material, as in Task I. Thus, the results of wet chemical analysis represent the actual composition of the oxidation samples. As a final step, the oxidation samples were hand-polished to remove any burrs resulting from the sectioning of test samples from the cold-rolled sheet material.

A cross-section of the 10-mil sheet material as-cold-rolled and after annealing is shown in Figure 34. The photomicrograph presented in Figure 34a represents both iron- and nickel-base alloys after cold rolling and illustrates the excellent surface conditions obtained. During sectioning of the oxidation samples from the 10-mil sheet, care was taken to avoid any defects which may have been present in the cold-rolled material. The microstructure shown in Figure 34 is that of alloy F22 (0.15Y) and was typical of Fe-Cr-Al alloys containing yttrium. The annealed structure (Figure 34b) shows the dispersed precipitate (Fe-Y) that was visible in all Fe-Cr-Al-Y alloys.

2. Furnace Oxidation Testing

Test samples, 2 x 0.5 x 0.010 in. thick, of the 18 Task II alloys were subjected to cyclic exposure at 2300°F to failure or to 800 hr. The cyclic conditions were identical to those used in Task I: 2 hr cycles to 20 hr, followed by 20 hr cycles to 800 hr. Triplicate samples of each alloy were included in the test; one sample of each material was sectioned at 100, 400, and 800 hr, or failure, for metallographic examination. After sectioning, the remainder of the sample to be used for metallography was returned for additional exposure. Thus, weight changes after 100 hr were obtained only on the two remaining samples of each alloy. As in Task I, both total and sample weight changes were determined during furnace exposure.

Test samples were contained in alumina crucibles during exposure in order to retain any spall products. This was necessary in order to obtain total weight change data for the alloys.

36

Because of the difference in sample geometry, it was necessary to use different alumina crucibles from those in Task I. The only crucibles available that would adequately contain the 2 in. long test samples were of porous alumina. It was discovered early in the 800 hr test that the porous alumina crucibles gained weight during cyclic exposure. This was readily apparent because of the considerable difference between total and sample weight change for all alloys in the absence of spalling. Accordingly, four empty crucibles were exposed along with the test samples to provide a means of calculating a correction for total weight change of the test samples.

Figure 35 is a plot of the average weight gain of the four empty alumina crucibles which were exposed along with the test samples. The reason for the weight gain of the crucibles is not definitely known, but the gain was fairly linear with time. An apparent change in slope occurs at about 300 hr, although the original slope is resumed after 600 hr. At 300 hr, the refractory brick used to hold the crucibles was changed due to fracture of the brick. This does not mean that visible interaction of the crucible and brick occurred; rather, the weight gain was apparently due to a gaseous reaction, possibly with water vapor. The data in Figure 47 were used to correct total weight gain only for the various samples in subsequent plots and tables of oxidation data. This correction does not alter total weight gain drastically, nor does it affect in any way the sample weight change data. For example, the crucible correction for alloy F26 after 120 hr was 22 mg of the total 88 mg weight change.

Total and sample weight changes for Task II alloys, TD Ni, and TD NiCr during cyclic furnace oxidation are summarized in Table 25. Data in Table 25 are presented only at 40 hr intervals, although weighing and calculations were made at each 20 hr interval during furnace exposure. Each value is the average of three samples up to 100 hr and only two specimens at times greater than 100 hr. Data for TD Ni and TD NiCr are based on a single oxidation sample. Failure of the first alloy, F28 (0.5Hf-0.5Ta), occurred at 140 hr, although all of the alloys had an excellent surface appearance after 100 hr. Termination of testing for the various alloys was based on visual observation of the samples rather than well-defined level of weight gain. This was because calculations of weight change were not performed continuously during the oxidation testing. Furthermore, attack of the 10-mil test samples was readily visible, although it was generally not uniform over the sample.

Obviously, the determination of oxidation failure was arbitrary, particularly because of the 10-mil thick oxidation samples. The use of thin specimens tended to accelerate failure at edges and corners because of high oxide stresses and a limited reservoir of substrate material. In general, the failure of all Fe-Cr-Al samples was due to initial extensive attack at the corners and/or edges of the samples. However, the use of thin specimens

did provide a more stringent selection of the better compositions. Although the use of thin samples did accelerate attack on some alloys, the superiority of alloys which did not fail was thereby further demonstrated.

Using the above criterion, failure of the various alloys was not based on the initial appearance of attack at an edge or corner. The samples were all permitted to be attacked to a point of considerable visible deterioration prior to removal from the test. Furthermore, in cases where only one of the samples of a given composition showed considerable attack, testing was continued. This was not a general condition, since reasonably good correlation between samples of the same composition was normally obtained. Spalling of the surface oxide was generally limited on all of the compositions tested. When it did occur, spalling consisted of fracture of relatively large pieces of oxide from edges and corners of the samples.

A summary of the time of removal and visual appearance of Task II alloys, TD Ni, and TD NiCr during cyclic furnace testing is presented in Table 26. Photographs of one oxidation sample for each alloy system at the time of removal from the oxidation test are shown in Figures 36 and 37. Each of the five basic alloy systems developed charateristic surface oxides so that the alloys in the various systems could be readily distinguished by their surface appearance. For example, Fe-Cr-Al alloys containing Hf had a mottled dark green surface, whereas the alloys containing Ti developed a light tan oxide. One difference in the behavior of Fe-Cr-Al and Ni-Cr-Al alloys was observable, as shown in Table 26. All of the alumina crucibles used for Ni-Cr-Al alloys, TD Ni, and TD NiCr had a green internal surface indicating evaporation of metallic and/or oxide species from the test samples. None of the Fe-Cr-Al alloys caused any appreciable discoloration of the crucibles.

The test samples described in Table 26 are presented as photographs in Figures 36 and 37. It is apparent that fracture as a result of oxidation did occur on some samples (F28, F30). Furthermore, distortion of the test samples also occurred during exposure, particularly for Fe-Cr-Al alloys. It is also apparent that some of the alloys suffered more extensive oxidation than other alloys. This was due primarily to the abrupt nature of failure in Fe-Cr-Al alloys, as will be discussed subsequently.

Weight gain data for alloys which were removed from test prior to 400 hr are plotted in Figures 38 and 39. All of the specimens removed were Fe-Cr-Al alloys, including all of the Hf- and Ti-modified alloys, except the alloy containing both Hf and Ti (F27). Both the sample and total weight change curves show similar shapes; a low oxidation rate for periods greater than 100 hr is followed by a rapid increase at exposure times between 140 and 320 hr. This is presumably due to depletion of the additive which

inhibits the oxidation rate. Thus, Ti additions which resulted
in the lowest 100 hr oxidation rates did not provide long-time
stability, at least at the concentrations investigated.

Analysis of the slope of the weight gain curves is diffi-
cult, since several competitive factors enter into the measured
values. The exposure temperature of 2300°F is sufficient to in-
clude vaporization of alloying elements and/or products as a factor
in weight change. Evaporation coupled with spalling and oxidation
can produce abrupt changes in slope of the oxidation curve since
all these processes can take place simultaneously. Consequently,
unusual variations in weight change can occur depending on the
relative importance of these competitive reactions over any time
interval.

Weight change data for Fe-Cr-Al alloys which did not
fail prior to 400 hr are plotted in Figures 40 and 41. The lowest
weight gains and best surface appearance were observed for the Y
additions in the Fe-Cr-Al alloys. The total weight gain curves
for alloys F14, F23, and perhaps F22, shown in Figure 40, indicate
an anomalous decrease in the total weight gain in the range of
300-600 hr. These alloys (and also TD NiCr) showed almost no
change in either the total or sample weight over this temperature
range. Thus, when the crucible correction was applied to these
alloys, the total weight gain decreased, although the crucible
correction merely magnifies the effect. This can only be accounted
for by evaporation of the alloy constituents or oxide products
which balances, or exceeds, the rate of oxygen uptake. However,
the weight changes are so small that minor variations can be ex-
pected. It is significant that no visible change in the Fe-Cr-Al
samples occurred in this range.

Weight change data for the Ni-base alloys, TD Ni and
TD NiCr, are plotted in Figures 42 and 43. Failure of nickel alloys
was not as abrupt as in the Fe-base systems. These alloys all had
a continuous band of oxide around the edges of the samples, which
tended to chip at the longer exposure times. This resulted in a
decrease in the sample weight gain for NA13 and NA16 at about
500 hr. In contrast, Fe-base alloys usually exhibited edge failure
primarily along the 0.5 in. dimension of the 2 x 0.50 x 0.010 in.
samples, generally initiating at a corner.

The oxidation behavior of TD Ni and TD NiCr correlated,
in general, with results obtained in Task I. Test samples of these
alloys were 0.060 in. thick since it was expected that this thick-
ness was required to provide oxidation data to 800 hr. It is ob-
vious that if 0.010 in. samples had been used, these alloys would
have failed prior to 800 hr. TD Ni developed the characteristic
thick, adherent oxide and the high weight gain previously obtained.
Similarly to Task I data, TD NiCr had a small sample weight loss
of about 1.5 mg/cm^2 at 100 hr. However, after this time oxidation
and spalling became accelerated as shown in Figure 43. As a result,
the sample external dimensions were considerably reduced after 800 hr,
as shown in Figure 37.

The apparently anomalous decrease in total weight gain for TD NiCr in Figure 42 in the range of 200 to 600 hr can be explained with more assurance than for the Fe-Cr-Al alloys. Figure 43 indicates that spalling of the oxides on TD NiC became accelerated at about 200 hr. This effect was apparently due to compositional changes in the alloy surface. While spalling would be expected to cause an acceleration in the rate of total weight gain, this was apparently offset by evaporation of metallic and/or oxide species. Spalling of the oxide obviously resulted in a large increase in the total effective surface for evaporation to occur. Thus, the observed decrease in total weight gain could be expected provided that the evaporating species did not condense on the crucible walls. Following this stage, the total weight gain for TD NiCr became essentially linear with time in the time interval of 600 to 800 hr.

One characteristic was often observed on the specimen sectioned for metallographic examination at 100 and 400 hr: The unexposed edge resulting from cutting off one-third as the metallographic sample often became the initiation point for edge attack. This observation is generally applicable to Fe-Cr-Al alloys which failed early and/or were particularly subject to edge attack. This effect is probably due to depletion of the alloying additions in the alloys. After 100 or 400 hr, migration of the alloy additions had already occurred so that little or none of the alloying addition or, for that matter, Al was available to affect the oxide developed on the freshly cut surface. Thus, the oxidation resistance of the new surface was equivalent to that of the Fe-Cr-Al matrix, with perhaps a lower concentration of aluminum.

In general, the results of the 800 hr cyclic oxidation test demonstrated that yttrium additions to the Fe-Cr-Al alloys provided the best oxidation resistance. All of the yttrium-containing alloys were exposed 800 hr without failure, although the data suggest that failure of alloy F22 (0.15Y) was imminent. The next best alloys were Fe-Cr-Al alloys with thorium additions. Nickel-base alloys exhibited considerable oxidation resistance, which was superior to Fe-Cr-Al alloys with Hf and Ti additions. Significantly, titanium additions which resulted in the lowest 100 hr weight gains resulted in early failures with no apparent effect of titanium concentration on the 2300°F life.

As expected, addition of tantalum as a secondary alloying element had no significant effect on the time to failure of any of the alloys. In general, the results indicate that tantalum in the range of 0.5 to 1.0 w/o may have provided slight improvement in the alloys with Hf and Ti additions. Alloy F27 does indicate that some possible synergistic effect may have occurred due to a combination of Ti and Hf. This alloy was significantly more oxidation-resistant than any of the alloys which contained either Hf or Ti alone. However, the significance of this combination was masked in this alloy. One of the F27 samples had very little

attack after 540 hr, whereas the other sample exhibited intensive attack. The reason for this behavior is not clear, assuming no segregation was present in this alloy, but may be related to edge attack on this alloy.

As previously stated, analysis of the slope of the weight gain curves is difficult because of competing reactions that are possible during exposure. These include oxygen consumption, oxide spalling, vaporization of oxide and/or metallic species, and alloy depletion due to edge effects, spalling, and possibly vaporization. Obviously, the relative importance of these factors determines slope changes and other distinct features of the weight gain curves. The results on the Fe-Cr-Al alloys which failed early, however, does indicate the overriding effect of oxygen as soon as the surface oxide layer is penetrated. It will be subsequently shown in the supplemental microprobe examination (Section III-B-4d) that this layer is rich in Al_2O_3. The oxidation results suggest that the major influence of the alloying elements is associated with modification of this oxide. However, the data obtained in this program were inadequate to define the mechanisms by which the Al_2O_3-rich oxide was influenced by alloying additions. Thus, it was not possible to define whether the influence is mechanical (improved oxide adherence), or an effect more directly associated with oxide layer, such as decreasing oxygen and cation diffusion in the oxide layer. It is likely that both effects occur in the various alloy systems investigated.

The Fe-Cr-Al alloys containing Y did permit some insight into the mechanism of oxidation. For most of the other alloys, the oxidation life was independent of the concentration of alloying limit. The oxidation data for Fe-Cr-Al-Y alloys suggest that this is also generally true for the Y-containing alloys. However, subtle differences in appearance of these alloys did occur during the oxidation test. During the exposure period of about 100 to 600 hr all of the Y-containing alloys had a smooth, light gray oxide which did not undergo any visible changes. At about 740 hr alloy F22 (0.15Y) began to develop surface pits. These pits did not result in immediate failure, although they are probably responsible for the higher total weight gain for this alloy. Furthermore, as the exposure period reached 740 hr, all of the Y-containing alloys began to develop green spots which slowly engulfed the sample as the exposure time increased. After 800 hr, the F22 samples were completely greenish in color, whereas samples of F14 (0.25Y) and F23 (0.25Y-0.5Ta) had only areas of greenish oxide or were only partially converted. At this point, edge and corner attack was observed on samples of alloy F22 and F23. All of these observations can be seen on the samples of these alloys in Figure 36.

The pitting defects observed primarily on alloy F22 were probably due to localized breakdown of the Al_2O_3-rich oxide. It is significant that these defects did not result in rapid oxidation of the samples, as would be expected based on the behavior of the

other Fe-Cr-Al alloys. The development of the greenish surface oxide suggests that this effect was due to diffusion of Cr and/or Ni either through the oxide layer or localized defects in the oxide layer. Thus, only in the Fe-Cr-Al-Y system was an apparent wearout mechanism determined by diffusion kinetics obtained. The remaining Fe-Cr-Al alloys, with the possible exception of Fe-Cr-Al-Th alloys, probably failed as a result of the lack of oxide adherence or continuity. The Fe-Cr-Al-Y alloys were the three best alloys in the 800 hr oxidation test. The indication of wear-out shows that the actual life of the best alloys was approached. Other additions and additive concentrations should, of course, be evaluated by anyone furthering this work.

3. Interdiffusion Studies

Interdiffusion studies were conducted to evaluate the thermal stability of potential cladding alloys and TD Ni materials at 2300°F. Three cladding alloys were selected, with approval of NASA, for interdiffusion evaluation in contact with both TD Ni and TD NiCr. All of the six cladding/substrate combinations were exposed at 2300°F in argon for 100 hr. Subsequently, the time of exposure of two of these combinations was extended to 300 hr at 2300°F. Clad samples of the six composites were evaluated by metallography, bend tests, and microprobe examination as fabricated and after interdiffusion at 2300°F.

The three cladding alloys selected for interdiffusion studies included F16 (0.5Ti), F18 (1.0Ta), and NA13 (0.5Th). Unfortunately, fabrication of the interdiffusion samples was initiated before the completion of the 800 hr furnace oxidation test. As a result, none of the Fe-Cr-Al-Y alloys, which had the best oxidation resistance at 2300°F, was selected for evaluation. The two Fe-Cr-Al alloys were selected to provide the maximum deviation of minor additions available in modified Task I and Task II alloys. The influence of Ti on interdiffusion was expected to be generally representative also of Y, Th, and Hf.

Interdiffusion couples were prepared by the picture-frame technique utilizing hot rolling as the method of bonding the cladding to the substrate. Cladding alloys were hot- and cold-rolled to 20 mil sheet, as previously described. The cladding alloys and TD Ni materials were polished through 320 grit paper, lightly glass bead peened, and washed in acetone. Prior to assembling the composite, a thin strip of ThO_2 was painted on the TD Ni and TD NiCr substrate as a diffusion marker. It was subsequently found that this was unnecessary since the original cladding/substrate interface was readily apparent metallographically. Composites about 2 x 1 in. were then prepared by forming an envelope and seam welding the cladding alloys around the 0.060 in. TD Ni and TD NiCr substrate. Following welding, the composites were encapsulated in sealed Vycor tubes and backfilled with argon. They were then heated at 2000°F for 15 min followed by hot rolling immediately after breaking the glass capsule. Encapsulation was intended to minimize oxidation of the cladding substrate interface

42

prior to rolling, which would limit bonding of the cladding. Hot rolling consisted of a single pass with a nominal reduction of 60%. It was subsequently found that the single-pass reduction resulted in varying cladding and substrate thickness. However, the diffusion studies were primarily intended to obtain qualitative interdiffusion data, so that the cladding thickness was not critical to interdiffusion studies.

After hot rolling, 2 x 0.5 in. interdiffusions specimens were sectioned from the approximately 4 x 1.0 in. clad composites. Samples for bend test, metallography, and microprobe examination were also sectioned from the hot-rolled material. The cladding surface was lightly polished to remove any surface oxide and finally weighed for determination of weight change during interdiffusion. The determination of any weight change during interdiffusion was part of the contract requirements. Consequently, interdiffusion samples were contained in Al_2O_3 crucibles during 2300°F exposure. Interdiffusion samples were heated in a Hastelloy X retort containing Ti-gettered argon for 100 hr or 300 hr at 2300°F. After exposure, the clad samples were weighed, bend tested, and sectioned for metallographic and microprobe examination. The results of these investigations are included in Section III-B-4.

As part of the work scope, test samples of the three cladding alloys (F16, F18, NA13), TD Ni, and TD NiCr were exposed in argon at 2300°F for 100 hr to determine if any evaporation losses could be measured. Test samples of the three cladding alloys were 2 x 0.5 x 0.01 in., and were sectioned from the cold-rolled sheet used for oxidation samples. TD Ni and TD NiCr samples were fabricated from 0.060 in. thick sheet material. Vaporization samples were lightly polished though 320 grit paper, washed in acetone, and placed in aluminum crucibles for exposure at 2300°F. The atmosphere was slowly flowing, Ti-gettered argon, since it was expected that a flowing system would aid in the migration of metallic vapor species away from the test samples. Obviously, this also had the effect of increasing the potential for oxidation of the samples due to oxygen and/or water vapor in the argon.

The results of evaporation studies are summarized in Table 27. All of the vaporization samples exhibited weight gains during exposure. The vaporization samples apparently removed residual impurities in the argon without significant evaporation of metallic species. The three cladding alloys had higher weight gains than TD Ni and TD NiCr, apparently because of aluminum and the other strong oxide formers in these alloys. It is interesting that the weight gains of the cladding alloys were about one-half that obtained in air at 2300°F. Both of the Fe-Cr-Al cladding alloys indicated a slight tendency toward spalling of surface layers. Thus, it may be that the oxidation behavior of Fe-Cr-Al alloys may be sensitive to oxygen pressure, although both F16 and F18 also had a tendency to spall slightly during air exposure.

Also, all of the interdiffusion samples gained weight during inter-diffusion in argon at 2300°F similar in magnitude to that shown in Table 27. These results suggest that evaporation of metallic species from the cladding alloys during exposure at 2300°F was minimal and could not be detected by gravimetric analysis.

4. Supplemental Evaluation

a. Chemical Analysis

Wet chemical analysis was conducted on all 18 Task II alloys to compare the actual composition with the nominal analysis. Samples for chemical analysis were sectioned from the cold-rolled sheet immediately adjacent to the oxidation samples. Consequently, the alloys were less subject to the sampling errors discussed in Section III-A-6a. As previously, analyses of all alloys except those containing Hf and Th were conducted by the Charles C. Kawin Company. Alloys with Hf and Th additions were analyzed by William A. Fahlbush Associates.

The results of chemical analyses of Task II alloys are summarized in Table 28. All of the analyses for chromium and aluminum were reasonably close to the nominal analysis; in no case was any major deviation obtained for these elements. The aluminum results show that analyses by Kawin tended to be slightly higher and those by Fahlbush were slightly lower than the nominal com-position. These differences are apparently due to the analytical technique employed. As in Task I, the concentrations of the strong oxide formers Y, Hf, and Th obtained by chemical analysis, with the exception of alloy F14, were 0.05 to 0.15 w/o lower than the nominal analysis. Titanium and tantalum determinations, however, were generally quite close to the nominal analysis. Furthermore, the concentrations determined for Th by Fahlbush were much nearer the nominal analysis in nickel-base alloys than in the Fe-Cr-Al alloys.

A possible explanation for these differences lies in the microstructures of the various alloys. The reduction in the minor alloying elements does not appear to be due only to gettering of strong oxide formers by oxygen during arc-melting. If this were the case, loss of Ti could also be expected. Rather, the results tend to show that values lower than the nominal analysis occurred primarily for alloying additions which were in excess of the solu-bility limit. Alloys containing Ti were all single-phase, whereas those containing Y, Hf, and Th additions exhibited precipitates, presumably intermetallic compounds. Thus, the analytical techniques used may have distinguished between the addition in the solid solu-tion from that in the precipitated form because of differences in solution rate. From the data in Table 28, this possibility appears to be a better explanation for the low analyses for Y, Th, and Hf. These conclusions probably apply also to Task I alloys, although the compositional data for Task I alloys may have had more tendency toward sampling errors.

b. Metallography

(1) Oxidation Test Specimens

Metallographic samples were sectioned from one of the
triplicate furnace oxidation samples for surface recession and
oxide penetration depth measurements as in Task I. Metallographic
measurements were initially scheduled after 100, 400, and 800 hr
of furnace exposure. However, alloys which failed between these
times were examined at the time of removal from the test program.
As previously discussed, sectioning of metallographic samples
tended to cause accelerated attack at the new edge of some of the
metallographic samples. Thus, the metallographic sample had
greater attack than the two weight change samples of the alloy in
some cases. Furthermore, because of the tendency toward edge
attack on some materials, the metallographic measurements could
be made only on the portion of the sample which had some remaining
metal. For these reasons, measurements may not have been repre-
sentative at the time of removal for the alloys which were removed
from the oxidation test prior to 800 hr.

A summary of metallographic measurements of the metal
recession and oxide penetration depths of Task II alloys during
cyclic furnace oxidation at 2300°F is presented in Table 29.
These data show that complete oxidation of the metallographic
sample occurred on four alloys at the time of removal from testing
(F29, F16, F31, NA17). The metal recession and maximum depth of
penetration for the various alloys generally corresponds with
Task II weight change data and metallographic measurements in
Task I. One difference, however, existed for Fe-Cr-Al alloys
with Hf additions. Complete penetration of the 10 mil sample by
internal oxidation occurred in 100 hr for both F17 and F28, which
did not occur on the 0.060 mil samples in Task I. Internal oxi-
dation was also visible throughout all other Fe-Cr-Al alloys at
the time of removal from the oxidation test, although it varied
in extent. In no case was internal oxidation as well defined in
Fe-Cr-Al alloys as in Ni-Cr-Al alloys. Thus, the resistance of
Fe-Cr-Al alloys to internal oxidation is dependent on the presence
of an adherent oxide layer. The low metal recession rates for all
Fe-Cr-Al-Y alloys is indicated by Table 29. Surface pitting on
alloy F22 is reflected in the relatively high depth of penetration
of 3.5 mils. In contrast, alloys F14 and F23 had depth of oxide
penetrations of only 1.0 to 1.5 mils in 800 hr.

Table 29 also indicates a significant difference in the
depth of oxidation of TD Ni and TD NiCr that is not apparent in
Figure 37. Visually, the TD NiCr sample revealed a considerable
change in dimensions whereas the TD Ni sample had little apparent
dimensional change. Metallographically, the depth of oxidation
on TD Ni was approximately three times that of TD NiCr; the mea-
sured metal recession for TD Ni and TD NiCr was 18 and 5.5 mils,
respectively. However, the TD NiCr specimen had internal porosity
completely throughout the sample after 800 hr.

The microstructures of selected Task II alloys, TD Ni, and TD NiCr after various exposure times are presented in Figures 44 through 51. Metallographic samples were electroplated with nickel prior to polishing. Alloy F8 after 100 and 320 hr is shown in Figure 44. Both microstructures illustrate the absence of an adherent oxide layer and localized penetration approximately though one-half of the sample thickness after 320 hr (Fig. 44b).

Microstructures of alloy F14 at 100, 400, and 800 hr are presented in Figures 45 and 46. These structures represent all of the Fe-Cr-Al-Y alloys (F14, F22, F23) at these conditions, except for alloy F22 after 800 hr. The oxidation samples display an adherent oxide layer and the absence of any significant internal oxidation at all exposure conditions. Figure 46b shows the effect of pitting on alloy F22 after 800 hr. Internal oxidation occurred on this alloy in the region of pitting, although metal recession is not extensive. These defects may also have influenced bend ductility (as will be discussed in Section III-B-4e).

Alloy F27 after 100 and 540 hr is shown in Figure 47, and alloy F30 after 400 and 760 hr is presented in Figure 48. Alloy F31 after 400 and 760 hr is shown in Figure 49. All of these alloys, and the other alloys which failed, show a similar oxidation behavior during the furnace oxidation test. After 100 hr, very little attack of the oxidation samples is apparent, as shown in Figure 47a. As the exposure time increases, localized defects are developed in the protective oxide (Fig. 47b), which subsequently caused significant oxidation, as shown in Figures 48b and 49a. Finally, complete oxidation of the sample occurred provided that the sample was not removed from the test (Fig. 49b). Obviously, the microstructures shown in Figures 47 through 49 represent only a generalized mechanism of the oxidation behavior of Fe-Cr-Al alloys, since minor differences in the various alloys may have occurred. However, the mechanism shown is probably the basis for edge attack that occurred for most alloys which were removed from testing prior to 800 hr.

The microstructures of the nickel-base alloy NA13 after 100, 400, and 560 hr is presented in Figure 50. These photomicrographs illustrate the difference in the oxidation behavior of the nickel-base alloys. Internal voids and/or oxidation is apparent after 100 hr, and no adherent oxide layer is shown even after only 100 hr. The alloy has significant localized attack after 400 hr, but apparently does not result in accelerated attack. Local surface defects do not cause the generalized attack observed in Fe-Cr-Al alloys; metal recession is generally uniform to 540 hr. Thus, the metallographic structures correlate with the weight change data in that the nickel-base alloys are not subject to the abrupt failure common to Fe-Cr-Al alloys.

TD Ni and TD NiCr samples after 800 hr are shown in Figure 51. The thick oxide layer on each side of the TD Ni sample (Fig. 51a) is greater than the thickness of remaining metal. In contrast, TD NiCr shows no adherent oxide and small, spherical voids are dispersed throughout the sample. In some cases, the spherical particles appear to be filled with oxide. Consequently, the internal structure appears to be a combination of Kirkendall porosity due to chromium depletion and internal oxidation.

(2) Interdiffusion Samples

Diffusion couples were examined metallographically in the as-fabricated state and after exposure at 2300°F for either 100 or 300 hr. All of the six diffusion couples were interdiffused for 100 hr. Subsequently, the F8/TD Ni and NA13/TD Ni composites were exposed for 300 hr. Examination of diffusion couples in the hot-rolled condition was intended only to determine the cladding thickness and the effectiveness of hot rolling in obtaining a good cladding/substrate bond. These samples were sectioned from the end of the nominal 2 x 0.5 x 0.060 in. diffusion couples. Metallographic and electron microprobe samples after interdiffusion were sectioned from the ends of the diffusion couples prior to bend testing.

The results of metallographic examination of diffusion samples are summarized in Table 30. In the as-fabricated condition, the cladding thickness, with the exception of F18 on TD Ni, was between 12 and 14.5 mils. Similarly, the substrate thicknesses varied from about 33 to 38.5 mils. The exception to these general dimensions were cladding and substrate thicknesses of 7.5 and 21.0 mils on the F18/TD Ni interdiffusion couple. One other exception was the NA13/TD Ni couple which was exposed 300 hr. This sample was sectioned from a different clad composite than the sample exposed for 100 hr. The cladding thickness on this sample was about 10 mils. Diffusion couples exhibited good interfacial bonding after hot rolling, except in the area where the ThO_2 interface marker was placed prior to hot rolling. The ThO_2 inhibited bonding in a region approximately the same width as the original strip of ThO_2 powder. Bonding was excellent on both extremities of the ThO_2 strip. Another effect of the ThO_2 strip was evident after interdiffusion. After exposure, the location of the ThO_2 could readily be seen because of blistering of this region. This effect was most apparent on the alloys interdiffused for 300 hr consisting of readily visible raised strip extending the full length of the 2 in. long sample.

Metallographic measurements on interdiffused samples were intended to provide a definition of the extent of interdiffusion which could be detected visually. Obviously, measurements of the width of the solid solution zone are subject to variation depending on the etching technique employed. Table 30

shows that a zone of porosity existed at or near the original cladding/substrate interface, particularly for Fe-Cr-Al cladding alloys. This porosity is apparently a Kirkendall effect resulting from the extensive interdiffusion that occurs at 2300°F. Alloy F16 (0.5Ti) had a greater tendency for the development of a well-defined porous zone than F18. Alloy F18 had random porosity throughout the cladding that is not well defined in Table 30, but will be shown in subsequent microstructures. Furthermore, porosity was more extensive with TD Ni than with TD NiCr substrates.

Comparison of the substrate thickness in Table 30 as-fabricated and after exposure indicates that there is only a minor reduction in substrate thickness after exposure. Consequently, the porous zone existed primarily at the original cladding interface and within the cladding alloys. This is reflected in a reduction in indicated cladding thickness during exposure for Fe-Cr-Al alloys. The nickel-base alloy NA13 in combination with either TD Ni or TD NiCr did not present a well-defined porous zone, except perhaps for the TD Ni/NA13 sample interdiffused for 300 hr. This is not surprising considering the number of possible cations diffusing in the various composite systems. Obviously, the number of diffusing species decreases as the substrate and cladding approach equivalence in composition. Excluding aluminum, the possible diffusing species varies from three (Fe, Cr, Ni) for the combination of iron-base alloys and TD Ni and to none for the system NA13 (20 w/o Cr)/TD NiCr (20w/o Cr). Similarly, the number of diffusing species are two (Fe, Ni) for the system Fe-Cr-Al/ TD NiCr and one (Cr) for the system NA13/TD Ni. Obviously, both aluminum and the minor addition also will tend to diffuse from the cladding into the substrate. Even in the case of iron-base alloys and TD NiCr, some chromium diffusion occurs since the cladding contains 25 w/o and the substrate 20 w/o chromium. Consequently, it is not surprising that greater porosity exists in the iron-base systems. The general rule that Kirkendall porosity exists on the side of the diffusion couple containing the faster diffusing species is indicated by the metallographic data in Table 30.

Microstructures of the six diffusion couples as-fabricated and after interdiffusion at 2300°F are presented in Figures 52 to 58. Photomicrographs of iron-base cladding after exposure, shown in Figures 52 through 55, demonstrate the extensive interfacial porosity observed in these structures. Etching tends to amplify the interfacial porosity because of differential solution rates. This effect is also evident at the interface of the as-fabricated specimen. Consequently, considerably less porosity is evident in the unetched condition than that indicated in Figures 52 through 55. This is also demonstrated by the 180°-4t bend tests described in Section III-B-4c.

The microstructures of NA13 interdiffusion samples are shown in Figure 56 and 57. In contrast to iron-base claddings, no well-defined interfacial porosity exists in these systems. Both of the diffusion couples exhibited dispersed porosity in the cladding layer, but porosity is more extensive in the NA13/TD Ni sample. This is consistent with the above discussion on inter-diffusing species, since chromium and aluminum can diffuse into the TD Ni substrate and only aluminum into the TD NiCr substrate. There is also a tendency for diffusion of nickel into the clad-ding in the NA13 (76 w/o Ni)/TD Ni (98 w/o Ni) composite because of the nickel gradient that exists in this system. This probably accounts for the limited porosity on the substrate side of the interface in Figure 56. Again, porosity in the cladding layer is probably amplified by etching of the metallographic samples.

The microstructures of the F18/TD Ni and NA13/TD Ni clad composites after 300 hr at 2300°F are shown in Figure 58. No major differences exist from the structures shown after 100 hr. There is an apparent tendency for pores to coalesce with increas-ing exposure time in both systems. Furthermore, a line of poro-sity at the interface is now apparent after 300 hr in the NA13/TD Ni microstructure. The NA13/TD Ni diffusion couple shown in Figure 58b does demonstrate that the original cladding thickness was less on this specimen than on the sample exposed at 100 hr (Fig. 56b).

c. Bend Test

(1) Oxidation Specimens

Bend tests were conducted on all Task II alloys as-fabricated and after cyclic furnace exposure at 2300°F. No pro-vision was made to provide an additional sample for 180°-4t bend testing. Consequently, bend tests in the exposure condition were performed on oxidation samples at the time of removal from the furnace oxidation test. As a result, the bend tests reflected the influence of the oxidation--i.e., in some cases localized oxi-dation had progressed to the point that bend failures occurred in these areas.

A summary of the results of bend tests and microhardness measurements of Task II alloys is exhibited in Table 31. All of the Fe-Cr-Al alloys were ductile after cold rolling, but the three nickel-base alloys cracked during bend testing. This was apparently due to the greater work hardening of nickel-base alloys as shown by microhardnesses of about 430 DPH for these alloys and about 330 DPH for the iron-base alloys. The nickel-base alloys were ductile after annealing the cold-rolled material at 2150°F for 15 min. The difference in bend ductility of cold-rolled and annealed NA13 alloy is shown in Figure 59. Cold-rolled nickel-base alloys cracked on the tension side of the bend, but no separa-tion occurred (Figure 59a). After annealing, the nickel-base

alloys exhibited excellent bend ductility as shown in Figure 59b, which also represents the behavior of all the iron-base alloys.

Bend ductility data in Table 31 after oxidation exposure are influenced by the degree of oxidation of the various alloys, as previously discussed. Consequently, the influence of composition and/or metallurgical structure on bend ductility cannot be defined in some cases. It is likely that some of the bend failures were associated with localized defects and/or internal oxidation resulting from the defects. In cases where complete oxidation existed, obviously abrupt fracture of the bend sample occurred. However, as a rule, samples which had brittle failures were ductile if the bend sample was positioned so that an area with minimal oxidation was placed in the region of maximum strain. Thus, it can be concluded that all of the bend samples exhibited some degree of ductility.

Bend data in Table 31 cannot be compared with the results for modified Task I alloys after oxidation exposure. Furthermore, the influence of tantalum on the bend ductility cannot be well defined, but some indications are apparent. Of the three Y-containing Fe-Cr-Al alloys (F14, F22, F23), only the F23 (0.5Ta) alloy did not suffer any cracking after exposure. Extension of this analysis to Fe-Cr-Al alloys containing Ti does not result in such a well-defined conclusion. Only one of the two Fe-Cr-Al alloys containing both Ti and Ta (F25, F26) was completely ductile after exposure (F25). Furthermore, of the three Fe-Cr-Al alloys with only Ti additions (F8, F16, F24), two exhibited some cracking and the sample with the highest Ti addition (F21) was ductile after exposure. Since the alloys with Ti additions were oxidized to greater degree than Fe-Cr-Al-Y alloys, bend data for Ti-containing alloys are more subject to influence of oxidation effects. Thus, the influence of tantalum in improving room-temperature ductility after exposure is not well defined, although the data suggest that Ta is effective in improving ductility.

The divergence of the bend test data for 10 mil samples after exposure can be attributed to factors other than localized internal oxidation. During exposure, both aluminum and the minor additions tend to diffuse to the oxidizing interface. Obviously, the rate of diffusion of the various alloying elements varies. The 2300°F exposure temperature and time in the furnace are probably sufficient to provide significant alloy depletion for most of the alloying additions. Thus, oxidation exposure tends to lower the ductile-to-brittle transition temperature for all of the Task II alloys through alloy depletion within the metal. The extent of depletion is obviously a function of the sample thickness and is a probable reason that the bend ductility of oxidized Fe-Cr-Al alloys is dependent on sample thickness. Comparison of Task I and Task II data suggests that alloys which were brittle in 0.060 in. samples are more ductile as oxidized 10 mil sheet.

(2) Diffusion Couples

Bend tests and microhardness measurements were performed on diffusion couples as hot rolled and after holding in argon at 2300°F. Microhardness surveys could not be conducted across the cladding-substrate interface because of the porosity present after exposure. As a result, microhardness measurements were made only within the portion of the cladding which was free from porosity and at the center of the substrate. The results of microhardness measurements and bend tests are summarized in Table 32. Photographs of the bend-tested diffusion couples after exposure are presented in Figure 60.

Microhardness measurements in Table 32 indicated that all of the cladding alloys decrease in hardness during exposure. The decrease in hardness of the cladding tended to be greater on TD Ni substrates. This can be expected because of diffusion of chromium into the substrate on TD Ni composites. It is expected, however, that the major part of the hardness reduction is due to diffusion of aluminum from the cladding. Change in the substrate hardness after exposure was less than that of the cladding layer. One reason for this effect is that the substrate thickness was considerably greater than the cladding thickness so that alloy depletion in the cladding layer is not reflected in a comparable increase in substrate composition. TD Ni, however, generally increased in hardness during exposure whereas TD NiCr decreased in hardness. Furthermore, some increase in hardness of the TD Ni and TD NiCr may have occurred during hot rolling and subsequently decreased by annealing during exposure. This possibility can explain some of the variation in substrate hardness that was obtained.

Bend tests of diffusion couples as-hot-rolled and after exposure resulted in somewhat surprising behavior. Table 32 shows that separation of the cladding and substrate occurred in several of the as-fabricated bend samples on the tension side of the specimen. This may have been due, in part, to the location of the as-fabricated bend samples in the hot-rolled composite. These samples were sectioned from the ends of the hot-rolled composite where bonding may not have been continuous. However, this was likely only for the F18/TD NiCr specimen which separated on both sides during bend testing. The remaining three failures of as-fabricated bend samples were probably the result of limited interdiffusion during hot rolling.

In spite of the extensive porosity at the interface, only one separation of the cladding and substrate occurred on exposure samples. This separation occurred on the compression side of the F16/TD Ni composite as shown in Figure 60. The nature of the separation of the F16/TD Ni sample indicated that it was due to incomplete bonding at one end of the sample which was propagated by the bend test. This is supported by the tendency of

as-fabricated samples to fail on the tension side. Thus, the porosity apparent in the microstructures in Figure 52 through 58 did not result in separation of the cladding from the substrate.

d. Microprobe Examination

(1) Furnace Oxidation Specimens

Oxidation samples of selected alloys were examined in the electron microprobe in both the as-fabricated and oxidized condition. Because of the number of samples examined, extensive analysis was not possible on any of the alloys. Microprobe examination normally consisted of a single scan across the sample for each of the major and minor elements in the alloy. The minor alloying elements could not always be detected because of their low concentration. Minor alloying elements were normally only detected in alloys in which these additions were concentrated in intermetallic compounds or at the surface. Definition of aluminum was also limited in some cases because of a relatively high detection limit of 1-2 w/o in the cladding alloys. This is because of high absorption of low energy aluminum radiation of the alloy resulting in a low intensity for aluminum.

A summary of the microprobe data for as-fabricated cladding alloys is presented in Table 33. In accordance with the contract requirements, 8 of the 18 cladding alloys were examined in the as-fabricated condition. Alloys selected and approved for examination included the alloys which were also scanned in more detail in the oxidized condition and/or were used for interdiffusion studies. Alloy F18 (1.25Ta) represents the latter case. An attempt was made to include any metallographically visible precipitates in the microprobe scans. Subsequently, some additional microprobe analysis was conducted on some of these precipitates to provide some indication of their composition.

Both of the Fe-Cr-Al-Y alloys (F14, F23) exhibited peaks in the Y scan. These results demonstrate that the solubility of Y in Fe-20Cr-4Al is less than 0.25 w/o; the metallography of as-fabricated alloys suggested that the Y solubility is less than 0.15 w/o. The peaks in the Y scan were distinct, but not as strong as the Th peaks obtained in scans of alloys F20, F31, and NA13. Obviously, the intensity of the peaks depends upon the scanning rate, atomic number, and particle size, as well as the composition of the particles. Peaks in the Y scan were coincident with a decrease in intensity of both Fe and Cr, but had no apparent effect on the Al intensity. This suggests that the particles may be a complex Fe-Cr-Y intermetallic compound and not Fe_9Y as might be expected. If the particles were Fe_9Y, the intensity of the iron scan in the particles should increase, since the concentration of iron in Fe_9Y is greater than that of the solid-solution matrix. These results, however, are only qualitative because of the limited microprobe work that was performed.

Microprobe examination of the two Fe-Cr-Al alloys containing Ti additions (F16 and F28) and the Fe-Cr-Al containing Ta (F18) indicated that both of these alloys were solid solutions. The intensity of both major and minor elements in these alloys was uniform across the samples.

Examination of the two Fe-Cr-Al alloys containing Th (F29, F31) and NA13 resulted in strong peaks in the Th scan for all three alloys. The Th solubility limit was also exceeded in these alloys. The change in intensity at these precipitation sites was considerably greater than for the Y peaks in Fe-Cr-Al alloys. This may have been due to composition and larger particles, as well as the higher atomic number of Th. As in Fe-Cr-Al-Y alloys, Th peaks were also associated with a minor decrease in Fe and Cr intensity, as expected. These decreases, however, were not sufficient to suggest that the particles were thorium-rich. Rather, the relative intensities of the precipitates and matrix suggested that the particles were complex Fe-Cr-Th intermetallic compounds. In contrast, the Th peak in NA13 was associated with a much greater decrease in Cr intensity in comparison to that of Ni. Thus, the particles in NA13 appeared to be a Ni-Th compound. Again, these observations are qualitative since no quantitative measurements could be attempted.

The results of electron microprobe examination of oxidation samples after exposure are summarized in Table 34. A total of 18 approved samples were examined in the oxidized condition. The specimen selected for analysis consisted of the alloys with the best oxidation resistance and were intended to indicate any detectable influence of exposure time on the compositional profile. Accordingly, the microprobe specimens were concentrated on Fe-Cr-Al-Y, Fe-Cr-Al-Th, and Ni-Cr-Al-Th alloys. As in as-fabricated samples, the majority of the analysis consisted of a single scan across the specimen.

The microprobe examination revealed that all Fe-Cr-Al alloys developed a well-defined Al-rich surface oxide. This has been reported previously as the reason for the good oxidation resistance of Fe-Cr-Al alloys.[3] An attempt was made to compare the Al surface peak width qualitatively with the oxide thickness measured metallographically. It was recognized that the peak width obtained by the microprobe scan tends to be greater than the actual thickness of the surface oxide due to scattering effects. Although the Al peak width tended to increase with increasing exposure time, especially in the time interval 100-400 hr, the peak intensity did not increase significantly with time. Thus, it appears that the surface layer did not increase in aluminum concentration after 100 hr. The thickness of the Al_2O_3-rich oxide layer estimated from the microprobe scans is included in Table 34. These measurements were made at the base of the Al surface peak, and compare reasonably well with the oxide thickness of Fe-Cr-Al alloys in Table 29.

All of the Fe-Cr-Al-Y alloys (F14, F22, F23) were ex-
amined at 100, 400, and 800 hr, except the 400-hr F23 sample. In
general, the microprobe scan indicated very little change with
increasing time, except that the width of the Al_2O_3 surface peak
increased from 100 to 400 hr. All of the samples exhibited a
decrease in the Fe, Cr, and Y intensity in the region of the Al
surface peak. Furthermore, the intensity of Fe, Cr, and Y gener-
ally remained constant across all of the samples, with one ex-
ception. The F22 samples exposed 800 hr had a minor increase in
chromium and a decrease in iron intensity just beneath the Al-rich
surface layer. A similar tendency was suggested by the microprobe
scans for the F14 sample after 800 hr, but not the F23 specimen.
This effect is not surprising if it is recalled that the Fe-Cr-Y-Al
alloys developed a green discoloration after about 700 hr. Thus,
it appears that the green discoloration was due to chromium oxide
resulting from Cr diffusion through the oxide layer. The increase
in chromium intensity therefore suggests that a slightly chromium-
rich oxide was developed beneath the Al_2O_3 surface layer after
about 700 hr.

In no case was any significant Y concentration observed
in any of the oxidized samples. The Y-containing precipitates
observed in as-fabricated alloys could not be detected after
100 hr, nor after subsequent exposure. These results suggest
that the Fe-Cr-Y precipitates were dissolved, presumably because
of a depletion of Y in solid solution due to migration to the
surface oxide. In no case, however, was any Y concentration
observed in the oxide layer in any of the samples. Thus, the
role of Y in improving the oxidation resistance could not be as-
certained from the microprobe data.

A limited study of particles present in metallographic
samples was attempted for Y-containing alloys. This was accom-
plished by locating the particles in the electron image and con-
ducting a spectral scan for the constituents of the alloys in the
particles and in the adjacent matrix. Spectral scans were con-
ducted on the Y-containing particles in as-fabricated alloy F23
and on one of the widely scattered oxide particles in the F23
sample oxidized 800 hr. The spectral scan of the intermetallic
particles in F23 showed that Fe, Cr, and Y were present. The Fe
and Cr intensity in the precipitate was only slightly lower in
the particles than in the matrix. In contrast, the oxide particles
were devoid of Y and contained only Fe, Cr, and Al. Thus, the
spectral scans verified the previous results in that the Y-
containing precipitates were not present in oxidized couples. In
both cases, however, the particles that could be examined were so
small that there was some doubt about the results obtained.

Samples of alloy F16 (0.5Ti) were examined after 100
and 320 hr, although the latter specimen was completely oxidized.
As for Y-containing alloys, an Al surface peak was observed on
the 100 hr sample, but could not be detected in the fully oxidized
specimen. This may have been due to spalling of the outer oxide

54

since an Fe-rich layer existed at the surface. A minor increase in Ti concentration was detectable beneath the Al-rich surface layer after 100 hr of oxidation exposure.

In contrast to Fe-Cr-Al-Y alloys, alloys F30 (0.3Th) and F31 (0.3Th, 0.5Ta) retained the Th peaks observed in the as-fabricated alloys. This may have been because of a much slower diffusion rate of Th than Y in the alloys. These peaks were not as strong in Fe-Cr-Al alloys as the Th peaks in Ni-Cr-Al alloys. The F30 alloy did not have an Al surface peak at either 100 or 400 hr. It is not known if this was because of spalling of the outer oxide or metallographic preparation. This alloy, however, failed earlier than the other Fe-Cr-Al-Th alloys so that spalling of the outer oxide may have occurred. In contrast, the F31 (0.3Th, 0.5Ta) alloy had an Al surface peak at both 100 and 400 hr.

Microprobe examination was conducted on the two nickel-base alloys NA16 and NA17 after 100 and 400 hr of oxidation exposure. These alloys were selected rather than NA13 because the three Task II nickel-base alloys were all removed from the oxidation test at the same time (540 hr). The selected alloys provided the maximum range of minor addition in the Ni-Cr-Al system. In contrast to Fe-Cr-Al alloys, the Ni-Cr-Al alloys did not indicate a strong Al surface peak after 100 hr, but a wide Al peak was present in samples oxidized 400 hr. In all samples where Th peaks were obtained, the intensity of these peaks was greater than in as-fabricated alloys. This suggests some agglomeration of the Th particles, which were probably internally oxidized to ThO_2. No Th peaks were detected in the scan of the NA16 alloy (0.3Th) exposed 400 hr. In the NA17 alloy (0.5Th, 1.0Ta), a Th-enriched surface layer existed just beneath the Al-rich surface oxide. This was evident in the microstructure as a thin band of fine dispersed oxide particles beneath the continuous surface oxide. Tantalum scans were not possible in alloy NA17 because of an interference of Ta L_α with Ni K_β radiation.

In general, microprobe examination did not provide an apparent reason for improvement in oxidation resistance afforded by the minor additions. Detailed analysis would be required to define the mechanism of improvement and the location of the additions after oxidation exposure. Such an analysis could not be conducted in this program.

(2) Interdiffusion Specimens

Interdiffusion samples were analyzed by the electron microprobe as hot-rolled and after interdiffusion at 2300°F. Examination of as-fabricated samples consisted of a single scan across the substrate/cladding interface. Interdiffused samples were examined by multiple scans from the external surface of the cladding to the center of the substrate.

A summary of the results of microprobe data for as-fabricated diffusion couples is presented in Table 35. The microprobe results within the cladding did not differ significantly from those obtained on as-fabricated cladding alloys. The microprobe data demonstrated a sharp change in composition across the interface indicating little interdiffusion after hot rolling. Both of the interdiffusion samples with F16 cladding exhibited a Ti peak at the cladding/substrate interface. The reason for the Ti concentration at the interface is not clear. It is possible that the Ti was concentrated at the surface prior to hot rolling the composite. This does not appear to be likely because of the surface preparation prior to fabrication of the composite. Thus, it appears that diffusion of titanium to the cladding/substrate interface occurred during preheating for hot rolling, or as a result of hot rolling. Aluminum had a similar tendency on TD NiCr substrates, although not as pronounced as Ti, as shown by the results obtained on F16/TD NiCr and F18/TD NiCr composites.

The results of microprobe examination after interdiffusion at 2300°F are summarized in Table 36 and plotted in Figures 61 through 68. Data in Table 36 are presented as the intensity of the various elements in counts/sec as a function of distance from the surface. These are observed intensities which have not been corrected for background or absorption. In diffusion couples with interfacial porosity, estimates of intensity could not be made in the zone of porosity. The intensity measurements are fairly linear over the full range of the intensity scale and, as such, represent a qualitative measure of the composition. It would be possible to calculate the composition at any given point by determining the actual composition anywhere in the scan and relating this known composition with the intensities obtained for each element. However, the intensity data do provide an equally acceptable qualitative indication of the extent of interdiffusion in the diffusion couples. Intensity data for any element in Table 36 can be compared within any given diffusion couple, but should not be compared with the intensity in another diffusion couple. Thus, for example, the intensity of Fe in the F16/TD Ni diffusion couple should not be compared with data for Fe in the F16/TD NiCr diffusion couple. This is because of possible variations in the operating parameters for the microprobe during examination of the various interdiffusion samples.

The intensities for the various elements in Table 36 are presented to a depth of 36 mils from the surface of the diffusion couples. This distance is sufficient to extend to the center of the substrate on all of the diffusion couples. Since the interdiffusion samples contained cladding on both sides, further extension of the intensity data would result in a mirror image of the data in Table 36. Three of the four diffusion couples with Fe-base cladding had porosity at the cladding/substrate interface. This is shown in Table 36 as a break in the intensity data at a

point approximating the original cladding/substrate interface. This did not happen in the scan of the F18/TD NiCr diffusion couple, although porosity was also present in this sample. Metallographic examination of this sample after microprobe examination showed that the scan had been made by chance through an area where a continuous metal path existed. Thus, the apparent absence of a porous zone in this sample was due to the location of the microprobe scan. All of the interdiffusion samples were examined unetched so that the interfacial porosity was less than that shown in the microstructures in Figures 52 through 60.

Data for the various elements in Table 36 are not corrected for background intensity, which normally is in the range of 20 to 50 counts/sec. Thus, in many cases, the intensities presented for minor elements consist only of background. These are included to provide a comparison of the intensities in cladding and substrate. For example, Th can be detected above background in TD Ni and TD NiCr when the intensity is compared to the background level of Fe-Cr-Al cladding alloys. In general, no significant conclusions can be made from the intensity data of the minor elements or, for that matter, aluminum. In most cases, minor aluminum gradients could be detected, but the low intensities obtained did not permit determination of the depth of diffusion into the substrate.

The intensity profiles for Fe, Ni, and Cr in the various diffusion couples are plotted in Figures 61 through 68. The composition gradients in F16/TD Ni and F16/TD NiCr diffusion couples after 100 hr at 2300°F are presented in Figures 61 and 62, respectively. Comparison of these composites suggests that iron diffuses more rapidly into TD Ni than into TD NiCr. In both diffusion couples, however, iron was detected at a distance greater than 20 mils from the original interface. Similarly, chromium could be detected at this distance within the TD Ni substrate in the F16/TD Ni system. However, a chromium gradient still existed in the F16/TD NiCr diffusion couple after 100 hr. Nickel appeared to diffuse into the cladding equally from either TD Ni or TD NiCr in the F16 diffusion couples.

The results of microprobe examination of F18/TD Ni and F18/TD NiCr diffusion couples after 100 hr at 2300°F are plotted in Figures 63 and 64, respectively. These results cannot be compared as readily as the F16 diffusion couples because of the thinner cladding on the F18/TD Ni diffusion couple. Again, Fe was detected at a distance greater than 20 mils from the original interface in both systems, as was Cr in the F18/TD Ni couple (Figure 63). Because of the thinner cladding, the nickel concentration within the cladding was also considerably greater in this couple. The data suggest that diffusion of Fe and Ni was more rapid with TD Ni than with TD NiCr substrates, as was observed with F16 cladding. Figure 64 shows that a minimum exists in the Cr intensity in the area of the original interface. This anomaly is probably due

to porosity in this area which reduces the Cr intensity. A similar effect is not observed in the Ni and Fe curves because the effect is obscured by the rapid change in intensity of Ni and Fe in this area.

The intensity profiles for Cr and Ni in the NA13/TD Ni and NA13/TD NiCr diffusion couples after 100 hr at 2300°F are presented in Figures 65 and 66, respectively. In both systems, the nickel concentration in the cladding was lower than that of the substrate; i.e., the nickel concentration is not equilibrated in 100 hr. As with the Fe-base cladding, chromium was detectable at greater than 20 mils from the surface. However, the rate of diffusion of Cr appears to be slower than from Fe-base cladding. Obviously, no chromium gradient existed in the NA13/TD NiCr system since both cladding and substrate originally contained 20 w/o Cr. There appeared to be a minor chromium gradient near the external surface of the NA13/TD NiCr couple (Fig. 66). This may have been due to some chromium migration to the surface, but it is likely this was due to some porosity or other defect in the microprobe scan.

Intensity data for the F18/TD Ni and NA13/TD Ni diffusion couples interdiffused for 300 hr at 2300°F is presented in Figures 67 and 68, respectively. Interdiffusion for 300 hr resulted in nearly equilibrated compositions. In the F18/TD Ni diffusion couple (Fig. 67), the Fe, Ni, and Cr intensities are nearly uniform across the scan. Minor Ni and Cr gradients were detected within the cladding of NA13/TD Ni couple. However, in both samples it appears that the Fe, Ni, and Cr concentrations could be calculated by assuming complete homogenization of the cladding and substrate.

The results of microprobe examination demonstrated that extensive interdiffusion occurred at 2300°F for all cladding/ substrate combinations. This occurred in spite of limited apparent influence on the microstructures, particularly for samples with NA13 cladding. Interdiffusion was more rapid in the systems with the greatest number of diffusing species--i.e., Fe-base claddings with TD Ni substrate in which Fe, Cr, and Ni are the diffusing species. This is because the concentration gradients were maximum in these systems. Thus, from a interdiffusion standpoint, the Ni-base alloys are preferable as cladding alloys, as expected. It is therefore possible that a composite system with Ni-base cladding may have a longer life than a composite with Fe-Cr-Al cladding, although the oxidation resistance of Fe-Cr-Al alloys alone is better. This will be discussed in more detail in Section III-B-6.

5. Fabrication of Foil Material

Six of the Task II cladding alloys were fabricated into 5-mil sheet and supplied to NASA for further evaluation as part of the contract requirements. The six alloys selected and approved were F8, F14, F22, F23, F30 and NA13, and represented three Fe-Cr-Al-Y alloys (F14, F22, F23), one Ti alloy (F8), one Th alloy (F30), and a single nickel-base alloy (NA13). Four pieces of each approved alloy with minimum dimensions of 4 x 3 in. were submitted. Two of the alloys (F8, F14) were supplied during the tenth month of contract performance on request by NASA. The remaining four alloys were fabricated after completion of the experimental program.

The fabrication schedule for fabrication of foil materials is summarized in Table 37. Arc-melted 150 g buttons of the six alloys were fabricated by the techniques used for the fabrication of the 10 mil oxidation samples in Task II. Foil material (5 mil) was obtained by simply continuing cold rolling to a sheet thickness of about 5.5 mils. It was found that two additional anneals were required in the final cold reduction from 10 to 5.5 mils. The cold-rolled material was then polished with metallographic paper to remove surface film resulting from the hot-cold rolling and/or surface defects. Finally, the 4 x 3 in. sheet samples were annealed in argon at 2150°F for 15 min. The final sheet thickness of all foil material was 5 $\pm$ 0.5 mil.

6. Discussion

The furnace oxidation tests of 10-mil samples in Task II demonstrated the superior oxidation resistance of Fe-Cr-Al alloys, particularly those containing Y. Task I oxidation results suggest that the life of unmodified Fe-25Cr-4Al would be about 100 hr at 2300°F. Thus, addition of as little as 0.15 Y resulted in at least an eight-fold increase in life. No apparent reasons for this improvement could be obtained by the analyses in this program, because the minor additions could not be detected after exposure. It was shown that Y probably migrates to the surface during oxidation exposure. This was suggested by the inability to detect the Y-containing precipitates after exposure that were present in as-fabricated alloys. In any case, Y, and the other minor alloying elements, would be expected to migrate to the oxidizing interface provided that they had sufficient mobility at 2300°F. The data in this program suggest that Ti and Y had sufficient mobility, whereas Th, and perhaps Hf and Ta, had limited mobility during exposure.

The following discussion on probable oxidation mechanisms is directed toward Fe-Cr-Al-Y alloys but applies, in general, to the other Fe-Cr-Al systems. In no case was the level of minor addition sufficient to change the basic oxidation mechanism of Fe-Cr-Al. The influence of the minor additions, therefore, consisted in their ability to improve the oxidation protection afforded

by the Al_2O_3-rich surface oxide. There appears to be little doubt
from the microprobe data that all of the Fe-Cr-Al alloys developed
an Al_2O_3-rich surface oxide. This is supported by the appearance
of the samples during oxidation testing. All of the alloys, with
the exception of Fe-Cr-Al-Hf alloys, had a thin, light gray sur-
face oxide after 100 hr. The surface oxide of Fe-Cr-Al-Hf alloys
was similar to the other alloys prior to 100 hr, but was mottled
green after 100 hr. Subsequently, most of the other alloys deve-
loped a characteristic surface appearance with further exposure.
Alloys containing Ti developed light tan oxides, whereas those
with Th additions were dark gray to black. The Y-containing alloys
retained the light gray appearance to about 700 hr, when localized
patches of green oxide developed on the surface. These observa-
tions suggest a similar mechanism in the mode of failure, exclud-
ing edge effects which are merely an acceleration of the normal
wear-out life. Edge effects will be discussed in more detail sub-
sequently.

As previously stated, there is little doubt that all of
the Fe-Cr-Al alloys developed an Al_2O_3-rich oxide very early during
oxidation exposure. Thus, the influence of the minor additions
in improving the protective capability of this oxide can only be
in (1) improving oxide adherence without changing rate of oxide
growth, or (2) reducing the rate of growth of the oxide. Ob-
viously, a single alloying addition can be effective in either or
both of these mechanisms. The second factor is related to the
first to some extent since a thin oxide will have a lesser ten-
dency to spall than a thick oxide (TD Ni is an apparent exception).
However, the rate of oxide growth is also separable since it con-
trols the amount of alloy depletion that occurs in a thin oxida-
tion sample. It is likely that Y, and perhaps Th, are influential
in both of the above factors. Hafnium, and perhaps Ti, appear to
affect only the adherence of the oxide rather than the kinetics
of oxide growth. Tantalum probably has a minor effect on the rate
of oxide growth, although the behavior is not well defined.

The mechanism of growth of the Al_2O_3-rich oxide is not
definitely known. However, it appears that it develops external
to the original interface, at least initially, by rapid diffusion
of aluminum from the substrate. This is evidenced by the nearly
complete absence of either Fe or Cr in the Al_2O_3 layer in the
microprobe scans. Subsequently, the oxide continues to grow either
by cation or oxygen diffusion through oxide layer. It is here that
the influence of the minor addition is probably most significant.
If the addition, such as Y, enters the Al_2O_3 oxide structure and
reduces the rate of oxygen or cation diffusion through the oxide,
the rate of oxide growth will be substantially decreased. This
can occur either by dispersion of the minor addition throughout
the oxide or by the development of a second oxide or complex oxide
beneath the outer oxide layer. The exact mechanism is not impor-
tant since either mechanism will effectively decrease the rate of
oxide growth. The resulting surface structure is thus an effective

60

diffusion barrier to uphill diffusion of aluminum from the substrate. This is verified by the oxide thickness (metal recession) of Fe-Cr-Al-Y alloys measured metallographically and presented in Table 29.

Edge oxidation is merely an acceleration of depletion of the substrate of aluminum by growth of the Al_2O_3-rich oxide. A relatively simple calculation will show that the growth of a uniform Al_2O_3 layer 0.2 mil thick requires about 25% of the aluminum present in the 2 x 0.5 x 0.010 in. oxidation sample. Obviously, depletion is greater at edges and corners where the unit volume of metal per unit area of surface is lower. Consequently, any defects in the oxide layer, which are more probable in these areas, results in the exposure of an Fe-Cr alloy significantly depleted in aluminum. Thus, it is not surprising that corners were generally the initial area of failure of Fe-Cr-Al alloys which did fail prior to 800 hr. The tendency of Fe-Cr-Al-Y alloys to be resistant to edge attack demonstrates the minimal Al depletion and/or continuity of the oxide layer on these alloys.

The oxidation mechanism of Ni-Cr-Al alloys differs somewhat from that of Fe-Cr-Al alloys. Although there is a tendency toward Al_2O_3 enrichment of the oxide in Ni-Cr-Al alloys, the Al_2O_3 layer is neither well defined nor as readily formed. This is probably due, in part, to a slower diffusion rate of aluminum in the Ni-Cr solid solution. There is some evidence to support this possibility since iron-base alloys can be aluminized at faster rates than nickel-base alloys, at least at lower temperatures. The oxides developed on Ni-Cr-Al alloys are not as adherent so that these alloys undergo a series of stages of oxide growth followed by spalling. As a result, depletion effects are of lesser importance to the failure mechanism in Ni-Cr-Al alloys. Furthermore, since the Ni-Cr-Al alloys initially contained 5 w/o Al, an additional reservoir of aluminum was available for development of the oxide. In any case, the Ni-Cr-Al alloys tended toward a uniform metal recession rate in comparison to Fe-Cr-Al alloys.

The above discussion suggests that more difficulties might be encountered with Fe-Cr-Al alloys than with Ni-Cr-Al cladding in composite systems. Diffusion of Al into the substrate will cause further depletion of Al from the cladding. Furthermore, the oxidation resistance of the cladding under stress may be considerably different from that obtained in the furnace oxidation test because of fracture of the Al-rich oxide layer. The above discussion does indicate that Fe-Cr-Al alloys may be self-healing provided that a sufficient reservoir of Al is available. Thus, it is likely that Fe-Cr-Al-Y alloys will be more subject to failure under load after some period of exposure at elevated temperature.

The basic oxidation resistance of the cladding alloys developed in this program is not the only factor limiting the usefulness of composite systems. Rather, the extensive interdiffusion obtained is of equal concern. Interdiffusion during exposure will be detrimental to the composite system if one or more of the following conditions prevails:

(1) Interfacial porosity causes spalling of the cladding layer because of thermal or mechanical stresses.

(2) Interdiffusion lowers the mechanical properties of the substrate.

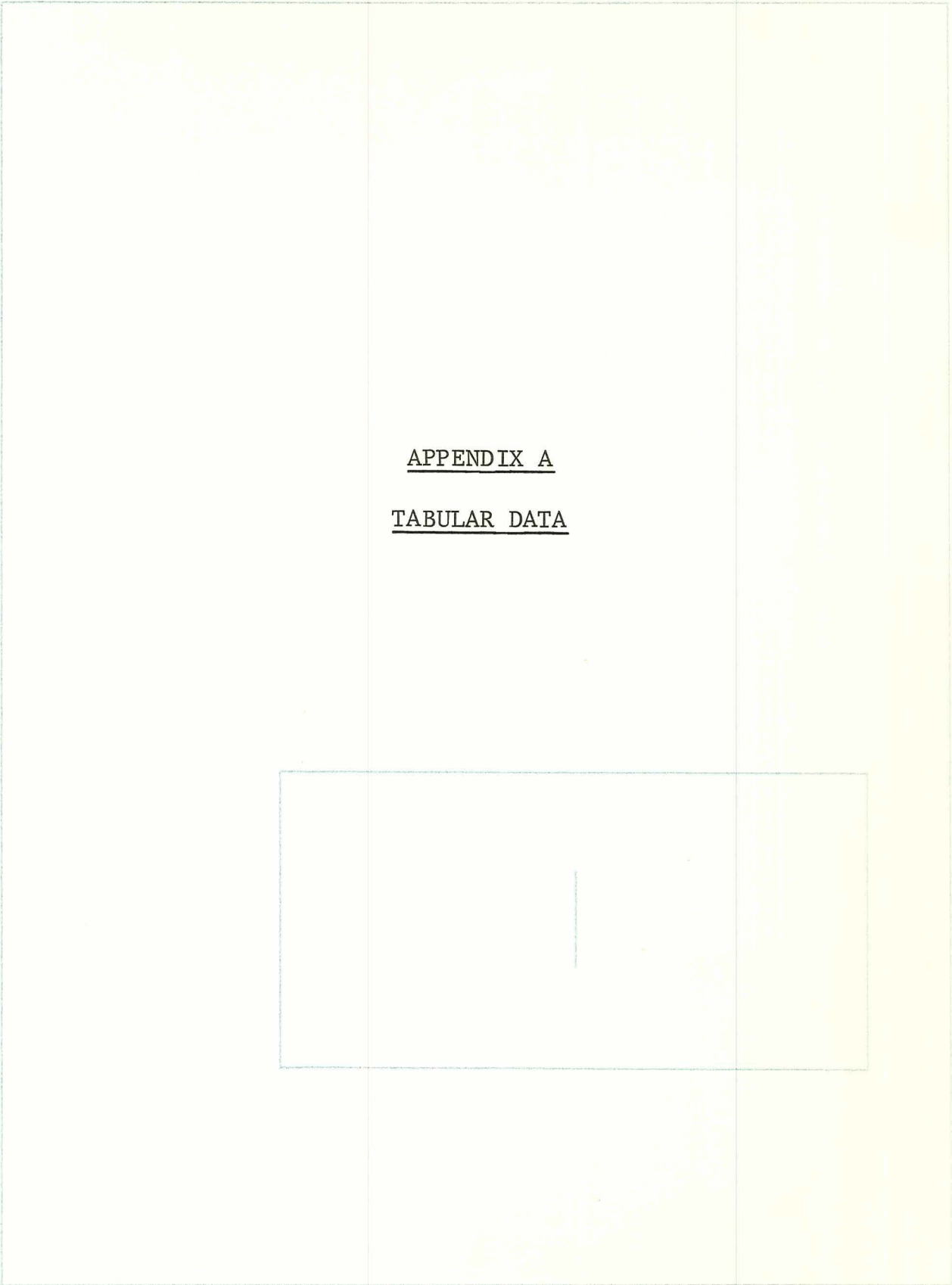(3) Interdiffusion reduces the oxidation resistance of the cladding alloy.

In this program, only the first of the above conditions was evaluated. Bend tests demonstrated that spalling of the cladding was not likely even with the extensive porosity that prevailed with Fe-Cr-Al cladding alloys. Thus, spalling of the ductile cladding layer does not appear to be the limiting factor in the life of a clad TD Ni or TD NiCr composite system. It is more likely that the life of the composite system will be determined by one, or both, of the remaining conditions.

The influence of interdiffusion on mechanical properties appears to be controlled by the cladding/substrate system under consideration. No data are available on influence of iron on the long-time elevated temperature mechanical properties of TD Ni materials. However, the maximum influence on mechanical properties can probably be expected from interdiffusion of iron-base cladding alloys. The minimal change in mechanical properties should be obtained with Ni-Cr-Al cladding on TD NiCr. These judgments are based simply on the minimal change in the composition of the substrate by interdiffusion of the major alloying elements. However, it is not known if diffusion of iron will be more detrimental, for example, than development of the internal porosity in TD NiCr during oxidation exposure. At this point, no conclusion can be made concerning the role of the minor alloying elements and aluminum. It is further possible that additional effects not considered in the initial analysis, such as agglomeration of the ThO_2, may be important during long exposure periods at elevated temperature. No effects of this type, however, were observed in this program.

The influence of interdiffusion on the oxidation resistance of the cladding alloy is likely to provide the greatest limitation on the life of a composite system. Furthermore, this may well be the result of diffusion of Al, which could not be determined by the microprobe data in this program. Depletion of alloy constituents was evaluated in the oxidation tests of 10-mil samples in Task II, as discussed previously.

In the composite system the effect of alloy depletion will be greater than in the cladding alloys alone because of the possibility of diffusion into the substrate. This does not necessarily imply that the oxidation life of the composite can be predicted on the basis of interdiffusion data alone. The mechanism of diffusion will be considerably different in an oxygen environment. There is little doubt that Al and Y will diffuse to the oxidizing interface rather than into the substrate in the presence of oxygen. An Fe-Cr-Al-Y cladding will therefore develop the protective outer oxide in spite of changing composition of the cladding by diffusion of nickel. Consequently, the basic protective mechanism of the Fe-Cr-Al alloy will be operative for some exposure period. The cladding alloy will be protective until the composition beneath the oxide is changed by interdiffusion to the degree that the basic Fe-Cr-Al oxidation mechanism is no longer operative. It is quite possible that this exposure time will be somewhere between the oxidation life of the cladding and the projected life suggested by interdiffusion. Similar effects can be expected with Ni-Cr-Al cladding alloys. Thus, the inter-diffusion data in this program cannot be projected into an es-timated life of a composite system in an oxygen environment.

The use of diffusion barriers is an obvious solution to interdiffusion problems. Oxidation data in this program de-monstrate that oxides are among the best diffusion barriers for the metal cations in the cladding and substrate. It is possible that other barrier systems could also be effective. These possi-bilities include refractory metals or multiple cladding layers whose compositions are adjusted to minimize concentration gra-dients across the cladding/substrate interface. An example of the multiple system might be Fe-Ni-Cr interlayer between an Fe-Cr-Al cladding and TD NiCr. Obviously, diffusion barriers are necessary only if interdiffusion results in a short life of the composite systems. In this event, the potential composite system developed in this program may be applicable to temperatures below 2300°F where interdiffusion should be a lesser problem. Accordingly, the composite systems developed in this program should be inves-tigated in air environments at 2100° to 2300°F to determine the effects of interdiffusion on the mechanical properties and oxidation life.

V. CONCLUSIONS AND RECOMMENDATIONS

The major objective of this program--to develop oxidation-resistant cladding alloys capable of operating several hundred hours at 2300°F--has been met. Oxidation lives greater than 500 hr were obtained as simulated 5 mil cladding in three systems: Fe-25Cr-4Al-Y, Fe-25Cr-4Al-Th, and Ni-20Cr-5Al-Th. All of these alloys are ductile (at least, in thin sections) and fabricable by conventional hot and cold rolling into thin sheet material.

Work conducted in this program, however, was inadequate to define the life of these alloys in a composite system. Additional work is required to define the potential life of the cladding/substrate systems in oxidation environments.

The results obtained in this program provide the following conclusions:

(1) The most oxidation-resistant alloys developed were Fe-25Cr-4Al with Y additions of 0.15 to 0.25 w/o. Higher Y additions may be applicable, but the alloys may tend to be brittle at room temperature after exposure. The quaternary addition of 0.5Ta to a 0.08Y alloy provided ductility before and after exposure. The other Fe-Cr-Al alloys were ductile as-fabricated, but not after oxidation exposure.

(2) Iron-base alloys with 0.5 w/o Th additions were the next most oxidation resistant alloys. Ni-20Cr-5Al alloys with Th additions are also potential cladding alloys for TD Ni and TD NiCr.

(3) The oxidation resistance of Fe-Cr-Al alloys depends upon the development of an Al_2O_3-rich surface oxide layer. Minor additions probably improve the oxidation resistance by modification of the transport properties of this oxide. Ni-Cr-Al alloys also tend to develop Al_2O_3 layers, but the rate of growth is greatly reduced. The oxidation mechanism of Ni-Cr-Al alloys consists of slow metal recession, in contrast to abrupt failure of Fe-Cr-Al alloys.

(4) Rapid interdiffusion occurs at 2300°F in Fe-Cr-Al and Ni-Cr-Al cladding on TD Ni and TD NiCr substrates. After 300 hr, nearly complete homogenization of the cladding and substrate constituents occurs. The results of interdiffusion, such as interfacial or cladding porosity, are predictable based on the composition of the cladding and substrate. Interfacial porosity due to interdiffusion does not readily result in separation of the cladding by external mechanical stresses.

Interdiffusion effects will likely result in a decrease in the composite life from that predicted by the oxidation life of the cladding alloys. In general, three distinct limiting conditions can result from interdiffusion:

(1) Interfacial porosity results in separation of the cladding by mechanical and/or thermal stresses.

(2) Interdiffusion lowers the mechanical properties of the substrate.

(3) Interdiffusion reduces the protective life of the cladding.

In this program, only the first condition was evaluated and found to be no major problem. It is recommended that the remaining conditions be evaluated by additional work. These studies should be conducted in air environments in order to provide the most practical information. In this program, composites were exposed in argon at 2300°F to isolate interdiffusion effects. The influence of interdiffusion on mechanical properties could be evaluated in inert atmospheres. However, it is possible that a difference in behavior will be obtained in oxygen environment because of a different interdiffusion mechanism in atmospheres containing oxygen. Furthermore, the evaluation of composite systems should be conducted below 2300°F since interdiffusion rates are strongly temperature dependent. Thus, an acceptable life may be obtained for a composite system at 2100°-2200°F based on the cladding alloys developed in this program.

It is further recommended that potential diffusion barriers be investigated. If an effective barrier system can be developed, the life of a composite system should approach the oxidation life of the cladding.

REFERENCES

1. Anonymous, High Temperature, High Strength Nickel Base Alloys, International Nickel Company, 1966.

2. Anonymous, Kanthal Handbook, Kanthal Corporation, 1953.

3. O. Kubaschewski and B. E. Hopkins, Oxidation of Metals and Alloys, Academic Press, Inc., New York, 1962, p. 237.

4. M. Hansen, Constitution of Binary Alloys, McGraw-Hill, New York, 1958, p. 563.

5. R. P. Elliott, Constitution of Binary Alloys, First Supplement, McGraw-Hill, New York, 1965, p. 362.

APPENDIX A

TABULAR DATA

TABLE 1

COMPOSITION OF ALLOYS SELECTED FOR TASK I OXIDATION TESTS

Desig-	Nominal Composition, w/o					
nation	Fe	Ni	Cr	Al	Ta	Other *
F1	71.0	--	25.0	4.0	--	--
F2	70.57	--	25.0	4.0	--	0.43 Y
F3	70.96	--	25.0	4.0	--	0.043Be
F4	70.88	--	25.0	4.0	--	0.12Mg
F5	70.32	--	25.0	4.0	--	0.68Ce
F6	70.34	--	25.0	4.0	--	0.66La
F7	69.94	--	25.0	4.0	--	1.06Th
F8	70.77	--	25.0	4.0	--	0.23Ti
F9	70.56	--	25.0	4.0	--	0.44Zr
F10	70.15	--	25.0	4.0	--	0.85Hf
F11	70.15	--	25.0	4.0	0.85	--
F12	70.87	--	25.0	4.0	--	0.13Si
F13	70.65	--	25.0	4.0	--	0.35Ge
M3	57.5	--	35.0	7.5	--	--
NA1	--	79.0	16.0	5.0	--	--
NA2	--	75.0	20.0	5.0	--	--
NA3	--	74.59	20.0	5.0	--	0.41Y
NA4	--	74.89	20.0	5.0	--	0.11Mg
NA5	--	74.36	20.0	5.0	--	0.64Ce
NA6	--	74.37	20.0	5.0	--	0.63La
NA7	--	73.99	20.0	5.0	--	1.01Th
NA8	--	74.78	20.0	5.0	--	0.22Ti
NA9	--	74.19	20.0	5.0	--	0.81Hf
NA10	--	74.87	20.0	5.0	--	0.13Si
NA11	--	74.67	20.0	5.0	--	0.33Ge
NA12	--	74.95	20.0	5.0	--	0.041Be
M1	20.0	58.85	20.0	--	--	1Mn, 0.15La
M2	--	70.0	20.0	5.0	5.0	--
NT1	--	75.0	20.0	--	5.0	--
NT2	--	70.0	20.0	--	10.0	--
NT3	--	65.0	20.0	--	15.0	--
NT4	--	70.0	25.0	--	5.0	--
NT5	--	65.0	25.0	--	10.0	--
NT6	--	60.0	25.0	--	15.0	--
NT7	--	62.5	27.5	--	10.0	--
NT8	--	65.0	30.0	--	5.0	--
NT9	--	60.0	30.0	--	10.0	--
NT10	--	55.0	30.0	--	15.0	--
NT11	--	57.5	32.5	--	10.0	--

TABLE 1 (Continued)

Desig-	Composition, w/o					
nation	Fe	Ni	Cr	Al	Ta	Other
NT12	--	60.0	35.0	--	5.0	--
NT13	--	55.0	35.0	--	10.0	--
NT14	--	50.0	35.0	--	15.0	--
NT15	--	52.5	37.5	--	10.0	--
NT16	--	55.0	40.0	--	5.0	--
NT17	--	50.0	40.0	--	10.0	--
NT18	--	45.0	40.0	--	15.0	--
NT19	--	64.63	25.0	--	10.0	0.37Y
NT21	--	64.90	25.0	--	10.0	0.10Mg
NT22	--	64.42	25.0	--	10.0	0.58Ce
NT23	--	64.43	25.0	--	10.0	0.57La
NT24	--	64.09	25.0	--	10.0	0.91Th
NT25	--	64.80	25.0	--	10.0	0.20Ti
NT26	--	64.63	25.0	--	10.0	0.37Zr
NT27	--	64.27	25.0	--	10.0	0.73Hf
NT28	--	64.88	25.0	--	10.0	0.12Si
NT29	--	64.70	25.0	--	10.0	0.30Ge

*All additions were 0.25 a/o, except in M1.

TABLE 2

ANALYSES OF MAJOR RAW MATERIALS USED FOR ALLOY FABRICATION

| Element | Raw Material (Vendor, Grade) Analysis, w/o | | | | |
	Iron (Glidden Co., A-104B)	Chromium (Shieldalloy Corp., H.P. flakes)	Nickel (Sherritt & Gordon Ltd., SG-100)	Tantalum (Kawecki Chem., arc-melted ingot)	Aluminum (UMC Corp., H.P. wire)
Fe	99.94	<0.0002	0.04	0.005	--
Ni	0.001	--	99.85 (min)	--	--
Cr	0.001	99.9 (min)	--	--	--
Co	0.001	--	0.08	--	--
Al	<0.001	<0.0002	--	0.005	99.999
Ta	<0.001	--	--	99.9	--
C	0.002	0.001	0.008	0.005	--
Mn	0.0015	--	--	--	--
Si	0.003	<0.001	--	0.03	--
S	0.003	0.003 (max)	0.003	--	--
P	0.002	--	--	--	--
O	0.013	0.06 (max)	--	0.015	--
N	0.002	0.003 (max)	--	0.005	--
H (loss)	0.04	0.006 (max)	--	0.001	--
Others	Cu 0.004	Cu 0.0002	Cu 0.006	Cb 0.01	--
	Mo <0.004	Pb <0.0002			
	All Others <0.001		All Others <0.001		

TABLE 3

TYPICAL COMPOSITIONS OF MINOR ALLOYING ELEMENTS

Element	Vendor	Purity	Form
Ce	Lunex Co.	99.9+	Ingot
La	Lunex Co.	99.9+	Ingot
Ti	UMC Corp.	99.9	Sponge
Zr	UMC Corp.	99.9	Sponge
Hf	UMC Corp.	99.7+	Sponge
Th	UMC Corp.	99.99	Crystal bar
Mg	UMC Corp.	99.97	Granules
Mn	UMC Corp.	99.99	Flake
Si	UMC Corp.	99.999	Ingot
Ge	UMC Corp.	99.999	Ingot

TABLE 4

WEIGHT LOSS OF TASK I ALLOYS DURING ARC MELTING

Alloy Designation	Percent Weight Loss	Alloy Designation	Percent Weight Loss	Alloy Designation	Percent Weight Loss
F1	0.25	NT7	0.13	NT28	0.07
F2	0.72	NT8	0.05	NT29	0.11
F3	0.13	NT9	0.06	NA1	0.09
F4	0.62	NT10	0.11	NA2	0.09
F5	0.52	NT11	0.12	NA3	0.28
F6	0.42	NT12	0.08	NA4	0.26
F7	0.50	NT13	0.06	NA5	0.15
F8	0.46	NT14	0.13	NA6	0.37
F9	0.32	NT15	0.11	NA7	0.75
F10	0.64	NT16	0.06	NA8	0.02
F11	0.38	NT17	0.06	NA9	0.13
F12	0.57	NT18	0.16	NA10	0.23
F13	0.26	NT19	0.32	NA11	0.17
NT1	0.07	NT21	0.52	NA12	+0.004
NT2	0.10	NT22	0.28	M1	0.62
NT3	0.15	NT23	0.22	M2	0.13
NT4	0.11	NT24	1.25, 0.14[*]	M3	0.49
NT5	0.08	NT25	0.06		
NT6	0.08	NT26	0.32		
		NT27	0.50		

[*] Percent weight loss of the second heat.

TABLE 5

OXIDATION RATE OF Fe-Cr-Al ALLOYS DURING CYCLIC FURNACE EXPOSURE AT 2300°F

Alloy Desig-nation	Weight Change, mg/cm^2									
	20 hr		40 hr		60 hr		80 hr		100 hr	
	Total*	Sample+	Total	Sample	Total	Sample	Total	Sample	Total	Sample
F1	9.45	-6.15	12.40	-10.60	15.50	-13.10	21.50	-10.20	24.00	-9.25
F2	1.60	1.36	2.38	1.71	2.65	1.96	3.24	2.24	3.50	2.35
F3	4.50	-3.02	6.06	-4.72	7.94	-6.18	9.68	-6.58	12.10	-6.94
F4	10.75	-6.63	13.60	-11.70	16.90	-13.80	23.40	-9.45	25.30	-8.97
F5	9.70	4.50	12.70	3.50	16.80	-2.97	20.00	-4.91	23.40	-5.74
F6	4.30	3.55	8.94	7.97	13.70	12.60	18.40	17.30	22.40	20.70
F7	1.74	1.37	3.06	1.73	3.48	1.92	4.36	2.18	4.67	2.26
F8	1.44	0.94	1.76	0.85	2.10	0.87	2.42	0.68	2.82	0.52
F9	12.25	10.60	14.40	10.90	16.00	13.50	17.50	14.60	18.60	15.50
F10	4.82	4.47	6.17	5.50	6.63	5.87	7.29	6.15	7.56	6.18
F11	3.50	-0.58	4.22	-2.43	5.51	-2.38	6.34	-3.36	7.52	-4.32
F12	8.89	-2.56	11.80	-1.28	18.60	-0.64	20.40	-2.07	21.70	-3.80
F13	10.02	-6.69	13.00	-11.10	16.00	-13.50	21.80	-10.80	25.10	-9.73
M3	7.81	-5.63	9.83	-7.34	11.40	-8.35	13.50	-9.40	15.40	-10.70

*Total (sample + spall products) weight change.

+Sample weight change.

TABLE 6

OXIDATION RATE OF Ni-Cr-Al ALLOYS DURING CYCLIC FURNACE EXPOSURE AT 2300°F

Alloy Designation	Weight Change, mg/cm²									
	20 hr		40 hr		60 hr		80 hr		100 hr	
	Total*	Sample+	Total	Sample	Total	Sample	Total	Sample	Total	Sample
NA1	6.47	-8.03	8.16	-11.10	10.90	-15.20	14.10	-20.40	17.00	-24.50
NA2	6.20	-7.23	7.62	-10.40	10.30	-13.30	12.60	-17.30	14.80	-21.10
NA3	4.48	-2.94	7.31	-1.13	11.20	2.08	15.00	4.86	19.10	7.40
NA4	7.75	-10.75	9.08	-12.50	11.60	-15.10	13.30	-17.80	15.00	-21.00
NA5	Specimen could not be fabricated.									
NA6	8.00	4.17	12.00	5.79	15.50	6.26	19.40	4.69	23.30	-0.36
NA7	2.53	-1.13	3.29	-2.01	4.49	-3.02	5.51	-3.82	6.08	-4.69
NA8	9.52	-13.00	11.70	-16.40	14.00	-19.80	16.20	-23.60	18.80	-28.10
NA9	5.34	-7.20	6.80	-9.58	8.03	-12.00	9.52	-13.90	10.60	-15.50
NA10	7.73	-10.90	9.29	-14.00	11.70	-17.80	13.80	-21.40	15.80	-24.30
NA11	9.22	-13.10	10.70	-15.00	13.10	-18.80	15.40	-22.40	17.80	-26.00
NA12	8.33	-11.40	9.85	-15.30	12.40	-19.40	15.20	-24.20	17.80	-29.60
TD NiCr	1.23	-0.21	1.60	-0.74	2.04	-1.67	2.53	-2.52	2.90	-3.34
M1	33.10	-84.10	44.50	-111.00	46.00	-114.00	48.50	-120.00	52.00	-129.00

*Total(sample + spall products) weight change.
+Sample weight change.

TABLE 7

OXIDATION RATE OF Ni-Cr-Ta ALLOYS DURING CYCLIC FURNACE EXPOSURE AT 2300°F

Alloy Desig- nation	Weight Change, mg/cm^2									
	20 hr		40 hr		60 hr		80 hr		100 hr	
	Total *	Sample +	Total	Sample	Total	Sample	Total	Sample	Total	Sample
NT1	21.6	-53.3	31.7	-83.5	38.6	-91.5	50.8	-123.0	64.3	-143.0
NT2	33.4	-96.7	40.2	-115.0	46.6	-139.0	64.7	-195.0	76.4	-236.0
NT3	41.75	-129.0	48.4	-156.0	54.7	-170.0	71.6	-250.0	92.2	-317.0
NT4	11.35	-14.5	16.1	-21.9	20.4	-29.2	26.5	-41.7	33.0	-58.4
NT5	20.6	-45.3	28.2	-62.5	32.0	-75.7	38.5	-96.1	47.4	-118.0
NT6	33.7	-87.5	42.2	-122.0	48.5	-129.0	63.4	-186.0	80.5	-235.0
NT7	19.1	-36.5	25.1	-53.2	29.7	-63.4	36.9	-83.0	44.8	-101.0
NT8	13.7	-15.7	18.7	-27.0	22.5	-34.2	27.3	-40.6	32.7	-51.9
NT9	18.3	-33.0	23.8	-49.8	28.8	-57.4	35.0	-70.3	42.2	-85.3
NT10	24.7	-40.2	29.0	-62.4	37.3	-72.0	46.7	-87.9	59.8	-123.0
NT11	17.7	-29.3	23.4	-47.3	29.7	-58.5	36.1	-67.8	42.1	-83.8
NT12	13.8	-15.9	18.9	-23.3	23.9	-30.9	28.8	-44.7	33.7	-53.0
NT13	17.5	-26.2	23.0	-41.0	29.5	-50.7	36.1	-56.0	41.7	-64.3
NT14	Melted									
NT15	22.1	-27.7	28.1	-38.6	34.0	-43.6	40.3	-48.8	47.0	-49.2
NT16	16.2	-22.0	22.6	-31.2	27.1	-39.5	32.1	-47.3	37.1	-57.5
NT17	28.9	-17.2	33.1	-28.8	40.8	-29.0	46.3	-32.6	51.6	-34.3
NT18	Melted									
NT19	12.0	-20.2	16.9	-32.7	22.0	-37.6	27.2	-47.8	33.1	-63.7

TABLE 7 (Continued)

Alloy Desig-nation	Weight Change, mg/cm^2									
	20 hr		40 hr		60 hr		80 hr		100 hr	
	Total	Sample	Total	Sample	Total	Sample	Total	Sample	Total	Sample
NT21	17.9	-34.3	24.1	-49.3	28.2	-69.6	37.1	-83.8	47.7	-115.0
NT22	48.6	-121.5	104.0	-70.4	137.0	-37.9	Complete Oxidation 60 hr			
NT23	9.63	-15.7	12.2	-22.2	18.4	-21.3	23.7	-23.5	32.3	-40.6
NT24	11.1	-22.4	13.9	-32.0	17.8	-37.5	21.3	-43.5	26.3	-53.4
NT25	17.6	-34.4	22.7	-46.4	27.2	-65.3	34.6	-81.5	42.9	-106.0
NT26	20.3	-38.2	26.8	-47.3	32.0	-63.8	40.2	-80.2	50.9	-105.0
NT27	24.8	-58.7	31.2	-75.9	34.6	-99.0	43.4	-114.0	51.9	-146.0
NT28	14.8	-33.4	18.7	-44.1	22.2	-53.5	26.6	-62.8	32.3	-78.0
NT29	14.9	-29.2	19.5	-42.0	22.9	-53.5	31.2	-69.3	36.7	-90.0

*Total(sample + spall products) weight change.

+Sample weight change.

TABLE 8

NOMINAL COMPOSITION OF MODIFIED TASK I ALLOYS

| Designation | Composition, w/o | | | | |
	Fe	Ni	Cr	Al	Other
F14	70.75	-	25.00	4.00	0.25Y
F15	70.85	-	25.00	4.00	0.15Ti
F16	70.50	-	25.00	4.00	0.50Ti
F17	70.50	-	25.00	4.00	0.50Hf
F18	69.75	-	25.00	4.00	1.25Ta
F19	70.50	-	25.00	4.00	0.50Ta
F20	70.50	-	25.00	4.00	0.50Th
F21	70.35	-	25.00	4.00	0.65Y
NA13	-	74.50	20.00	5.00	0.50Th
NA14	-	74.40	20.00	5.00	0.60Hf
NA15	-	74.00	20.00	5.00	1.00Ta

TABLE 9

WEIGHT LOSS OF MODIFIED TASK I ALLOYS
DURING ARC MELTING

Alloy	Percent Weight Loss
F14	0.10
F15	0.11
F16	0.09
F17	0.05
F18	0.03
F19	0.09
F20	0.24
F21	0.12
NA13	0.02
NA14	0.29
NA15	0

TABLE 10

OXIDATION RATE OF MODIFIED TASK I ALLOYS DURING CYCLIC FURNACE EXPOSURE AT 2300°F

Alloy Desig- nation	Weight Change, mg/cm^2									
	20 hr		40 hr		60 hr		80 hr		100 hr	
	Total*	Sample+	Total	Sample	Total	Sample	Total	Sample	Total	Sample
F14	1.88	1.18	2.26	1.45	2.85	1.70	3.18	1.89	3.43	2.03
F15	1.20	0.93	1.54	1.03	1.81	1.14	1.82	1.17	2.19	1.33
F16	1.84	1.10	2.34	1.38	2.84	1.55	3.15	1.65	3.36	1.73
F17	3.44	3.22	3.76	3.55	4.21	3.80	4.30	3.95	4.88	4.37
F18	3.17	-0.12	3.71	-1.78	5.12	-1.75	5.90	-2.20	6.35	-2.57
F19	3.06	-0.73	4.36	-3.04	5.91	-4.10	7.33	-4.32	8.40	-5.27
F20	1.29	1.08	1.59	1.15	2.02	1.73	2.01	1.74	2.48	1.63
F21	1.38	1.24	1.72	1.39	2.25	1.65	2.18	1.64	2.84	2.00
NA13	2.02	-0.61	2.33	-1.13	2.84	-1.20	2.85	-1.61	3.46	-2.10
NA14	3.45	-4.47	4.02	-7.10	5.35	-7.52	5.88	-9.35	7.18	-11.1
NA15	9.36	-16.8	10.3	-17.8	12.2	-19.6	13.5	-23.4	15.4	-26.2
TD Ni	14.1	13.7	19.3	18.7	24.1	23.1	28.0	26.9	31.9	30.7
TD NiCr	1.26	0.04	1.65	-0.26	1.99	0.58	2.20	-0.97	2.31	-1.43
									0	-129.00

*Total (sample + spall products) weight change.

+Sample weight change.

TABLE 11

OXIDATION RATE OF MODIFIED TASK I ALLOYS DURING CYCLIC TORCH TESTING AT 2300°F

Alloy Desig- nation	Sample Weight Change, mg/cm^2									
	20 hr		44 hr		60 hr		84 hr		100 hr	
	Total*	Front+	Total	Front	Total	Front	Total	Front	Total	Front
F14	0.56	1.38	0.80	1.97	0.78	1.92	1.15	2.83	1.27	3.12
F15	0.19	0.47	0.25	0.63	0.19	0.48	0.46	1.16	0.45	1.13
F17	1.42	3.42	1.86	4.48	1.97	4.74	2.31	5.55	2.15	5.18
F18	-0.62	-1.53	-1.76	-4.33	-2.38	-5.86	-3.63	-8.93	-4.17	-10.3
F20	0.67	1.62	0.87	2.10	1.00	2.42	1.28	3.10	1.13	2.74
NA13	-0.22	-0.54	-0.94	-2.23	-1.45	-3.44	-2.60	-6.36	-3.50	-8.57
TD Ni	7.98	19.0	7.30	17.4	6.67	15.9	2.17	5.16	-1.42	-3.38
TD NiCr	-3.63	-8.41	-8.64	-20.0	-13.0	-30.2	-19.6	-45.5	-24.0	-55.6

* Calculated using total surface area.

+ Calculated using flame impingement front area.

TABLE 12

CHEMICAL ANALYSES OF TASK I AND MODIFIED TASK I ALLOYS

Alloy	Fe	Ni	Cr	Al	Other	Source+
			Composition, w/o*			
F1	Bal	--	24.81	5.40	--	K
F2	Bal	--	24.77	4.34	0.48Y	K
F7	Bal	--	24.78	3.96	0.93Th	F
F8	Bal	--	24.77	4.40	0.25Ti	K
F9	Bal	--	24.58	3.96	0.39Zr	K
F10	Bal	--	25.14	3.91	0.66Hf	F
F11	Bal	--	24.96	3.40	0.80Ta	K
F12	Bal	--	24.76	4.02	0.12Si	K
F14	Bal	--	24.15	4.16	0.08Y	K
F15	Bal	--	24.96	4.36	0.14Ti	K
F16	Bal	--	24.76	4.18	0.47Ti	K
F17	Bal	--	24.40	3.92	0.40Hf	F
F18	Bal	--	23.88	4.10	0.98Ta	K
F19	Bal	--	24.08	4.06	0.35Ta	K
F20	Bal	--	24.37	3.95	0.33Th	F
F21	Bal	--	24.68	4.00	0.51Y	K
NA2	--	Bal	19.76	6.80	--	K
NA7	--	Bal	19.89	5.09	0.96Th	F
NA9	--	Bal	20.14	5.06	0.81Hf	F
NA13	--	Bal	19.59	5.01	0.41Th	F
NA14	--	Bal	19.86	4.99	0.34Hf	F
NA15	--	Bal	15.82	5.20	1.03Ta	F
NT5	--	Bal	23.10	--	8.12Ta	K

*Nominal Analysis: Fe-25Cr-4Al, Ni-20Cr-5Al, Ni-25Cr-10Ta

+K = Charles C. Kawin Company.
 F = William A. Fahlbush Associates.

80

TABLE 13

METAL RECESSION AND OXIDE PENETRATION DEPTH FOR TASK I Fe-Cr-Al ALLOYS

Alloy Desig-nation	Exposure Time, hr					
	20 hr		60 hr		100 hr	
	Metal Recession, Mils	Max. Depth of Penetration, Mils	Metal Recession, Mils	Max. Depth of Penetration, Mils	Metal Recession, Mils	Max. Depth of Penetration, Mils
F1	1.1	>30	1.6	>30	3.8	>30
F2	<0.5	<0.5	<0.5	2.6	0.8	3.4
F3	0.5	0.5	1.0	1.0	1.6	1.6
F4	1.2	>30	1.4	>30	2.7	>30
F5	<0.5	>30	1.5	>30	2.5	>30
F6	<0.5	>30	0.7	>30	2.4	>30
F7	<0.5	2.0	<0.5	4.2	0.8	4.9
F8	<0.5	<0.5	<0.5	<0.5	<0.5	<0.5
F9	2.2	16.0	2.9	19.0	3.1	>30
F10	1.7	3.0	2.3	4.2	3.1	5.6
F11	<0.5	<0.5	0.5	0.5	0.7	1.1
F12	<0.5	>30	1.5	>30	2.8	>30
F13	<0.5	>30	0.7	>30	1.0	>30
M3	<0.5	>30	0.6	>30	1.5	>30

TABLE 14

METAL RECESSION AND OXIDE PENETRATION DEPTH FOR TASK I Ni-Cr-Al ALLOYS

Alloy Desig- nation	Exposure Time, hr					
	20 hr		60 hr		100 hr	
	Metal Recession, Mils	Max. Depth of Penetration, Mils	Metal Recession, Mils	Max. Depth of Penetration, Mils	Metal Recession, Mils	Max. Depth of Penetration, Mils
NA1	<0.5	17.0	<0.5	>30	<0.5	>30
NA2	<0.5	17.0	<0.5	>30	0.7	>30
NA3	<0.5	>30	0.5	>30	0.7	>30
NA4	<0.5	16.0	<0.5	>30	0.6	>30
NA6	<0.5	>30	<0.5	>30	<0.5	>30
NA7	<0.5	16.0	<0.5	>30	<0.5	>30
NA8	<0.5	<0.5	<0.5	<0.5	1.4	>30
NA9	<0.5	<0.5	<0.5	>30	0.7	>30
NA10	<0.5	16.5	<0.5	>30	<0.5	>30
NA11	<0.5	22.0	<0.5	>30	0.9	>30
NA12	<0.5	16.0	<0.5	>30	1.4	>30
TD NiCr	<0.5	4.0	<0.5	5.5	<0.5	10.0
M1	4.6	5.9	6.3	16.0	8.8	>30

TABLE 15

METAL RECESSION AND OXIDE PENETRATION DEPTH FOR TASK I Ni-Cr-Ta ALLOYS

| Alloy Desig- nation | Exposure Time, hr | | | | | |
| | 20 hr | | 60 hr | | 100 hr | |
	Metal Recession, Mils	Max. Depth of Penetration, Mils	Metal Recession, Mils	Max. Depth of Penetration, Mils	Metal Recession, Mils	Max. Depth of Penetration, Mils
NT1	3.2	14.0	7.1	18.0	10.5	27.0
NT2	4.9	10.0	6.9	18.0	12.0	> 30
NT3	6.2	12.0	7.1	22.0	15.0	> 30
NT4	0.5	10.0	1.2	18.0	4.7	> 30
NT5	2.3	10.1	3.4	19.0	5.5	21.5
NT6	3.2	11.0	4.4	16.0	11.0	21.0
NT7	0.6	12.0	1.7	19.0	3.3	24.0
NT8	0.9	4.8	1.7	19.0	3.9	> 30
NT9	0.7	11.0	1.3	18.0	2.9	21.0
NT10	0.8	6.0	2.6	16.0	3.9	16.0
NT11	1.2	5.2	2.0	15.0	2.8	18.0
NT12	0.8	4.7	1.4	18.0	2.5	23.5
NT13	0.9	13.0	1.5	18.0	2.1	17.0
NT14	MELTED --					
NT15	1.1	9.0	1.5	16.0	2.2	25.0
NT16	0.9	7.2	1.5	18.0	2.1	> 30
NT17	2.5	>30	3.3	>30	3.6	> 30
NT18	MELTED --					
NT19	0.7	>30	1.2	>30	2.2	> 30
NT21	1.0	2.2	1.8	8.1	4.5	18.5
NT22	4.5	>30	Total conversion to oxide 60 hr-----------------			
NT23	< 0.5	>30	< 0.5	>30	1.4	> 30
NT24	< 0.5	12.0	< 0.5	>30	0.6	> 30
NT25	1.4	4.6	2.5	6.4	4.2	20.0

TABLE 15 (Continued)

| Alloy Desig- nation | 20 hr | | 60 hr | | 100 hr | |
	Metal Recession, Mils	Max. Depth of Penetration, Mils	Metal Recession, Mils	Max. Depth of Penetration, Mils	Metal Recession, Mils	Max. Depth of Penetration, Mils
NT26	<0.5	14.0	1.1	23.0	4.0	>30
NT27	2.6	5.8	3.6	9.9	6.0	21.0
NT28	0.9	4.9	1.2	5.2	2.5	20.5
NT29	1.2	5.1	1.7	9.6	2.9	22.0

Exposure Time, hr

TABLE 16

METAL RECESSION AND OXIDE PENETRATION DEPTH FOR MODIFIED TASK I ALLOYS

Alloy Designation	Exposure Time, hr					
	20 hr		60 hr		100 hr*	
	Metal Recession, Mils	Max. Depth of Penetration, Mils	Metal Recession, Mils	Max. Depth of Penetration, Mils	Metal Recession, Mils	Max. Depth of Penetration, Mils
F14	<0.5	1.0	<0.5	1.6	<0.5	2.6
F15	<0.5	<0.5	<0.5	<0.5	<0.5	<0.5
F16	<0.5	<0.5	<0.5	<0.5	<0.5	<0.5
F17	1.7	2.5	2.0	3.2	2.2	3.4
F18	<0.5	<0.5	0.7	0.7	1.0	1.0
F19	<0.5	<0.5	0.6	0.6	0.8	0.9
F20	<0.5	1.4	<0.5	2.0	<0.5	2.0
F21	<0.5	1.4	<0.5	2.0	<0.5	2.0
NA13	<0.5	>30	<0.5	>30	<0.5	>30
NA14	<0.5	>30	<0.5	>30	<0.5	>30
NA15	0.9	16	<1.3	>30	1.5	>30
TD Ni	1.8	1.8	4.2	4.2	5.7	5.7
TD NiCr	<0.5	5.0	<0.5	8.0	<0.5	12.0

*Duplicate specimen

TABLE 17

METAL RECESSION AND OXIDE PENETRATION DEPTH OF MODIFIED TASK I ALLOYS DURING CYCLIC TORCH TESTING AT 2300°F

Alloy	Metal Recession, mils	Max. Depth of Penetration, mils	Hardness at Given Distance (mils) from Center, DPH (100-g load)							
			0	4	8	12	16	20	24	28
F14	<0.5	2.0	206	206	203	213	202	205	207	201
F15	1.2	1.2	203	202	206	197	201	202	198	195
F17	<0.5	1.5	193	190	193	193	190	193	193	190
F18	0.7	2.7	189	190	188	190	188	187	187	188
F20	<0.5	2.0	205	190	206	199	202	206	205	199
NA13	<0.5	>30.0	270	274	281	238	238	228	228	203
TD Ni	2.3	4.1	165	165	163	165	163	160	160	464*
TD NiCr	2.1	15.0	309	317	322	309	317	292	254	203

*Hardness of the oxide layer.

TABLE 18

EFFECT OF SULFIDATION EXPOSURE ON MODIFIED TASK I ALLOYS EXPOSED AT 1650°F FOR 20 HR

Alloy Desig- nation	Specific Weight Change, mg/cm^2	Metal Loss, mils	Metallographic Observations
F14	+0.20	<0.5	Very thin adherent oxide. No subsurface attack.
F15	+0.13	<0.5	Very thin adherent oxide. No subsurface attack.
F17	+0.14	<0.5	Very thin adherent oxide. No subsurface attack.
F20	+0.13	<0.5	Very thin adherent oxide. No subsurface attack.
NA13	-0.31	<0.5	Nonuniform subsurface attack in form of internal and intergranular oxidation. Sulfide-like phase also present.
TD Ni	+1.4	<0.5	Thin adherent oxide. No subsurface attack.
TD NiCr	-0.58	<0.5	Thin adherent oxide. No subsurface attack.

TABLE 19

BEND DUCTILITY AND MICROHARDNESS OF TASK I ALLOYS
AFTER EXPOSURE AT 2300°F FOR 100 HR

Alloy Desig-nation	Results of 180°-4t Bend Test*	As Fabri-cated	Microhardness, DPH (100g load)							
			After Exposure, at Given Distance (mils) from Center							
			0	4	8	12	16	20	24	28
F1	Cracked after slight bend.	211	170	174	163	171	163	168	165	-
F2	Cracked almost immediately.	218	213	209	238	207	219	213	219	206
F7	Cracked almost immediately.	216	199	209	216	212	207	206	205	207
F8	Cracked almost immediately.	211	179	193	188	189	193	192	189	-
F10	Passed.	226	194	190	195	192	190	193	170	-
F11	Passed.	219	198	199	201	195	199	201	203	198
NA2	Passed.	316	297	283	292	294	270	233	193	147
NA7	Sample bent 180° but numerous small cracks present on tension side.	337	333	281	325	314	314	302	297	302
NA9	Passed.	329	297	283	304	322	306	276	279	281

*Samples cut from oxidation specimens.

TABLE 20

BEND DUCTILITY AND MICROHARDNESS OF MODIFIED TASK I ALLOYS

Alloy Desig-nation	Bend Ductility, 180°-4t Hot Rolled	Oxidized 2300°F-100 hr	As Fabri-cated	Microhardness, DPH (100 g load) After Exposure, at Given Distance (mils) from Center							
				0	4	8	12	16	20	24	28
F14	Bent ~90° and cracked. Cracked immediately when another bend was attempted.	Cracked immediately.	208	203	202	203	201	205	205	207	203
F15	Bent 180°, no cracks.	Cracked almost immediately.	-	Not determined							
F16	Bent 180°, one small edge crack.	Cracked immediately.	205	221	216	212	215	219	213	217	215
F17	Bent 180°, few small cracks on tension side.	Bent 180°, no cracks.	216	189	189	193	189	194	190	189	-
F18	Bent ~90° and cracked.	Bent 180°, one small edge crack.	219	201	203	202	201	201	201	203	-
F19	Bent 180°, no cracks.	Bent 180°, no cracks.	203	187	185	183	185	185	182	183	-
F20	Bent 180°, no cracks.	Cracked almost immediately.	200	207	205	199	203	201	201	203	201
F21	Cracked after slight bend.	Cracked after slight bend.	-	Not determined							
NA13	Bent 180°, no cracks.	Bent 180°, no cracks.	308	330	339	304	299	319	302	249	256
NA14	Bent 180°, no cracks.	Bent 180°, no cracks.	-	Not determined							
NA15	Bent 180°, few small edge cracks.	Bent 180°, no cracks.	-	Not determined							

TABLE 21

COMPARISON OF THE WEIGHT CHANGE
OF TASK I AND MODIFIED TASK I ALLOYS
AFTER EXPOSURE AT 2300°F FOR 100 HR

| | Task I | | | Modified Task I | | |
| | Specific Weight Change, mg/cm^2 | | | Specific Weight Change, mg/cm^2 | |
Alloy Designation	Total*	Specimen+	Alloy Designation	Total*	Specimen+
F2 (0.43Y)	3.5	2.35	F14 (0.25Y)	3.43	2.03
			F21 (0.65Y)	2.84	2.0
F7 (1.06Th)	4.67	2.26	F20 (0.5Th)	2.48	1.63
F8 (0.23Ti)	2.82	0.52	F15 (0.15Ti)	2.19	1.33
			F16 (0.5Ti)	3.36	1.73
F10 (0.85Hf)	7.56	6.18	F17 (0.5Hf)	4.88	4.37
F11 (0.85Ta)	7.52	-4.32	F18 (1.25Ta)	6.35	-2.57
			F19 (0.5Ta)	8.40	-5.27
NA7 (1.01Th)	6.08	-4.69	NA13 (0.5Th)	3.46	-2.10
NA9 (0.81Hf)	10.6	-15.5	NA14 (0.6Hf)	7.18	-11.1
--			NA15 (1.0Ta)	15.4	-26.2

*Total (sample + spall products) weight change.
+Sample weight change.

TABLE 22

NOMINAL COMPOSITION OF TASK II ALLOYS

| Alloy | Composition, w/o | | | | |
	Fe	Ni	Cr	Al	Other
F22	Bal	--	25	4	0.15Y
F14*	Bal	--	25	4	0.25Y
F23	Bal	--	25	4	0.25Y, 0.5Ta
F8*	Bal	--	25	4	0.23Ti
F16*	Bal	--	25	4	0.50Ti
F24	Bal	--	25	4	0.75Ti
F25	Bal	--	25	4	0.50Ti, 0.50Ta
F26	Bal	--	25	4	0.50Ti, 1.0Ta
F27	Bal	--	25	4	0.23Ti, 0.20Hf
F17*	Bal	--	25	4	0.50Hf
F28	Bal	--	25	4	0.30Hf
F29	Bal	--	25	4	0.30Hf, 0.50Ta
F20*	Bal	--	25	4	0.50Th
F30	Bal	--	25	4	0.30Th
F31	Bal	--	25	4	0.30Th, 0.50Ta
NA13*	--	Bal	20	5	0.5Th
NA16	--	Bal	20	5	0.30Th
NA17	--	Bal	20	5	0.50Th, 1Ta
NA18	--	Bal	20	6	0.75Si

*Task I alloy.

91

TABLE 23

WEIGHT LOSS OF TASK II ALLOYS
DURING ARC MELTING

Alloy	Percent Weight Loss
F8	0.11
F14	0.36
F16	0.11
F17	0.03
F20	0.23
F22	0.09
F23	0.12
F24	0.10
F25	0.02
F26	0.07
F27	0.08
F28	0.04
F29	0.05
F30	0.32
F31	0.21
NA13	0.03
NA16	0.02
NA17	0.03
NA18*	+0.01
NA18*	0.01

*Duplicate arc-melt.

TABLE 24

MECHANICAL BEHAVIOR OF TASK II ALLOYS DURING HOT ROLLING AT 2150°F

Alloy Desig- nation	Final Thickness, in.	Total Reduction, %	Appearance
F8	0.074	82	No surface or edge cracking
F14	0.073	75	No surface or edge cracking
F16	0.075	85	Very light edge cracking
F17	0.095	78	Very light surface and edge cracking
F20	0.082	75	No surface or edge cracking
F22	0.080	80	No surface or edge cracking
F23	0.074	80	Very light surface cracking
F24	0.080	76	Very light edge cracking
F25	0.078	83	No surface or edge cracking
F26	0.090	70	No surface or edge cracking
F27	0.091	75	No surface or edge cracking
F28	0.090	80	No surface or edge cracking
F29	0.082	75	Light surface cracking
F30	0.082	80	No edge or surface cracking
F31	0.083	70	Light edge cracking
NA13	0.092	70	Moderate edge and surface cracking
NA16	0.090	72	Light edge and surface crack- ing
NA17	0.093	70	Moderate edge and surface cracking
NA18	0.095	70	Very heavy surface and edge cracking

TABLE 25

OXIDATION RATE OF TASK II ALLOYS DURING CYCLIC FURNACE EXPOSURE AT 2300°F

Alloy Desig-nation	Weight Change, mg/cm^2																			
	40 hr		80 hr		120 hr		160 hr		200 hr		240 hr		280 hr		320 hr		360 hr		400 hr	
	Total	Sample	Total	Sample	Total	Sample	Total	Sample	Total	Sample	Total	Sample	Total	Sample	Total	Sample	Total	Sample	Total	Sample
F14	2.31	1.24	2.90	1.46	3.07	1.63	3.59	1.84	4.10	1.98	4.26	2.03	4.65	2.12	3.95	2.17	3.92	2.17	3.50	2.23
F22	3.37	1.37	3.91	1.60	5.05	1.81	5.47	1.95	7.64	2.08	7.95	2.17	8.27	2.27	7.09	2.32	7.38	2.36	8.02	2.38
F23	3.46	1.34	3.98	1.60	5.76	1.85	6.96	2.01	5.88	2.01	6.00	2.06	6.64	2.16	6.65	2.21	6.85	2.25	7.27	2.27
F8	3.20	1.36	4.07	1.59	4.64	1.78	5.67	1.90	6.55	2.17	7.04	2.30	8.29	2.57	11.10	6.21	Stopped after 320 hr			
F16	3.44	1.38	4.38	1.65	5.27	1.90	6.35	2.15	8.06	2.32	8.81	2.56	12.99	5.96	19.48	13.27	Stopped after 320 hr			
F24	2.37	1.48	3.04	1.69	3.28	2.01	3.62	2.30	4.78	2.89	9.77	7.11	Stopped after 240 hr							
F25	2.06	1.47	2.47	1.64	3.29	1.90	3.60	2.09	5.50	2.97	11.25	7.38	Stopped after 240 hr							
F26	2.20	1.50	4.55	1.66	5.80	1.97	6.03	2.18	7.79	2.67	9.50	3.78	11.48	5.16	19.32	11.85	Stopped after 320 hr			
F27	2.20	1.24	3.89	1.33	4.02	1.44	4.51	1.67	5.07	1.73	5.68	1.87	6.66	2.06	6.10	2.32	6.73	2.53	6.72	3.09
F17	2.09	1.41	4.24	1.01	6.71	1.99	17.54	8.74	20.37	10.18	(180 hr) Stopped after 180 hr									
F28	1.38	0.93	3.39	0.59	10.57	8.57	19.15	15.26	(140 hr) Stopped after 140 hr											
F29	2.89	0.46	3.27	0.45	4.02	0.89	5.18	1.61	7.65	3.85	(180 hr) Stopped after 180 hr									
F20	2.34	1.36	3.56	1.50	4.03	1.63	4.77	1.69	5.61	1.85	6.58	2.04	7.16	2.15	7.18	2.28	7.41	2.32	7.27	2.41
F30	3.96	1.25	5.03	1.35	6.17	1.32	6.92	1.03	7.02	1.00	7.60	0.84	8.55	1.06	9.19	1.22	9.03	1.40	9.79	2.06
F31	3.26	1.29	3.96	1.52	4.62	1.47	5.60	1.76	6.41	1.76	7.15	1.16	7.59	1.98	7.06	2.13	7.16	2.10	7.58	2.18
NA13	2.31	1.43	4.20	1.64	5.50	1.86	5.33	2.02	6.81	2.37	7.66	2.60	8.04	2.85	8.41	3.22	9.01	3.65	9.43	4.23
NA16	2.93	1.34	3.21	1.53	3.19	1.76	3.37	1.93	4.48	2.27	4.97	2.50	5.56	2.77	5.43	3.10	5.81	3.36	5.98	3.65
NA17	1.75	1.29	2.46	1.46	2.71	1.62	2.91	1.72	3.45	1.94	3.82	2.10	4.23	2.28	4.85	2.59	5.53	2.90	5.68	3.31
TD Ni	11.09	9.21	17.03	15.97	23.51	21.34	28.74	26.08	33.45	30.60	37.89	35.16	42.33	39.16	46.33	42.82	48.11	44.31	52.60	47.61
TD NiC	1.53	-0.64	2.00	-1.38	3.80	-2.25	3.58	-3.29	--	--	3.04	-5.43	2.76	-7.16	1.72	-9.57	1.75	-10.85	1.53	-14.2

TABLE 25 (Continued)

Weight Change, mg/cm^2

Alloy Designation	440 hr Total	440 hr Sample	480 hr Total	480 hr Sample	520 hr Total	520 hr Sample	560 hr Total	560 hr Sample	600 hr Total	600 hr Sample	640 hr Total	640 hr Sample	680 hr Total	680 hr Sample	720 hr Total	720 hr Sample	760 hr Total	760 hr Sample	800 hr Total	800 hr Sample
F14	2.68	2.30	3.43	2.31	4.50	2.38	4.63	2.41	4.79	2.46	5.04	2.52	4.88	2.57	5.03	2.64	5.32	2.82	5.30	2.84
F22	7.58	2.35	8.10	2.34	8.30	2.49	7.85	2.58	8.39	2.59	8.30	2.65	8.65	2.70	8.97	2.73	9.10	2.79	8.99	2.79
F23	6.51	2.48	6.87	2.53	7.18	2.61	7.08	2.69	6.91	2.20	7.20	2.74	7.33	2.75	7.30	2.79	7.41	2.78	7.72	3.23
F8																				
F16																				
F24																				
F25																				
F26																				
F27	9.86	6.16	16.00	11.72	22.90	18.68	25.88	22.26	(540 hr) Stopped after 540 hr											
F17																				
F28																				
F29																				
F20	9.21	2.51	10.61	2.62	10.65	2.67	10.95	2.72	11.71	3.15	12.95	3.68	15.48	6.01	20.93	10.91	25.7	14.35	Stopped after 780 hr	
F30	11.90	4.01	29.41	22.3	Stopped after 440 hr															
F31	6.56	2.30	7.45	2.32	7.58	2.48	7.68	2.56	8.59	2.59	11.18	4.19	27.48	19.2	Stopped after 680 hr					
NA13	10.23	4.25	11.77	4.68	12.83	4.32	13.35	3.91	(540 hr) Stopped after 540 hr											
NA16	8.51	4.02	10.12	4.44	10.50	4.08	10.92	4.24	(540 hr) Stopped after 540 hr											
NA17	6.15	4.30	10.34	6.77	11.28	7.72	11.73	8.85	(540 hr) Stopped after 540 hr											
TD Ni	53.25	52.7	55.7	55.8	58.63	58.8	61.21	61.6	64.24	64.3	64.65	66.2	70.7	70.2	71.26	70.8	83.2	71.8	84.4	75.8
TD NiC	0.44	-24.21	9.36	-31.50	1.45	-41.50	3.29	-54.40	6.09	-68.80	7.87	-84.70	11.73	-111.8	12.99	-122.0	16.20	-143.5	17.45	-157.0

TABLE 26

LIFE OF 10-MIL SHEET SAMPLES OF TASK II ALLOYS
DURING CYCLIC FURNACE OXIDATION AT 2300°F

Alloy* (Addition, w/o)	Removal Time, hr	Remarks
F28 (0.3Hf)	140	Dark green; complete oxidation one-half both specimens.
F17 (0.5Hf)	180	Dark green; complete oxidation one-half of one sample; complete penetration in large area on second sample.
F29 (0.3Hf-0.5Ta)	180	Dark green; extensive oxidation at edges and corners; very rough surface appearance.
F24 (0.75Ti)	240	Tan oxide; considerable oxidation at edges and corners; one-fifth of one sample consumed.
F25 (0.5Ti-0.5Ta)	240	Tan oxide, extensive oxidation at edges and corners; one-fifth of one sample consumed.
F8 (0.23Ti)	320	Tan oxide; considerable oxidation at edges and corners; one-fifth of one sample consumed.
F16 (0.5Ti)	320	Tan oxide; extensive attack at edges and corners; one-third of each sample badly attacked.
F26 (0.5Ti-1.0Ta)	320	Tan oxide; extensive oxidation at edges and corners.
F30 (0.3Th)	440	Dark gray; extensive attack edges and corners; both samples broken due to oxide fracture.

TABLE 26 (Continued)

Alloy[*] (Addition, w/o)	Removal Time, hr	Remarks
F27 (0.23Ti, 0.20Hf)	540	Light to dark gray; one sample complete oxidation; second sample moderate edge attack.
NA13 (0.5Th)	540	Light to dark green; edge attack all edges and corners; spalling of oxide at edges; crucible green.
NA16 (0.3Th)	540	Light to dark green; edge attack all edges and corners; spalling of oxide at edges; crucible green.
NA17 (0.5Th, 1.0Ta)	540	Light to dark green; edge attack all edges and corners; one sample broken in half; spalling of oxide at edges; crucible green.
F31 (0.3Th, 0.5Ta)	680	Dark gray; extensive attack edges and corners; both samples broken due to oxide fracture.
F20 (0.5Th)	780	Dark gray; extensive attack edges and corners; both samples broken due to oxide fracture.
F14 (0.25Y)	800	Light gray oxide with dark green patches; no apparent edge effect.
F22 (0.15Y)	800	Light gray oxide with dark green patches; no apparent edge effect.
F23 (0.25Y, 0.5Ta)	800	Light to dark gray oxide; slight attack one end of sample.
TD Ni	800	Black with little spall product; crucible green; minor dimensional change
TD NiCr	800	Gray to black oxide with extensive spalling; crucible green; dimensions decreased extensively

[*]F alloys, Fe-25Cr-4Al; NA alloys, Ni-20Cr-5Al

TABLE 27

WEIGHT CHANGE OF INTERDIFFUSION ALLOYS
DURING EXPOSURE IN ARGON AT 2300°F FOR 100 HR

Alloy Designation	Specimen Dimensions, in.	Weight Change, mg/cm^2	
		Total	Specimen
F16	2 x 0.5 x 0.01	+2.5	+0.6
F18	2 x 0.5 x 0.01	+3.0	+2.5
NA13	2 x 0.5 x 0.01	+1.0	+0.75
TD Ni	2 x 0.5 x 0.06	+0.2	+0.1
TD NiCr	2 x 0.5 x 0.06	+0.8	+0.5

TABLE 28

RESULTS OF CHEMICAL ANALYSIS OF TASK II ALLOYS

Alloy Designation	Composition, w/o*					Source+
	Fe	Ni	Cr	Al	Other	
F22	Bal	–	24.52	4.14	0.07Y	K
F14	Bal	–	24.43	4.06	0.27Y	K
F23	Bal	–	24.82	4.16	0.08Y, 0.54Ta	K
F8	Bal	–	25.02	4.08	0.24Ti	K
F16	Bal	–	24.82	4.16	0.49Ti	K
F24	Bal	–	24.80	4.18	0.70Ti	K
F25	Bal	–	24.5	4.06	0.5Ti, 0.56Ta	K
F26	Bal	–	24.82	4.16	0.5Ti, 0.88Ta	K
F27	Bal	–	24.88	3.78	0.23Ti, 0.11Hf	F
F17	Bal	–	24.83	3.88	0.32Hf	F
F28	Bal	–	24.91	3.82	0.18Hf	F
F29	Bal	–	25.15	3.82	0.15Hf, 0.52Ta	F
F20	Bal	–	24.81	3.93	0.16Th	F
F30	Bal	–	25.0	3.92	0.15Th	F
F31	Bal	–	24.99	3.92	0.15Th, 0.49Ta	F
NA13	–	Bal	20.04	4.88	0.44Th	F
NA16	–	Bal	19.89	4.80	0.23Th	F
NA17	–	Bal	19.78	4.83	0.39Th, 0.99Ta	F

+K = Charles C. Kawin Company.
 F = William A. Fahlbush Associates.

* Nominal Analysis: Fe-25Cr-4Al, Ni-20Cr-5Al

TABLE 29

METAL RECESSION AND OXIDE PENETRATION DEPTH FOR TASK II ALLOYS
DURING CYCLIC FURNACE EXPOSURE AT 2300°F

Alloy Designation	Exposure Time, hr					
	100 hr		400 hr		800 hr	
	Metal Recession, Mils	Max. Depth of Penetration, Mils	Metal Recession, Mils	Max. Depth of Penetration, Mils	Metal Recession, Mils	Max. Depth of Penetration, Mils
F28(0.3 Hf)	0.5	5.0*	2.0	5.0*(140 hr)	--	--
F17(0.5 Hf)	1.0	5.0*	1.5	5.0*(180 hr)	--	--
F29(0.3 Hf, 0.5 Ta)	0.75	1.5	(180 hr) Complete oxidation		--	
F8(0.23 Ti)	<0.5	<0.5	0.75	5.0*(320 hr)	--	--
F16(0.5 Ti)	<0.5	<0.5	(320 hr) Complete oxidation		--	
F24(0.75Ti)	<0.5	<0.5	0.7	5.0*(240 hr)	--	--
F25(0.50Ti, 0.5 Ta)	<0.5	<0.5	0.8	5.0*(240 hr)	--	--
F26(0.5 Ti, 1.0 Ta)	<0.5	<0.5	0.7	5.0*(320 hr)	--	--
F27(0.23Ti, 0.50Hf)	0.7	1.0	0.8	5.0*	0.7	5.0*(540 hr)
NA13(0.5Th)	<0.5	5.0*	2.0	5.0*	2.7	5.0*(540 hr)
NA16(0.3Th)	<0.5	5.0*	1.5	5.0*	1.5	5.0*(540 hr)
NA17(0.5Th, 1.0Ta)	<0.5	5.0*	2.0	5.0*	Complete oxidation (540 hr)	

TABLE 29 (Continued)

Alloy Desig- nation	100 hr		400 hr		800 hr	
	Metal Recession, Mils	Max. Depth of Penetration, Mils	Metal Recession, Mils	Max. Depth of Penetration, Mils	Metal Recession, Mils	Max. Depth of Penetration, Mils
F30 (0.3 Th)	< 0.5	< 0.5	1.5	5.0*	1.6	5.0* (440 hr)
F20 (0.5 Th)	< 0.5	< 0.5	0.75	5.0*	1.0	5.0* (780 hr)
F31 (0.3 Th, 0.5 Ta)	< 0.5	< 0.5	1.0	5.0*	Complete oxidation (680 hr)	
F22 (0.15 Y)	< 0.5	< 0.5	< 0.5	0.7	0.8	1.4
F14 (0.25 Y)	< 0.5	< 0.5	< 0.5	< 0.5	0.6	1.5
F23 (0.25 Y, 0.5 Ta)	< 0.5	< 0.5	< 0.5	1.0	0.6	1.0
TD Ni	--	--	--	--	18	18
TD NiCr	--	--	--	--	5.5	30 *

*Complete penetration as scattered oxide particles and/or large pores throughout sample.

TABLE 30

RESULTS OF METALLOGRAPHIC EXAMINATION OF DIFFUSION COUPLES
AS-FABRICATED AND AFTER EXPOSURE AT 2300°F

Diffusion Couple	Average Cladding Thickness, mils	Average Porous Zone Thickness, mils	Average Substrate Thickness, mils	Comments
		As Fabricated		
F16/TD Ni	14.5	--	38.5	Good interfacial bond
F16/TD NiCr	12.5	--	38.5	Good interfacial bond
F18/TD Ni	7.5	--	21.0	Good interfacial bond
F18/TD NiCr	12.2	--	32.7	Good interfacial bond
NA13/TD Ni	13.0	--	34.2	Good interfacial bond
NA13/TD NiCr	12.2	--	36.0	Good interfacial bond
		2300°F-100 hr		
F16/TD Ni	5.5	9.5	38.0	Extensive interfacial porosity; extensive porosity in cladding.
F16/TD NiCr	7.5	8.5	36.0	Extensive interfacial porosity; some porosity in cladding.
F18/TD Ni	5.5	4.5	19.0	Extensive interfacial porosity; extensive porosity in cladding.
F16/TD NiCr	10.0	4.0	29.5	Extensive interfacial porosity; some porosity in cladding.
F18/TD Ni	14.2	--	33.5	No uniform interfacial porosity; minor cladding porosity.
NA13/TD NiCr	12.5	--	36.0	No interfacial porosity; no significant cladding porosity.
		2300°F-300 hr		
F18/TD Ni	5.5	4.0	20.0	Extensive interfacial porosity; extensive cladding porosity.
NA13/TD Ni	9.0	1.5	24.0	Some interfacial porosity, moderate cladding porosity.

TABLE 31

MICROHARDNESS AND BEND DUCTILITY OF TASK II ALLOYS
AS FABRICATED AND AFTER EXPOSURE AT 2300°F

Alloy Desig- nation	Microhardness, DPH (100 g)			Bend Ductility, 180°-4t	
	Hot Rolled	Cold Rolled	Oxidized [a]	As-Fabricated	Oxidized [a]
F8	210	336	167	Pass	First crack appeared at 90°, no separation.
F14	235	322	198	Pass	First crack appeared at 110°, no separation.
F16	241	332	190	Pass	First crack appeared at 90°, no separation.
F17	216	322	194	Pass	Very brittle [b]
F20	228	357	178	Pass	Very brittle [b]
F22	226	360	195	Pass	Crack appeared at 110°, no separation
F23	206	297	190	Pass	Pass
F24	215	322	200	Pass	Pass
F25	249	336	210	Pass	Pass
F26	245	325	205	Pass	Crack appeared at 85°, no separation.
F27	230	315	195	Pass	Crack appeared at 85°, no separation.
F28	235	333	230	Pass	Very brittle [b]

TABLE 31 (Continued)

Alloy Desig-nation	Microhardness, DPH (100 g)			Bend Ductility, 180°-4t	
	Hot Rolled	Cold Rolled	Oxidized[a]	As-Fabricated	Oxidized[a]
F29	228	317	1000	Pass	Very brittle[b]
F30	213	322	190	Pass	Very brittle[b]
F31	219	330	1000	Pass	Very brittle[b]
NA13	287	433	150	Pass[c]	Pass
NA16	280	428	160	Pass[c]	Pass
NA17	295	437	1000	Pass[c]	Very brittle[b]

(a) After maximum oxidation exposure for each alloy, as indicated in Table 26.

(b) Ductile bend of that part of specimen with minimal oxidation.

(c) After annealing at 2150°F for 15 min.

TABLE 32

MICROHARDNESS AND BEND DUCTILITY OF DIFFUSION COUPLES
AS FABRICATED AND AFTER EXPOSURE AT 2300°F

| Diffusion Couple | Condition | Microhardness, DPH (100 g) | | Bend Test Results, 180°-4t |
		Cladding	Substrate[*]	
F16/TD Ni	As fabricated	245	217	Separation on tension side.
	2300°F-100 hr	113	297	Separation on compression side.
F16/TD NiCr	As fabricated	247	336	Pass
	2300°F-100 hr	139	310	Pass
F18/TD Ni	As fabricated	296	197	Separation on tension side.
	2300°F-100 hr	110	259	Pass
	2300°F-300 hr	94	210	Pass
F18/TD NiCr	As fabricated	285	339	Separation on both sides.
	2300°F-100 hr	139	247	Pass
NA13/TD Ni	As fabricated	230	177	Pass
	2300°F-100 hr	152	187	Pass
	2300°F-300 hr	124	207	Pass
NA13/TD NiCr	As fabricated	285	309	Slight separation on tension side.
	2300°F-100 hr	157	300	Pass

[*]Located at center of substrate.

TABLE 33

ELECTRON MICROPROBE DATA FOR AS-FABRICATED
TASK II CLADDING ALLOYS

Alloy Designation	Elements Scanned	Observations
F14	Fe,Cr,Al,Y	Several small Y peaks, possibly Fe-Cr-Y compound; remaining elements uniform.
F23	Fe,Cr,Al,Y,Ta	Several small Y peaks, possibly Fe-Cr-Y compound; remaining elements uniform.
F16	Fe,Cr,Al,Ti	All elements uniform.
F26	Fe,Cr,Al,Ti,Ta	All elements uniform.
F20	Fe,Cr,Al,Th	Several strong Th peaks, possibly Fe-Cr-Th compound; other elements uniform.
F31	Fe,Cr,Al,Th,Ta	Several strong Th peaks, possibly Fe-Cr-Th compound; other elements uniform.
F18	Fe,Cr,Al,Ta	All elements uniform.
NA13	Ni,Cr,Al,Th	Strong Th peaks, possibly Ni-Th compound; other elements uniform.

TABLE 34

ELECTRON MICROPROBE DATA FOR CLADDING ALLOYS

AFTER CYCLIC FURNACE OXIDATION AT 2300°F

Alloy Designation	Elements Scanned	Exposure Time, hr	Observations
F14 (0.25Y)	Fe, Cr, Al, Y	100	Al peak at surface (~1.0 mil); Fe, Cr, Y depletion at Al surface peak; no other significant Fe, Cr, Y variation.
		400	Al peak at surface (~1.2 mils); Fe, Cr, Y depletion at Al surface peak; no other significant Fe, Cr, Y variation.
		800	Al peak at surface (~1.5 mils); Fe, Cr, Y depletion at Al surface peak; tendency toward minor Cr increase, Fe decrease beneath Al-rich surface layer.
F22 (0.15Y)	Fe, Cr, Al, Y	100	Al peak at surface (~0.5 mil); Fe, Cr, Y depletion at Al surface peak; no other significant Fe, Cr, Y variation.
		400	Al peak at surface (~1.2 mils); Fe, Cr, Y depletion at Al surface peak; no other significant Fe, Cr, Y variation.
		800	Al peak at surface (~1.1 mils); Fe, Cr, Y depletion at Al surface peak; slight Cr peak, Fe depletion beneath Al-rich surface layer.
F23 (0.25Y, 0.5Ta)	Fe, Cr, Al, Y, Ta	100	Al surface peak (~0.5 mil), possible minor Y peaks; Fe, Cr, Y depletion at Al surface peak; no other significant Fe, Cr variation.
		800	Al surface peak (~1.4 mils); Fe, Cr, Y depletion at Al surface peak; no other significant Fe, Cr, Y variation.

TABLE 34 (Continued)

Alloy Designation	Elements Scanned	Exposure Time, hr	Observations
F16 (0.5Ti)	Fe, Cr, Al, Ti	100	Al surface peak ($\sim$0.6 mil); minor Ti peak beneath Al layer; Fe, Cr, Ti depletion at Al surface peak.
		320	Completely oxidized; no Al surface peak; Fe concentrated at surface. Very irregular concentration profile due to porosity.
F30 (0.3Th)	Fe, Cr, Al, Th	100	Al surface peak; internal Th peaks; no significant Fe, Cr variation.
		400	No Al peak at surface; internal Th peaks; slight Fe, Cr increase at surface.
F31 (0.3Th, 0.5Ta)	Fe, Cr, Al, Th, Ta	100	Al peak at surface ($\sim$0.6 mil); internal Th peaks; Cr, Fe depletion at Al surface peak; no other significant Fe, Cr variation.
		400	Al peak at surface ($\sim$1.5 mils); internal Th peaks; possible Ta peaks associated with Th peaks. Slight Cr, Fe increase at surface.
NA16 (0.3Th)	Ni, Cr, Al, Th	100	No Al peak at surface; strong internal and surface Th peaks (ThO_2?); Ni, Cr, Al depletion at Th peak near surface.
		400	Al peak at surface ($\sim$2.2 mils); no major Th peaks; Ni, Cr depletion at Al surface peak, minor Cr peak beneath Al surface peak.
NA17 (0.5Th, 1.0Ta)	Ni, Cr, Al, Th, Ta	100	Al peak at surface ($\sim$0.2 mil); strong internal Th peaks; Cr, Ni depletion at strong Th peak near surface; Ni K_β interference with Ta L_α.
		400	Al peak at surface ($\sim$1.1 mils); Th peak near surface; Cr, Ni, depletion at Th peak; Ni K_β interference with Ta L_α.

TABLE 35

RESULTS OF ELECTRON MICROPROBE EXAMINATION
OF AS-FABRICATED DIFFUSION COUPLES

Diffusion Couple	Elements Scanned	Observations
F16/TD Ni	Fe,Cr,Ni,Al,Ti,Th	Ti peak at interface; remaining elements uniform in cladding and substrate.
F16/TD NiCr	Fe,Cr,Ni,Al,Ti,Th	Strong Ti, slight Al, peak at interface; remaining elements uniform in cladding and substrate.
F18/TD Ni	Fe,Cr,Ni,Al,Th,Ta	All elements uniform.
F18/TD NiCr	Fe,Cr,Ni,Al,Th,Ta	Slight Al peak,Cr depletion at interface. All other elements uniform.
NA13/TD Ni	Ni,Cr,Al,Th	Th peaks in cladding, Ni, Cr depletion at Th peaks; all other elements uniform.
NA13/TD NiCr	Ni,Cr,Al,Th	Several small Th peaks in cladding, all other elements uniform.

TABLE 36

ELECTRON MICROPROBE DATA FOR DIFFUSION COUPLES
AFTER INTERDIFFUSION AT 2300°F FOR 100 AND 300 HR

Diffusion Couple	Element	Intensity at Given Distance from Surface (mils), counts/sec								
		Surface	5	7.2	10.8	14.4	18	21.6	28.8	36
					100 hr					
F16/TD Ni	Fe	5400	4600	4000	--	2900	2700	2300	1500	1000
	Ni	800	1500	2000	--	3000	3800	4300	5200	6000
	Cr	1620	1600	1500	--	870	840	690	450	300
	Al	51	48	46	--	36	36	36	36	36
	Ti	40	20	20	--	20	21	23	26	--
	Th	18	18	18	--	13.5	39	39	36	39
F16/TD NiCr	Fe	5600	5400	5000	4200	--	1900	1500	600	300
	Ni	700	1000	1400	1800	--	3200	3700	4400	5000
	Cr	3200	3150	3100	2900	--	2450	2500	2500	2500
	Al	63	63	62	58	--	54	35	35	35
	Ti	59	25	30	25	--	25	25	25	25
	Th	26	26	25	25	--	42	42	46	--
F18/TD Ni	Fe	3300	3050	--	2100	1800	1400	1300	1200	1200
	Ni	2700	3300	--	4200	4900	5500	5700	5700	5750
	Cr	930	870	--	720	640	520	490	490	490
	Al	60	49	--	44	44	44	44	44	44
	Ta	700	50	--	50	50	50	50	50	50
	Th	22	23	--	47	42	40	40	40	40
F18/TD NiCr	Fe	3200	2350	2300	1400	1100	800	500	200	300
	Ni	300	360	450	159	2020	2280	2460	2670	2670
	Cr	3100	2900	2150	1900	1900	2000	2200	2200	2200
	Al	100	30	26	24	22	23	22	23	23
	Th	15	13	18	18	34	37	37	36	36
	Ta	17	17	17	19	19	17	17	18	18

TABLE 36 (Continued)

Diffusion Couple	Element	Intensity at Given Distance from Surface (mils), counts/sec								
		Surface	5	7.2	10.8	14.4	18	21.6	28.8	36
NA13/TD Ni	Ni	4400	4500	4600	4780	4800	4900	5000	5000	5000
	Cr	1200	1110	1020	780	570	330	165	60	60
	Al	25	25	26	23	22	20	20	20	20
	Th	18	18	18	21	30	30	30	30	30
NA13/TD NiCr	Ni	4500	4800	4900	4900	5200	5200	5300	5200	5200
	Cr	1770	1590	1680	1710	1770	1830	1800	1800	1800
	Al	38	38	37	36	36	36	34	33	33
	Th	21	21	18	18	27	27	27	27	27
				300 hr						
F18/TD Ni	Fe	1350	1290	1230	1260	1260	1260	1260	1260	1260
	Ni	2340	2370	2140	2460	2460	2460	2460	2460	2460
	Cr	410	390	380	410	420	420	420	420	420
	Al	19	16	15	16	15	16	16	16	16
	Th	13	14	20	17	17	17	17	17	17
	Ta	40	39	39	39	40	39	39	39	39
NA13/TD Ni	Ni	3500	3700	3800	3900	4000	4000	4000	4000	4000
	Cr	590	560	520	510	500	490	490	490	490
	Al	98	21	19	18	17	17	17	17	17
	Th	17	17	17	18	18	18	18	18	18

TABLE 37

ROLLING SCHEDULE FOR FABRICATION OF 5 MIL FOIL MATERIAL

Rolling Condition	No. of Passes	Final Thickness, mil	% Reduction per Pass*
Hot	20	0.080	5-10
Cold	7	0.030^{+}	10
Cold	4	0.015^{+}	10
Cold	3	0.010^{+}	10
Cold	3	0.0075^{+}	10
Cold	4	0.005	10

[+] Samples annealed 2100°F-15 min prior to subsequent reduction scheduling.

*Approximate percent of reduction due to springback.

APPENDIX B

ILLUSTRATIONS AND PHOTOMICROGRAPHS
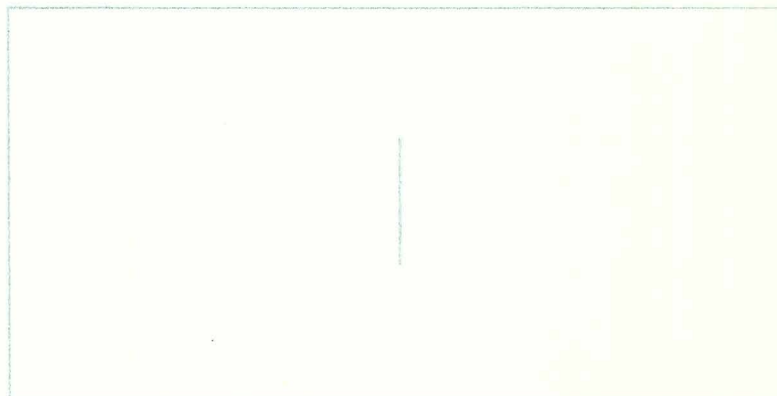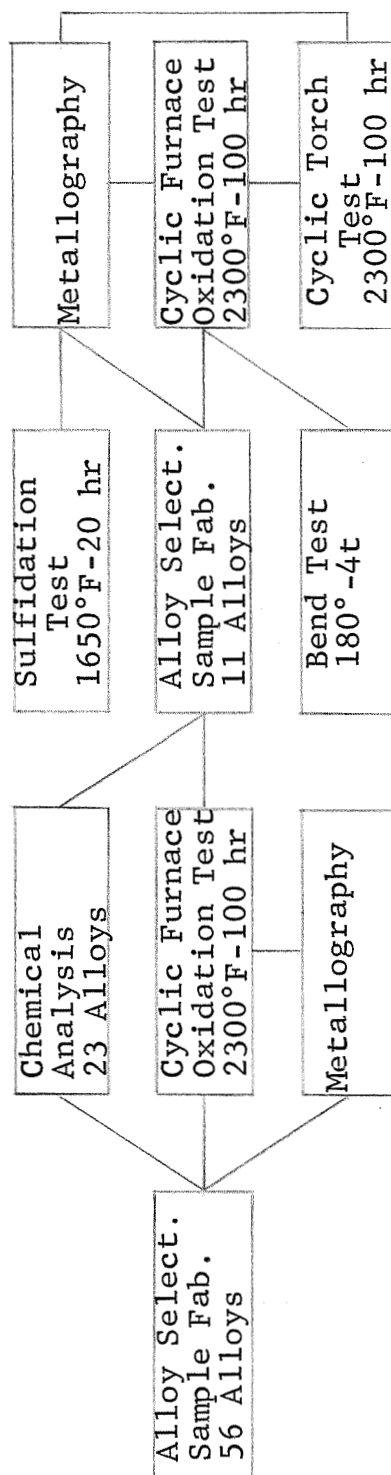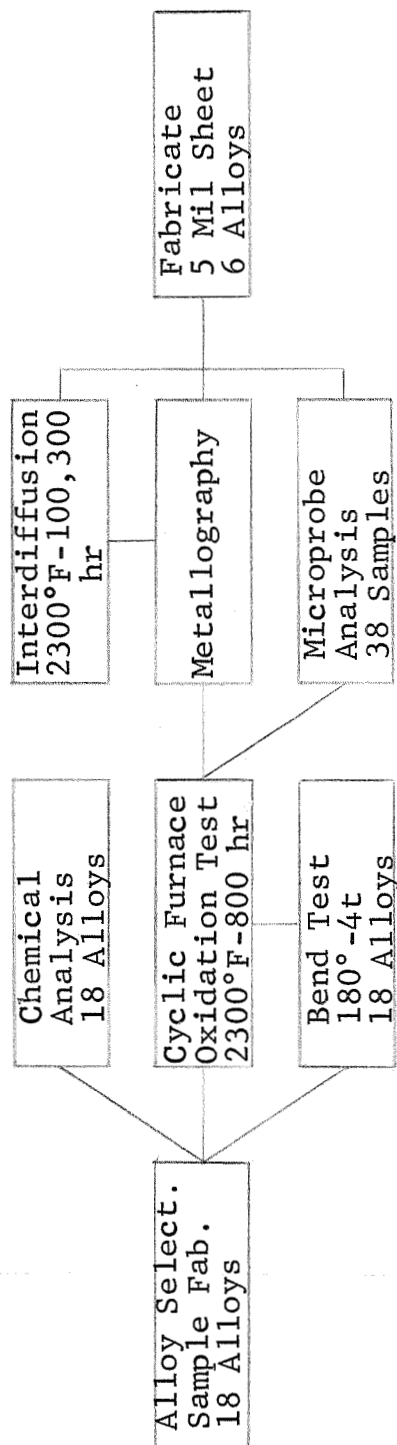
TASK I

TASK II

Fig. 1 – Flow Sheet of Experimental Program

114

F5

M1

NA2

NT10

NT2
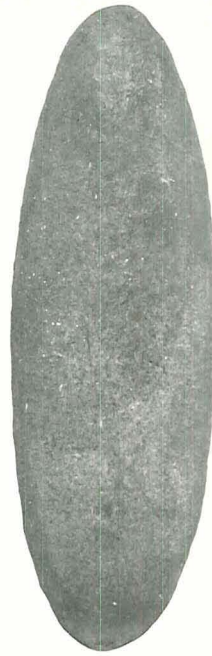
F1

Fig. 2 - Surface Condition of Selected Task I Alloys
After Hot Rolling
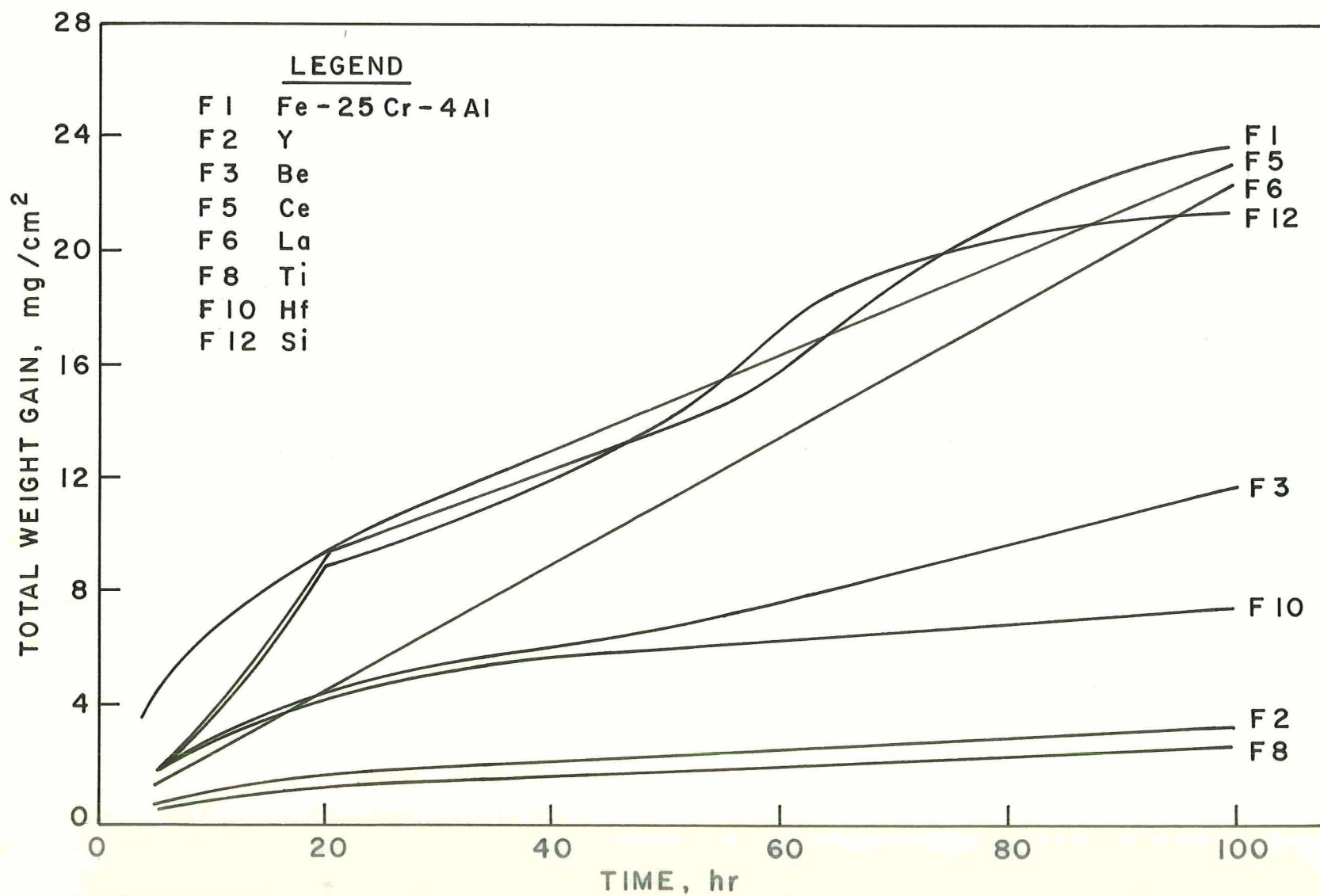
Fig. 3 - Effect of 0.25 a/o Additions on Total Weight Gain of Fe-25Cr-4Al
During Cyclic Furnace Oxidation at 2300°F.
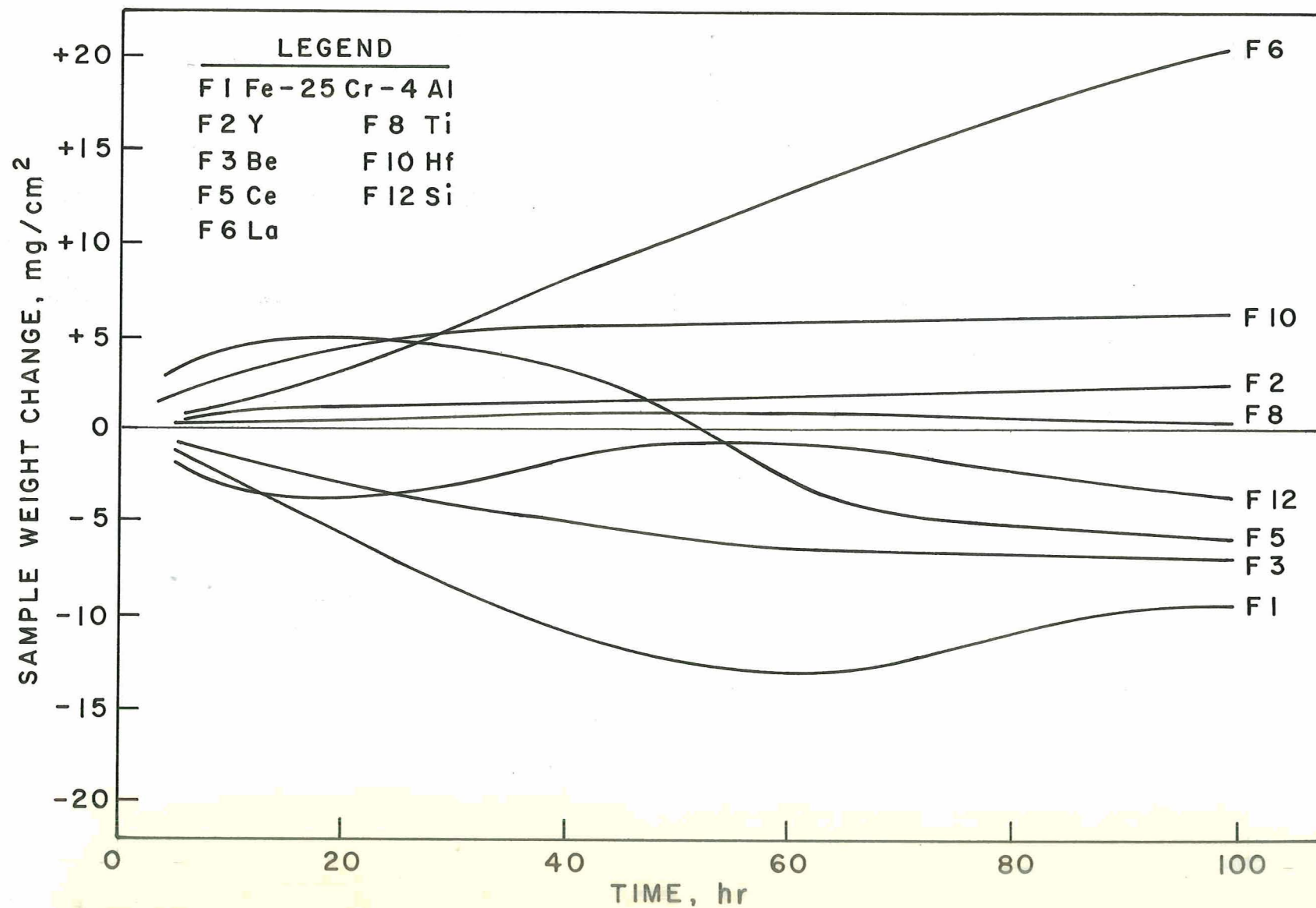
Fig. 4 - Effect of 0.25 a/o Additions on Sample Weight Change of Fe-25Cr-4Al During Cyclic Furnace Oxidation at 2300°F.
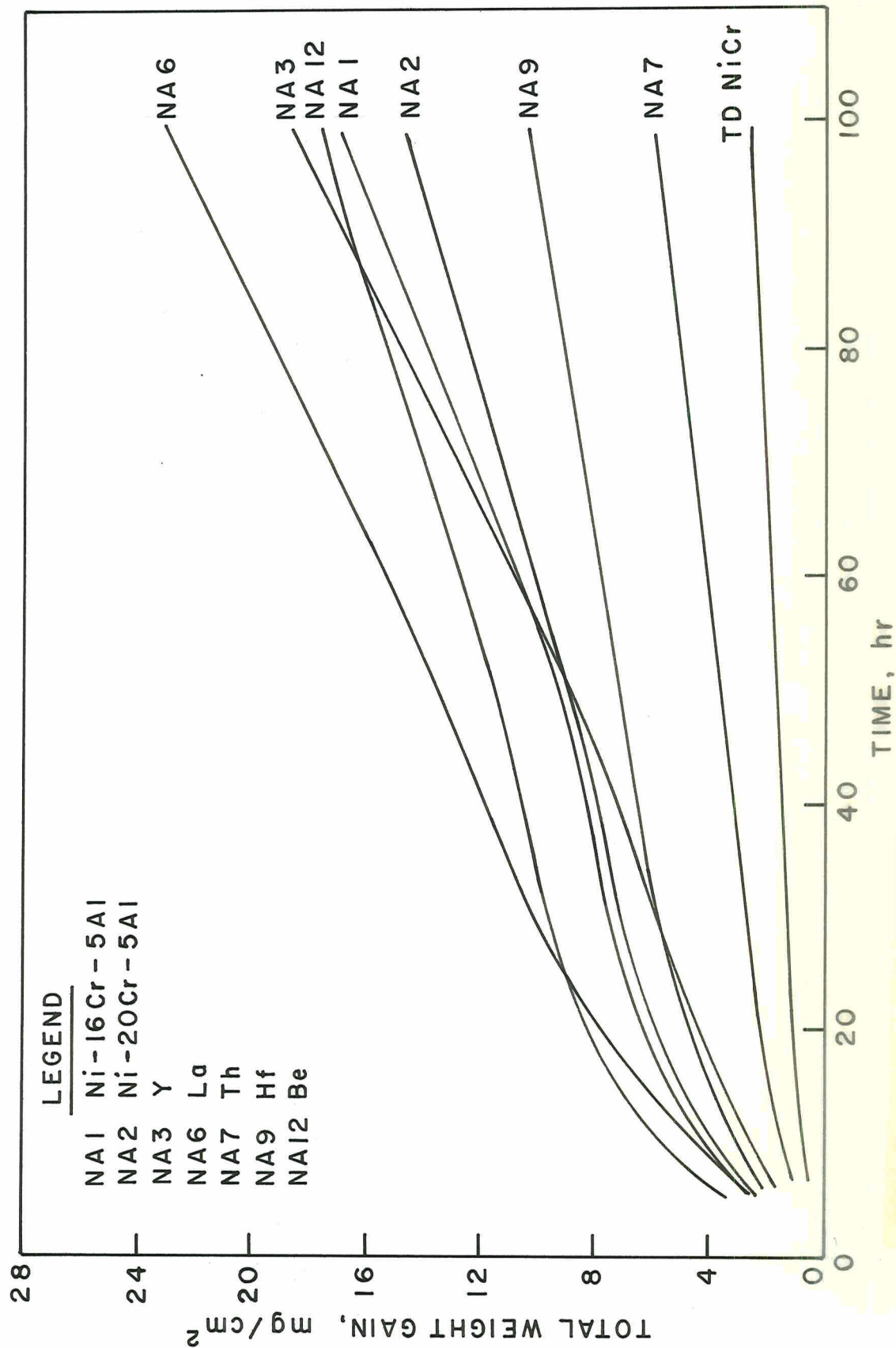
Fig. 5 - Effect of 0.25 a/o Additions on Total Weight Gain of Ni-20Cr-5Al During Cyclic Furnace Oxidation at 2300°F.

LEGEND

NA1	Ni-16Cr-5Al
NA2	Ni-20Cr-5Al
NA3	Y
NA6	La
NA7	Th
NA9	Hf
NA12	Be

118
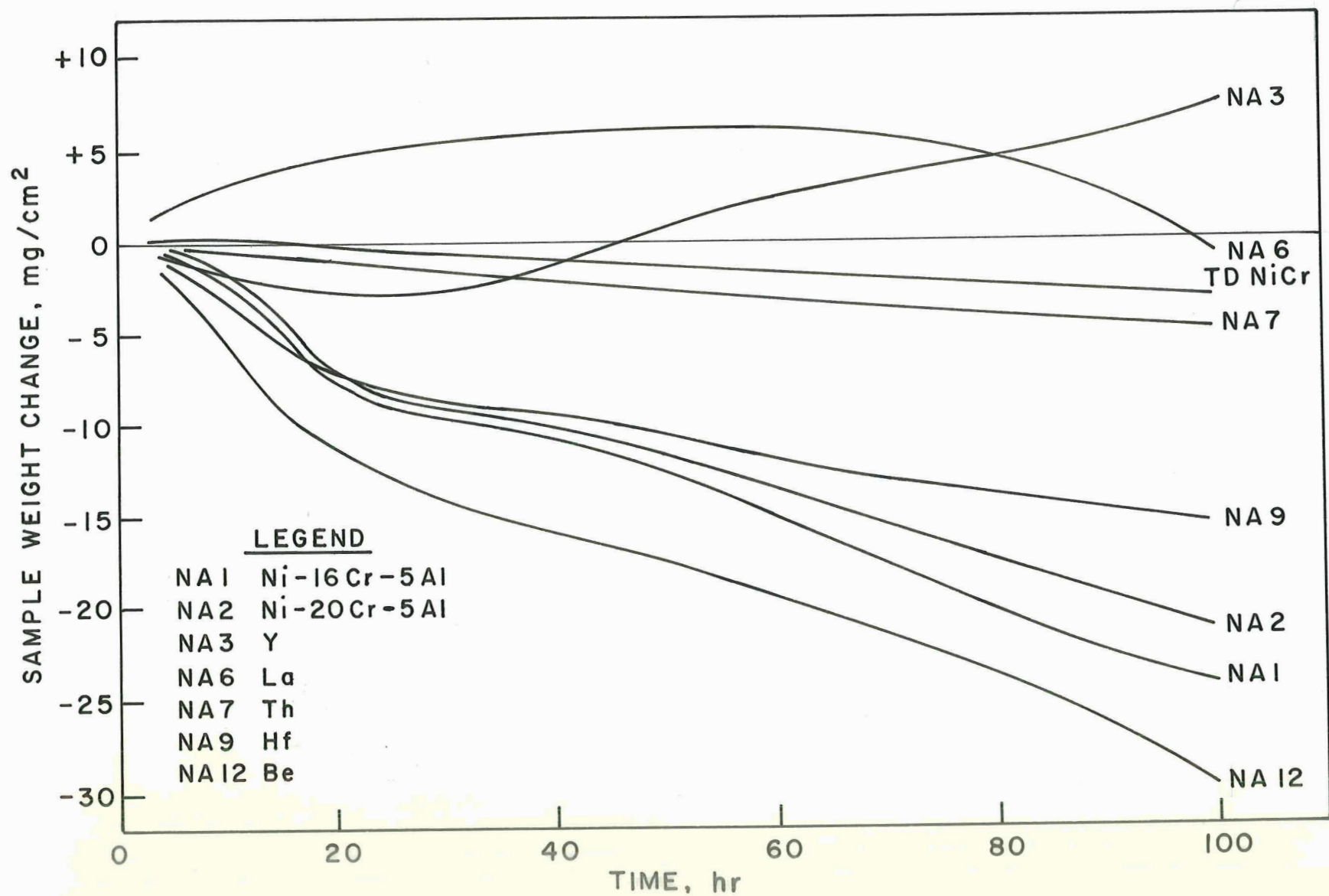
Fig. 6 - Effect of 0.25 a/o Additions on Sample Weight Change of Ni-20Cr-5Al During Cyclic Furnace Oxidation at 2300°F.
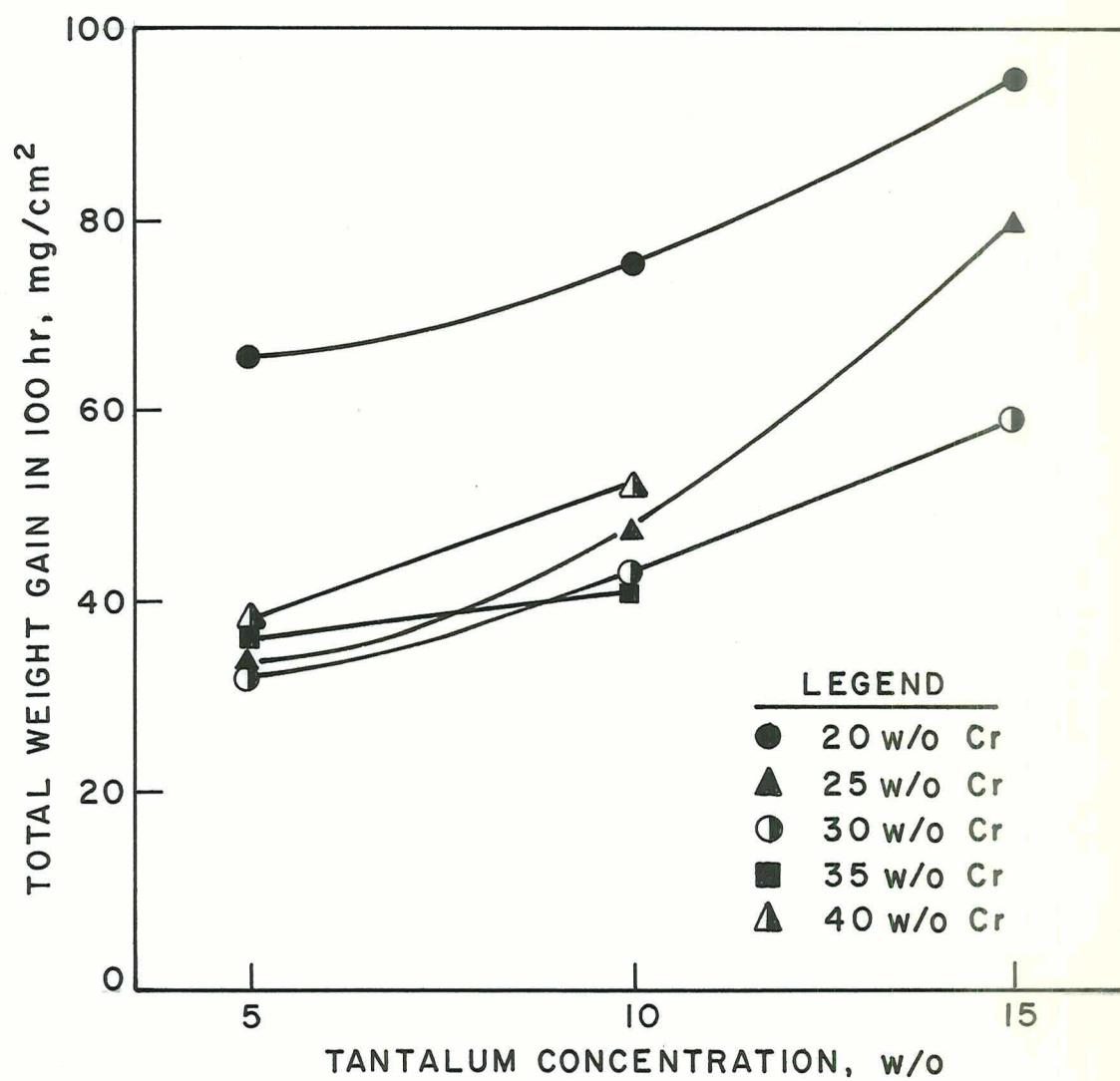
Fig. 7 - Effect of Tantalum on the Total Weight Gain of
Ni-Cr-Ta Alloys After 100 hr at 2300°F.
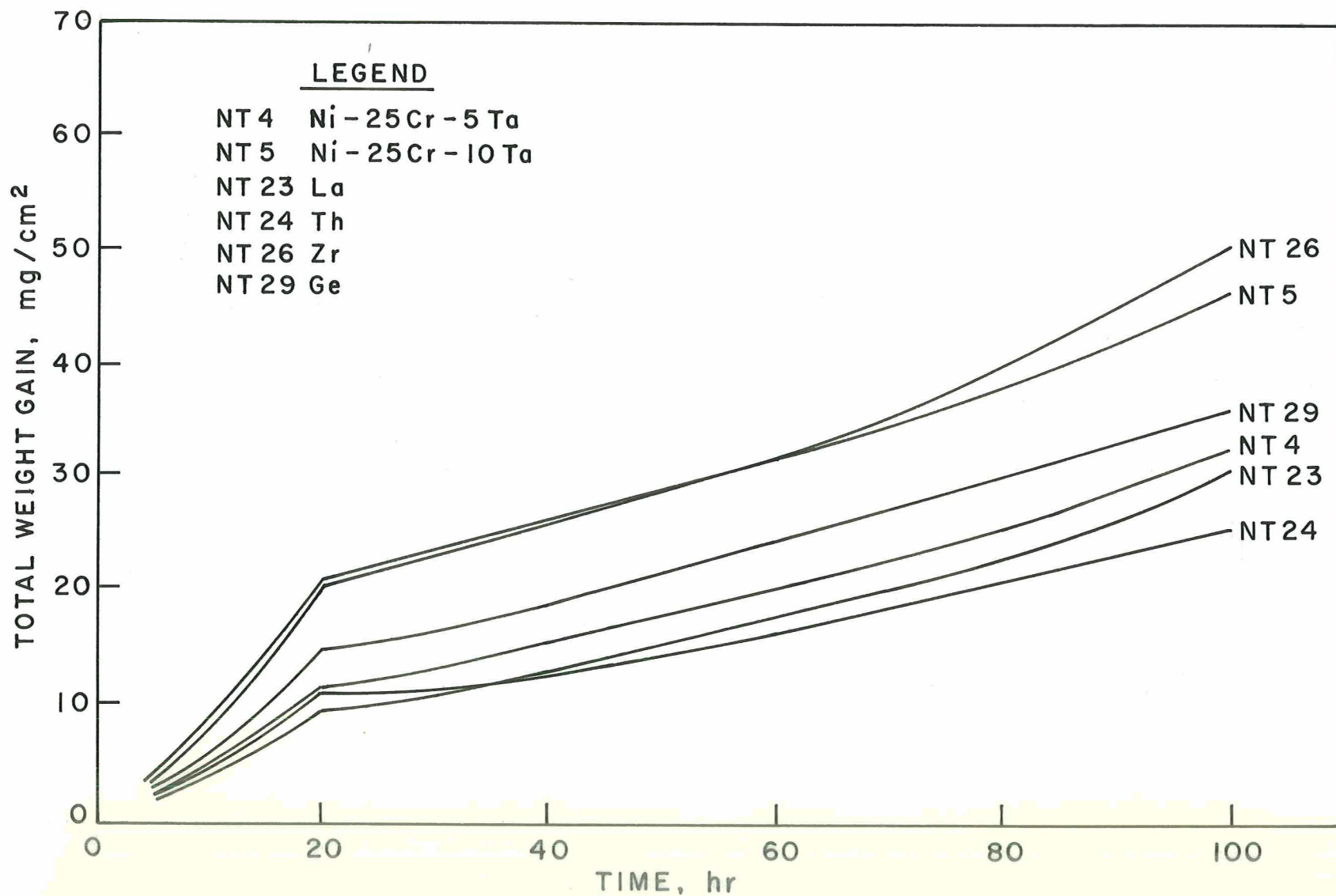
Fig. 8 - Effect of 0.25 a/o Additions on Total Weight Gain of Ni-25Cr-10Ta
During Cyclic Furnace Oxidation at 2300°F.
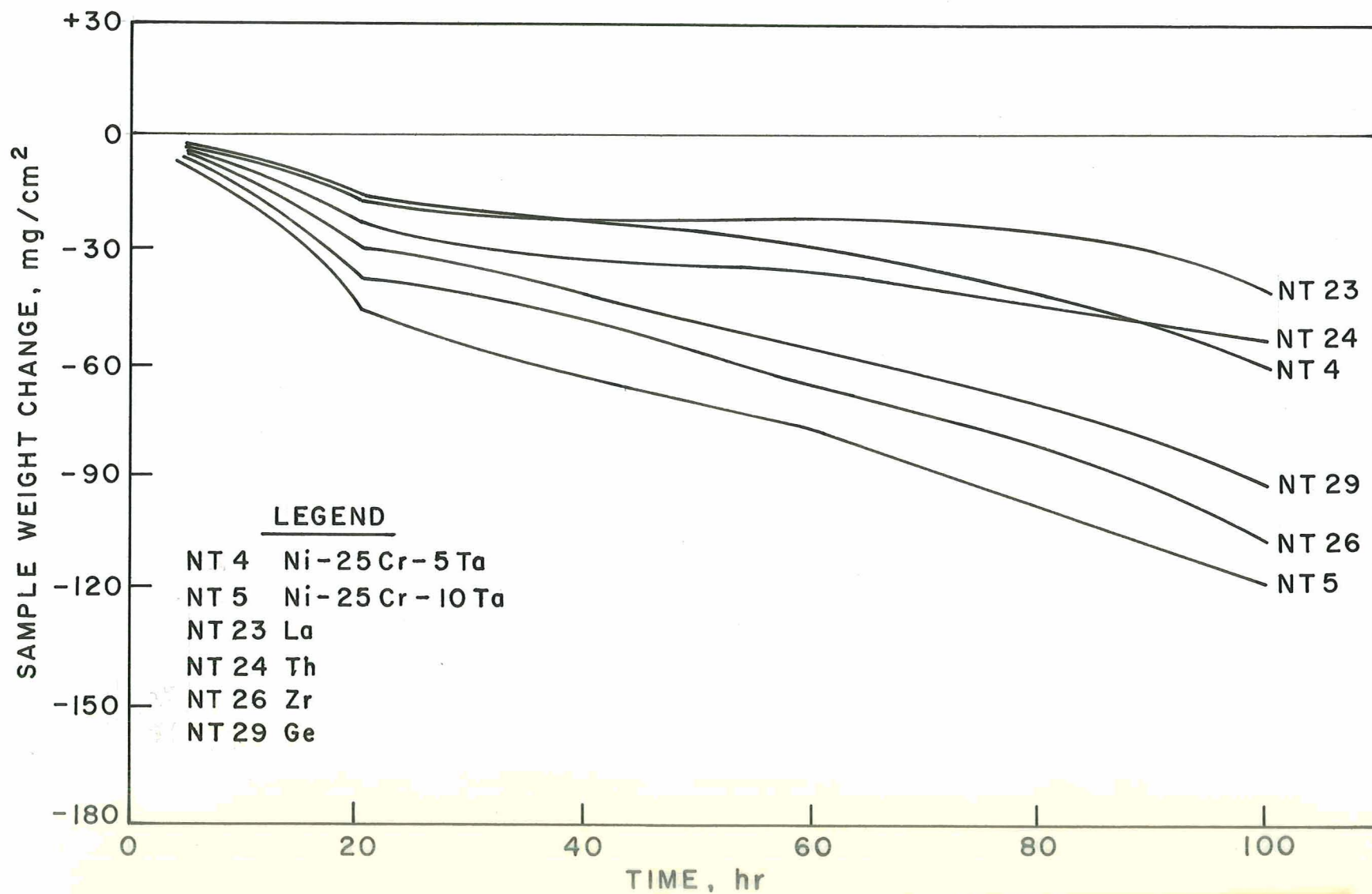
Fig. 9 - Effect of 0.25 a/o Additions on Sample Weight Change of Ni-25Cr-10Ta During Cyclic Furnace Oxidation at 2300°F.
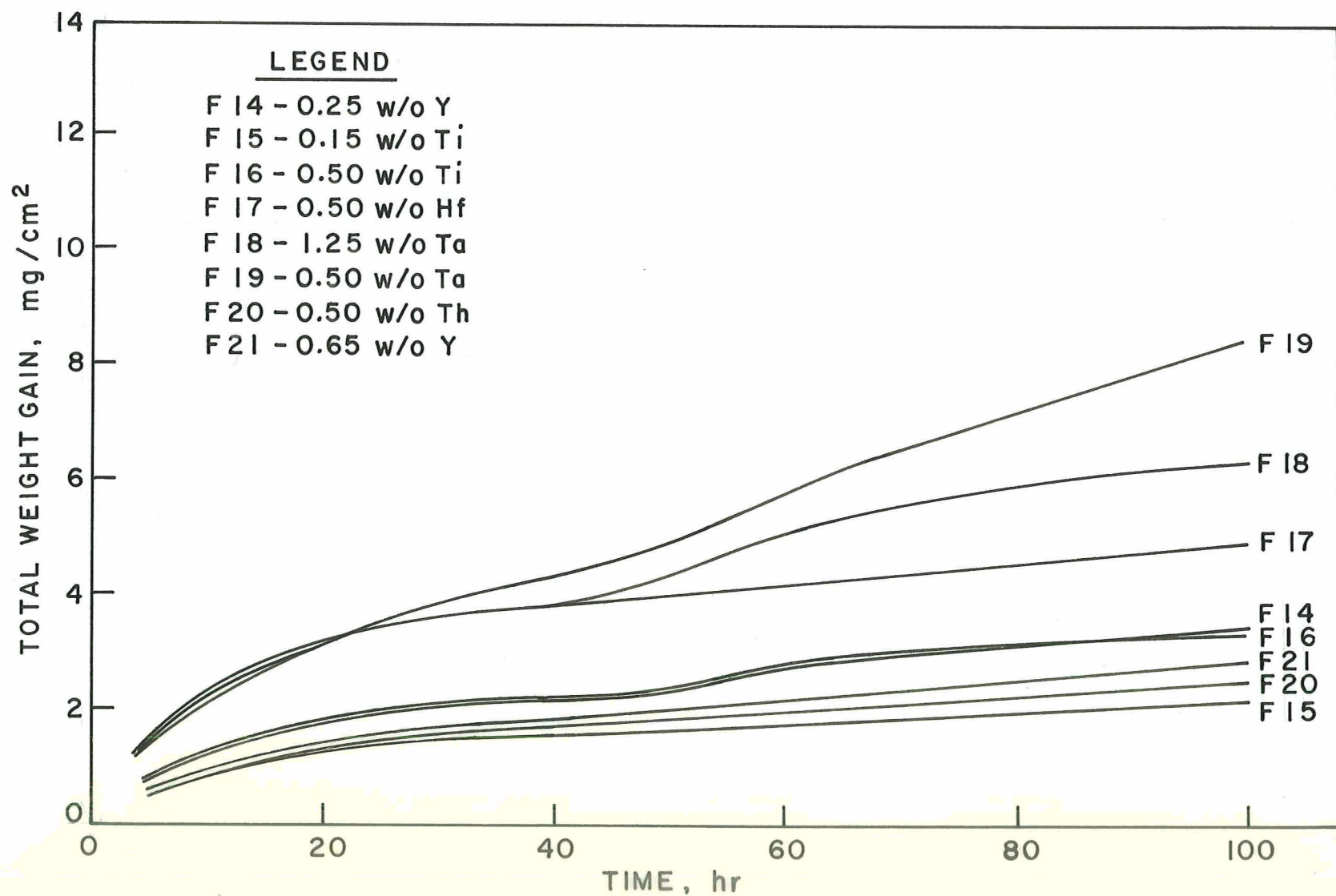
Fig. 10 - Total Weight Gain of Modified Fe-25Cr-4Al Alloys During Cyclic Furnace Oxidation at 2300°F.
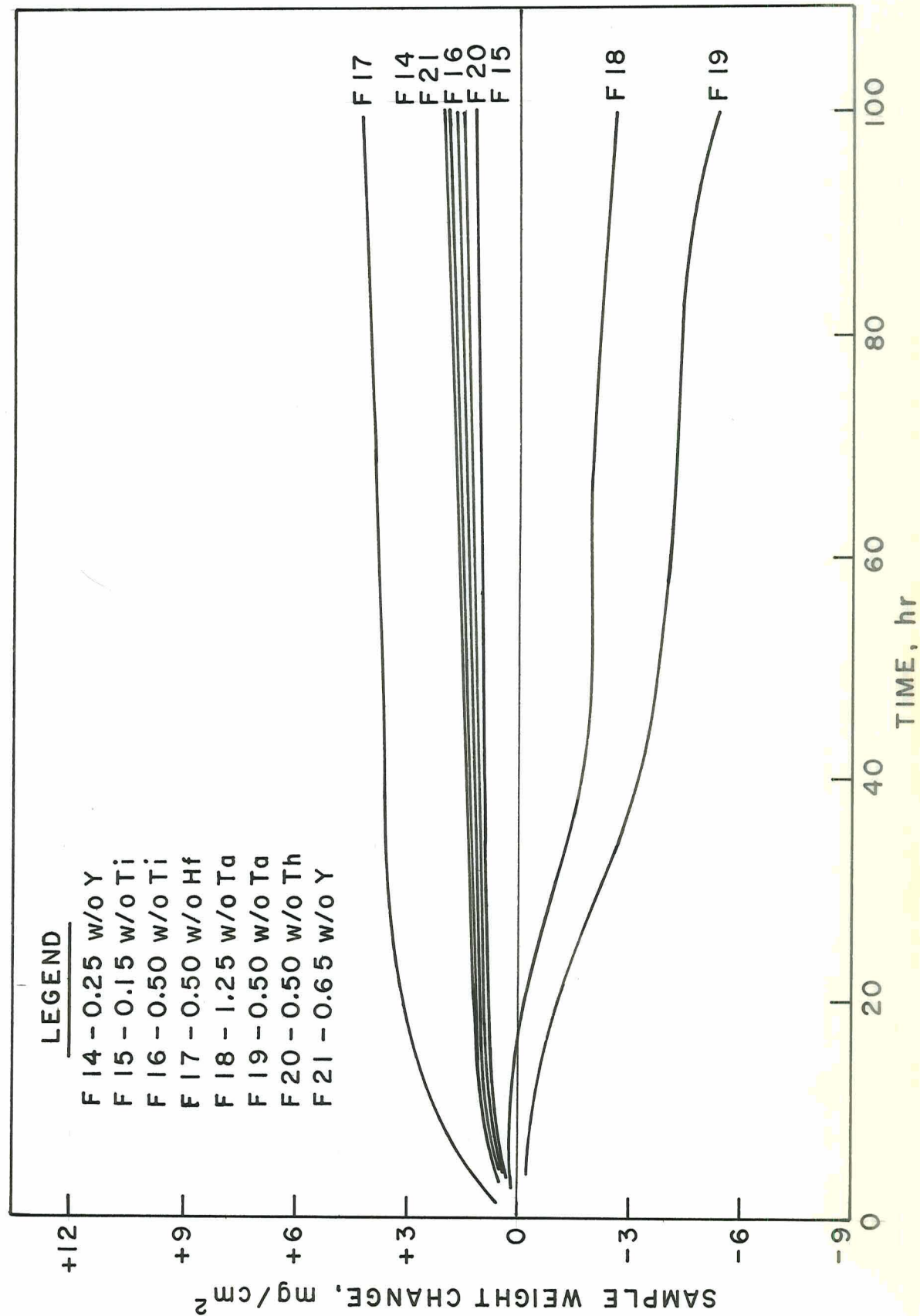
Fig. 11 – Sample Weight Change of Modified Fe-25Cr-4Al Alloys During Cyclic
Furnace Oxidation at 2300°F.

124
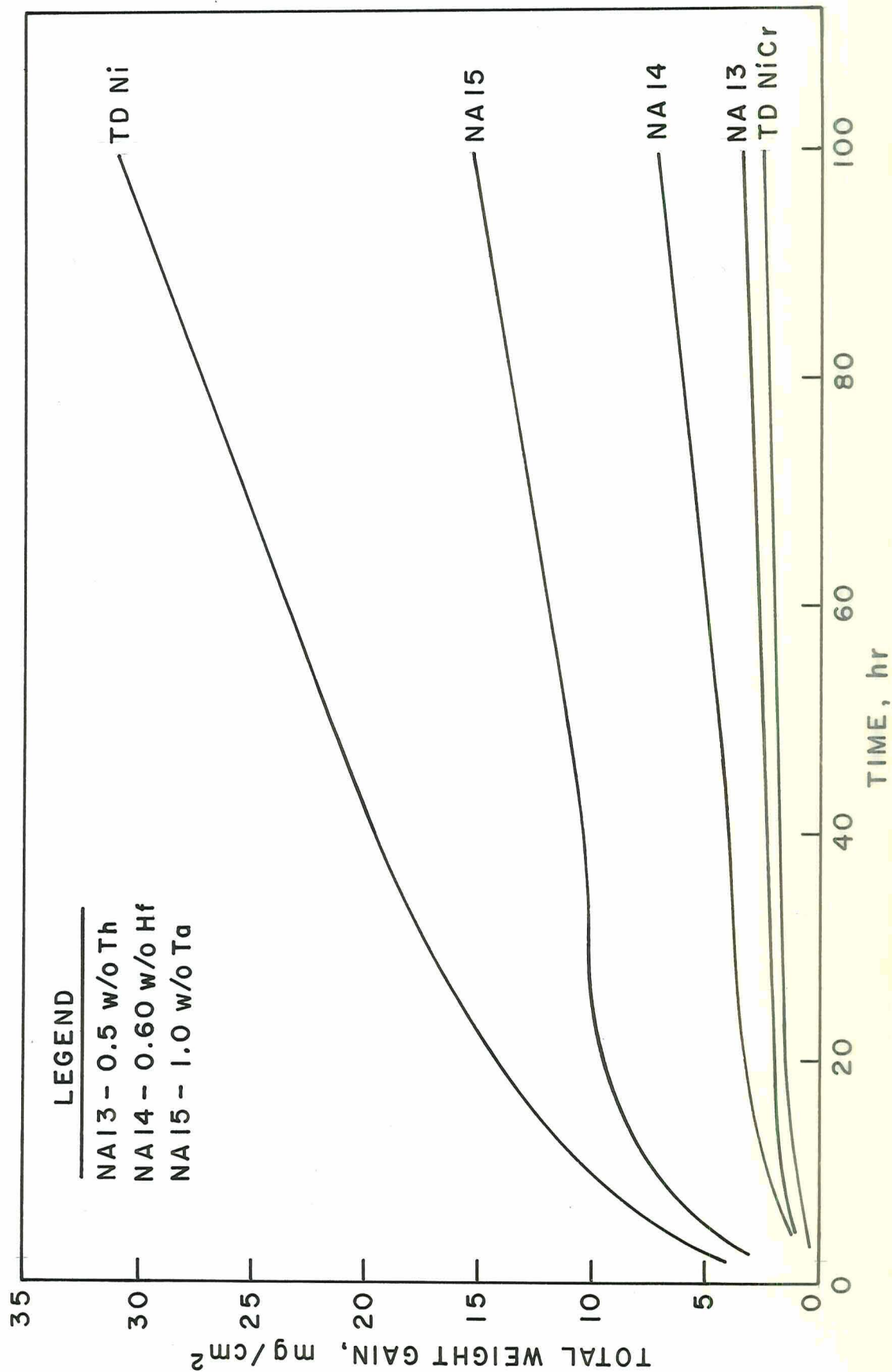
Fig. 12 - Total Weight Gain of Modified Ni-20Cr-5Al Alloys During Cyclic Furnace Oxidation at 2300°F.

125
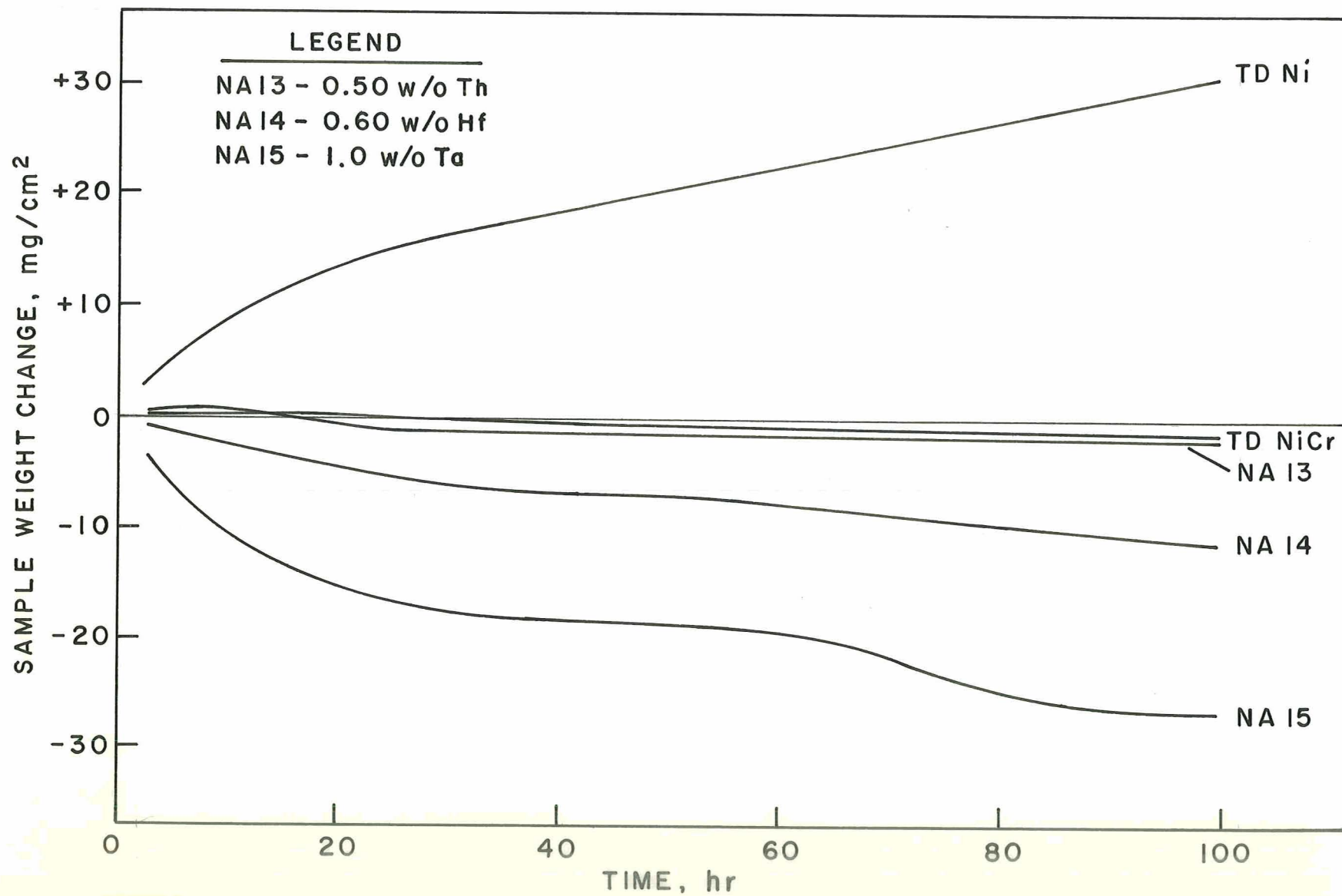
Fig. 13 - Sample Weight Change of Modified Ni-20Cr-5Al Alloys During Cyclic Furnace Oxidation at 2300°F.
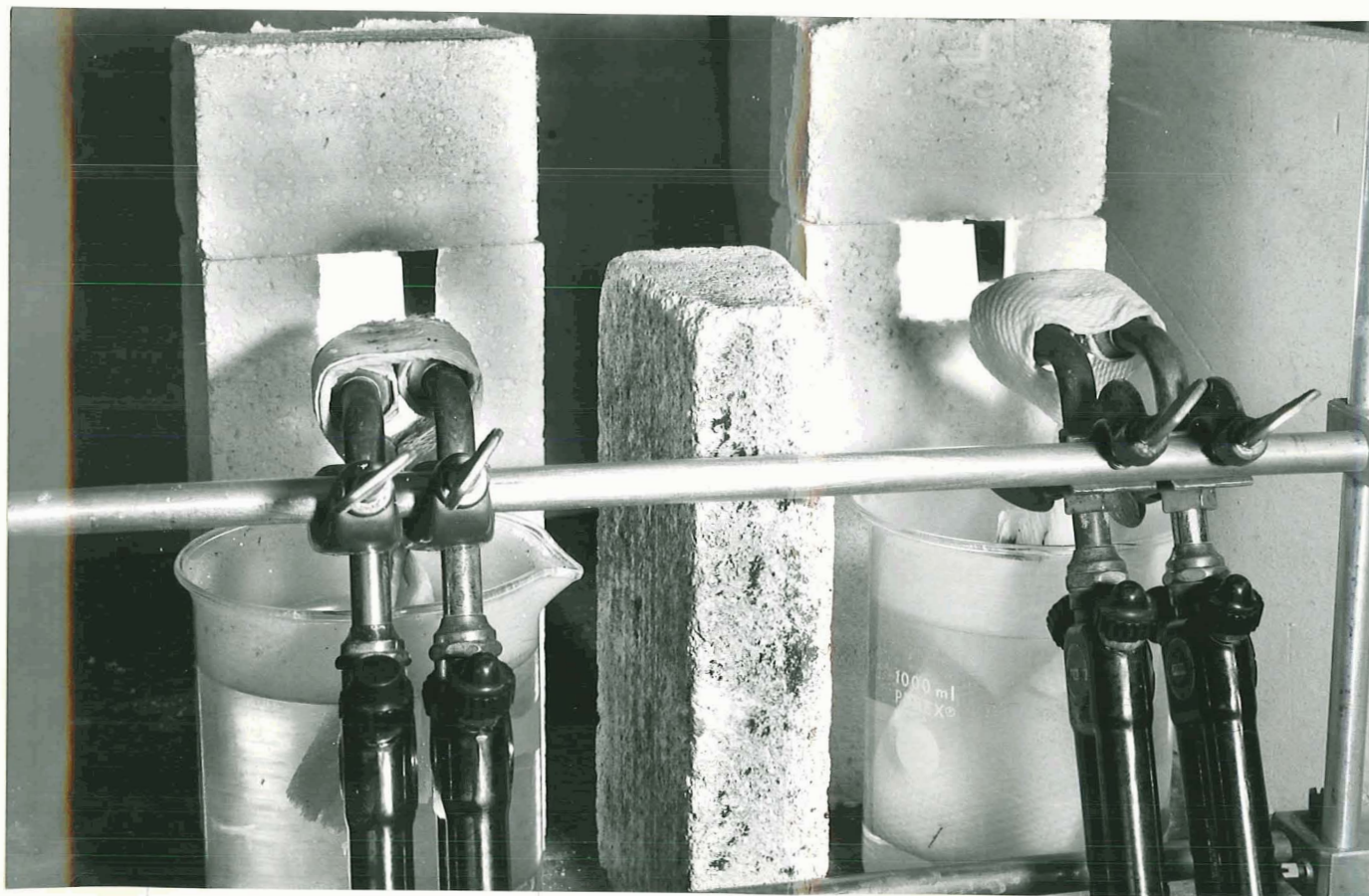
Neg. No. 34796

Fig. 14 - Test Facility for Air-Natural Gas Torch Evaluation
of Modified Task I Alloys
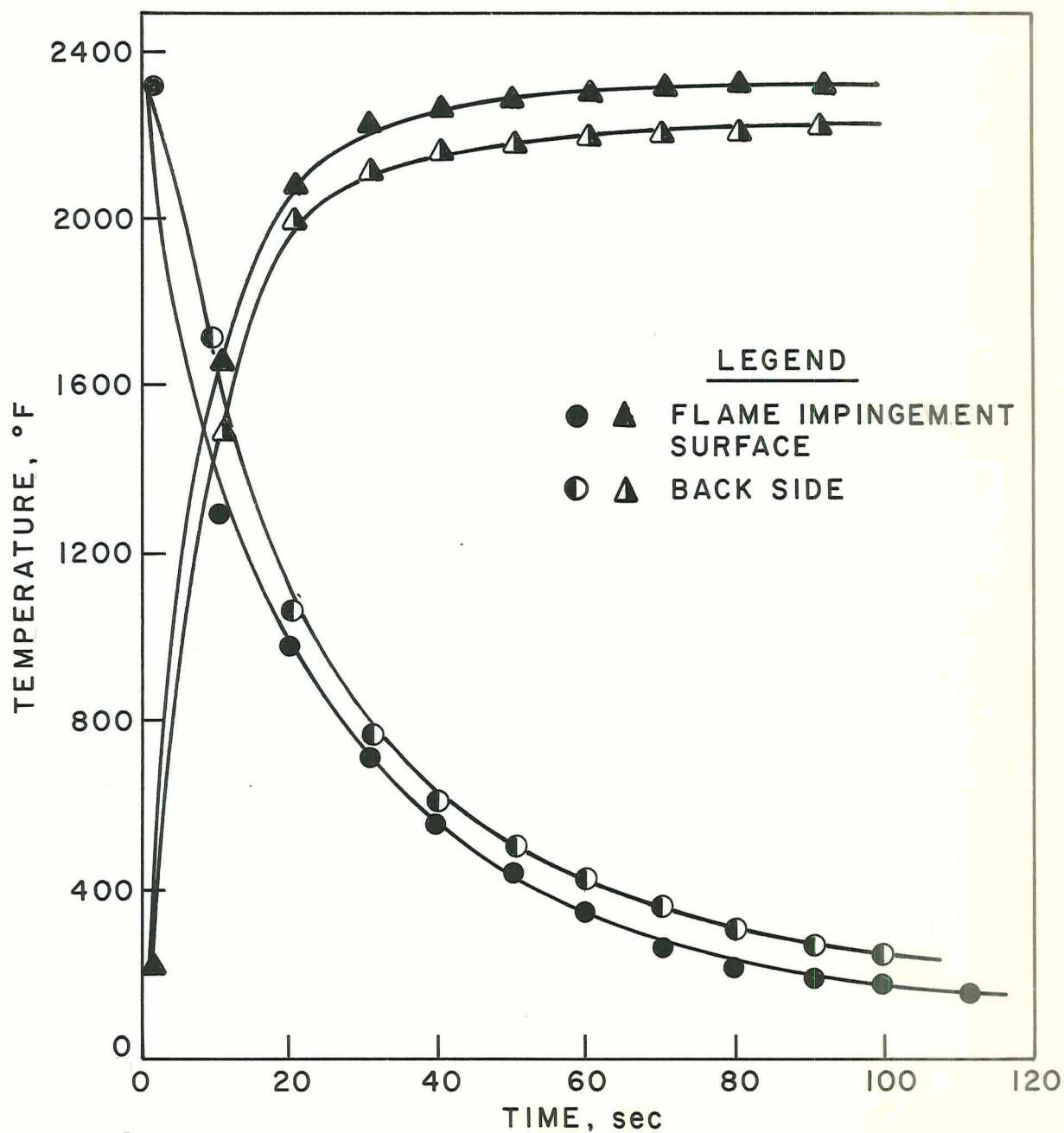
Fig. 15 - Approximate Heating and Air-Quench Cooling Rates of TD Nickel in Air-Natural Gas Torch Facility for 2300°F Optical Temperature Torch Settings.
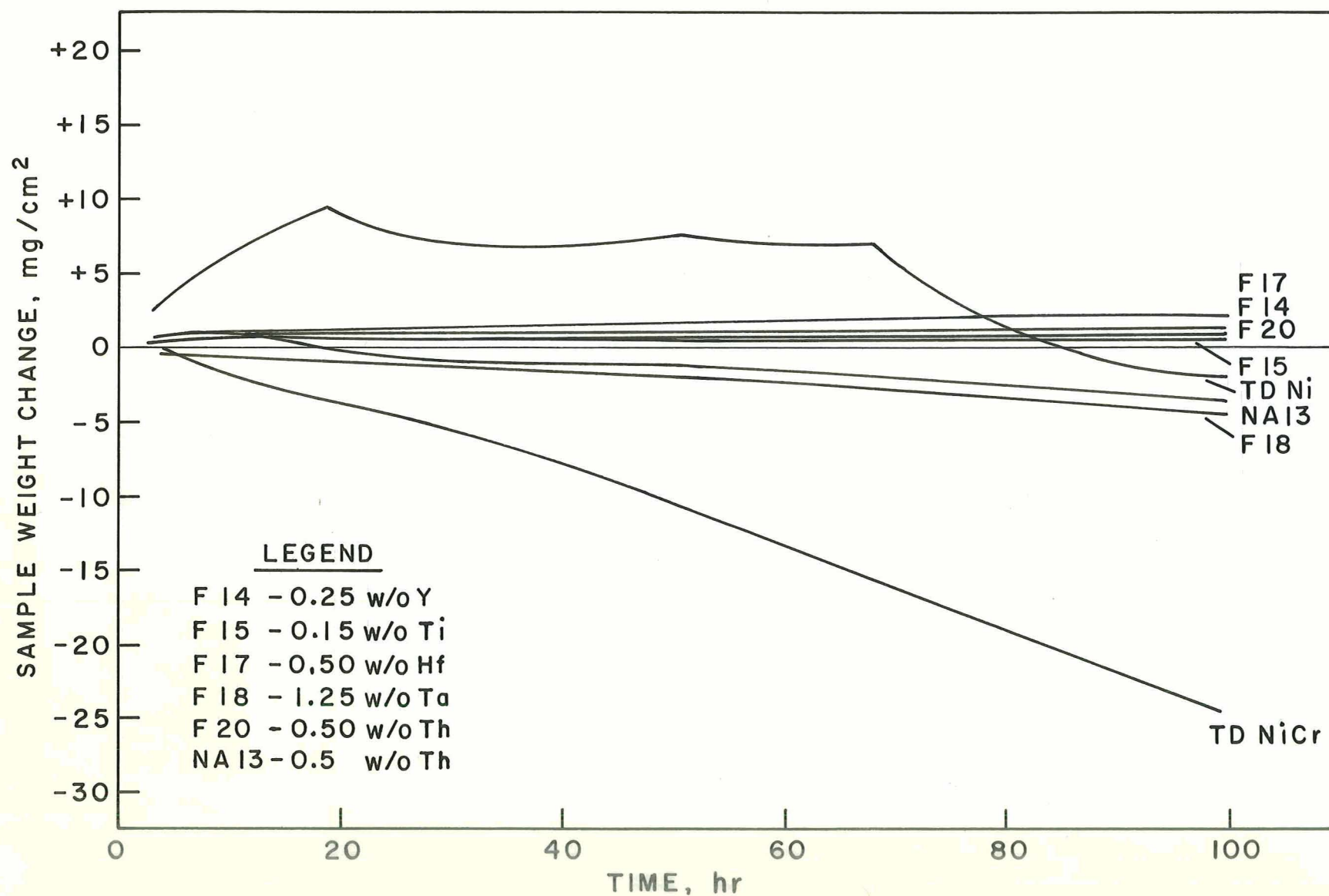
Fig. 16 - Sample Weight Change of Modified Fe-25Cr-4Al and Ni-20Cr-5Al Alloys
During Cyclic Torch Testing at 2300°F.
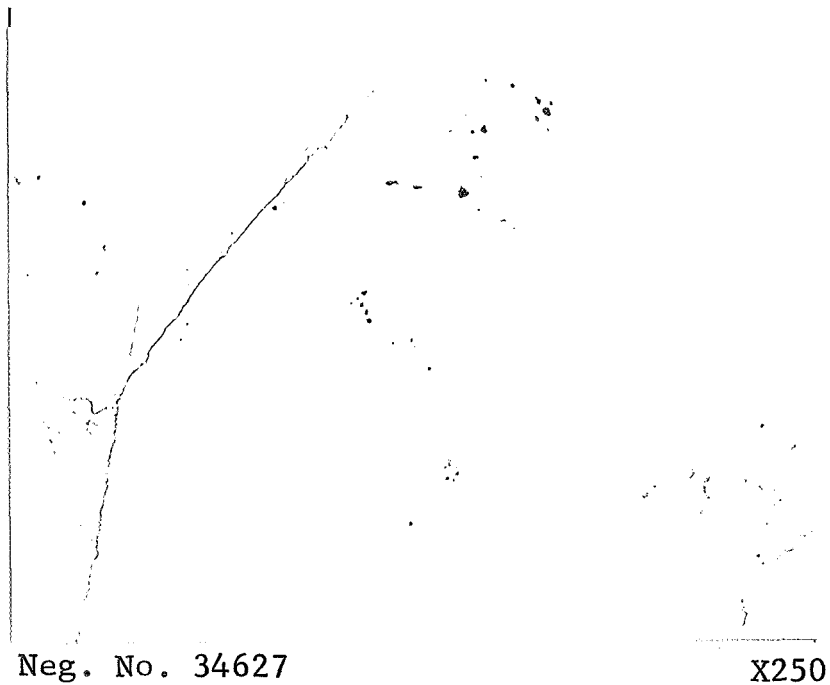
Neg. No. 34627   X250

(a) Hot Rolled
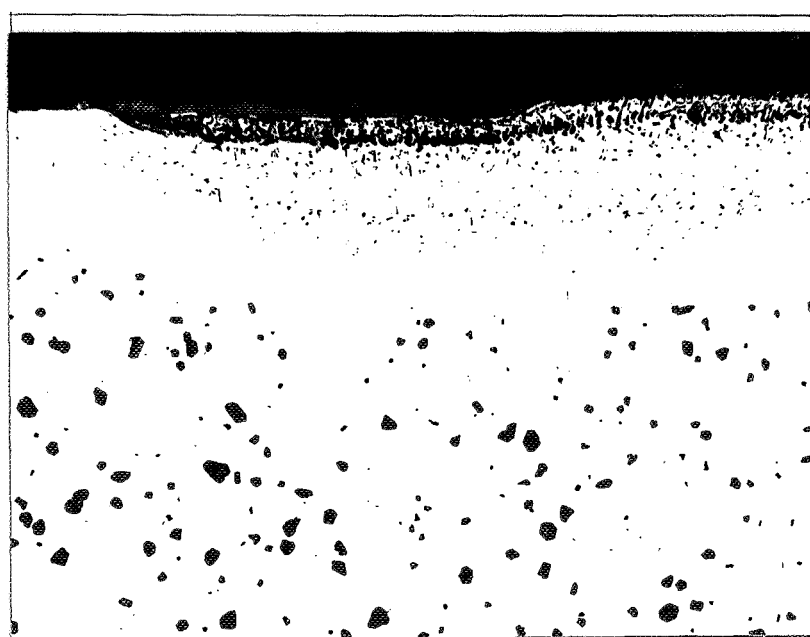
Neg. No. 34497   X100

(b) 2300°F-100 hr.

Fig. 17 — Alloy F1 As Hot Rolled and
              After 100 hr of Cyclic
              Furnace Oxidation at 2300°F.
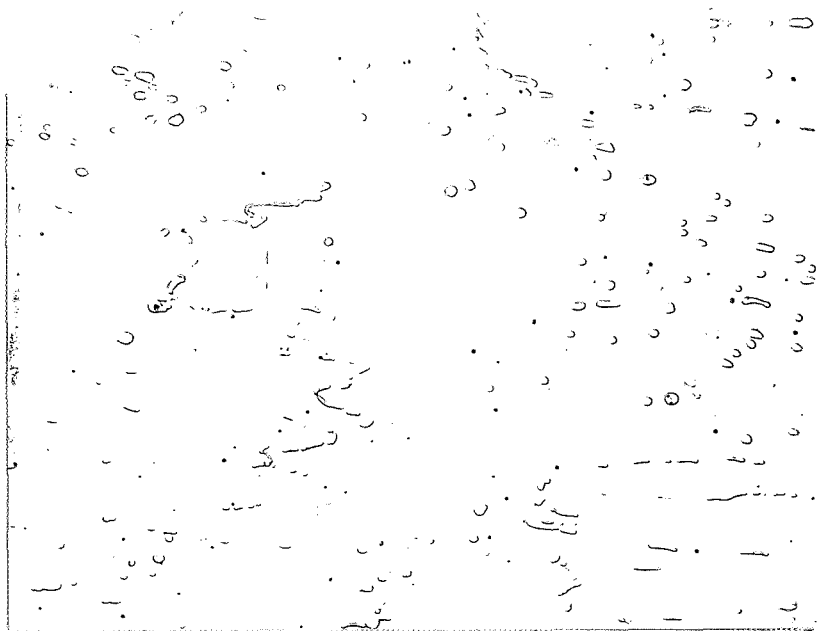
Neg. No. 34626   X250

(a) Hot Rolled
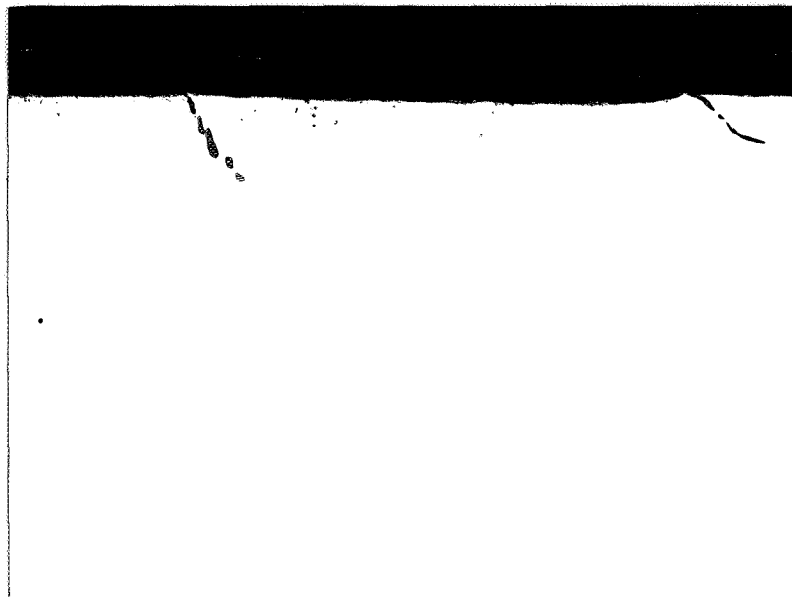
Neg. No. 34499   X250

(b) 2300°F-100 hr

Fig. 18 - Alloy F2 As Hot Rolled and
              After 100 hr of Cyclic
              Furnace Oxidation at 2300°F.

131
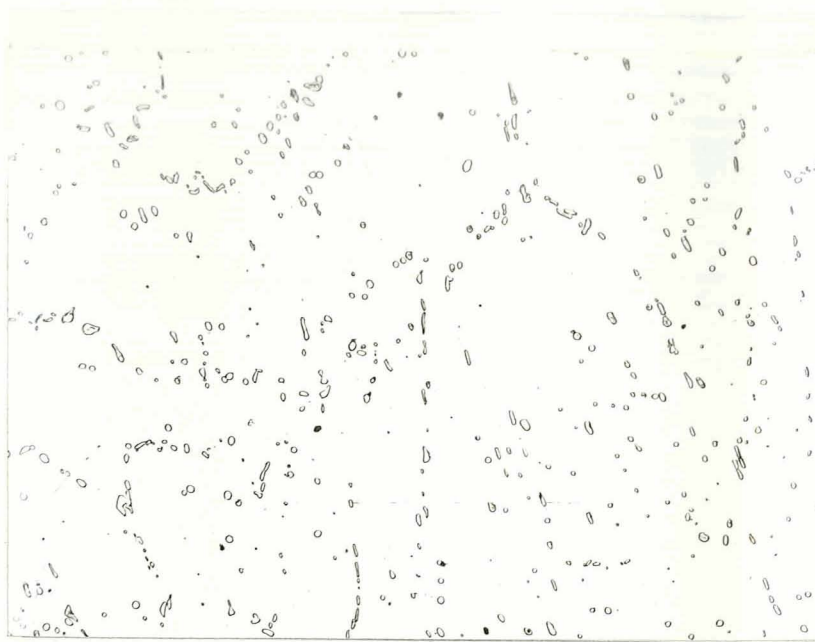
Neg. No. 34631   X250

(a) Hot Rolled
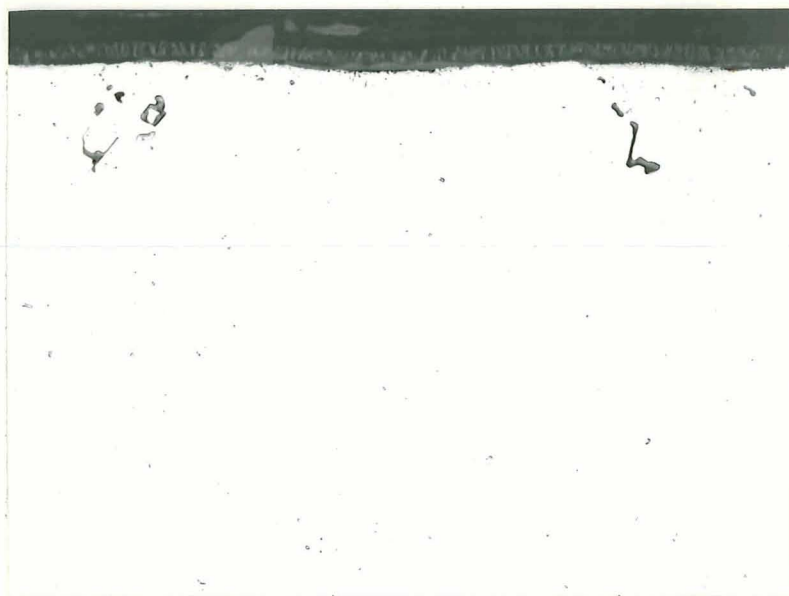
Neg. No. 34500   X250

(b) 2300°F-100 hr

Fig. 19 - Alloy F7 As Hot Rolled and After 100 hr of Cyclic Furnace Oxidation at 2300°F.

132

Neg. No. 34628   X250

(a) Hot Rolled

Neg. No. 34501   X250

(b) 2300°F-100 hr

Fig. 20 - Alloy F8 As Hot Rolled and
            After 100 hr of Cyclic
            Furnace Oxidation at 2300°F.

Neg. No. 34629   X250

(a) Hot Rolled

Neg. No. 34502   X250

(b) 2300°F-100 hr

Fig. 21 - Alloy F10 As Hot Rolled and
After 100 hr of Cyclic
Furnace Oxidation at 2300°F.
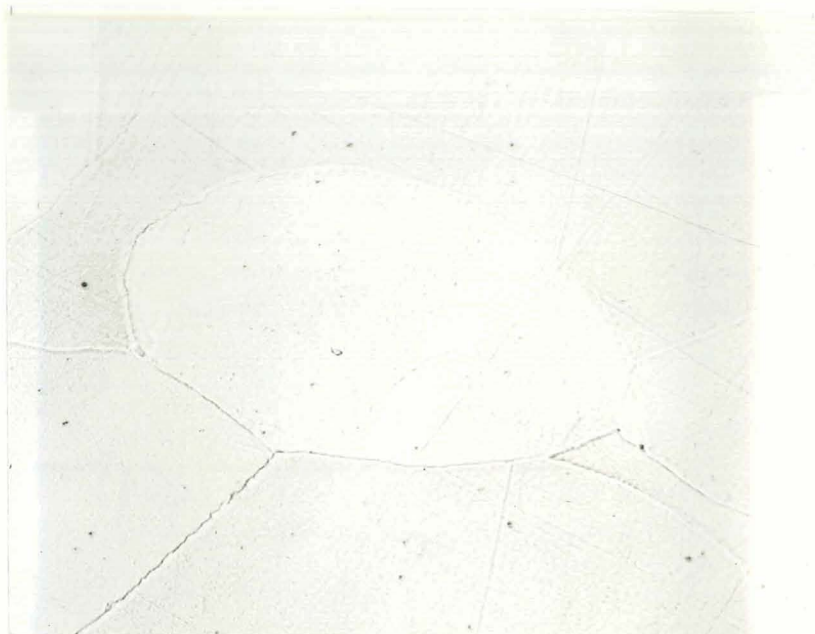
Neg. No. 34630   X250

(a) Hot Rolled

Neg. No. 34503   X250

(b) 2300°F-100 hr

Fig. 22 - Alloy F11 As Hot Rolled and
              After 100 hr of Cyclic
              Furnace Oxidation at 2300°F.
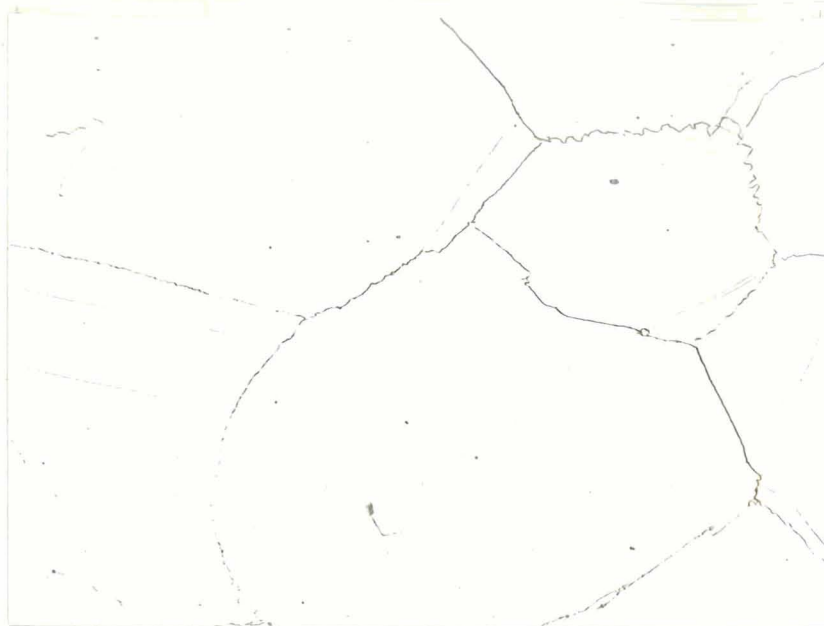
Neg. No. 34632   X250

(a) Hot Rolled

Neg. No. 34496   X100

(b) 2300°F-100 hr

Fig. 23 - Alloy NA2 As Hot Rolled and
             After 100 hr of Cyclic
             Furnace Oxidation at 2300°F.

136

Neg. No. 34634   X250

(a) Hot Rolled

Neg. No. 34504   X100

(b) 2300°F-100 hr

Fig. 24 - Alloy NA7 As Hot Rolled and
After 100 hr of Cyclic
Furnace Oxidation at 2300°F.

137

Neg. No. 34633   X250

(a) Hot Rolled
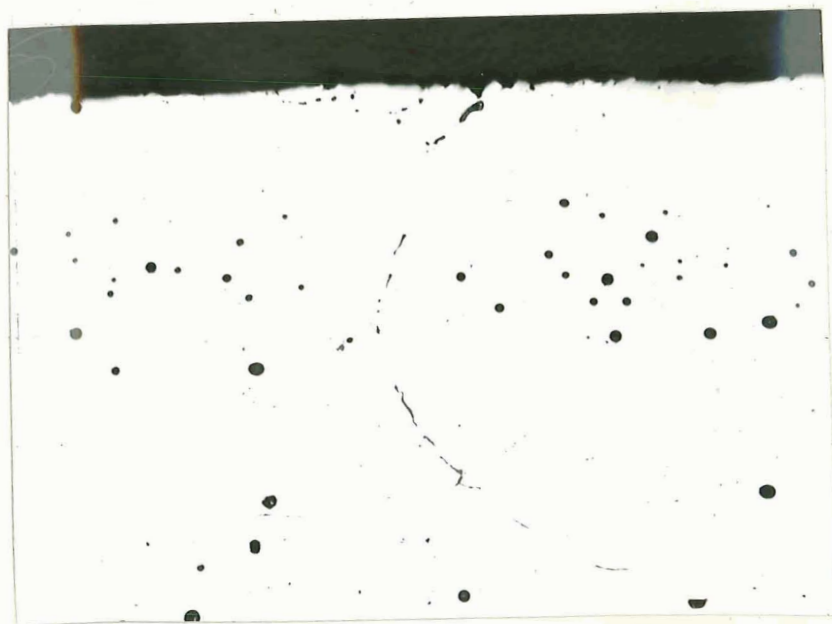
Neg. No. 34505   X100

(b) 2300°F-100 hr

Fig. 25 - Alloy NA9 As Hot Rolled and
             After 100 hr of Cyclic
             Furnace Oxidation at 2300°F.
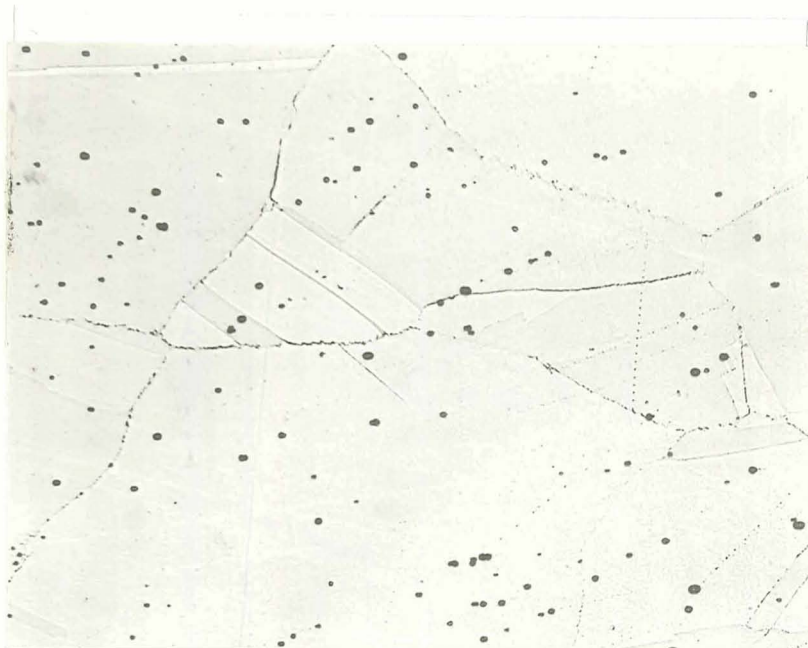
Neg. No. 34635   X250

(a) Hot Rolled
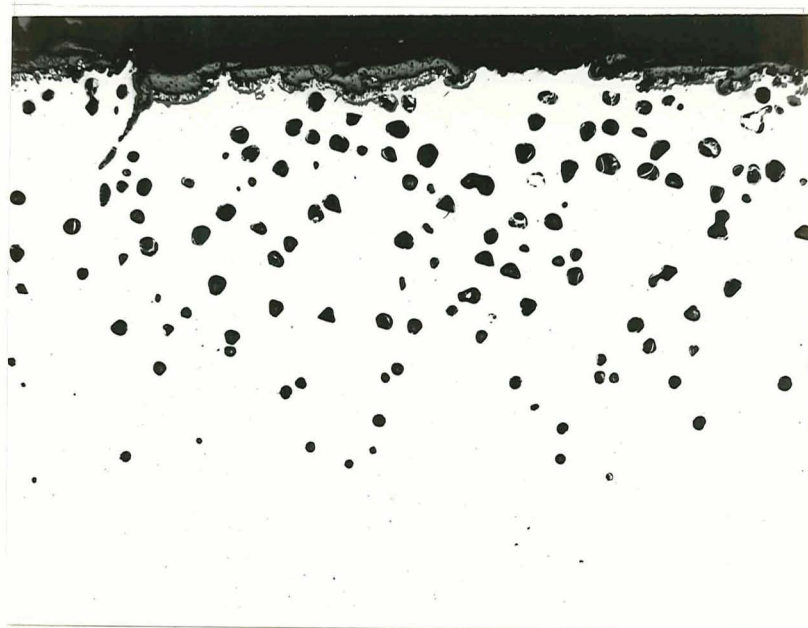
Neg. No. 34498   X100

(b) 2300°F-100 hr

Fig. 26 - Alloy NT5 As Hot Rolled and
After 100 hr of Cyclic
Furnace Oxidation at 2300°F.
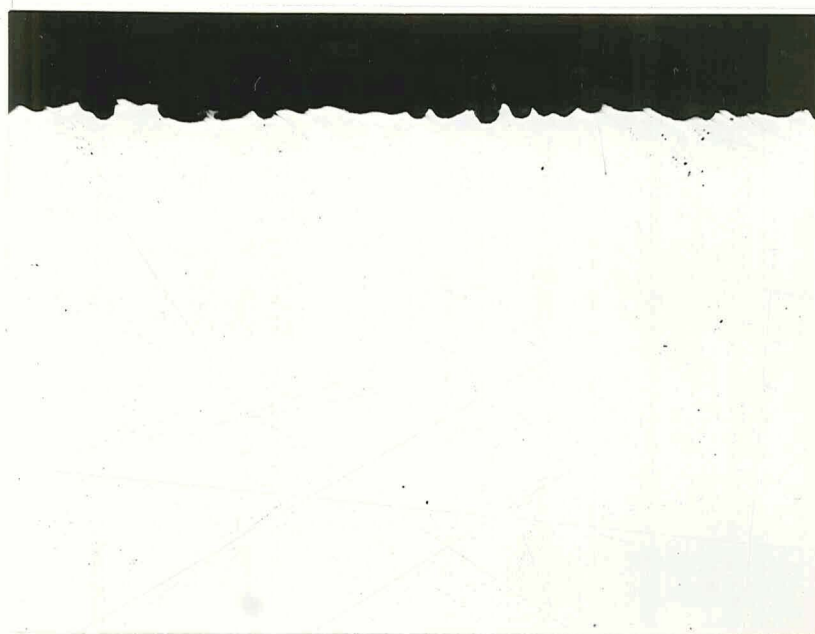
Neg. No.   X200

(a) F15
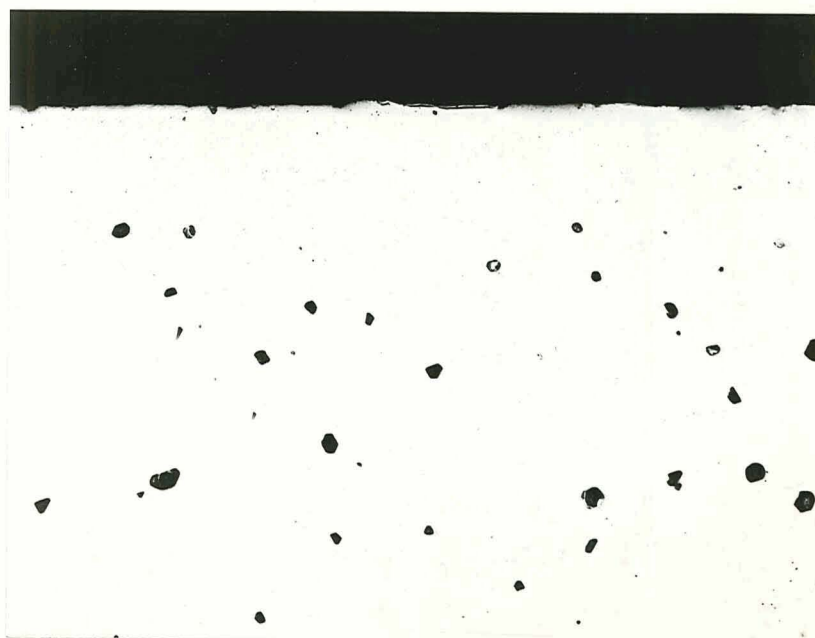
Neg. No. 31931   X200

(b) NA13

Fig. 27 – Surface of Modified Task I Alloys
          After Cyclic Torch Oxidation at
          2300°F for 100 hr.
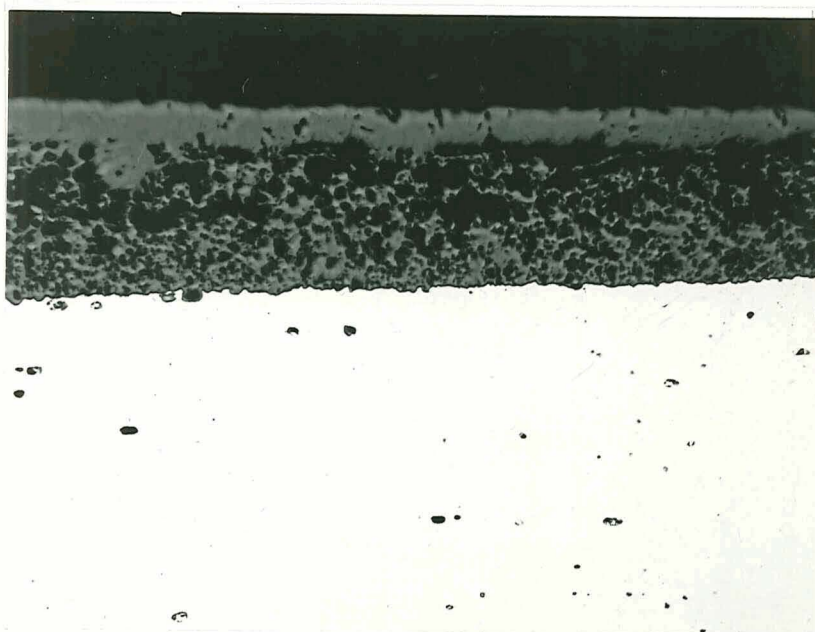
Neg. No. 34929　　　　　　　　　　　　　X200

(a) TD Ni
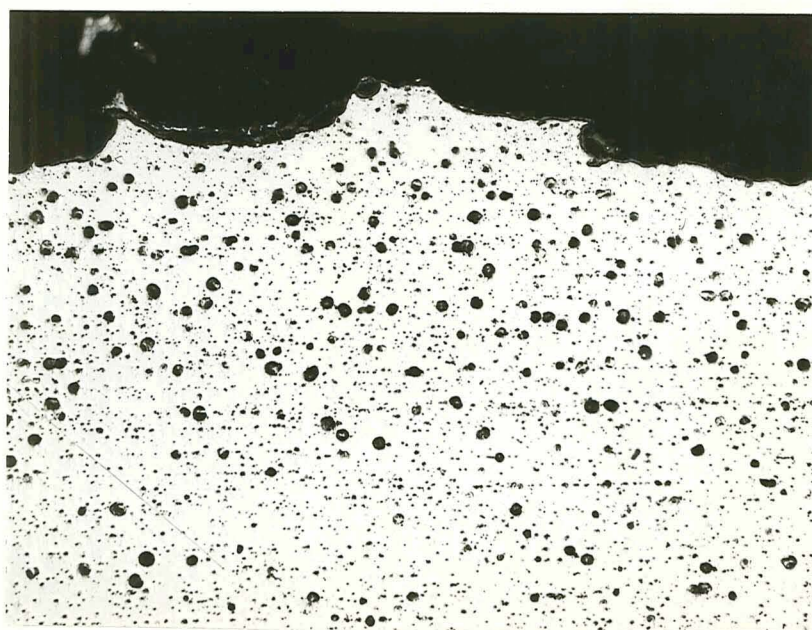
Neg. No. 34933　　　　　　　　　　　　　X200

(b) TD NiCr

Fig. 28 - Surface of TD Ni and TD NiCr After
　　　　　Cyclic Torch Oxidation at 2300°F
　　　　　for 100 hr.

X200

Neg. No. 34927

(a) F15

X200

Neg. No. 34934

(b) NA13

X200

Neg. No 34928

(c) TD Ni

Fig. 29 - Surface of Selected Alloys after Sulfidation Exposure at 1650°F for 20 hr.

142
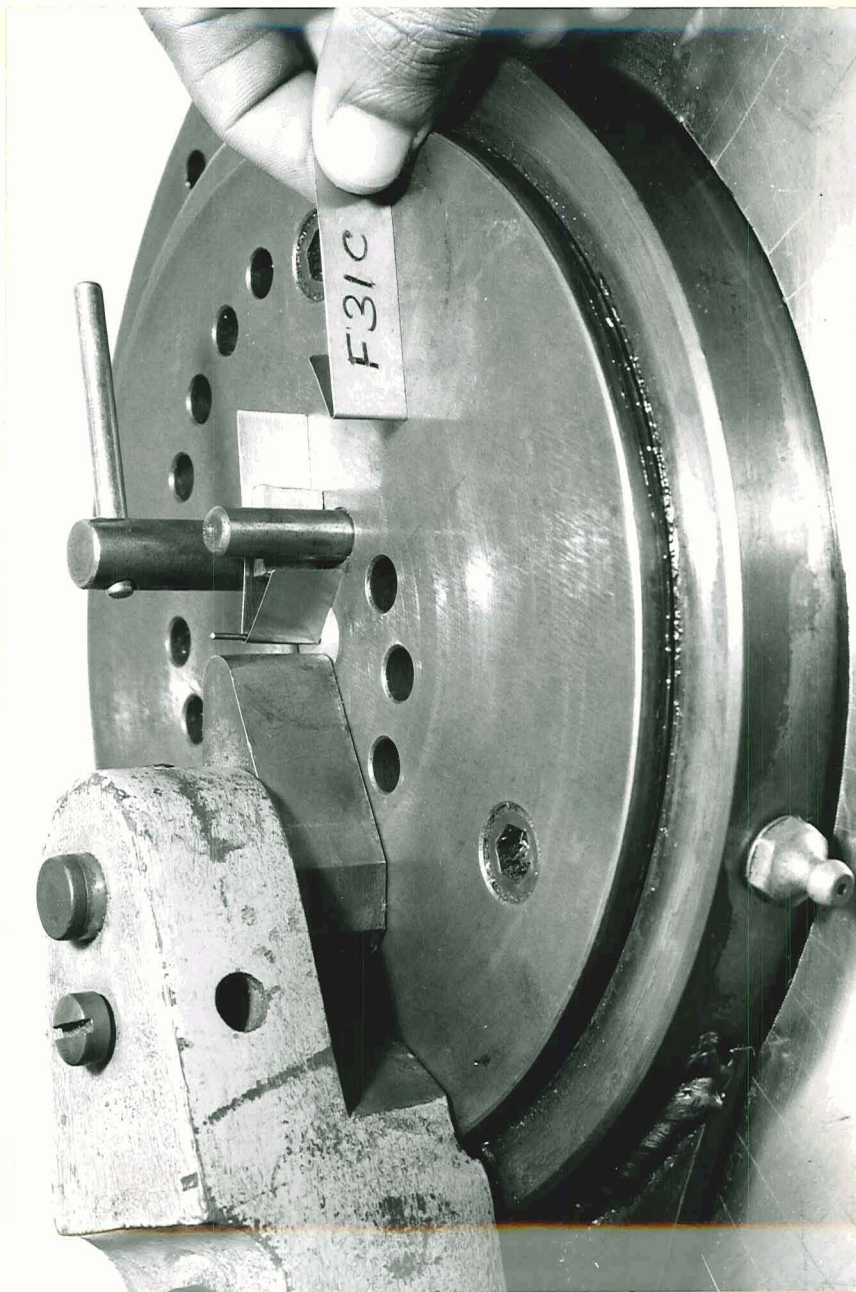
Neg. No. 35423   Fig. 30 - Test Fixture for 180°-4t Bend Testing.

143

F7

F11

TD NiCr

F2

F10

NA7

F1

F8

NA9

NA2
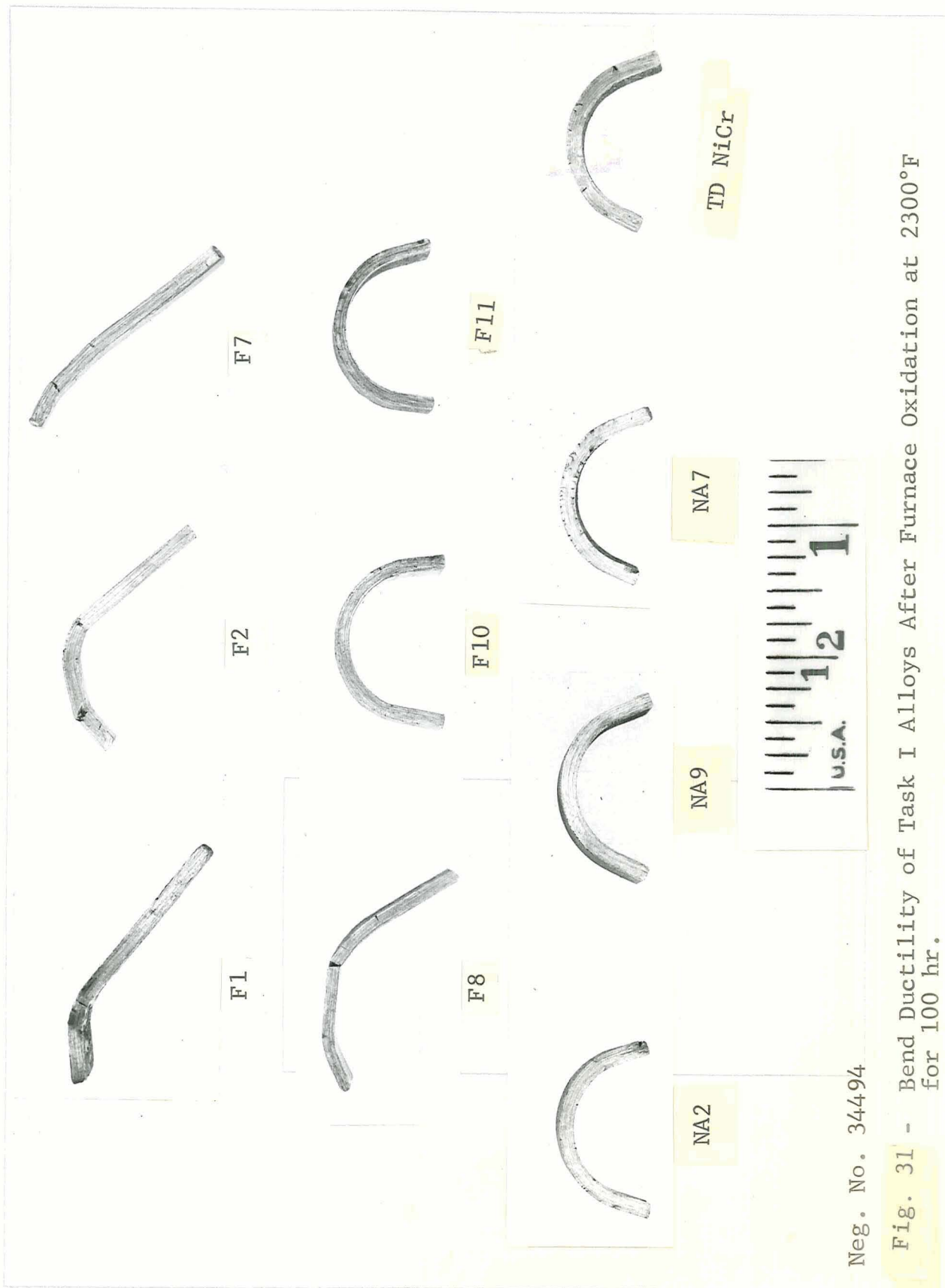
Neg. No. 34494

Fig. 31 – Bend Ductility of Task I Alloys After Furnace Oxidation at 2300°F for 100 hr.

144
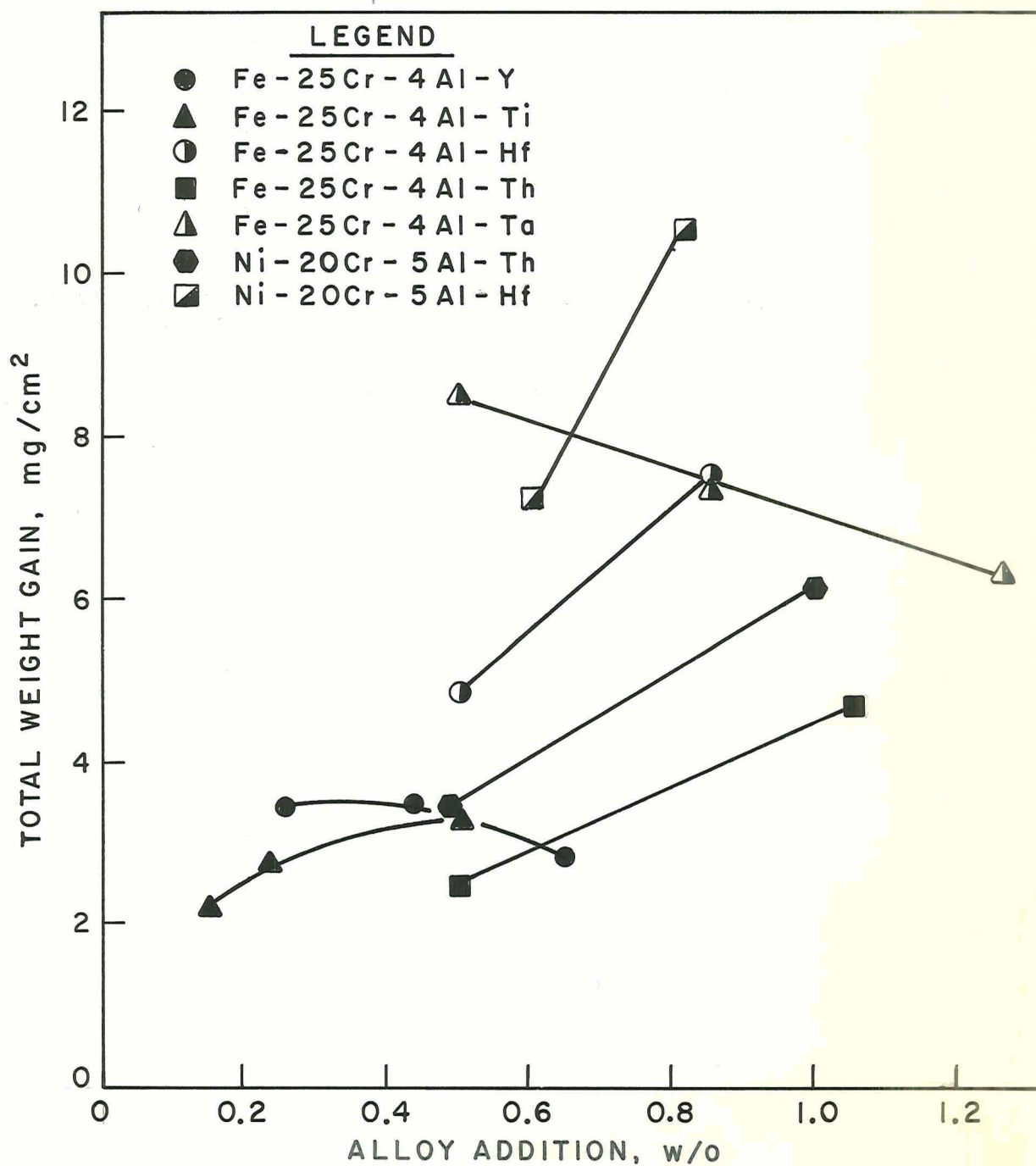
Fig. 32 - Total Weight Gain for Task I Alloys After 100 hr
Cyclic Furnace Oxidation at 2300°F.

145

Oxidation
Specimen

Cold Rolled

Sectioned
and Ground

Hot Rolled
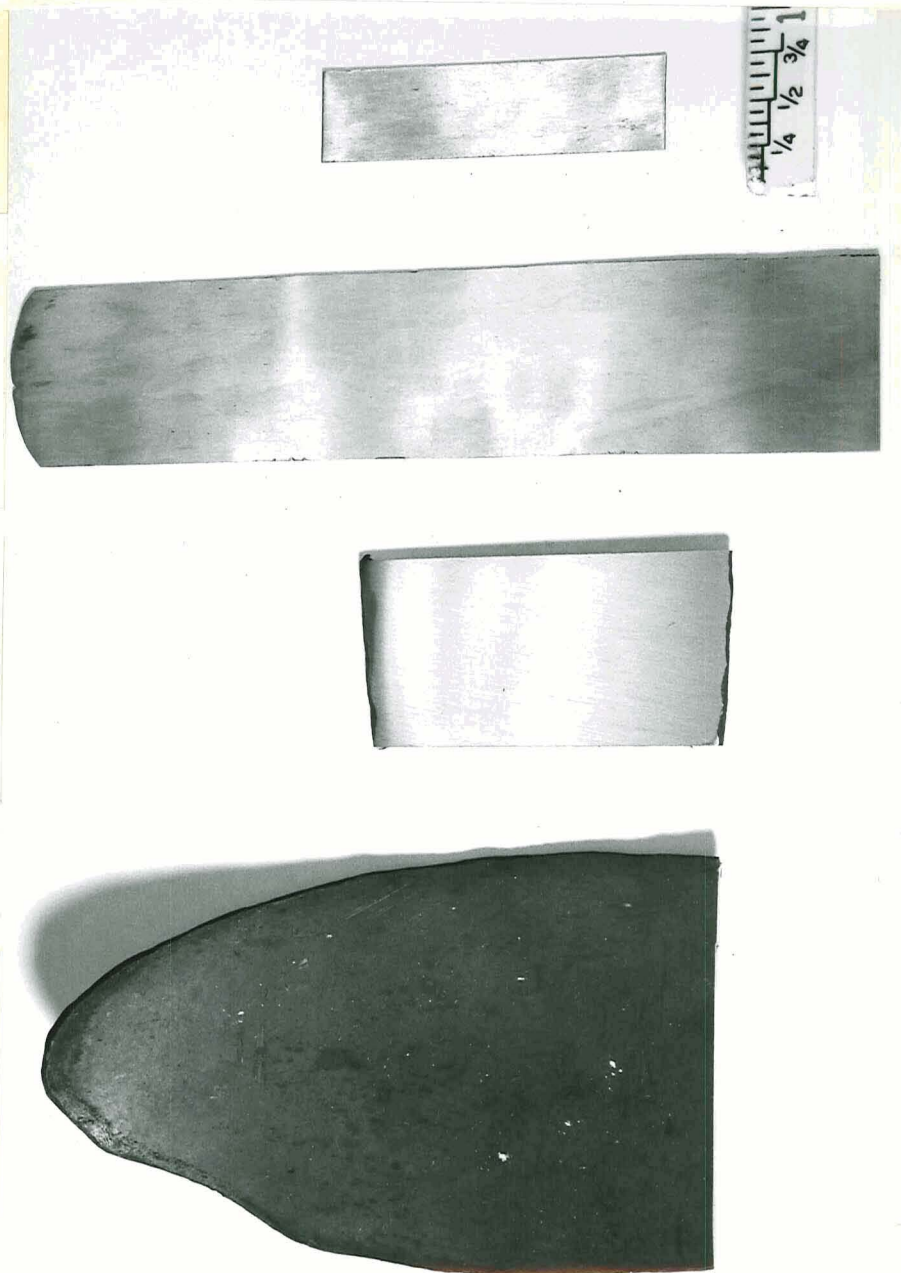
Neg. No. 35812

Fig. 33 - Fabrication Procedure for 10-Mil Oxidation Specimen in Task II.
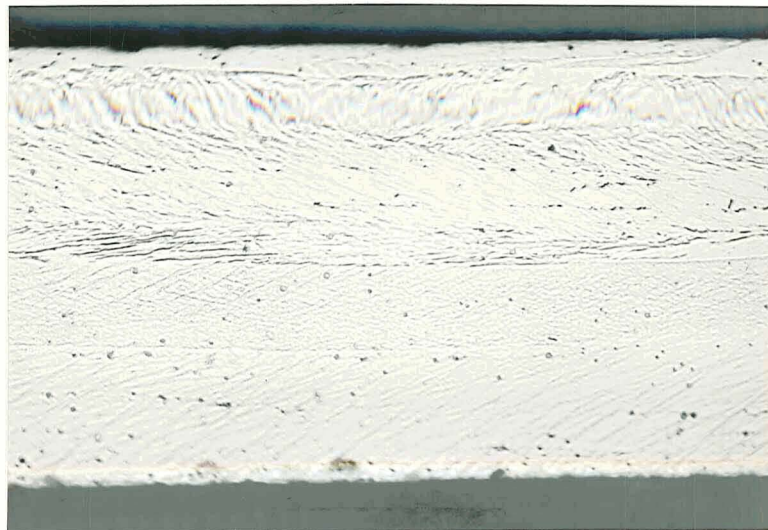
Neg. No. 35608   X200

(a) Cold Rolled
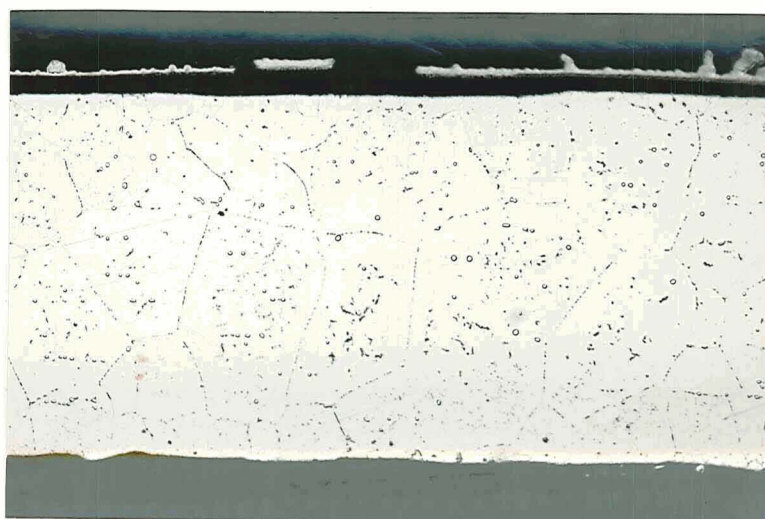
Neg. No. 35609   X200

(b) Annealed

Fig. 34 - Microstructure of Alloy F22 As
         Cold Rolled and After Annealing
         at 2150°F for 15 Min.
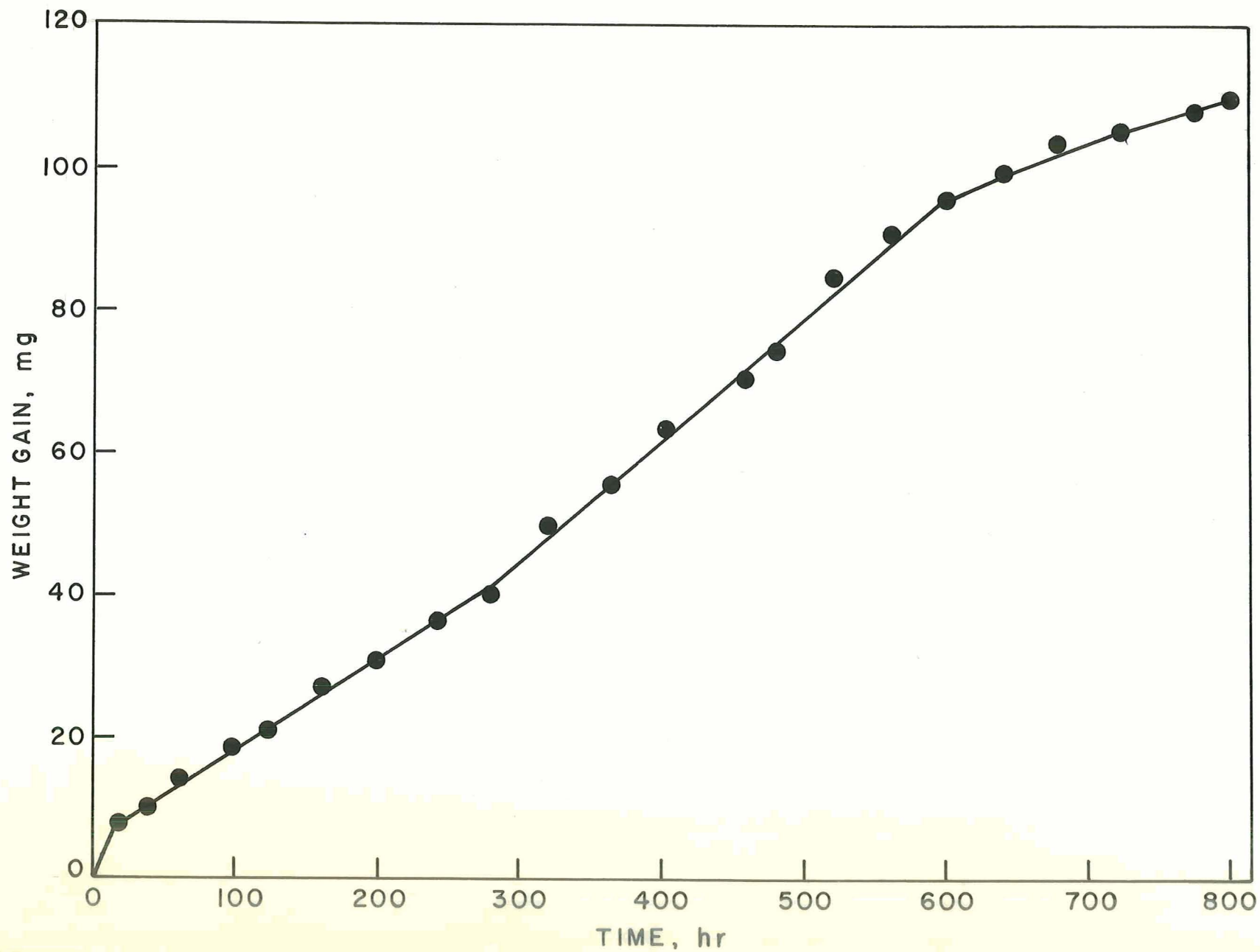
Fig. 35 - Average Weight Gain of Alumina Crucibles During Cyclic Oxidation at 2300°F.
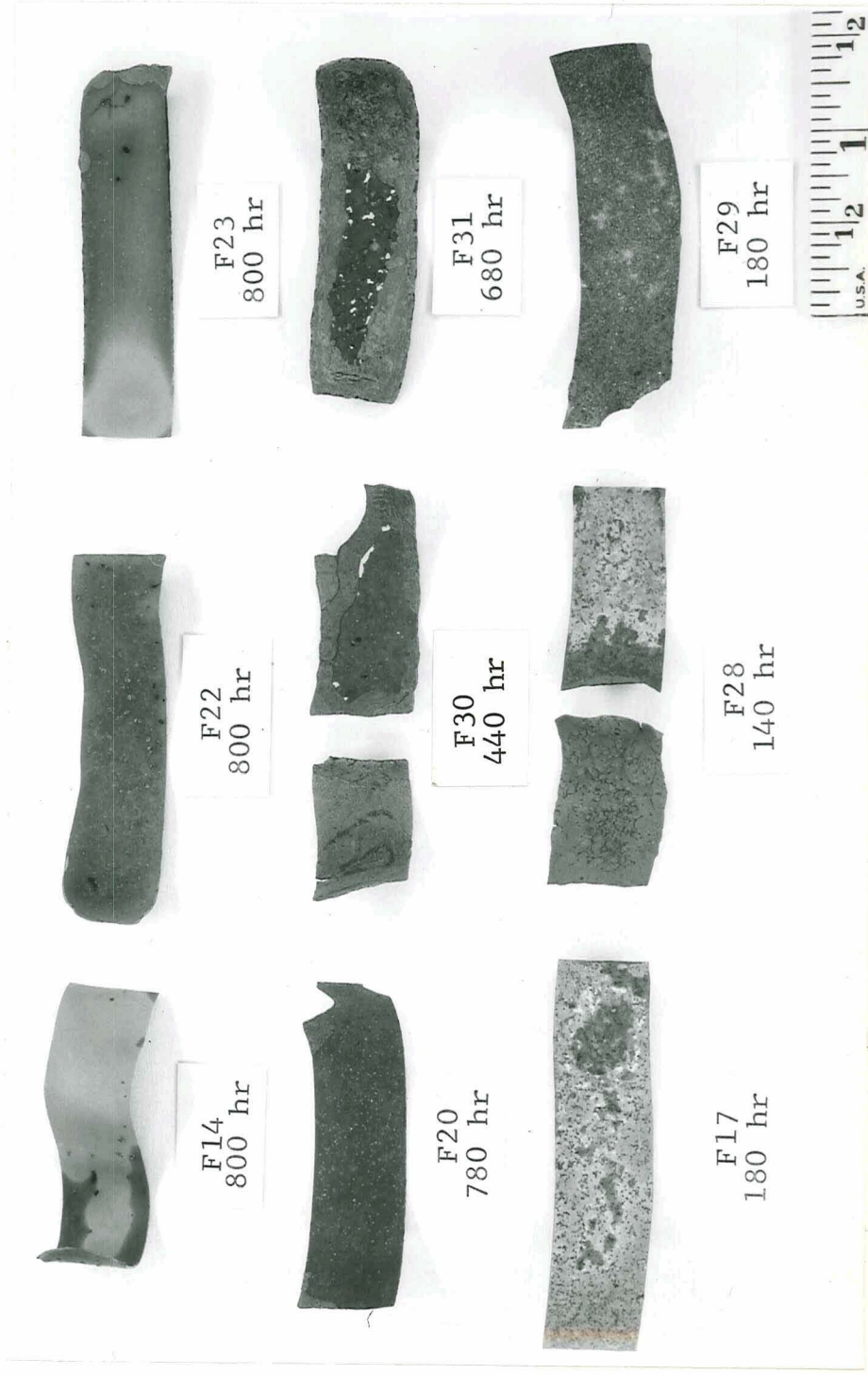
F23
800 hr

F31
680 hr

F29
180 hr

F22
800 hr

F30
440 hr

F28
140 hr

F14
800 hr

F20
780 hr

F17
180 hr

Fig. 36 - Task II Oxidation Samples after Cyclic Furnace Oxidation at 2300°F.

F24
240 hr

F27
540 hr

NA17
540 hr

F16
320 hr

F26
320 hr

NA16
540 hr

TD NiCr
800 hr

TD Ni
800 hr

F8
320 hr

F25
240 hr

NA13
540 hr
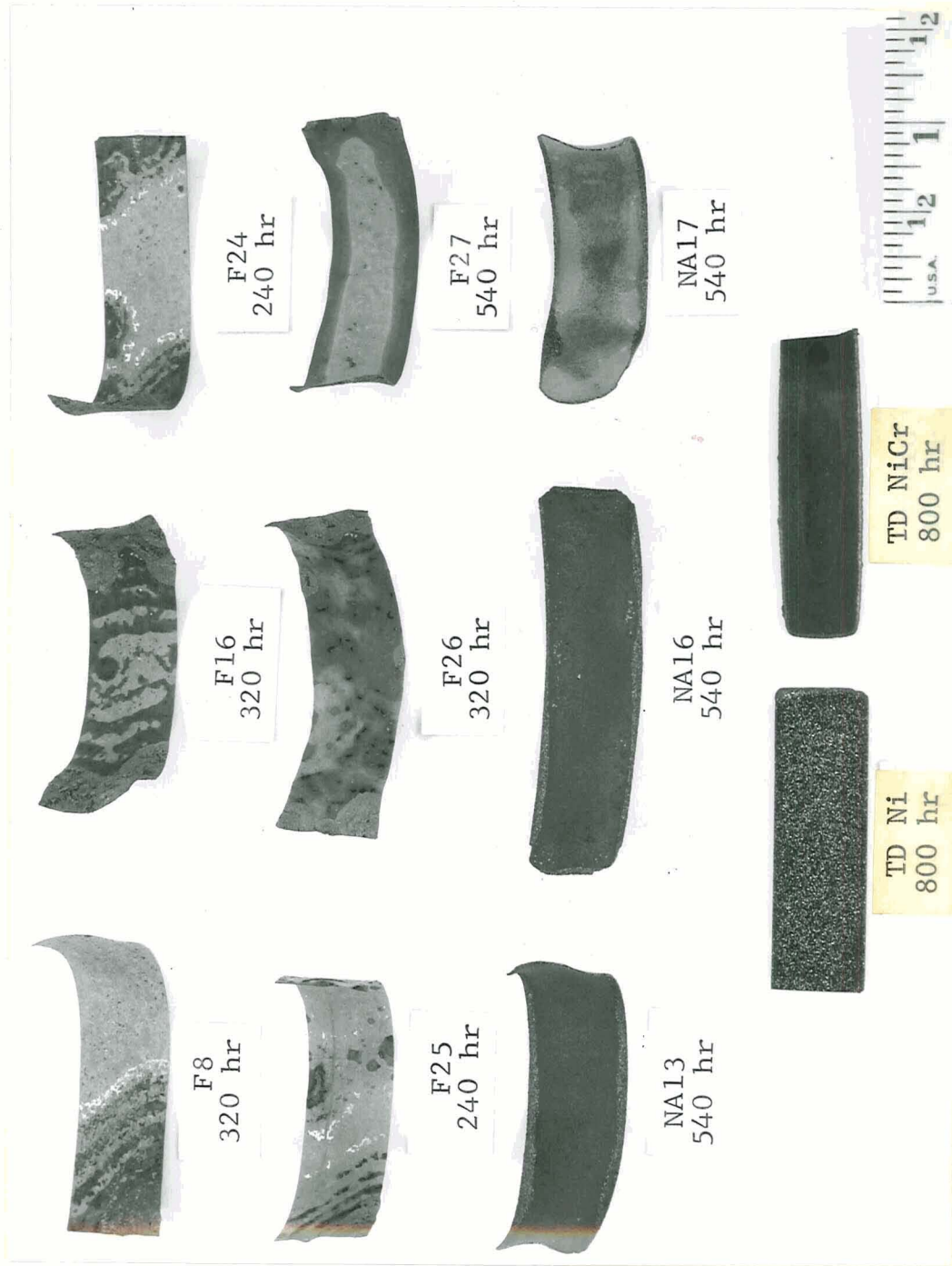
Neg. No. 35711

Fig. 37 – Task II Oxidation Samples After Cyclic Furnace Oxidation
at 2300°F.

LEGEND

F 8 — 0.23 Ti
F 16 — 0.5 Ti
F 17 — 0.5 Hf
F 24 — 0.75 Ti
F 25 — 0.5 Ti, 0.5 Ta
F 26 — 0.5 Ti, 1.0 Ta
F 28 — 0.3 Hf
F 29 — 0.3 Hf, 0.5 Ta
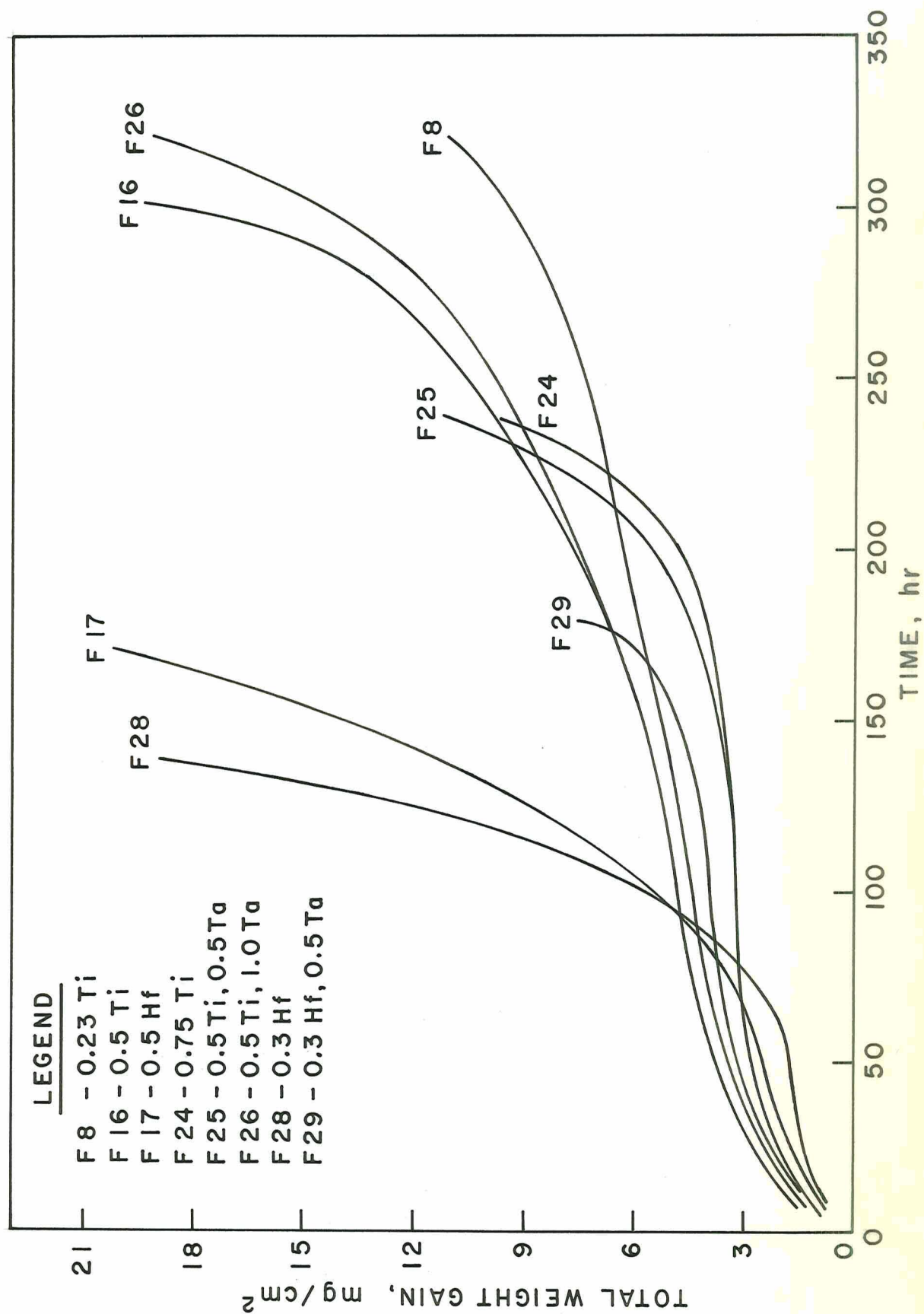
Fig. 38 – Total Weight Gain of Fe-25Cr-4Al Alloys Removed Prior to 400 hr Cyclic Furnace Oxidation at 2300°F.

Fig. 39 - Sample Weight Change of Fe-25Cr-4Al Alloys Removed Prior to 400 hr Cyclic Furnace Oxidation at 2300°F.

LEGEND

F 14 – 0.25 Y
F 20 – 0.50 Th
F 22 – 0.15 Y
F 23 – 0.25 Y, 0.5 Ta
F 27 – 0.23 Ti, 0.20 Hf
F 30 – 0.30 Th
F 31 – 0.30 Th, 0.50 Ta
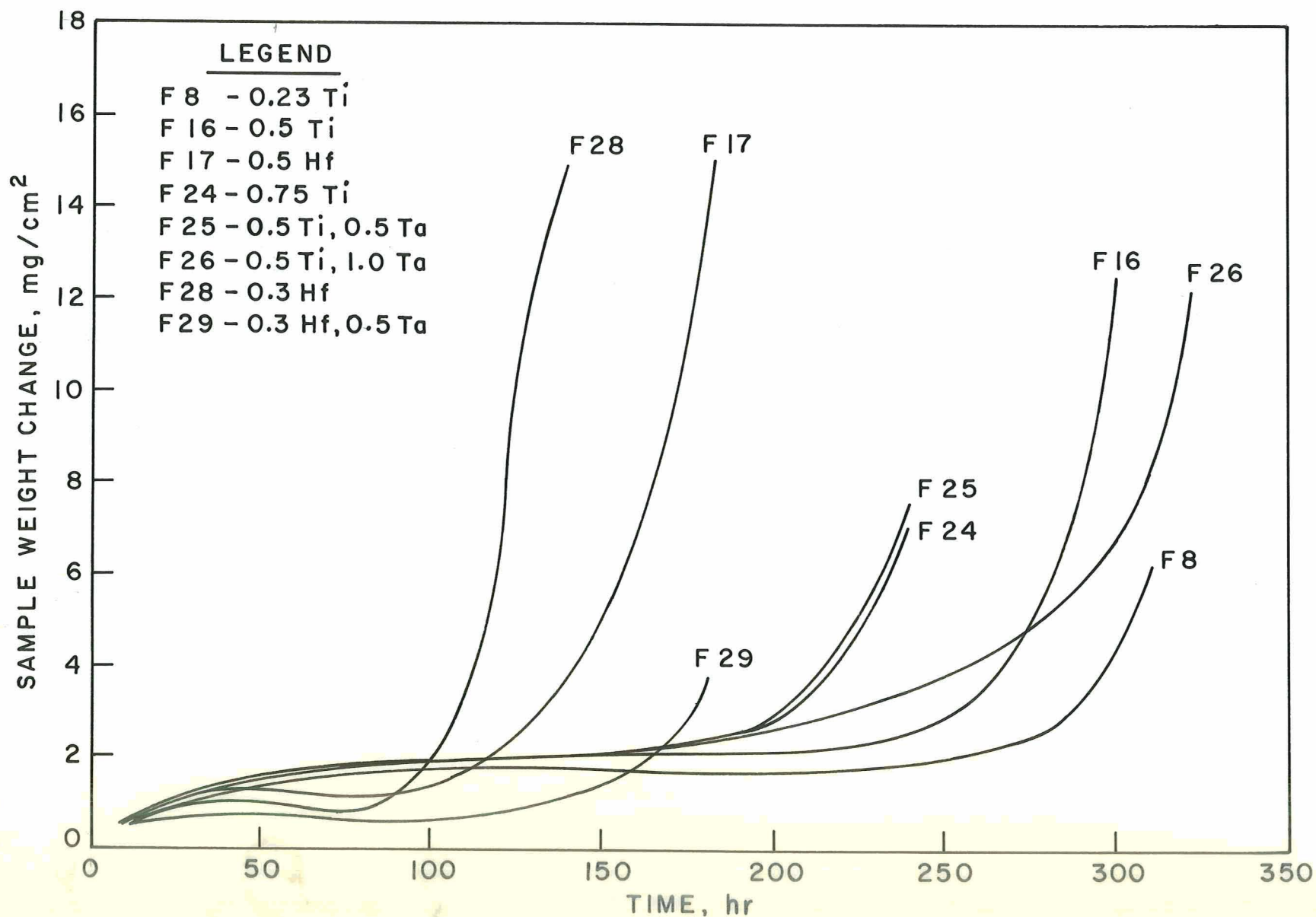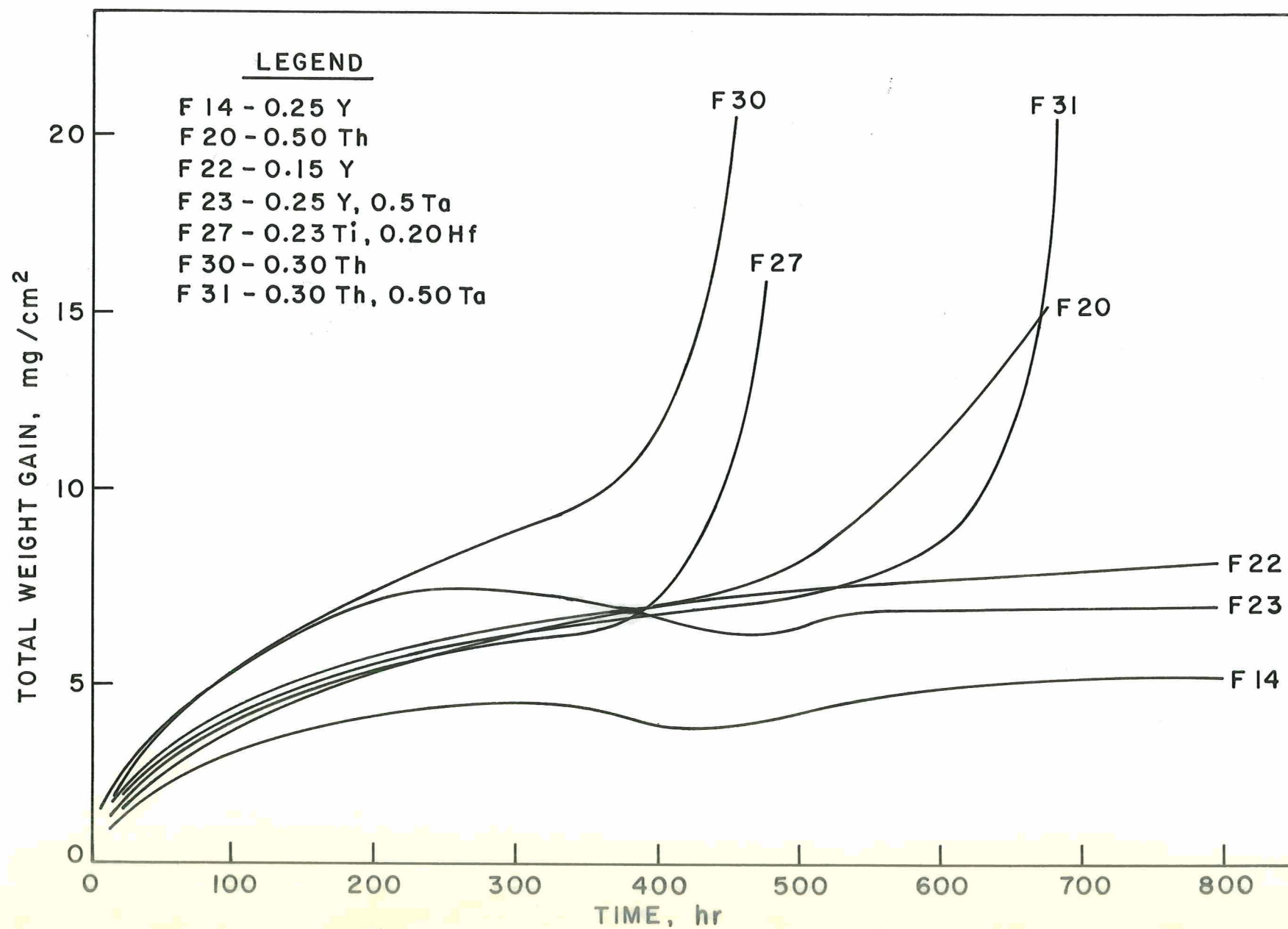
Fig. 40 - Total Weight Gain of Fe-25Cr-4Al Alloys During Cyclic Furnace Oxidation at 2300°F.

154
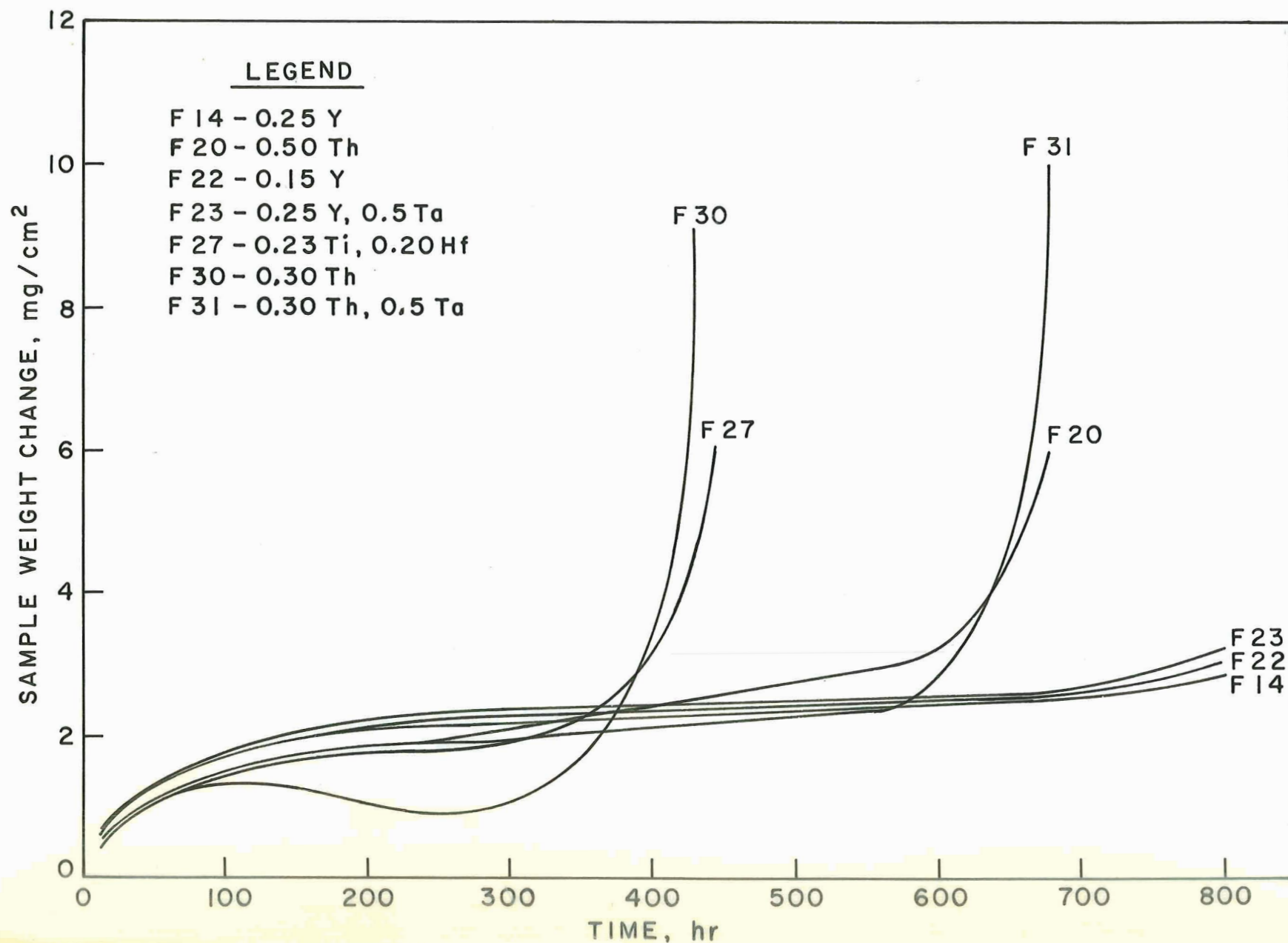
Fig. 41 - Sample Weight Change of Fe-25Cr-4Al Alloys During Cyclic Furnace Oxidation at 2300°F.
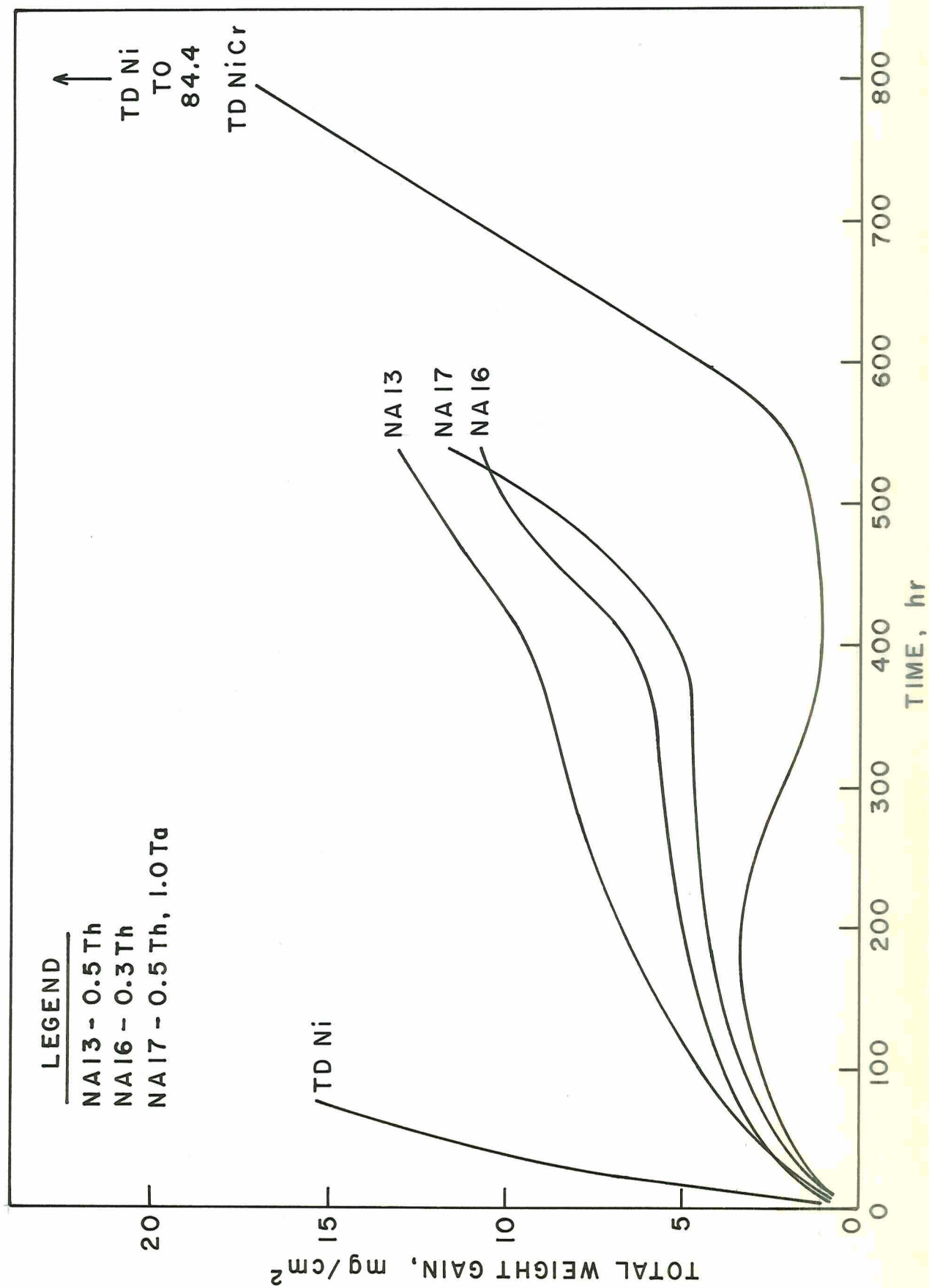
Fig. 42 - Total Weight Gain of Ni-20Cr-5Al Alloys During Cyclic Furnace Oxidation at 2300°F.
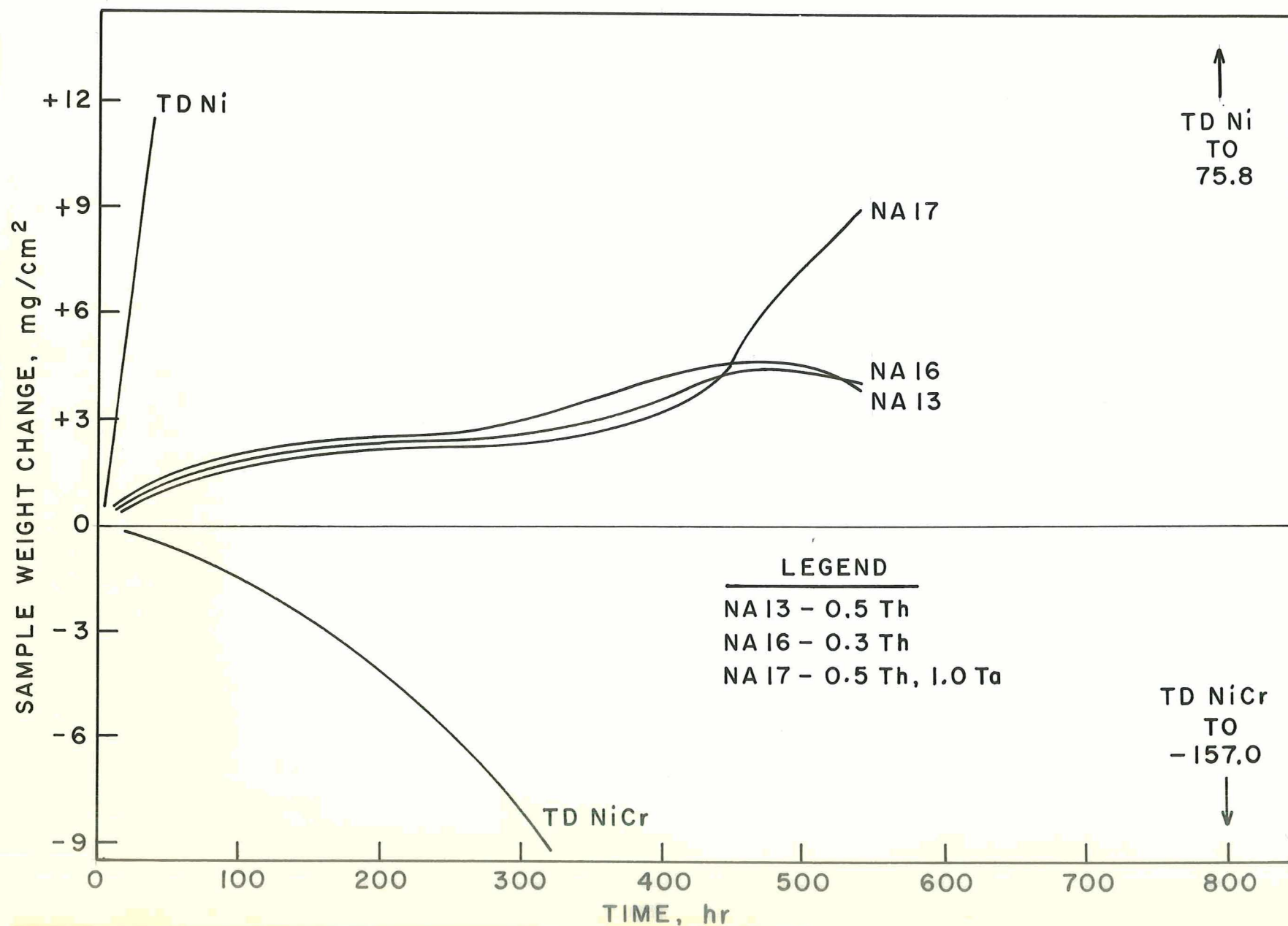
Fig. 43 - Sample Weight Change of Ni-20Cr-5Al Alloys During Cyclic Furnace Oxidation at 2300°F.
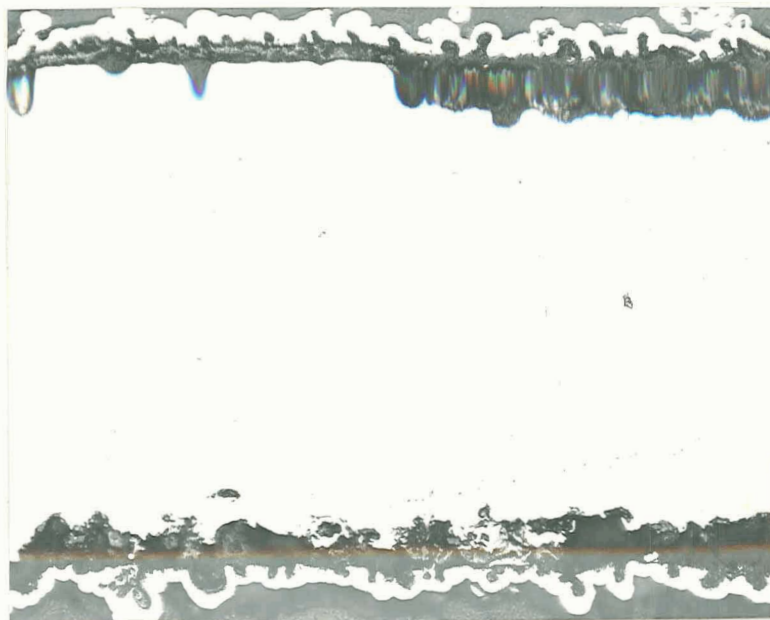
Neg. No. 35587   X200

(a) 100 hr
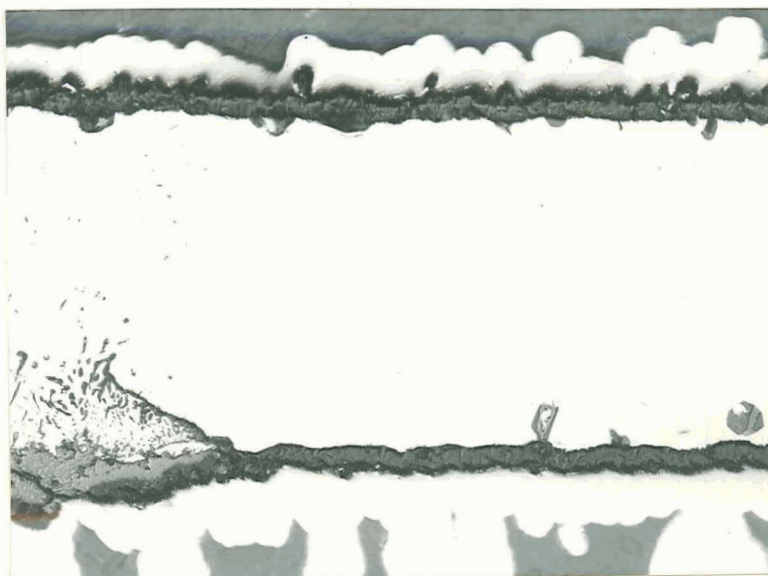
Neg. No. 35588   X200

(b) 320 hr

Fig. 44 - Microstructure of Alloy F8 (0.23Ti)
          after Cyclic Furnace Oxidation at
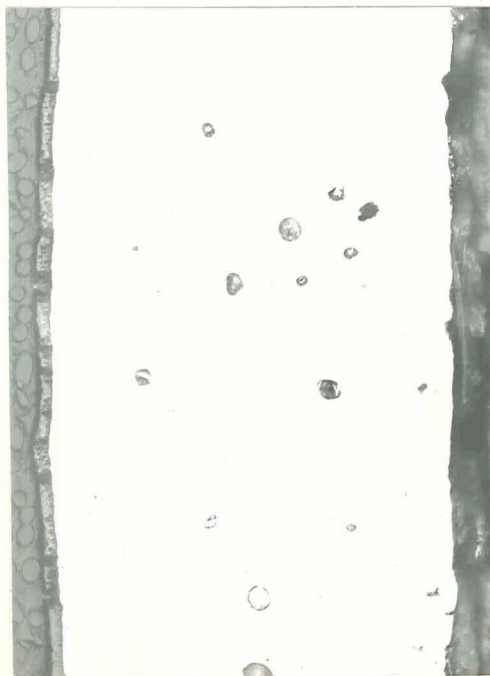   2300°F.
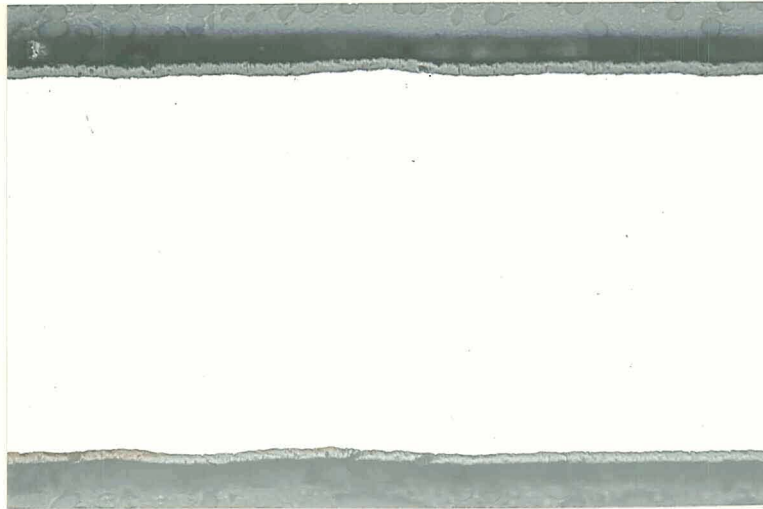
Neg. No. 35578   X200

(a) 100 hr
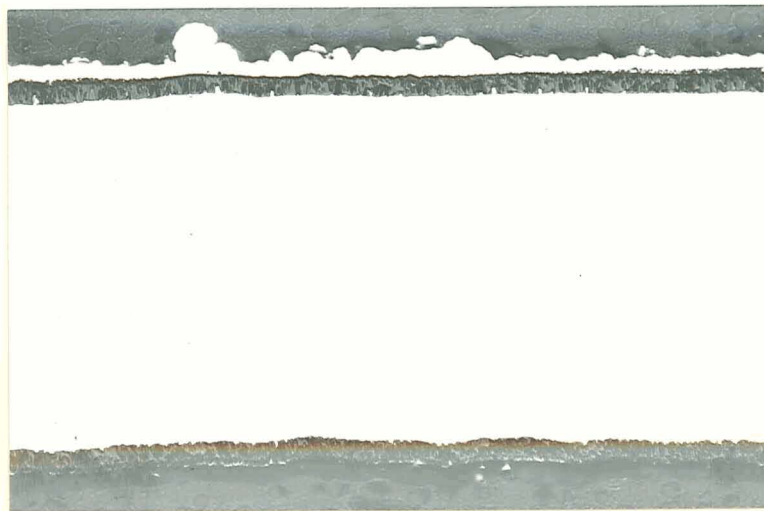
Neg. No. 35579   X200

(b) 400 hr

Fig. 45 - Microstructure of Alloy F14 (0.25Y) after Cyclic Furnace Oxidation at 2300°F.
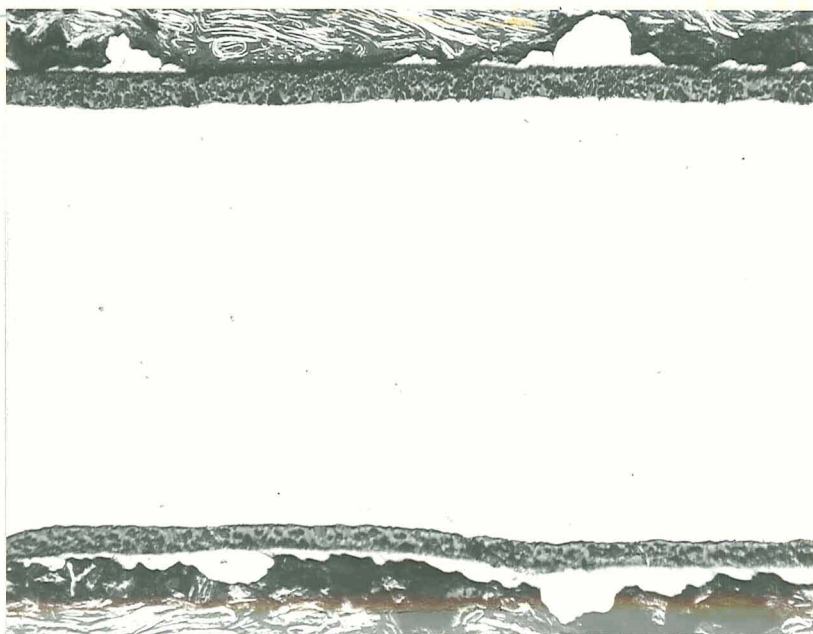
Neg. No. 35580   X200

(a) F14
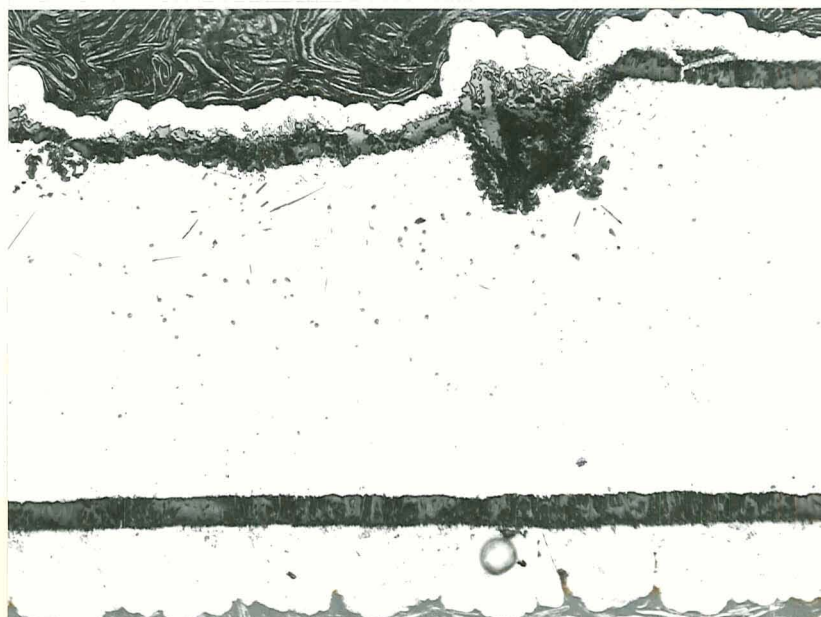
Neg. No. 35756   X200

(b) F22

Fig. 46 - Microstructure of Alloys F14 (0.25Y)
          and F22 (0.15Y) after Cyclic Furnace
          Oxidation at 2300°F for 800 hr.
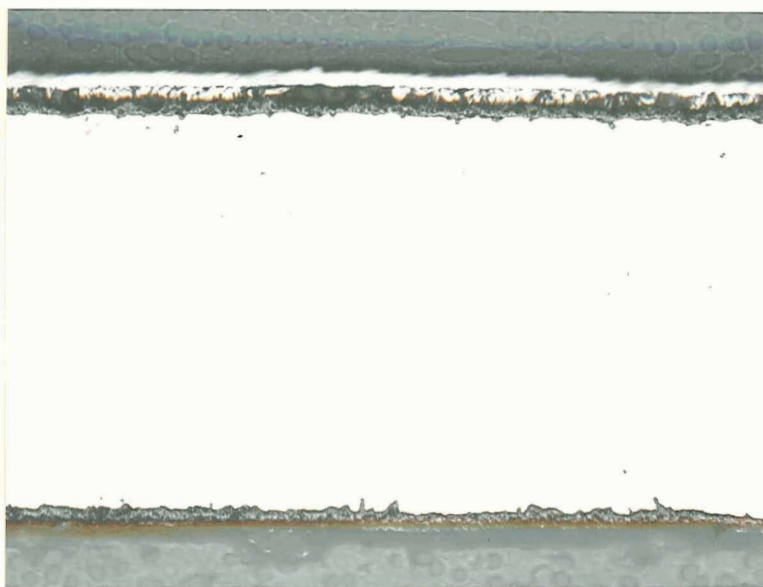
Neg. No. 35590 X200

(a) 100 hr

Neg. No. 35592 X200

(b) 540 hr

Fig. 47 - Microstructure of Alloy F27
(0.23Ti-0.2Hf) after Cyclic
Furnace Oxidation at 2300°F.

160
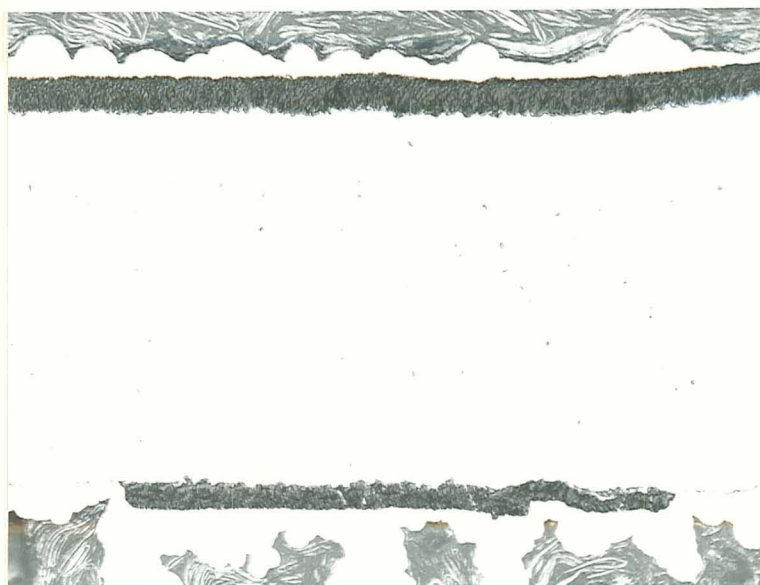
Neg. No. 35586　　　　　　　　　　　X200

(a) 400 hr
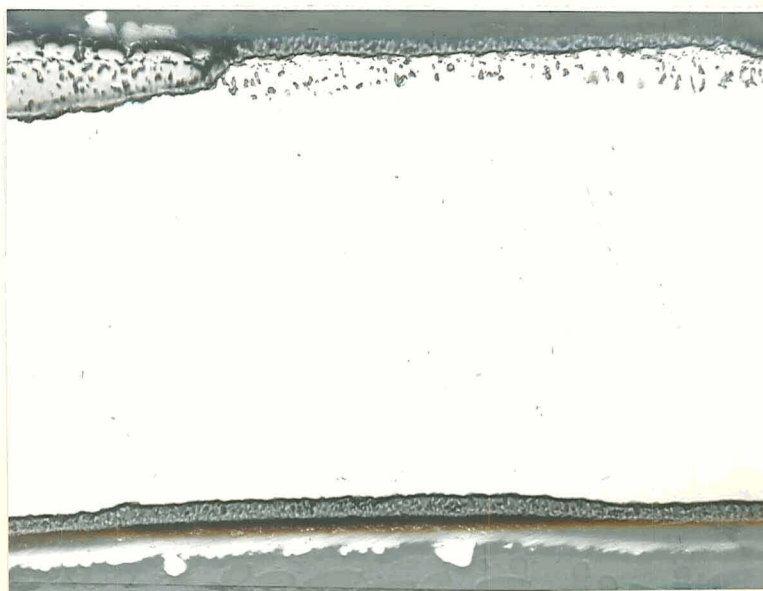
Neg. No. 35585　　　　　　　　　　　X200

(b) 440 hr

Fig 48 - Microstructure of Alloy F30
(0.5Th) after Cyclic Furnace
Oxidation at 2300°F.
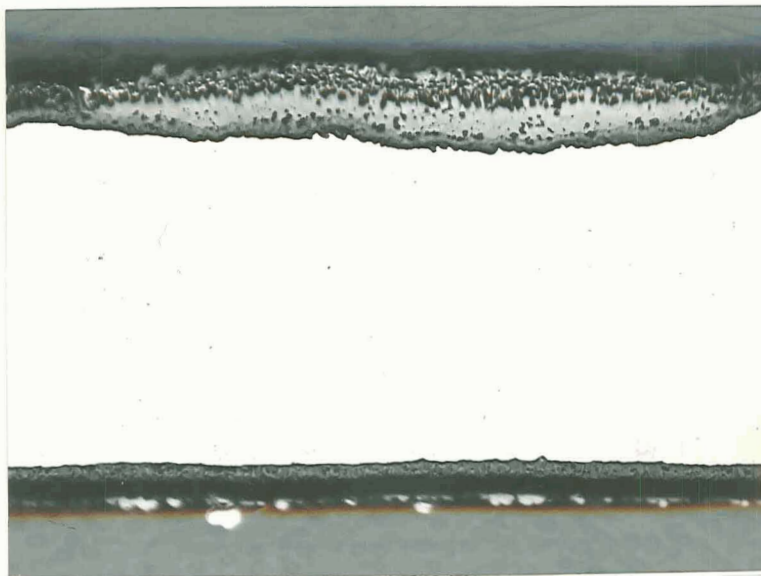
Neg. No. 35585   X200

(a) 400 hr
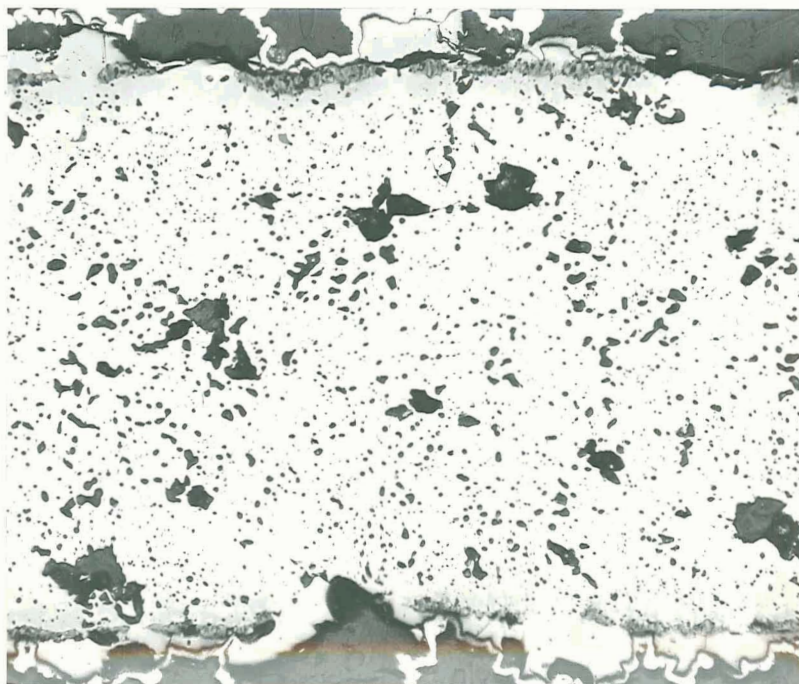
Neg. No. 35584   X200

(b) 680 hr

Fig. 49 - Microstructure of Alloy F31
             (0.5 Th, 0.5 Ta) after Cyclic
             Furnace Oxidation at 2300°F.

162

Neg. No. 35596   X200
(a) 100 hr

Neg. No. 35599   X200
(b) 400 hr
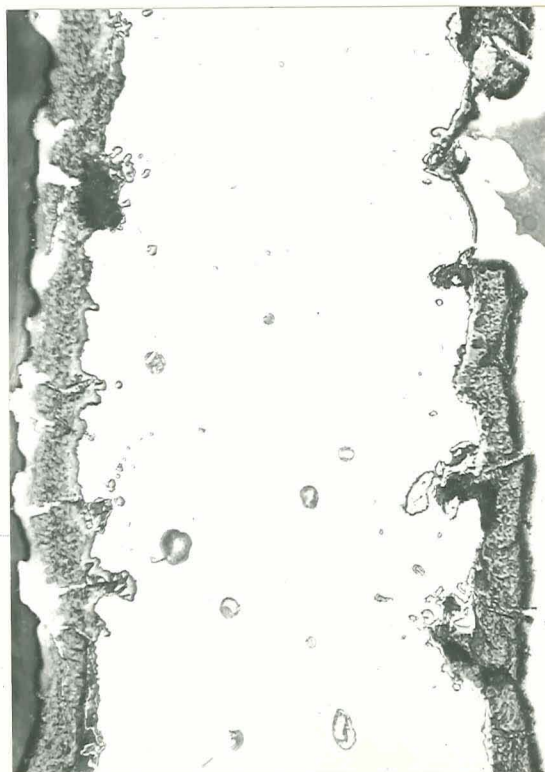
Neg. No. 35600   X200
(c) 560 hr

Fig. 50 - Microstructure of Alloy NA13 (0.5Th) After Cyclic
Furnace Oxidation at 2300°F.

Neg. No. 35601   (a) TD Ni   X50
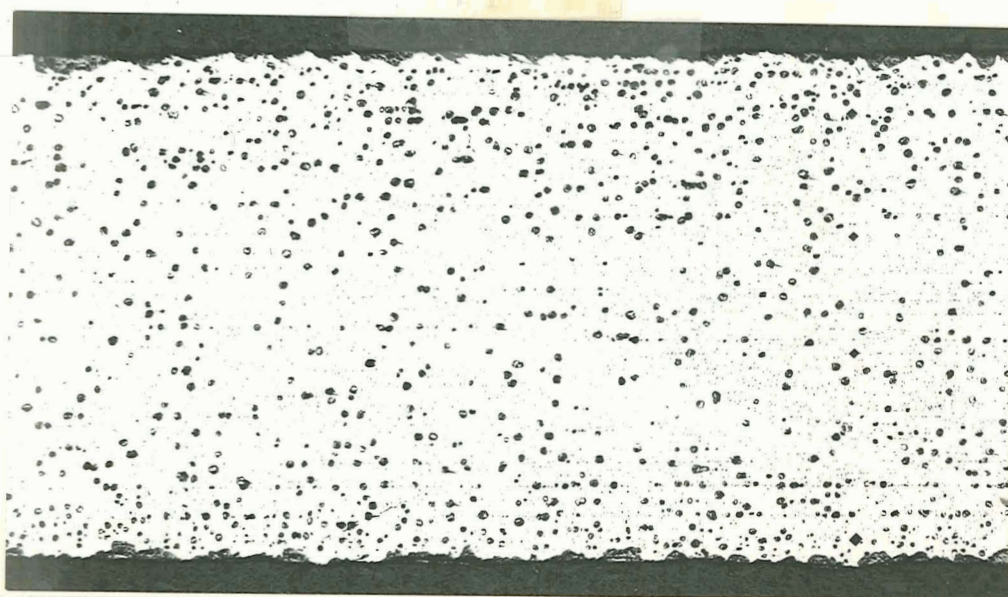
Neg. No. 35602   (b) TD NiCr   X50

Fig. 51 - Microstructure of TD Ni and TD NiCr After
          Cyclic Furnace Oxidation at 2300°F for
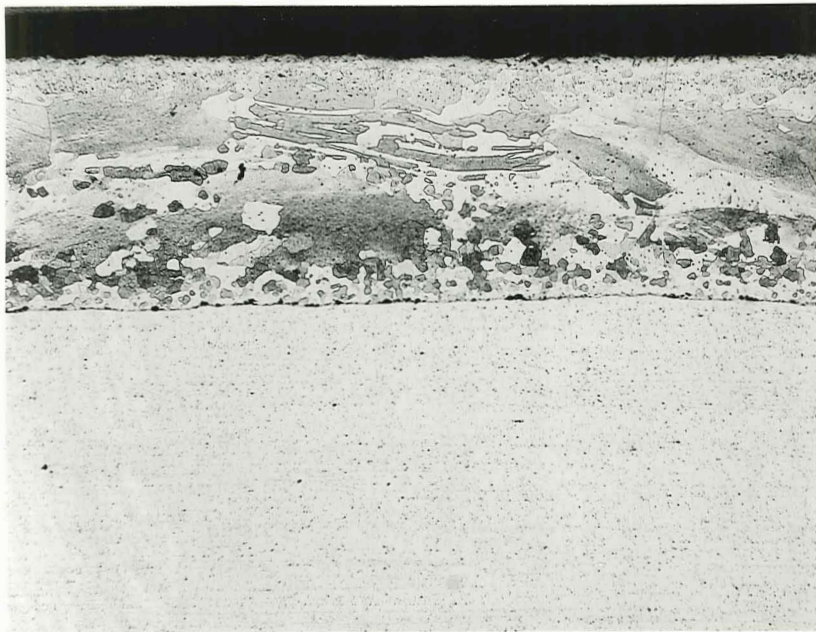   800 hr.
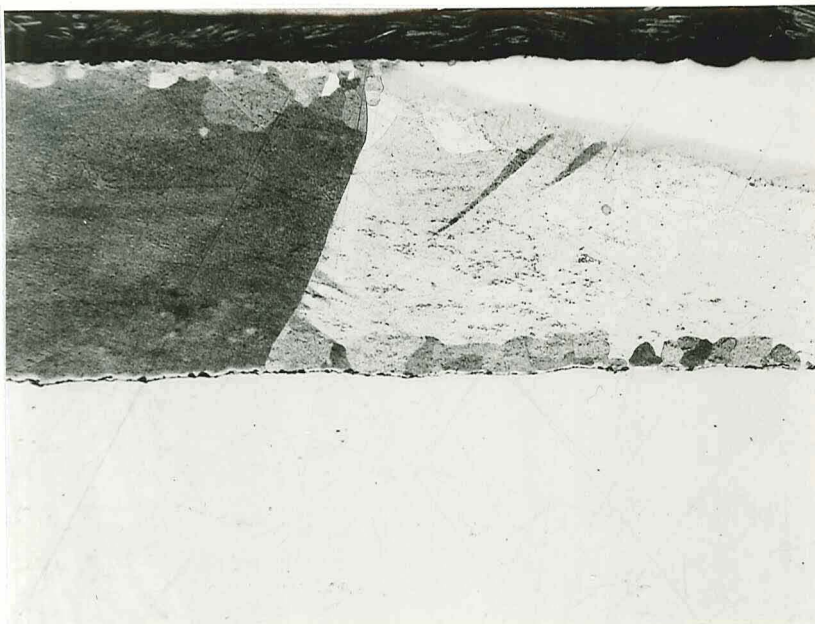
Neg. No. 35841   X100

(a) Hot Rolled
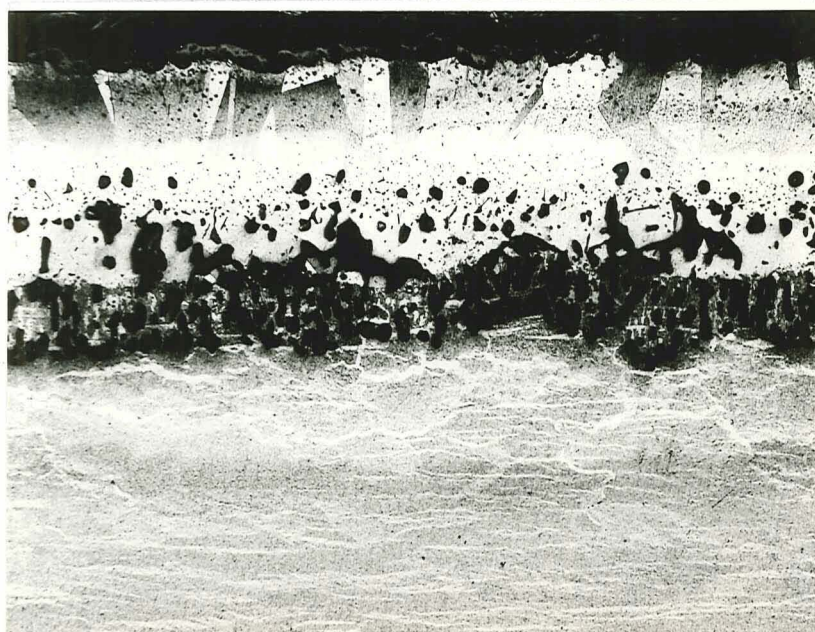
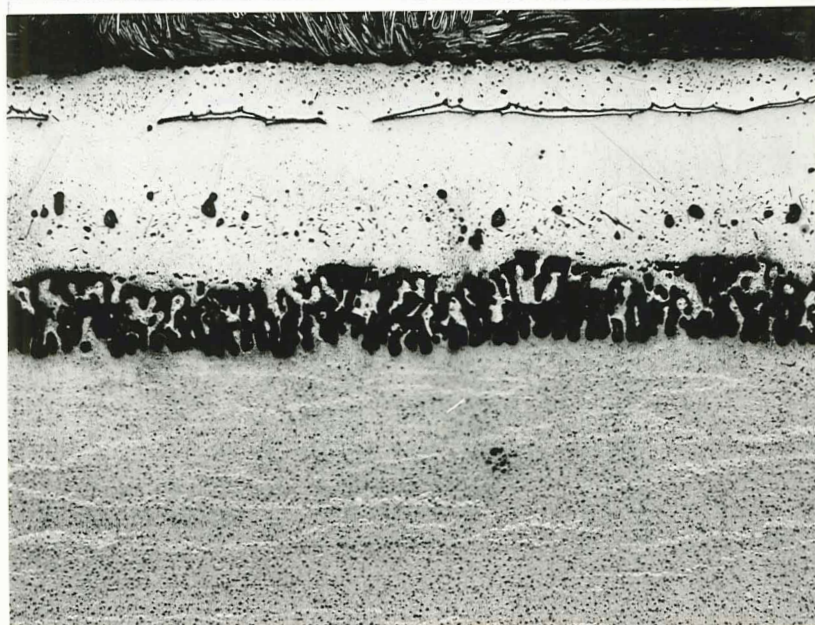Neg. No. 35846   X100

(b) 2300°F-100 hr

Fig. 52 - Diffusion Couple F16/TD Ni As
            Fabricated and After Interdiffusion
            at 2300°F for 100 hr.

Neg. No. 35842   X100
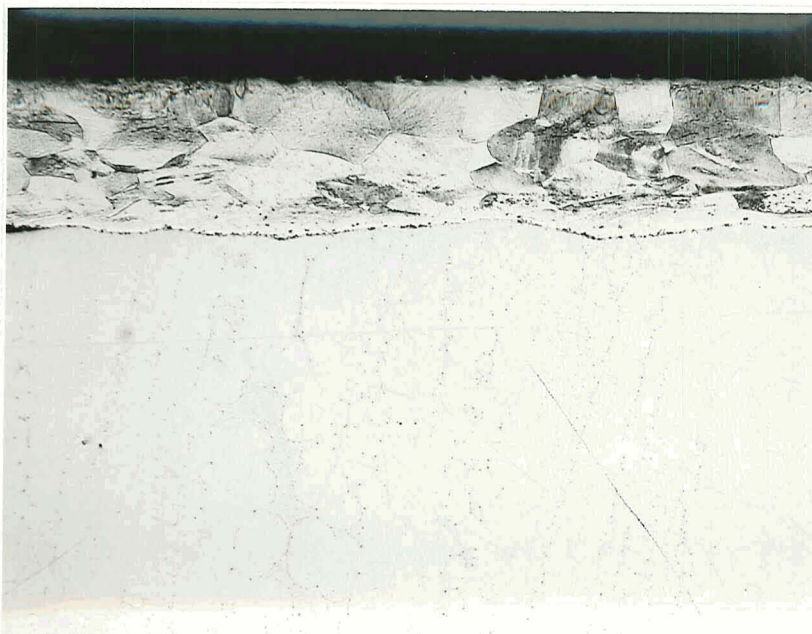
(a) Hot Rolled

Neg. No. 35845   X100

(b) 2300°F-100 hr
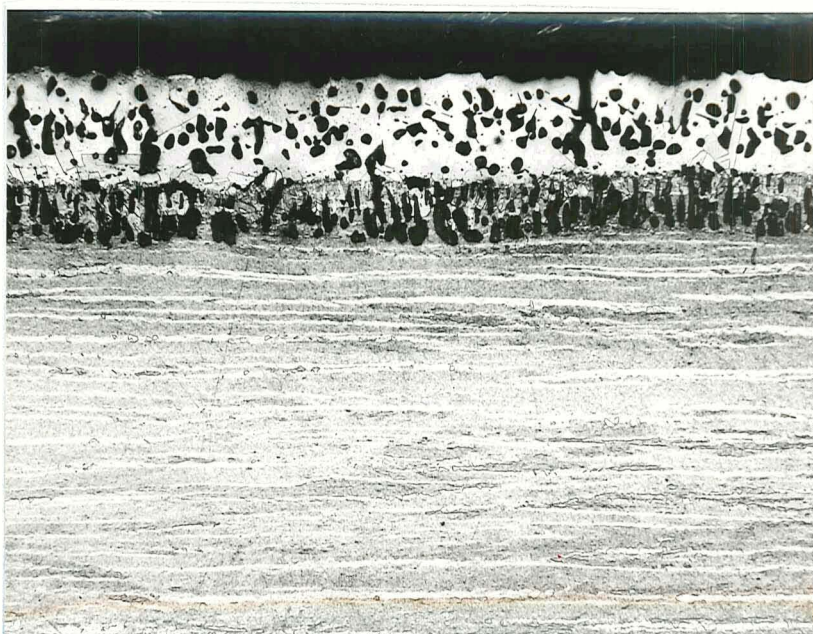
Fig. 53 - Diffusion Couple F16/TD NiCr As
Hot Rolled and After Inter-
diffusion at 2300°F for 100 hr.

Neg. No.   35843   X100

(a) Hot Rolled

Neg. No.   35844   X100
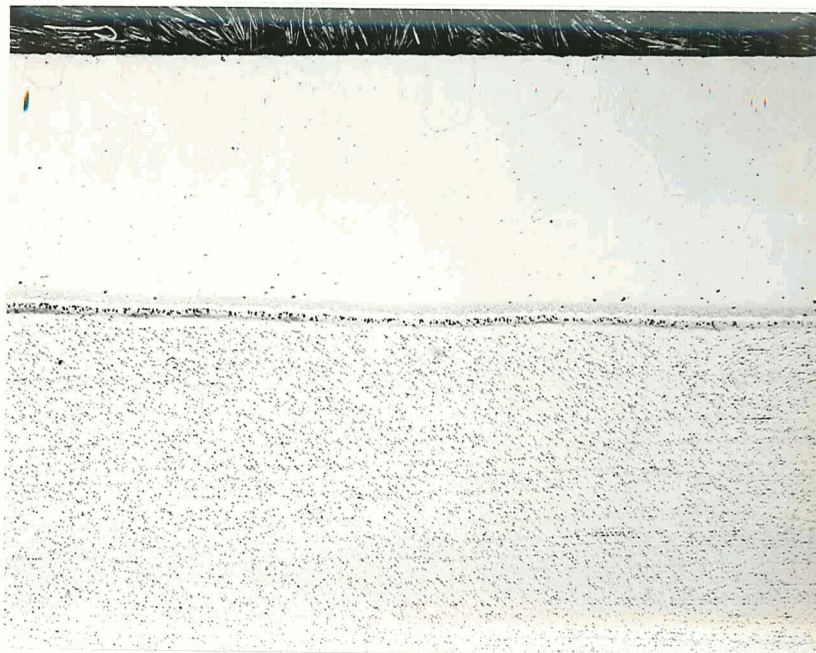
(b) 2300°F-100 hr

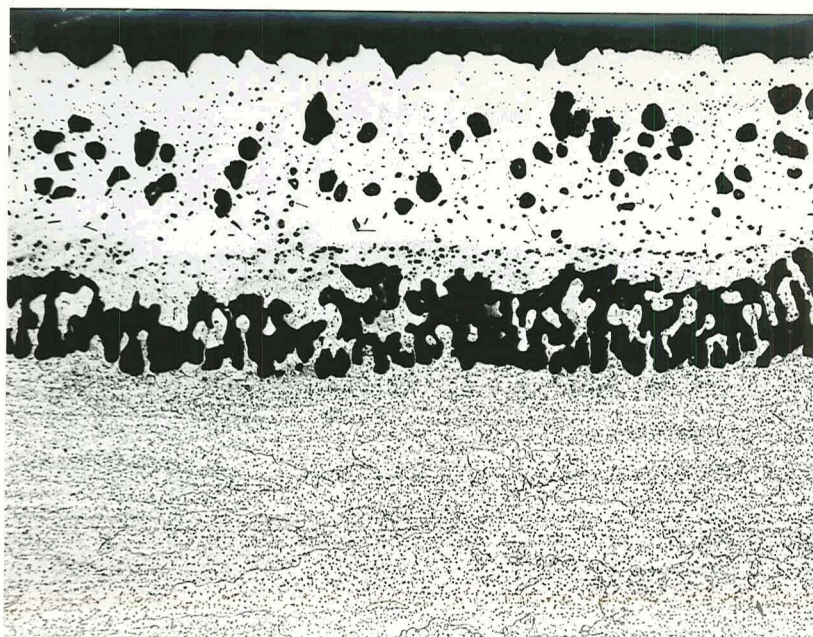Fig. 54 - Diffusion Couple F18/TD Ni As
             Hot Rolled and After Interdiffusion
             at 2300°F for 100 hr.

Neg. No. 35651   X100

(a) Hot Rolled

Neg. No. 35653   X100

(b) 2300°F-100 hr

Fig. 55 - Diffusion Couple F18/TD NiCr As
          Hot Rolled and After Inter-
          diffusion at 2300°F for 100 hr.

Neg. No. 35687   X100

(a) Hot Rolled

Neg. No. 35686   X100

(b) 2300°F-100 hr

Fig. 56 - Diffusion Couple NA13/TD Ni As
            Hot Rolled and After Interdiffusion
            at 2300°F for 100 hr.

Neg. No. 35689   X100

(a) Hot Rolled
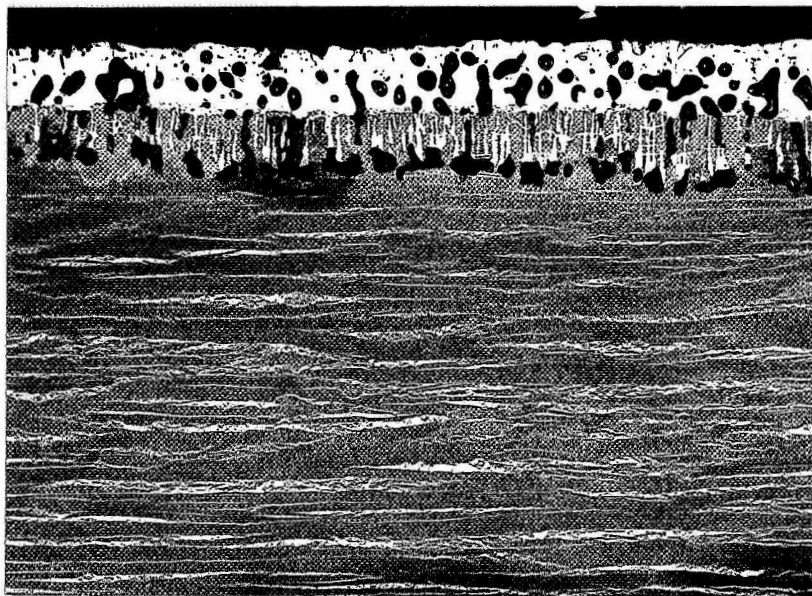

Neg. No. 35688   X100

(b) 2300°F-100 hr
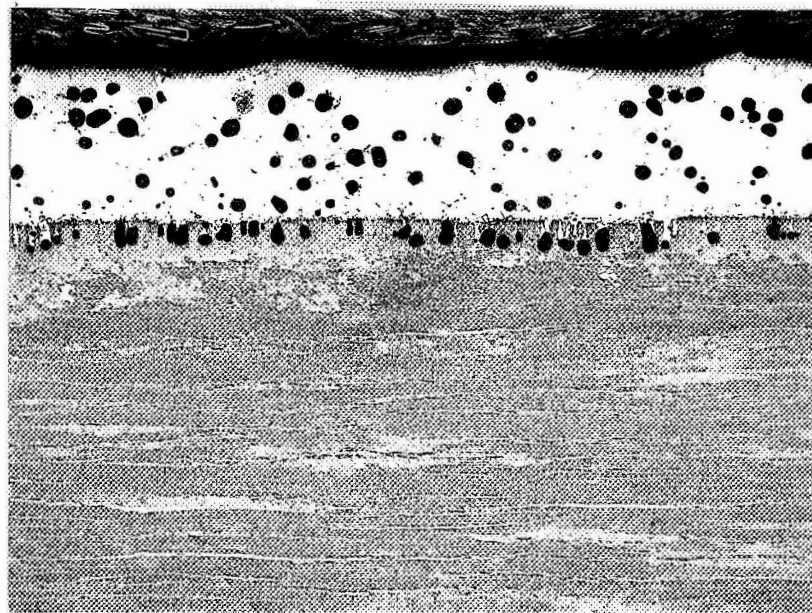
Fig. 57 - Diffusion Couple NA13/TD NiCr As
          Hot Rolled and After Inter-
          diffusion at 2300°F for 100 hr.
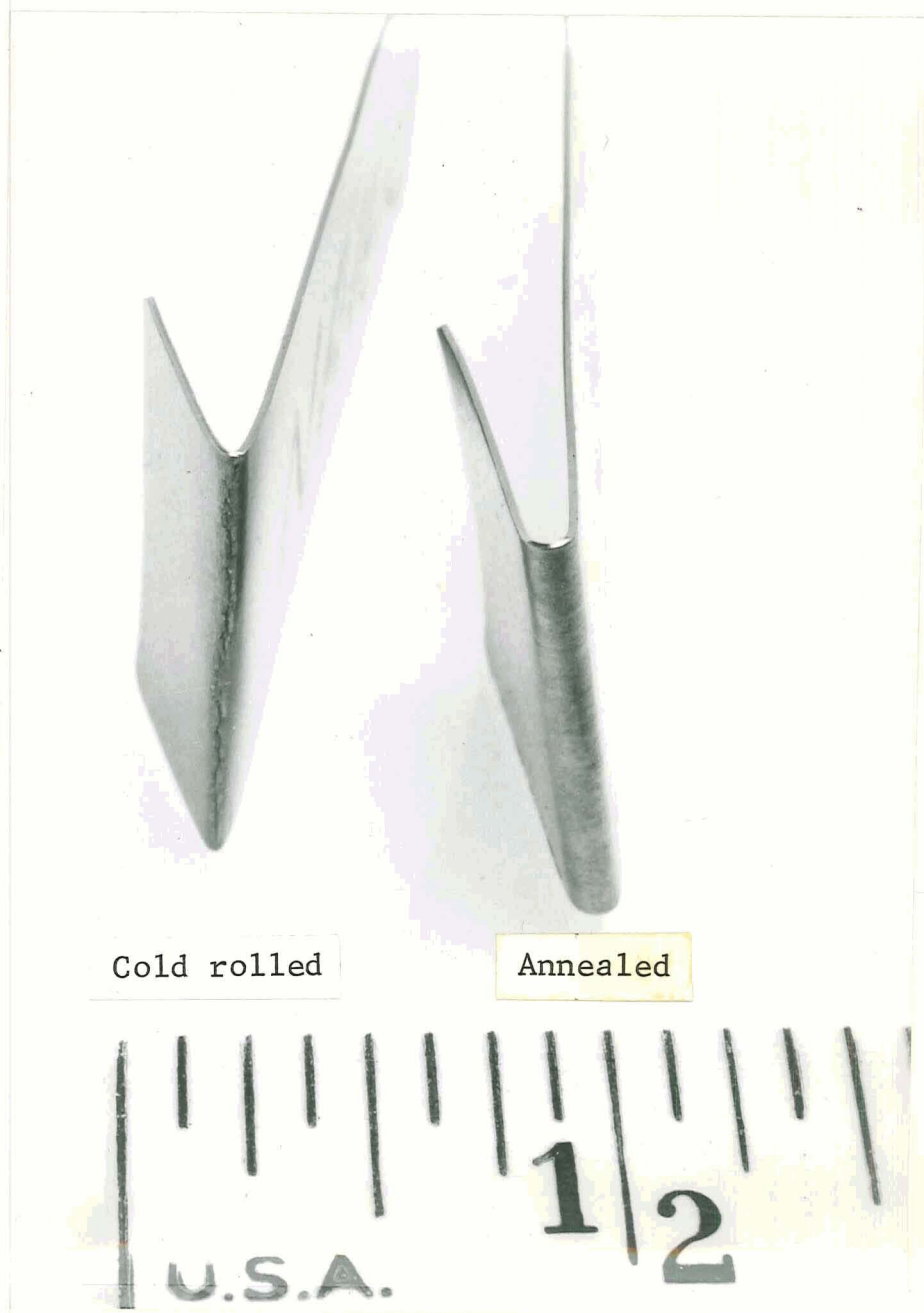
Neg. No. 35652   X100

(a) F18/TD Ni

Neg. No. 35653   X100

(b) NA13/TD Ni

Fig. 58 - Diffusion Couples F18/TD Ni and
            NA13/TD Ni After Interdiffusion
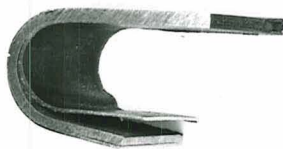   at 2300°F for 300 hr.

171

Cold rolled   Annealed

Neg. No. 35119

Fig. 59 - Bend Ductility of Alloy NA13 in Cold
Rolled and Annealed Conditions.

F18/TD Ni

F18/TD NiCr

NA13/TD Ni

F16/TD Ni

NA13/TD NiCr

F16/TD NiCr

Neg. No. 35709

Fig. 60 - Bend Ductility of Diffusion Couples After Exposure at 2300°F for 100 hr.
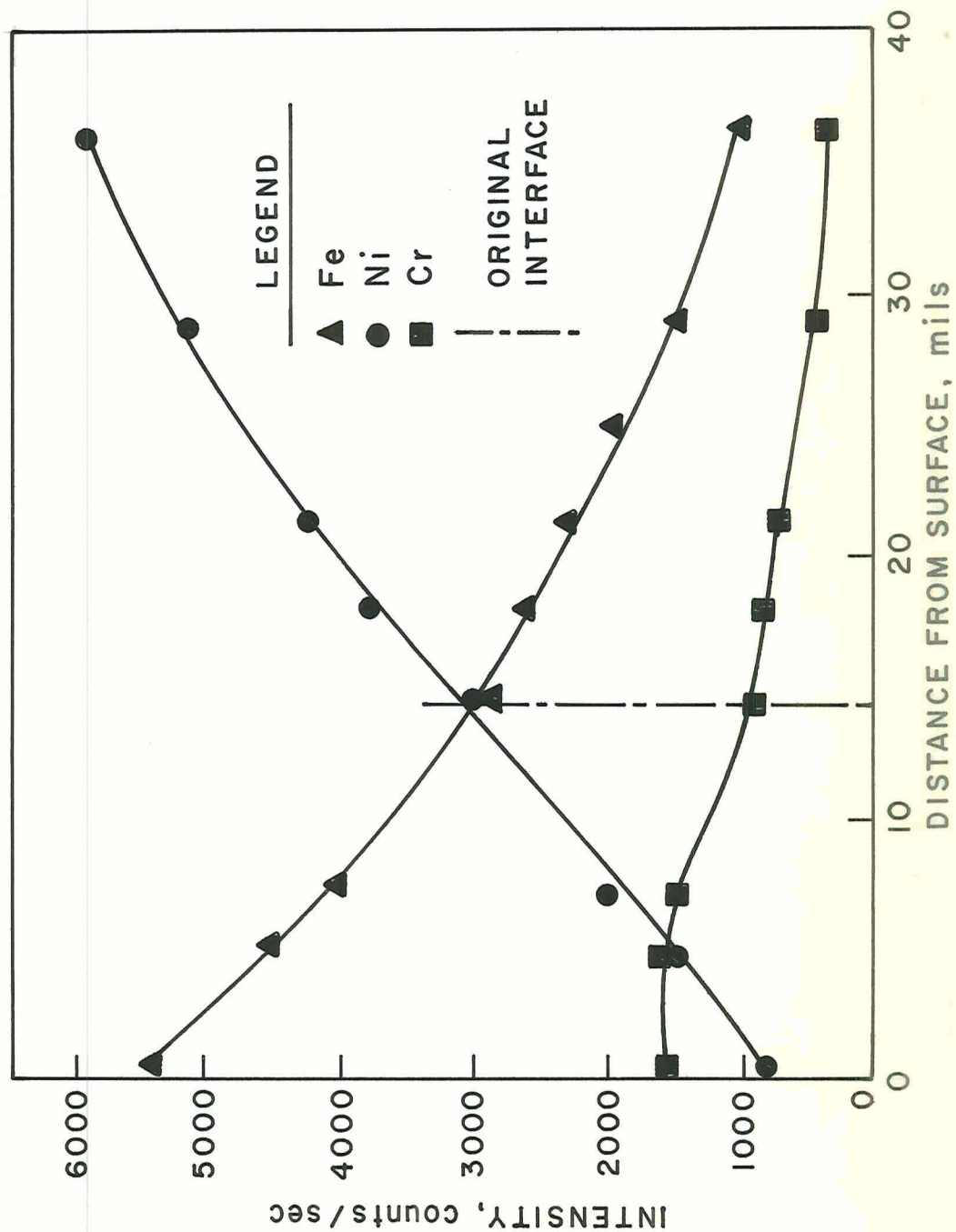
173

Fig. 61 - Composition Gradients in F16/TD Ni Diffusion Couple
After 100 hr at 2300°F.

Fig. 62 - Composition Gradients in F16/TD NiCr Diffusion Couple
After 100 hr at 2300°F.

Fig. 63 - Composition Gradients in F18/TD Ni Diffusion Gradients After 100 hr at 2300°F.

Fig. 64 - Composition Gradients in F18/TD NiCr Diffusion Couple
After 100 hr at 2300°F.

Fig. 65 - Composition Gradients in NA13/TD Ni Diffusion Couple
After 100 hr at 2300°F.
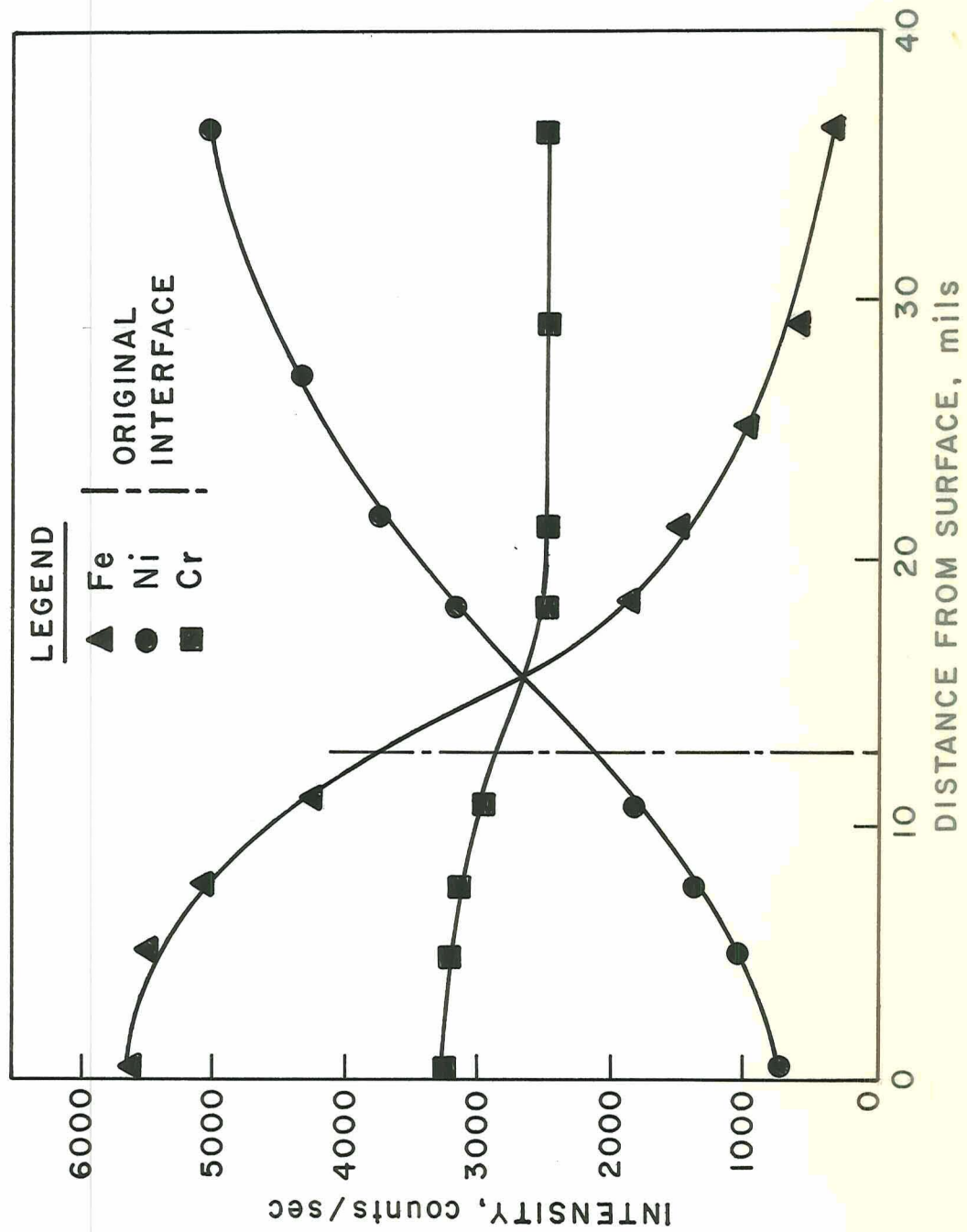
Fig. 66 – Composition Gradients in NA13/TD NiCr Diffusion Couple After 100 hr at 2300°F.

Fig. 67 - Composition Gradients in F18/TD Ni Diffusion Couple After 300 hr at 2300°F.

Fig. 68 - Composition Gradients in NA13/TD Ni Diffusion Couple
After 300 hr at 2300°F.
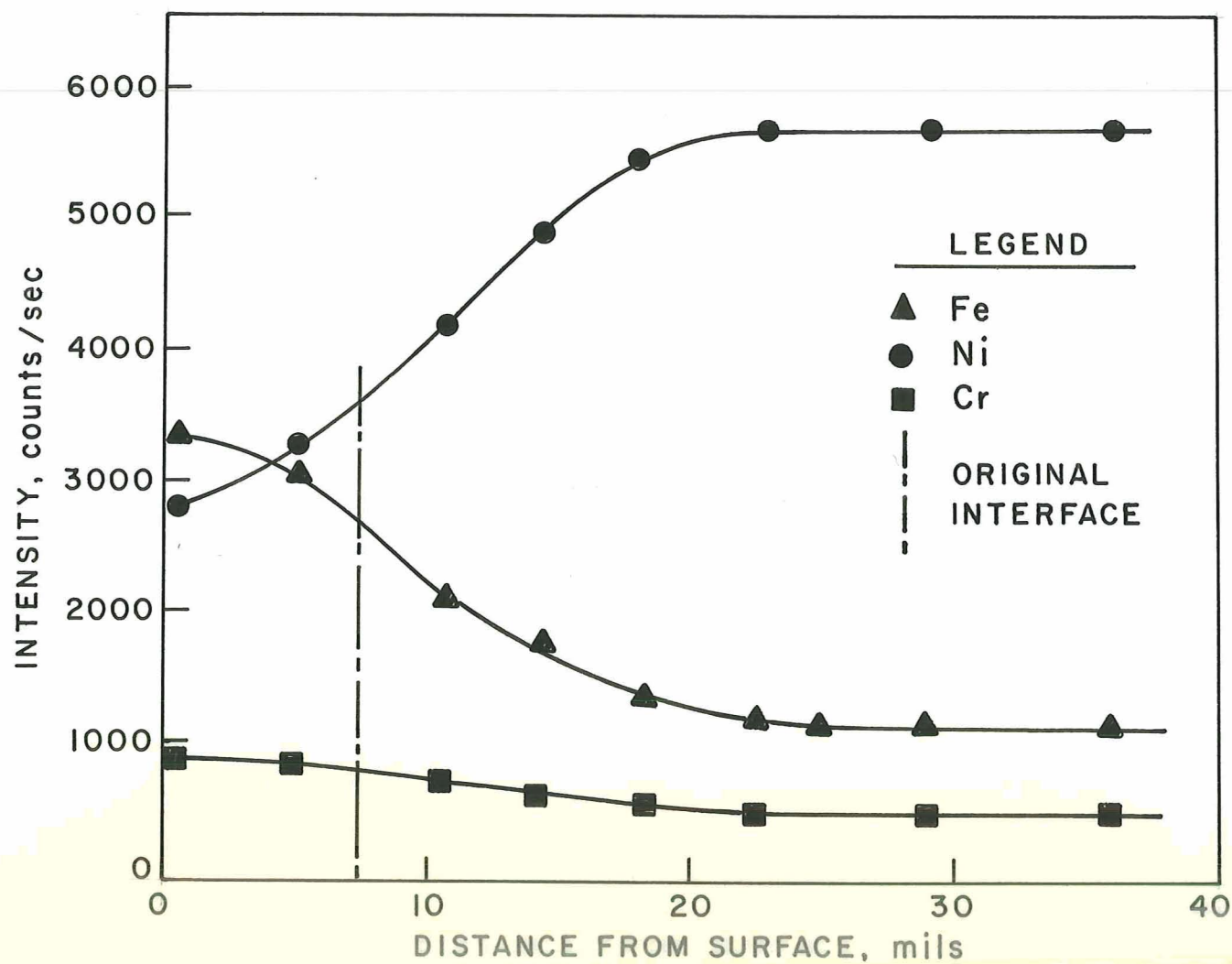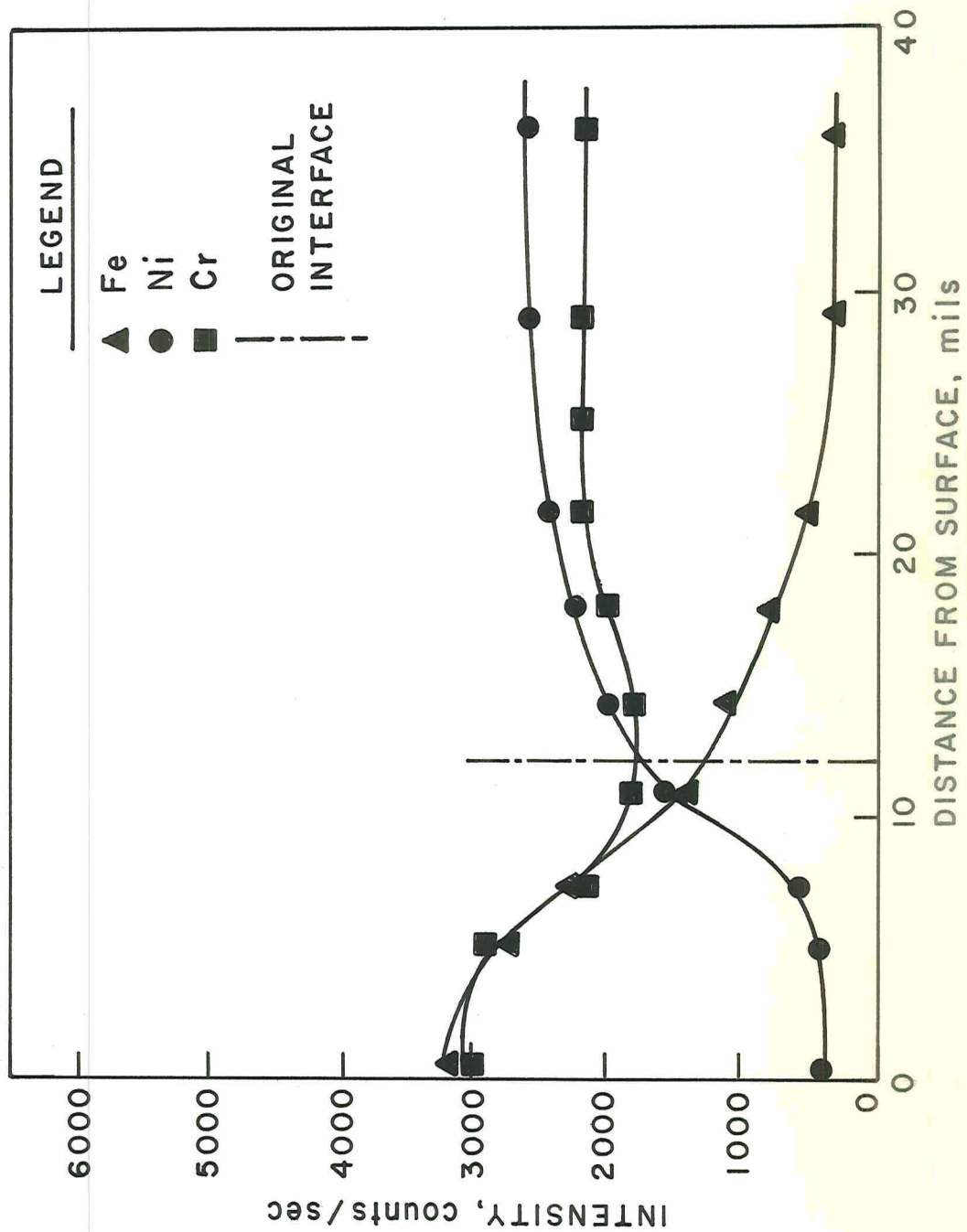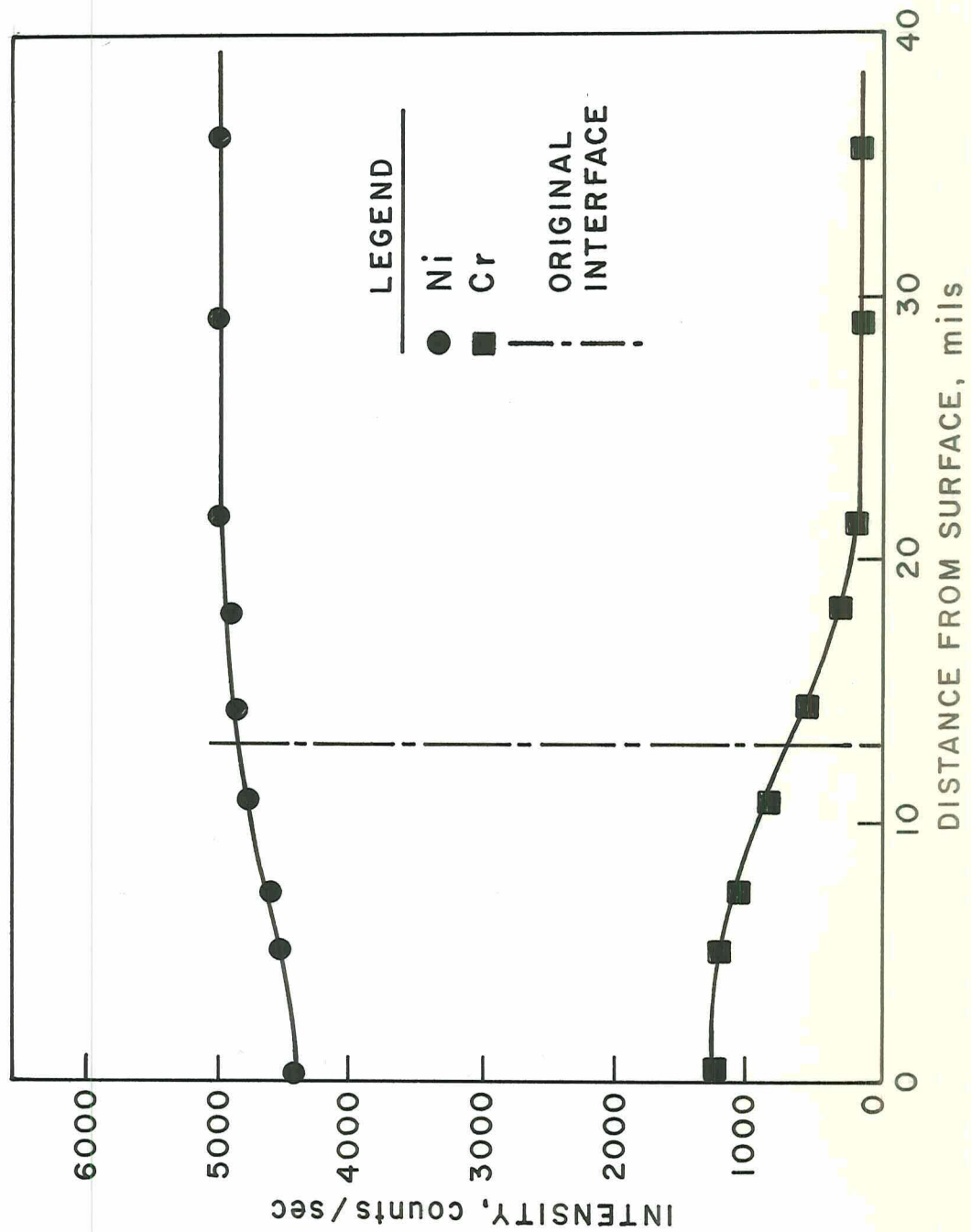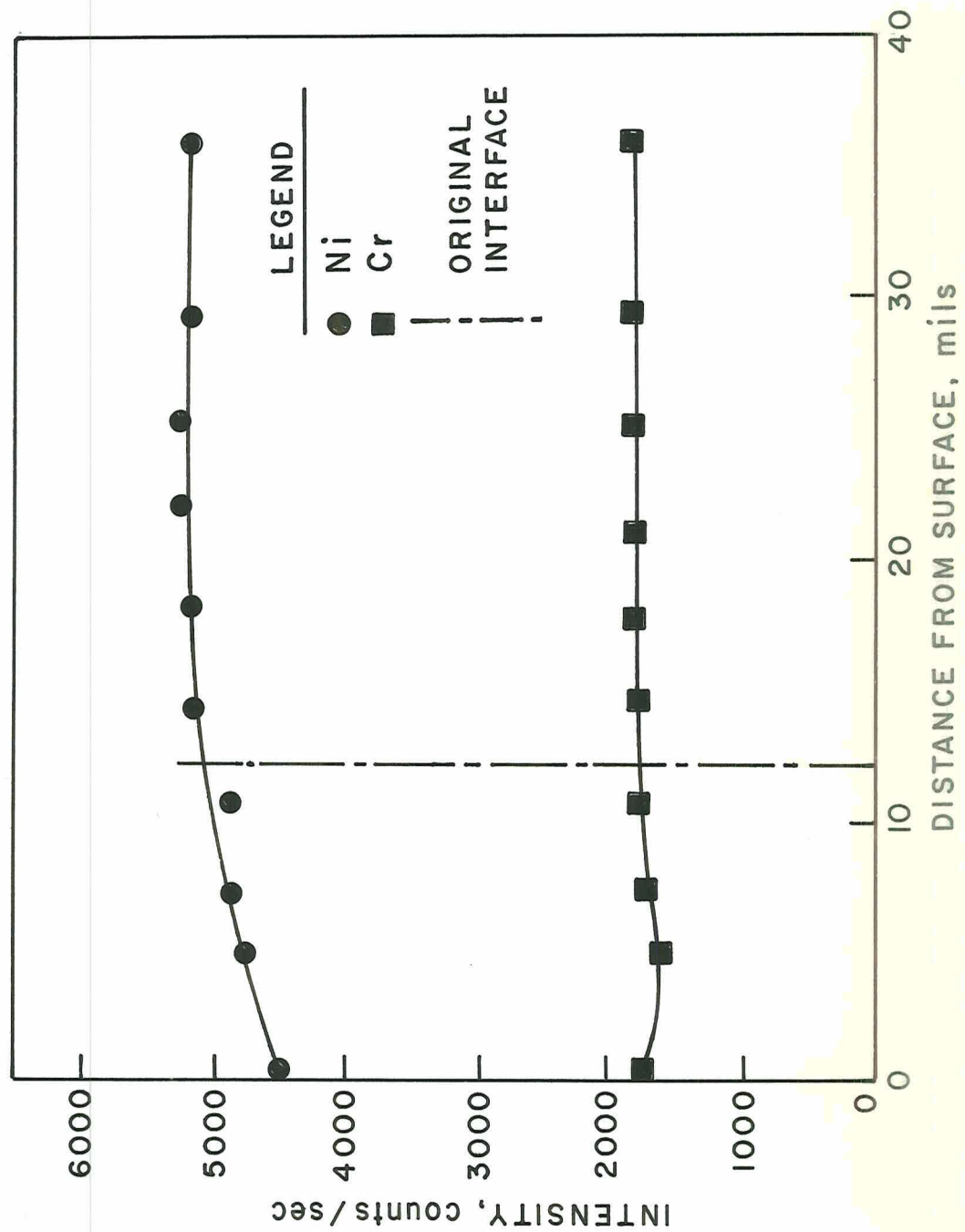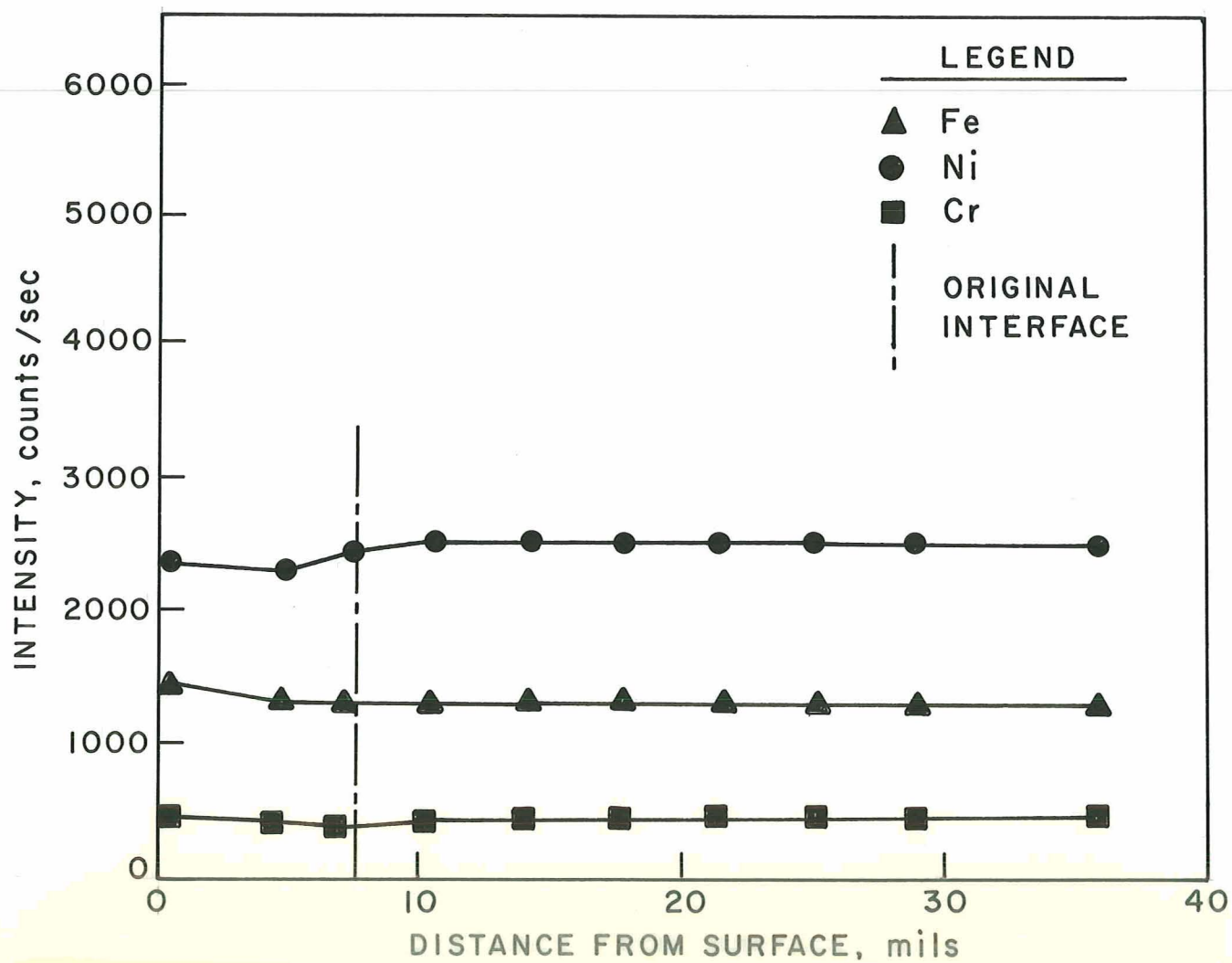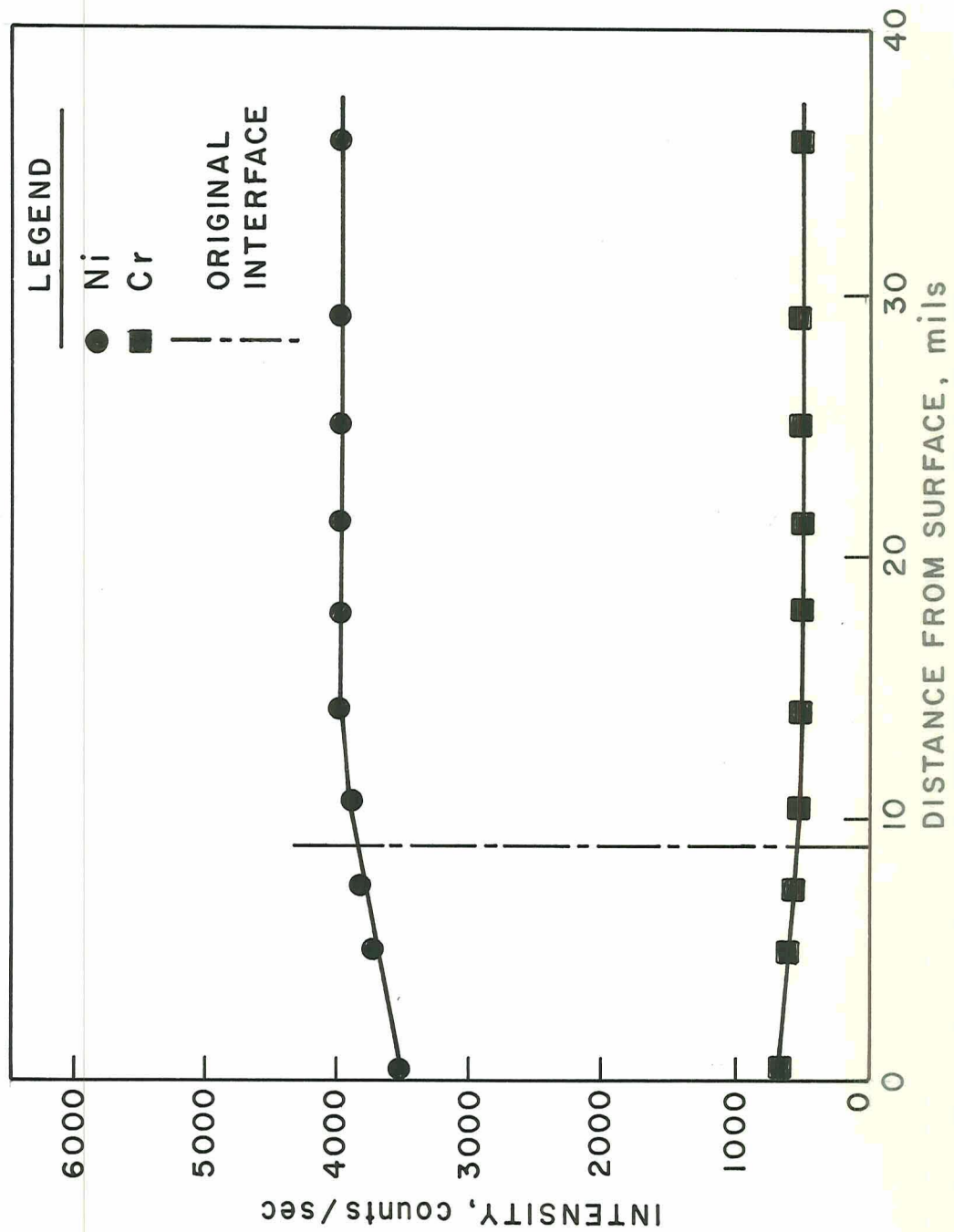
FINAL REPORT - DISTRIBUTION LIST
CONTRACT NAS3-10494

(The number in parentheses is the number of copies
sent to each addressee)

NASA Headquarters
600 Independence Avenue
Washington,D.C. 20546

Attention: RAP/N. F. Rekos (1)
            RRM/G. C. Deutch (1)
            RRM/R. H. Raring (1)

NASA-Ames Research Center
Moffett Field, California 94035
Attention: Library (1)

NASA-Flight Research Center
P.O. Box 273
Edwards, California 93523
Attention: Library (1)

NASA-Goddard Space Flight Center
Greenbelt, Maryland 20771
Attention: Library (1)

Jet Propulsion Laboratory
4800 Oak Grove Drive
Pasadena, California 91102
Attention: Library (1)

NASA-Langley Research Center
Langley Field, Virginia 23365
Attention: 214/Irvin Miller (1)
            Library (1)

NASA-Manned Space Flight Center
Houston, Texas 77058
Attention: Library (1)

NASA-Marshall Space Flight Center
Huntsville, Alabama 35812
Attention: Library (1)

Air Force Office of Scientific
    Research
Propulsion Research Division
USAF Washington, D.C. 20525
Attention: Library (1)

Defense Documentation Center (DDC)
Cameron Station (1)
5010 Duke Street
Alexandria, Virginia 22314

NASA-Lewis Research Center
21000 Brookpark Road
Cleveland, Ohio 44135

Attention: 105-1/G. M. Ault (1)
            3-19/Technology
                Utilization
                Office (1)
            49-1/S. Grisaffe (2)
            105-1/N. T. Saunders (1)
            60-3/Library (2)
            5-5/Report Control
                Office (1)
            106-1/R.E. Oldrieve (10)
            106-1/A.E. Anglin (1)
            77-3/John H. DeFord (1)
            5-3/A. Ginsburg (1)
            60-4/J. Howard Childs (1)
            105-1/W.D. Klopp (1)
            105-1/R.W. Hall (1)
            49-1/J.C. Freche (1)
            49-1/H.B. Probst (1)

NASA Scientific and Technical
    Information Fac.
P.O. Box 33
College Park, Maryland 20740 (6)

FAA Headquarters
800 Independence Avenue, S.W.
Washington, D.C. 20553

Atten.: Brig. Gen. J.C. Maxwell(1)
         SS/210/F.B. Howard (1)

U.S. Atomic Energy Commission
Washington, D.C. 20545
Attention: Technical Reports
            Library (1)

182

Distribution List

Oak Ridge National Laboratory
Oak Ridge, Tennessee 37830
Attention: Technical Reports
             Library (1)

Department of the Navy (1)
ONR
Code 429
Washington, D.C. 20525

Headquarters
Wright-Patterson AFB, Ohio 45433

Attention: MAMP (1)
             MATB (1)
             MAAM/Technical
               Library (1)
             AFSC-FTDS (1)
             AFML:MAM (1)
             MAG/Directorate
               of Materials (1)

U.S. Army Aviation Materials
   Laboratory
Port Eustis, Virginia 23604
Atten.:   SMOFE-APG/John White,
          Chief (1)

Bureau of Naval Weapons
Department of the Navy
Washington, D.C. 20525
Atten.:   RRMA-2/T. F. Kearns,
          Chief (1)

Army Materials Research Agency
Watertown Arsenal
Watertown, Massachusetts 02172
Attention: Director (1)

Battelle Memorial Institute
505 King Avenue
Columbus, Ohio 43201

Attention: Defense Metals
             Information Center
             (DMIC) (1)
             Dr. R. I. Jaffee (1)

Aerospace Corporation (1)
Reports Acquisition
P.O. Box 95085
Los Angeles, California 90045

Advanced Metals Research Corp.
149 Middlesex Turnpike
Burlington, Massachusetts 01804
Attention: J. T. Norton (1)

Allegheny Ludlum Steel Corp.
Research Center
Alabama and Pacific Avenues
Brackenridge, Pennsylvania 15014
Attention: Library (1)

American Society for Metals
Metals Park
Novelty, Ohio 44073
Attention: Library (1)

Avco Space Systems Division
Lowell Industrial Park
Lowell, Massachusetts 01851
Attention: Library (1)

The Bendix Corporation
Research Laboratories Division
Southfield, Michigan 48075
Attention: Library (1)

Boeing Co.
P.O. Box 733
Renton, Washington 98055
Attention: SST Unit Chief,
             W.E. Binz (1)

Case Western Reserve University
University Circle
Cleveland, Ohio 44106
Attention: Library (1)

Chromalloy Corp.
169 Western Highway
West Nyack, New York 10994
Attention: Mr. L. Maisel (1)

Distribution List

Denver Research Institute
University Park
Denver, Colorado 80210
Attention: Library (1)

Douglas Aircraft Co. MFSD
3000 Ocean Park Blvd.
Santa Monica, California 90406
Attention: Library (1)

Fansteel Metallurgical Corp.
Number One Tantalum Place
North Chicago, Illinois 60064
Attention: Library (1)

Ford Motor Company
Materials Development Dept.
20000 Rotunda Drive
P.O. Box 2053
Dearborn, Michigan 48123
Attention: Mr. Y. P. Telang (1)

Firth Sterling, Inc.
Powder Metals Research
P.O. Box 71
Pittsburgh, Pennsylvania 15230
Attention: Library (1)

General Electric Co.
Advanced Technology Lab.
Schenectady, New York 12305
Attention: Library (1)

General Electric Co.
Materials Development Lab. Oper.
Advance Engine and Tech. Dept.
Cincinnati, Ohio 45215
Attention: Mr. L.P. Jahnke (1)

General Motors Corporation
Allison Division
Indianapolis, Indiana 46206
Attention: Mr. D. K. Hanink (1)
            Materials Lab.

General Technologies Corp.
708 North West St.
Alexandria, Virginia 22314
Attention: Library (1)

E.I. DuPont de Nemours and Co. Inc.
Pigments Dept. Metal Products
Wilmington, Delaware 19898
Attention: Library (1)

IIT Research Institute
Technology Center
Chicago, Illinois 60616
Attention: Mr. V. Hill (1)
            Library (1)

Ilikon Corporation
Natick Industrial Center
Natick, Massachusetts
Attention: Library (1)

International Nickel Company
P.D. Merica Research Lab.
Sterling Forest
Suffern, New York 10901
Attention: Library (1)

Arthur D. Little, Inc.
20 Acorn Park
Cambridge, Massachusetts
Attention: Library (1)

Lockheed Palo Alto Research Labs.
Material and Science Lab. 52-30
3251 Hanover Street
Palo Alto, California 94304
Atten.: Technical Info. Center(1)
         Mr. E. C. Burke (1)

Massachusetts Institute of Tech.
Metallurgy Dept., RM 8-305
Cambridge, Massachusetts 02139
Attention: Library (1)

Distribution List

Narmco Research & Development Div.
Whittacker Corporation
3540 Aero Court
San Diego, California 92123
Attention: Library (1)

Nuclear Materials Company
West Concord, Massachusetts 01781
Attention: Library (1)

Ohio State University
Columbus, Ohio 43210
Attention: Library (1)

Rensselaer Polytechnic Institute
Troy, New York 12180
Attention: Library (1)

Sherritt Gordon Mines, Ltd.
Research and Development Division
Fort Saskatchewan, Alberta, Canada
Attention: Library (1)

Solar Division
International Harvester Corp.
San Diego, California 92112
Attention: Mr. A.R. Stetson (1)

Stanford Research Institute
Menlo Park, California
Attention: Library (1)

Stanford University
Palo Alto, California 94305
Attention: Library (1)

Westinghouse Electric Corporation
Westinghouse Astronuclear Lab.
P.O. Box 10864
Pittsburgh, Pennsylvania 15236
Attention: Mr. R. Begley (1)

TRW Electromechanical Division
TRW Inc.
23555 Euclid Avenue
Cleveland, Ohio 44117
Attention: Mr. J. Gadd (1)

Union Carbide Corporation
Stellite Division
Technology Department
Kokomo, Indiana 46901
Attention: Technical Library (1)

United Aircraft Corporation
400 Main Street
East Hartford, Connecticut 06108
Attention: Research Library (1)
            E.F. Bradley, Chief(1)
            Materials Engineering

United Aircraft Corporation
Pratt and Whitney Division
West Palm Beach, Florida 33402
Attention: Library (1)

Universal-Cyclops Steel Corp.
Bridgeville, Pennsylvania 15017
Attention: Library (1)

Vitro Laboratories
200 Pleasant Valley Way
West Orange, New Jersey 07052
Attention: Mr. M. Ortner (1)

Wah Chang Corporation
Albany, Oregon 97321
Attention: Library (1)

AFML (MAMP)
Wright-Patterson AFB, Ohio 45433
Attention: Mr. N. Geyer (1)

Bureau of Naval Weapons
Department of the Navy
Washington D.C. 20525
Attention: Mr. I. Machlin (1)

Alloy Surfaces, Inc.
100 South Justison Street
Wilmington, Delaware 19899
Attention: Mr. George H. Cook(1)

Battelle Memorial Institute
505 King Avenue
Columbus, Ohio 43201
Attention: Mr. E. Bartlett (1)

City College of New York
Department of Chemical Engineering
New York, New York 10031
Attention: Mr. R.A. Graff (1)
            Mr. M. Kolodney (1)

E. I. DuPont de Nemours and Co.
1007 Market Street
Wilmington, Delaware 19898
Atten.: Dr. Warren I. Pollack (1)

General Electric Company
Materials Development Lab Oper.
Advance Engine and Tech. Dept.
Cincinnati, Ohio 45215
Attention: Mr. M. Levinstein (1)
            Mr. J. W. Clark (1)

Howmet Corporation
Misco Division
One Misco Drive
Whitehall, Michigan 49461
Attention: Mr. S. Wolosin (1)

Pratt & Whitney Division of (1)
United Aircraft Corp.
Manufacture Engineering
Aircraft Road
Middletown, Conn. 06457

Sylvania Electric Products
Sylcor Division
Cantiague Road
Hicksville L.I., New York 11802
Attention: Mr. L. Sama (1)

Texas Instruments, Inc.
Materials and Controls Division
P.O. Box 5474
Dallas, Texas 75222
Attention: Mr. Gene Wakefield (1)

U.S.A.F.
San Antonio Air Material Area
Kelly Air Force Base, Texas 78241
Attention: SANEPJ/A. E. Wright,
                 Chief
                 Jet Engine Section (1)

University of Dayton
Research Institute
300 College Park Avenue
Dayton, Ohio 45409
Attention: Library (1)

University of Illinois
Department of Ceramic Engineering
Urbana, Illinois 61801
Attention: Mr. J. Wurst (1)

University of Pittsburgh
Center for Study of Thermodynamic
  Properties of Materials
409 Engineering Hall
Pittsburgh, Pennsylvania 15213
Attention: Dr. G.R. Fitterer (1)

University of Washington
Ceramics Department
Seattle, Washington   98101
Attention: Dr. J. Mueller (10)

Westinghouse Electric Corporation
Research Laboratories
Beulah Road, Churchill Buro.
Pittsburgh, Pennsylvania   15235
Attention: Mr. R. Grekila (1)

Whitfield Laboratories (1)
P. O. Box 287
Bethel, Connecticut   06801